The marine geology of Mossel Bay, South Africa

Hayley C. Cawthra

Submitted in fulfilment of the requirements
For the degree of

Doctor of Philosophy

In the
Department of Geological Sciences
Faculty of Science
University of Cape Town

Supervisor: Professor John S. Compton

May 2014

These studies, except where otherwise indicated and suitably acknowledged in the text, represent original work by the author and have not been submitted in any form to another university. Parts of this thesis which have been published in peer-reviewed publications and reports were the original work of the first author in terms of data analysis, interpretations and production of figures.

ABSTRACT

This thesis presents work undertaken to better understand the complex evolution of the terrestrial landscape now submerged by high sea levels offshore of Mossel Bay along the South Coast of South Africa. Three marine geophysical surveys and scuba diving were used to examine evidence of past sea-level fluctuations and interpret geological deposits on the seafloor. Additional geological mapping of coastal outcrops was carried out to link land and sea features and rock samples were dated using Optically Stimulated Luminescence (OSL). Geophysical investigations include a regional seismic survey extending from Still Bay in the west to Buffels Bay in the east out to a maximum water depth of 110 m; a high-resolution investigation of the Mossel Bay shelf using multibeam bathymetry, side-scan sonar and sub-bottom profiling; and a shallow seismic pinger survey of Swartvlei, the most prominent coastal lake in the Wilderness Embayment. This study presents 9 discrete seismic sequences, and describes major offshore geomorphic features such as submerged sea cliffs, palaeo-coastal zones and fluvial systems. Oscillation in sea level between ~2.7 and 0.9 Ma likely resulted in the formation of the prominent -45 m terrace, which separates a relatively steep inner from a low-gradient mid shelf. Beach and dune deposits span from Marine Isotope Stage 15 (MIS 15) (582 ka) to Recent based on an age model that integrates OSL ages and the established eustatic sea-level record. The most prominent deposits date from the MIS 6 glacial to MIS 5 interglacial periods and include incised lowstand river channels and regressive aeolianites that extended at least 10 km inland from their associated palaeoshorelines. The MIS 5 deposits include transgressive beachrock, an extensive foreshore unit which prograded on the MIS 5e highstand, and regressive beach and dune deposits on the shelf associated with the subsequent fall in sea level. MIS 4 lowstand incised river channels were infilled with sediment truncated during rapid landward shoreface migration at the MIS 4 termination. Low-energy, back-barrier MIS 4/3 sediments are preserved as a result of overstepping associated with meltwater pulses of the MIS 2 termination. The MIS 1 sediment wedge comprises reworked sediment and is best developed on the inner shelf. Holocene highstand sedimentation continues to prograde. Accommodation space for coastal deposits is controlled by antecedent drainage pathways and the gradient of the adjacent inner continental shelf. The geological deposits on the emergent shelf indicate a greatly expanded glacial coastal plain that potentially received more rain feeding low-gradient meandering rivers and wetland lakes. These extensive wetland environments provided a rich source of diverse food types which along with abundant marine resources on the shoreline made the Southern Coastal Plain an ideal habitat for our ancestors.

Hayley Candice Cawthra

The Marine Geology of Mossel Bay, South Africa

May 2014

ACKNOWLEDGEMENTS

The research presented in this thesis was undertaken from March 2011 to March 2014 in the University of Cape Town Department of Geological Sciences and the Council for Geoscience, under the supervision of Professor John Compton. The geophysical datasets collected for this project were funded by the National Geographic Society Expeditions Council (Grant number EC0482-10 awarded to C.W. Marean, H.C. Cawthra & E.C. Fisher), the Council for Geoscience Annual Technical Programme (Project number ST-2011-1139 led by H.C. Cawthra) with additional support provided by J.S. Compton (University of Cape Town), and the National Research Foundation (P.J. Holmes). Supplementary geophysical data from near Mossel Bay were provided by PetroSA. My colleagues in the Marine Geoscience Unit are thanked most sincerely for their invaluable role in a study clearly relying on extensive teamwork in both geophysical data collection and scuba diving. Michael MacHutchon (Mac), Wilhelm van Zyl and Willem Kupido have provided unwavering support which I greatly appreciated. This was also achieved with the constant backing and leadership of our manager, Dr Luc Chevallier, and additional administrative support from Khanyo Ngwenya and Hanneke Malherbe. Dr Chiedza Musekiwa assisted with GIS queries and Ishaam Davids is thanked for his assistance digitising Figures 2-1, 2-6, 6-8 and 6-10 presented in this thesis. There are a few people I wish to thank most sincerely for valued professional input and thoughtful advice, as well as support on a personal level. My supervisor, Prof John Compton; members of the Mossel Bay SACP4 project members and notably Drs Curtis Marean and Erich Fisher from Arizona State University; Prof Dr Ulrich Glasmacher (University of Heidelberg) and colleagues at the Council for Geoscience: Michael MacHutchon, Coenie de Beer, Dr Jurie Viljoen, Nicky Flint and Dr Dave Roberts. Two hydrographic companies in Cape Town supported this research programme. Marine Data Consultants (Gordon Rigg) and C&C Technologies (Aubrey Price) are acknowledged for the hire of a QINSy software key and differential GPS signal, respectively. Dr Zenobia Jacobs, University of Wollongong, is thanked for determining luminescence ages on offshore samples collected for this study. Thin sections were made by David Wilson, University of Cape Town, and SEM-EDS analyses guided by Miranda Waldron (Scanning Electron Microscope facility). Carbonate content was calculated by Clive Botha, Council or Geoscience. The seismic survey of Swartvlei, Wilderness, was undertaken with Prof Mark Bateman (University of Sheffield), Dr Andy Carr (University of Leicester) and Prof Peter Holmes (University of the Free State). Many weeks were spent in Mossel Bay over the past 3 years and the following groups and people are acknowledged for their contributions to make this a success: The Mossel Bay Yacht and Boat Club for the provision of a boat mooring, Estienne and Nadia Arndt for warm hospitality and logistical support. Oceans Research, and specifically Enrico Gennari, are thanked for providing a shark cage for divers to use and for accommodating us on their premises. Dive support from Dave van Beuningen, Ben Southall, Sarah Webb, John Wiley, Braham Smit and Thomas Morrell was greatly appreciated. Diving supervisor Daniel Rogers, from Adventure's Edge, and his team (Edward Terblanche, Alison Farron and Christiaan Coetzee) are thanked for joining our dive team and for multiple cylinder fills.

LIST OF PUBLICATIONS RELATED TO THIS THESIS

CONFERENCE ABSTRACTS

Cawthra, H.C., Fisher, E.C., Compton, J.S., Marean, C.W. Drowned Quaternary environments and the significance for the South African Southern Cape Archaeological Record. SplashCos 2013, Under the sea: Archaeology and palaeolandscapes, Szczecin (Poland).

Cawthra, H.C., Compton, J.S. A marine geophysical study of the continental shelf off Mossel Bay, South Africa: Sea-level fluctuations, human evolution and submerged landscapes. 2013 SANCOR workshop Kirstenbosch Research Centre, Cape Town, South Africa.

Cawthra, H.C. Reconstructing submerged landscapes: clues from the continental shelf. Quaternary climate and vegetation of Southern Africa, East-West-North-South. 2013 BPI Palaeontology, University of the Witwatersrand, Johannesburg, South Africa.

Cawthra, H.C., Marean, C.W., Fisher, E.C., Compton, J.S. Marine geophysics and geological modelling of offshore Late Quaternary palaeoshorelines in the Southern Cape, South Africa SASQUA 2012, Gobabeb, Namibia.

Cawthra, H.C., Marean, C.W., Fisher, E.C., Compton, J.S. The application of marine geophysics to understanding late Quaternary palaeoenvironments and early modern human dispersal in the Southern Cape, South Africa. IGC 2012, Brisbane, Australia.

Cawthra, H.C. Uken, R., Compton, J.S, 2011. Aeolianites and beachrocks on the continental shelf along the South African east- and South Coasts: High resolution marine geophysics, stratigraphy and relevance to understanding Quaternary sea level fluctuations. GeoSynthesis (Cape Town, Western Cape).

TECHNICAL AND SCIENTIFIC REPORTS

Marean, C.W., Cawthra, H.C., Fisher, E.C., 2013. Follow the coast: marine geophysical study of early human use of the continental shelf of the South Coast, South Africa. National Geographic Expeditions Council Final Report for Grant #EC0482-10, 13 pp.

Cawthra, H.C., 2013. Report on the first 'ground-truth' survey of Mossel Bay, South Africa: scuba diving and sediment sampling programme. Council for Geoscience Report 2013-0171, 23 pp.

Cawthra, H.C., 2013. Quaternary deposits of the Mossel Bay shoreline. Council for Geoscience Report 2013-0176, 33 pp.

Cawthra, H.C., MacHutchon, M.R., 2013. Surficial geology of the Mossel Bay continental shelf. Council for Geoscience Report 2013-0169, 30 pp.

Cawthra, H.C., 2013. Interpretation of cliff retreat and incision of coastal caves along the Mossel Bay shoreline, South African South Coast. Council for Geoscience Report 2013-0170, 18 pp.

Cawthra, H.C., 2013. Evaluation of offshore mineral resources in the Western Cape Province: presentation of processed sub-bottom profiling data collected between Knysna and Stilbaai. Council for Geoscience Report 2013-0172, 24 pp.

Cawthra, H.C., 2012. Evaluation of offshore mineral resources in the Western Cape Province: Implications for a new continental shelf exploration programme. Phase 1: Cruise report for sub-bottom profiling between Knysna and Stilbaai. Council for Geoscience Report 2012-0131, 26 pp.

Cawthra, H.C., 2012. Seismic survey of two Wilderness lakes (Swartvlei and Eilandvlei), Southern Cape, South Africa: Cruise and sediment sampling report. Council for Geoscience Report 2012-0129, 30 pp.

Cawthra, H.C., 2011. Processing methodology and presentation of multibeam bathymetric data acquired offshore of Mossel Bay and surrounds (Southern Cape, South Africa). Council for Geoscience Report 2011-0162, 14 pp.

Cawthra, H.C., 2011. Cruise report for the Mossel Bay seismic survey, Southern Cape, South Africa. Phase 2: Boomer and pinger sub-bottom profiling. Council for Geoscience Report 2011-0134, 33 pp.

Cawthra, H.C., 2011. Cruise report for the Mossel Bay geophysical and hydrographic survey, Southern Cape, South Africa. Phase 1: Multibeam bathymetry and side-scan sonar. Council for Geoscience Report 2011-0133, 44 pp.

Cawthra, H.C., 2011. Preliminary assessment of the geology of the continental shelf offshore of Pinnacle Point, Southern Cape, South Africa. Council for Geoscience Report 2011-0105, 17 pp.

Cawthra, H.C., 2011. Mapping of submerged geological deposits: planning, sampling, cataloguing and interpretation of results. Council for Geoscience Report 2011-0104, 10 pp.

Cawthra, H.C., 2011. A guideline to the interpretation and classification of marine geophysical data (bathymetry, side-scan sonar and sub-bottom profiling). Council for Geoscience Report 2011-0102, 12 pp.

TABLE OF CONTENTS

LIST OF FIGURES

LIST OF TABLES

LIST OF COMMON ABBREVIATIONS

AMSL: above Mean Sea Level

BMSL: below Mean Sea Level

CFB: Cape Fold Belt

CGS: Council for Geoscience

DEM: Digital Elevation Model

dGPS: differential Global Positioning System

GIS: Geographic Information System

ka: thousands of years (referring specifically to an age)

kyr: thousands of years before present (when referring to a range in time)

LGM: Last Glacial Maximum

Ma: millions of years (referring specifically to an age)

MGU: Marine Geoscience Unit

MWP: Meltwater Pulse

Myr: millions of years before present (when referring to a range in time)

MIS: Marine Isotope Stage

MPT: Mid-Pleistocene Transition

MSL: Mean Sea Level

OSL: Optically Stimulated Luminescence

PMT: post-glacial marine transgression

RSL: Relative sea-level

SACP4: South African Coast Palaeoclimate, Palaeoenvironment, Palaeoecology, Palaeoanthropology

SCP: Southern Coastal Plain

yrs BP: years before present

1 INTRODUCTION

1.1 Background

With the onset of the rhythmic Quaternary glacial-interglacial climate cycles, shorelines have shifted between a maximum lowstand depth of 130 m below and a maximum highstand elevation of 13 m above present-day sea level approximately every 100 thousand years (100 kyr) since 900 thousand years before the present (900 ka) (Bintanja et al., 2005; Lisiecki and Raymo, 2005). During most of this time (~90 %) sea level has been significantly lower than it is at present, exposing a now submerged terrestrial ecosystem of what is now the continental shelf and drastically altering the landscape. The ~500 km long South African South Coast, extending from Cape Hangklip in the west to Plettenberg Bay in the east (Figure 1-1), represents a tract of relatively low-relief coastal plain bordered at its landward geographic limit by the Cape Fold Belt (CFB) and at the seaward margin by the Indian Ocean. During times of minimum sea level during the Pleistocene the South Coast coastal plain was at least doubled and through much of the Pleistocene, there was a large rather flat landmass exposed that is now submerged as the Agulhas Bank (Dingle and Rogers, 1972; van Andel, 1989; Compton 2011). Using modern marine geophysical techniques the offshore submerged landscape and its deposits can now be mapped in ultrahigh-resolution and inform us of how the margin has evolved over glacial to interglacial cycles of the Quaternary.

The South Coast of South Africa has one of the richest Middle Stone Age archaeological records in the world, with sea cliff caves and open-air sites on the exposed landscape holding rich archives of early humans. While there are a number of archaeological sites along the South Coast (Figure 1-2), recent work has revealed rich records from the vicinity of Mossel Bay centrally located on the South Coast. In particular, there are well preserved archaeological records from coastal caves at Pinnacle Point. The coastal caves and rock shelters at Pinnacle Point contain evidence extending back 164 kyr for the emergence of modern behaviours in our species *Homo sapiens* (Marean et al., 2007). The South African Coast Palaeoclimate, Palaeoenvironment, Palaeoecology and Palaeoanthropology Project (SACP4) endeavours to develop a high-resolution and continuous palaeoclimatic and palaeoenvironmental reconstruction of the South Coast of South Africa from Marine Isotope Stage (MIS) 11 through to MIS 3 (440 to 40 ka) and contextualise within the reconstruction a detailed record of adaptive change across early modern humans. The focus of SACP4 is to determine where, when and why modern humans evolved, and much of the research effort targets the interval between 200 and 50 ka.

Figure 1-1. The Southern Coastal Plain (SCP), Western Coastal Plain (WCP), Cape Fold Belt (CFB) and broad continental shelf at water depths of 45, 75 and 120 m (from Compton, 2011). The area of study in this thesis is outlined by yellow infilled and black boxes offshore of Mossel Bay.

The extent to which the continental shelf was exposed in the past and the type of environments play an important role in the SACP4 endeavour (e.g., Fisher et al., 2010). However, our understanding of the marine geology is not well known and a more detailed understanding of the geology of the offshore region is paramount to the furthering of the SACP4 research effort. Compton (2011) suggested that correlations drawn between glacio-eustatic sea-level records and preserved archaeological evidence from the South African South Coast are indicative of periodic expansion and contraction of the environment in which humans lived. Selection pressures would, according to this hypothesis, have intensified during the periodic contraction of isolated groups living on the southern coastal plain (SCP) of South Africa. In this way, the SCP may have acted as a geographical region of origin during human evolution if groups were isolated over glacial to interglacial cycles to diverge away from other populations in Africa. Middle Stone Age people generally inhabited the coastal zone because of the abundant resources (Marean et al., 2007) and so for most of their history would have occupied what is now the submerged shelf. A pressing question therefore, is the nature of this offshore environment – how it fluctuated through time and how it may have influenced human development. Remnant coastal features such as dunes,

beaches, wave-cut platforms and fluvial systems have been documented on parts of the South African shelf, but have never been systematically mapped and sampled in this area of interest. It was, therefore, realised with the recent archaeological results from the Pinnacle Point site (Marean et al., 2007; Marean, 2010) the obvious need to extend the research offshore. It was out of geological scientific interest in the Quaternary depositional history of the coastal region in general and, more specifically, how changes in the palaeoenvironments may relate to human evolution that this marine geology project was initiated under the auspices of the SACP4 programme.

1.2 Locality

The study area lies on the South African South Coast and encompasses three zones. At the broadest scale, regional pinger seismic transects were collected between Still Bay in the west and Buffels Bay in the east (Figure 1-2). A total of 9 coast-perpendicular and coast-parallel seismic lines were collected across this ~200 km long area and up to 80 km out to sea. The area investigated in the highest resolution, offshore of Mossel Bay, occupies 255 km^2 of continental shelf with the Pinnacle Point archaeological site centrally located within the surveyed block (Figure 1-3). Here, multibeam echosounder, side-scan sonar, boomer seismic and pinger seismic data were collected with full seafloor coverage. The third component of the study is the largest coastal lake in the Wilderness Embayment, Swartvlei, which is situated 100 km east of Mossel Bay. A pinger seismic survey was undertaken, covering the entirety of this lake.

1.3 Hypothesis, questions and objectives

The key issues being addressed in this study relate to the highly complex coastal zone that shifts over the continental shelf though time. How did the extent of the coastal plain vary in response to Quaternary glacial-interglacial climate cycles, and what can the depositional history of this submerged landscape reveal of the variation in human habitats? The hypothesis is that the submerged landscape differs significantly to the currently sub-aerially exposed coastal plain, and this was addressed using marine geophysics, geological interpretation and sedimentology. The primary objective of this work was to apply the most appropriate techniques in marine geophysics and quantification of geological processes to create a base from which to derive palaeoenvironments through the middle to late Quaternary. This involved the acquisition of datasets on varying scales and resolution, from building a sequence stratigraphic model for the evolution of the shelf elements at the broadest view, to analytical quantification of microfacies using scanning electron microscopy at the finest resolution. Mapping of seafloor geology was achieved using geophysics, and samples and observations obtained by mapping the shoreline and offshore area, the latter using scuba diving. The combination of surficial information with sub-bottom profiling data allowed the depositional history of this shelf to be investigated. The culmination of these methods allowed the presentation of a geological and sedimentological model reflecting the character of ancient

landscapes and shorelines at key times of interest as defined by the archaeological record. Land-sea interactions and the response of the coastal zone to changes in sea level were comprehensively investigated.

1.3.1 Regional seismic survey: Still Bay to Buffels Bay

The regional seismic survey aimed to facilitate the development of a sequence stratigraphic model for the South Coast shelf, incorporating all significant Quaternary deposits and features, and providing a link to the underlying geological successions. Mapping the distribution of palaeo-drainage systems on the shelf by the interpretation of seismic data and the response of the South Coast rivers to sea level regressions and transgressions was also an objective of this seismic study. This included understanding the nature of transgressive infill facies into incised channels.

1.3.2 Mossel Bay

The purpose of the high-resolution geophysical and geological survey offshore of Mossel Bay was to:

1) Conduct intensive marine geophysical and sampling surveys, using the most appropriate technologies and develop a high-resolution geophysical/geomorphic/palaeoenvironmental database for a sector of the South Coast shelf off Mossel Bay.
2) Integrate these data with geological modelling to reconstruct past ecosystems with a focus on major sea-level changes. The timing and magnitude of relative sea-level fluctuations on the South Coast were based on eustatic sea-level records available in the literature (e.g. Waelbroeck et al., 2002; Bintanja et al., 2005; Rohling et al., 2009). The large-amplitude, high-frequency sea-level fluctuations, along with climate change, would have had a large impact on the dynamics of the near shore and shelf environments. This study considers palaeoshorelines, sediment supply of river sources as well as reworked older sediment deposits to infer processes such as longshore drift, aeolian dune formation, rocky versus sandy beach shorelines and the extent of estuarine and wetland environments. In addition inferences on vegetation biomes were based on bedrock geology, aspect and shelf gradient. The distribution of these elements of the coastal zone and how they changed through time would have been critical to humans living in the area and this study helps to delineate the distribution and dynamic of coastal environments in relation to sea-level fluctuations.
3) Integrate the results of this study with the already acquired onshore data, at the highly informative Pinnacle Point archaeological site, to generate more holistic models of changing ecosystems and their influence on human development. Offshore of the Pinnacle Point site, the need for marine mapping addresses the question of availability of food resources and the use of the marine environment by humans. Rocky coastlines within a 10 km radius of the site were mapped and modelled, spanning the

time of occupation when sea levels were similar to or lower than the present day. Identification of palaeosols and deflation surfaces offshore was carried out by interpreting seismic data with sequence stratigraphic principles.

1.3.3 Wilderness/Swartvlei

The Swartvlei seismic survey aimed to map the bedrock bathymetry of this coastal lake; identify possible submerged remnant dunes in the lake; and refine the understanding of palaeochannels in the Wilderness Embayment. These questions are also relevant to the preservation of the barrier systems in response to sea-level change in this area (e.g. post-glacial flooding of the lake systems) and allow an understanding of similar systems in the palaeo record. Swartvlei represents a modern back-barrier coastal wetland environment and, as such, provides a useful analogue and a crucial link in the land-sea connection.

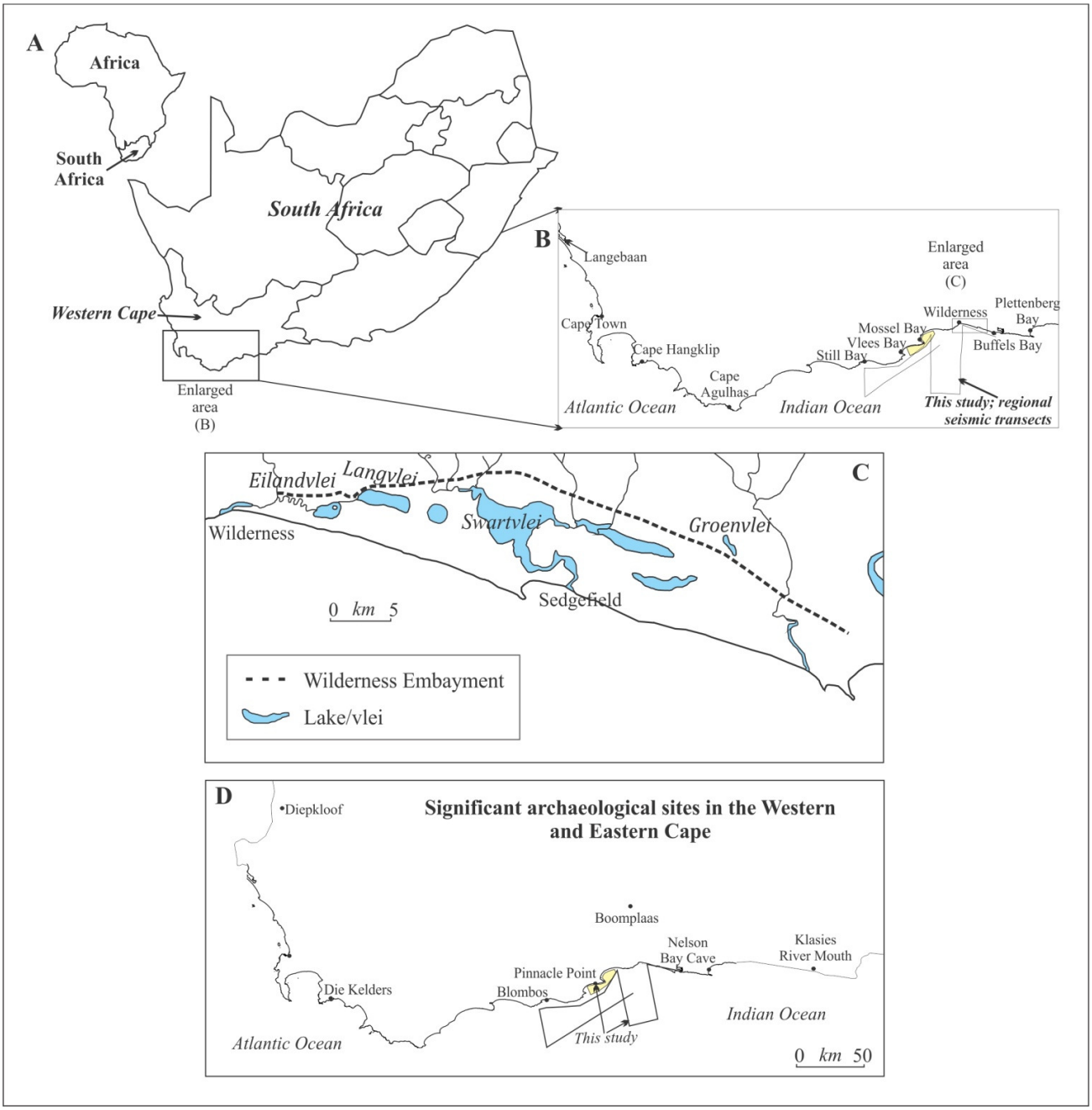

Figure 1-2. Locality of the study area in relation to A. South Africa, and B. The South Coast. C. Inset of the Wilderness Embayment, showing Swartvlei. D. Prominent archaeological sites along the South Coast and adjacent areas.

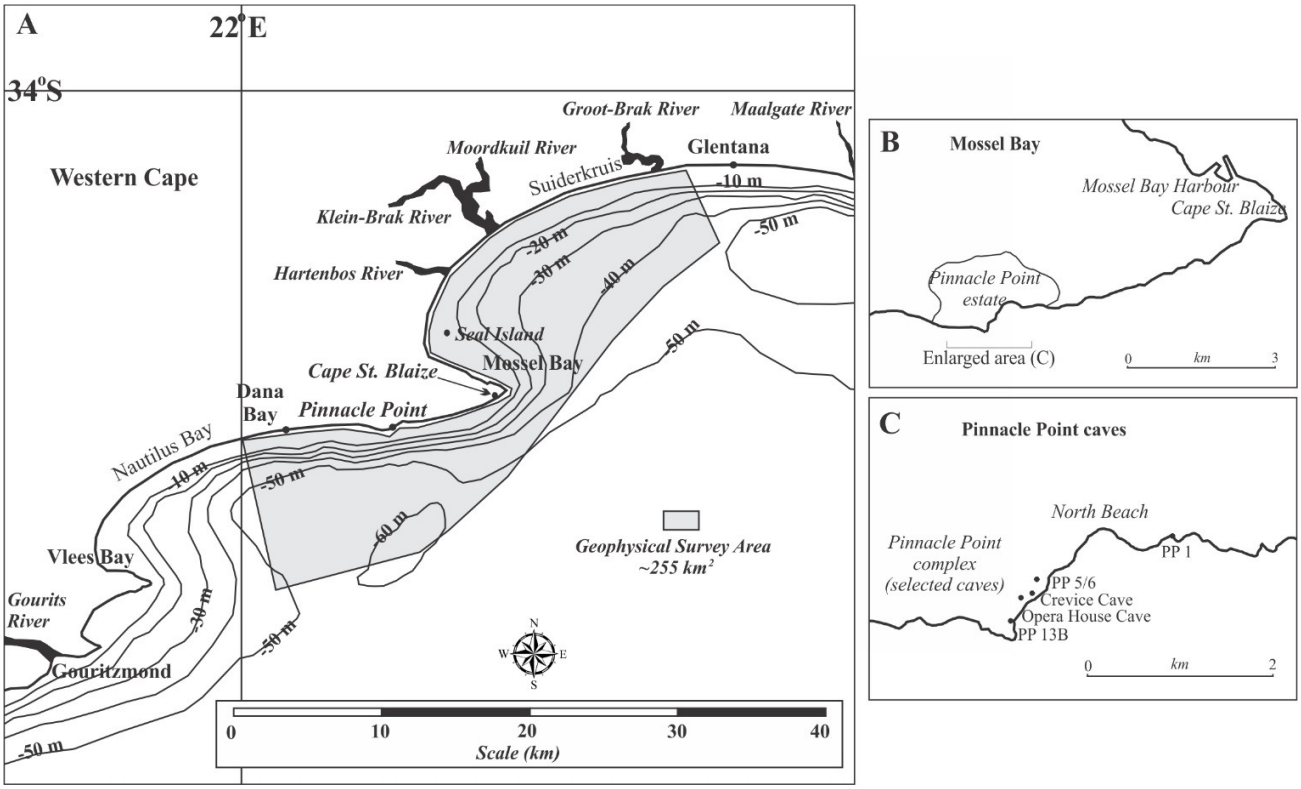

Figure 1-3. A. The Mossel Bay region and offshore high-resolution geophysical survey area shown in grey. B, C. Cape St. Blaize and Pinnacle Point.

1.4 Thesis format

This thesis takes the form of eight chapters, and is arranged in a logic flow determined by the nature of the interpretive process. Following a regional setting for context and an introduction to the methods applied to derive the interpretations, the presentation of results initially expands outward in scope from a high-resolution investigation of the Mossel Bay area, followed by consideration of the context of its placement on the South Coast in a seismic and sequence stratigraphy between Still Bay in the west and Buffels Bay in the east, and, finally, focusing back on Pinnacle Point. The succession of significant events which shaped this composite emerged landscape and submerged seascape is described chronologically from oldest to youngest, where possible. The reason for the chapters being laid out as such was based on the integration of datasets on varying scale and resolution, as well as the onland and offshore investigations carried out.

2 REGIONAL SETTING

2.1 Evolution of the landscape surface of the coastal plain and adjacent continental shelf

2.1.1 Topographic and bathymetric characteristics of the South Coast

The distinctive topography of Southern Africa is characterised by a high-relief inland plateau (backed by the Great Escarpment), the Cape Fold Belt (CFB) mountainous terrain, flanked by a low average elevation coastal plain (Figure 2-1). The regionally exposed onshore Southern Coastal Plain (SCP) extends semi-continuously from Cape Hangklip in the west to Plettenberg Bay in the east (Compton, 2011) and is characterised by a low-relief coastal plain incising the base of the CFB which dips consistently seaward where it terminates near or at the coast. Scattered authigenic deposits on this surface are suggested to be Cretaceous in age (Guillocheau et al., 2013) but the exhumation of the land surface may have occurred subsequent to the sedimentation. The lithology of pre-Cenozoic bedrock around the South African coast is variable, creating differences in geomorphic expression. Resistant lithologies, such as the quartz arenites of the Palaeozoic Cape Supergroup on the West and South Coasts, and the equivalent Natal Group and Msikaba Formation on the East Coast tend to form steep sea cliffs at the shoreline.

The adjacent offshore passive continental margin of Southern Africa varies extensively in width and relief, with the area off the South Coast being particularly broad (up to 270 km wide off Cape Agulhas). The major bathymetric features of the Agulhas Bank are shown in Figure 2-1. The South Coast is characterised by a broad, flat outer shelf, a middle shelf rise around 60 - 80 m BMSL, a relatively flat inner-shelf and a narrow (~2 – 14 km wide) sediment-free rocky nearshore zone (Birch, 1980). No major valleys or canyons transect the part of the South Coast continental shelf investigated in this study (Gentle, 1987), but the Breede River to the southwest is the most prominent fluvial system which characterises the shelf environment. A series of nick points across the shelf, preserved at water depths of ~40 m, 55 – 50 m, 80 – 75 m and 105 - 100 m BMSL, suggest erosion by previous sea-level stillstands, coinciding with the occurrence of aeolianite ridges on the continental shelf to support this argument (Martin and Flemming, 1986, 1987).

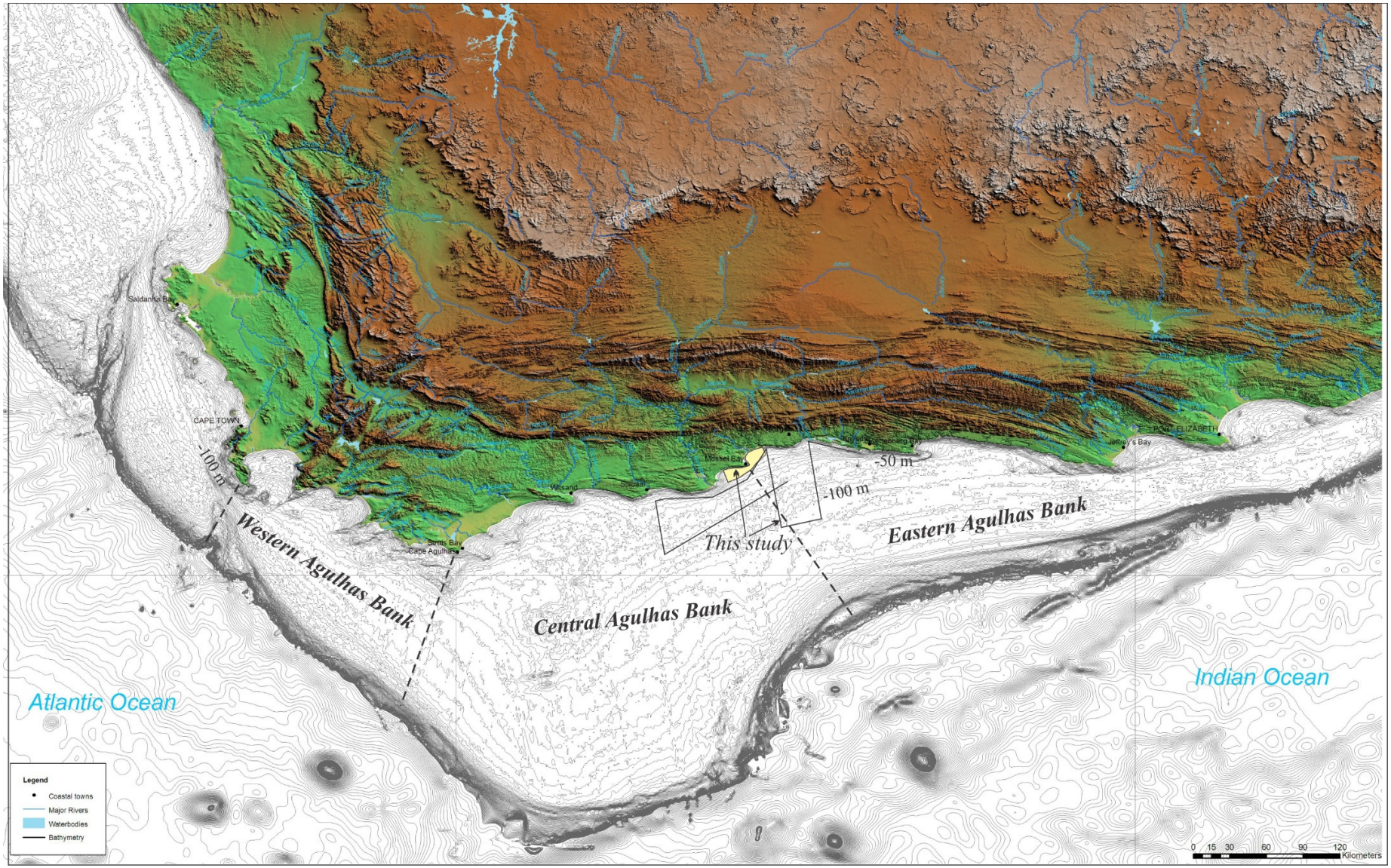

Figure 2-1. Physiographic setting of the South Coast, from de Wet (2013). Divisions of the Agulhas Bank zones are derived from Dingle and Siesser (1975).

2.1.2 Models for the uplifted land surface

While the mechanism of uplift will not be considered for the purposes of this study, the uplift of the South African plateau and development of associated scarps and planation surfaces, pediments and incised valleys has been debated since the initial work of du Toit (1937, 1954) and King (1951, 1962). In addition to the timing of the events, the role of deformation versus climate in the shaping of elevated intercontinental plateaus generally remains unresolved. With the improvement and availability of methods and techniques to study ancient landscapes, numerous models have been proposed for the timing of uplift of the Southern African plateau, suggesting that the exhumation occurred either during the early Cretaceous associated with Gondwana rifting (Hendey, 1983; Gilchrist and Summerfield, 1991; Pysklwec and Mitrovica, 1999; van der Beek et al., 2002; Doucouré and de Wit, 2003), during the late Cretaceous (Nyblade and Sleep, 2003; de Wit, 2007; Tinker et al., 2008 a ,b), during the Oligocene (Burke, 1996) or during the Pliocene (Partridge and Maud, 1987, 2000; van Zyl, 1997; Maud, 2012). These schools of thought can broadly be classified into two categories, namely (1) an argument for slow to no uplift associated with continuous erosion and (2) a theory suggesting episodic pulses of rapid uplift.

Links between the onshore record and offshore domain have recently been drawn to examine the system holistically (Tinker et al., 2008a, b; Guillocheau et al., 2013), and have shown that the timing of increased offshore sediment accumulation closely matches the timing of increased onshore denudation, so the largest volume of sediment was transported from source to sink during the early Cretaceous (136 – 120 Ma) and the late Cretaceous (93 – 67 Ma). The South African plateau with its distinctive associated planation surfaces is most recently considered to be a relatively old structure (Late Cretaceous: 75 – 65 Ma) with little erosion since the Middle Miocene (15 Ma). Stratigraphic evidence from sedimentary basins (Brown et al., 1995; Broad et al., 2006) suggests that the initial late Cretaceous uplift of the plateau likely occurred as a result of east (95 – 90 Ma), and then west (75 – 65 Ma) movement of Africa over a mantle plume. Tinker et al. (2008b) suggest that this increased landscape denudation during the mid-late Cretaceous in accordance with models of accelerated periods of Mesozoic denudation. The relief has subsequently been reshaped twice since the late Cretaceous with minor uplift phases occurring during (1) the Palaeocene to the Early Eocene (65 – 60 Ma) in the southwestern part of Southern Africa, and (2) the late Eocene to Oligocene (40 – 35 Ma) in the southeastern region (Guillocheau et al., 2013).

The correlation between Cenozoic basin-scale erosion rates and mean basin slope in the Southern Cape area (Portenga and Bierman, 2011) is consistent with a steady base level and suggests no further evidence for differential uplift. Evidence for slow and relatively uniform rates of erosion in the Cenozoic are therefore generally favoured (Fleming et al., 1999; Bierman and Caffee, 2001; Brown et al., 2002; Tinker et al., 2008a;

Kounov et al., 2007). These slow erosion and uplift rates are derived from dating surfaces using cosmogenic nuclides and analysis of denudation from fission track data. These studies suggest that the South Coast and associated hinterland form part of a geomorphologically stable area. Erosion rates and isostatic uplift are considered to be very low when compared to similar global settings (Portenga and Bierman, 2011; Scharf et al., 2013). Interestingly, erosion rates on the continental shelf have been high since the Cretaceous and onshore denudation estimations outweigh the preserved sediments reserved in the Outeniqua Basin (Tinker et al., 2008b). The loss of sediment has been attributed to dissolution during chemical weathering (Tinker et al., 2008a), or removal of sediment by the Agulhas Current since the onset of open ocean circulation since the early Cenozoic (Uenzelmann-Neben et al., 2007). Although the South Coast is suggested to be associated with relative stability in landscape evolution, Wigley and Compton (2006) argued for evidence for Pliocene uplift on the West Coast. Erlanger et al. (2012) presented tectonic uplift rates for the eastern margin of South Africa that are incompatible with the idea of rapid Pliocene uplift proposed by Partridge and Maud (1987).

2.2 Regional geology

The geological history of the South Coast spans the last 700 Myr from the Neoproterozoic sequences to Recent unconsolidated beach and dune sediments flanking the modern shoreline (Figure 2-2, Figure 2-3). The oldest South Coast 'basement' rocks comprise the Malmesbury, Kaaimans, Kango Groups and the Cape Granite Suite (~650 – 510 Ma), related to Pan African orogenesis during the formation of Gondwana (Rozendaal et al., 1999; Johnson et al., 2006; Milani and de Wit, 2008). Overlying deposits of the Cape Supergroup form a 6 – 10 km thick siliciclastic sequence, divided into the Table Mountain, Bokkeveld and Witteberg Groups (Thamm and Johnson, 2006). The lower Table Mountain Group sandstones were deposited along a regionally subsiding shelf from ~500 Ma and are overlain by middle Table Mountain Group glaciogenic deposits (Rust and Theron, 1964). Increased downwarping facilitated the deposition of the Devonian Bokkeveld Group shales during a marine transgression and the overlying Witteberg Group sandstones and mudstones represent the last phase of shelf sedimentation prior to the onset of the ~300 – 350 Ma Dwyka glaciation and the Cape Orogeny (~278 – 230 Ma; Newton et al., 2006). The CFB formed by crustal shortening associated with subduction and accretion of the palaeo-Pacific plate below the Gondwana plate (de Wit and Ransome, 1992; Milani and de Wit, 2008). Deposits of the Karoo Supergroup were laid down in a foreland basin adjacent to this orogeny and Karoo sedimentation was terminated by the extrusion and intrusion of the extensive Drakensberg basalts and dolerites, respectively (~183 Ma, Duncan et al., 1997). The fragmentation of Gondwana in the South Coast region and the opening of the South Atlantic commenced in the Early Cretaceous (~136 Ma) as South America was sheared westward along the Falkland Agulhas Fracture Zone (AFFZ) (Martin and Hartnady, 1986; Eagles, 2007). This rifting was accompanied by extensive mafic igneous activity along the entire west coast of Southern Africa, from the Walvis Ridge in the north, to the Cape Peninsula in the south (Day, 1986; Trumbull et al., 2007). Compressional CFB

faults were subsequently reactivated as listric extensional faults (Paton et al., 2006; Stankiewicz et al., 2007), and the newly created accommodation space in basins was filled with clastic sediments of the Uitenhage Group (~145 – 130 Ma). Offshore, arcuate normal faults bounded several graben and half graben structures that became the depocentres for terrigenous sediment sourced from the onshore areas (Brown et al., 1995; Broad et al., 2006; Tinker et al., 2008a, b).

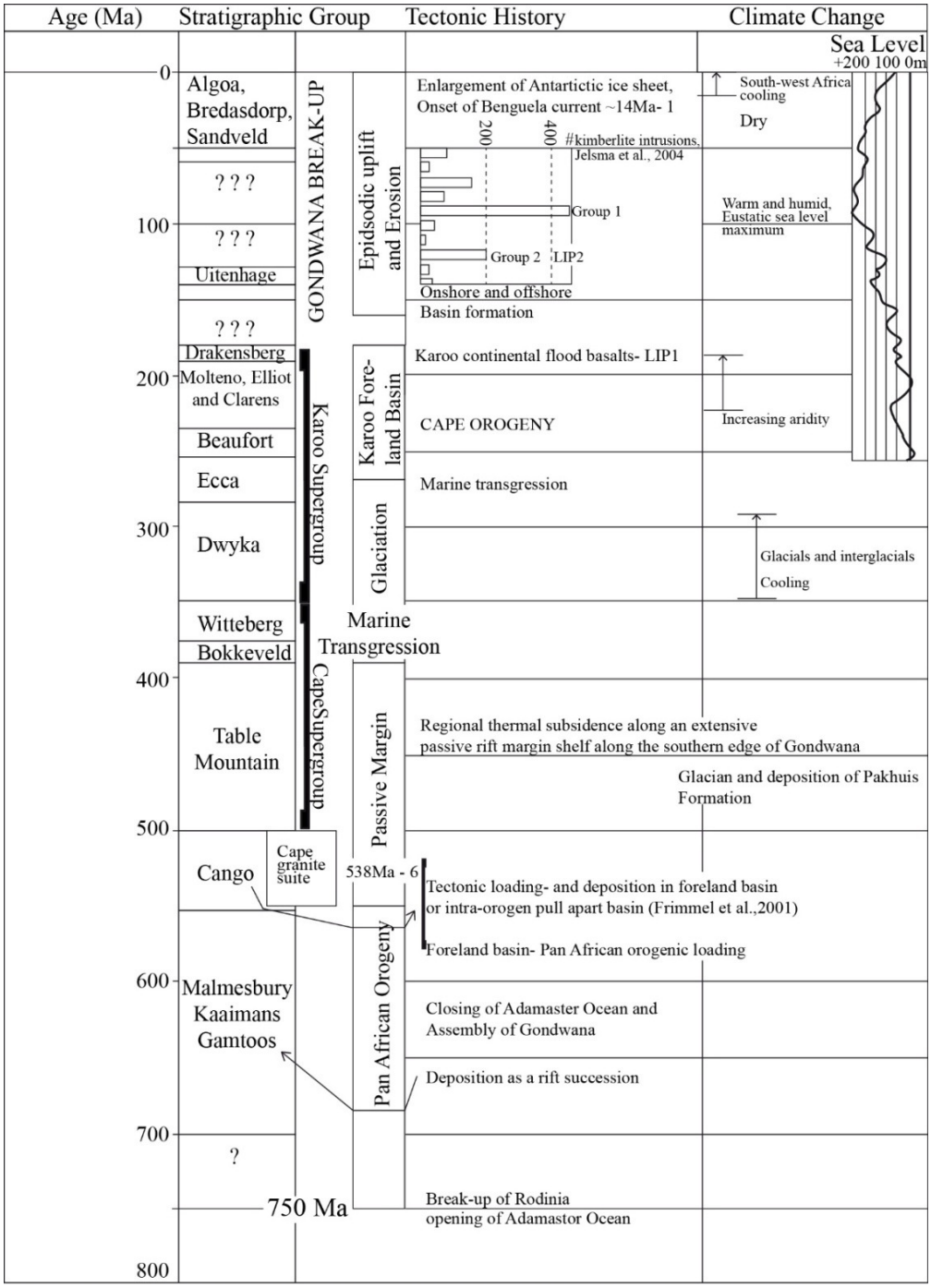

Figure 2-2. Stratigraphic column summarising the regional geology of the South Coast described above. Modified from Tinker et al. (2008a).

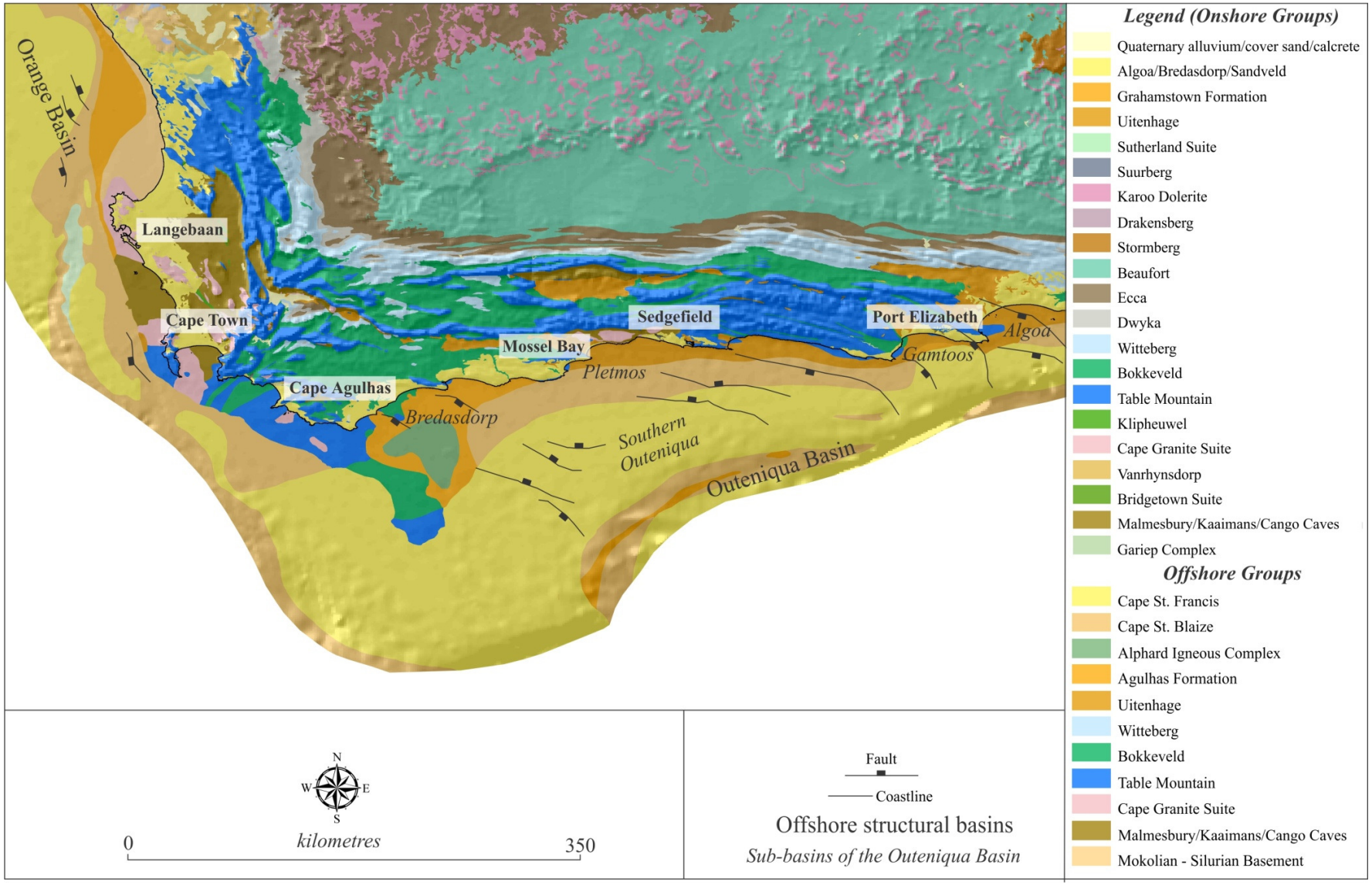

Figure 2-3. Geology of the southern part of South Africa, from the CFB, extending to the edge of the continental margin. Onshore data obtained from the Council for Geoscience 1:250 000 database, simplified to Group level. Offshore data derived from Dingle et al. (1983) and Gentle (1987).

2.3 Local geology

2.3.1 Stratigraphy of Mossel Bay and the adjacent continental shelf

The basement geology outcrop of Mossel Bay, generally dominated by the pre-Mesozoic Cape Supergroup, is typically confined to a narrow coastal strip approximately 2 km wide (Figure 2-4; Gentle, 1987; Viljoen and Malan, 1993). Anticlinoria comprised of Table Mountain Group quartz arenites form a series of east-trending headlands, such as at Cape St. Blaize and Vlees Bay, where erosion of the less resistant Bokkeveld Group shales in the synclinoria, or softer Mesozoic sequences, has led to formation of sweeping embayments (Rogers, 1971). To the west, the George and Woodville plutons of the Cape Granite Suite (Scheepers and Schoch, 2006) and adjacent Kaaimans Group metasediments (Gresse et al., 2006) are exposed along the coastline as an inlier in an unroofed mega-anticlinorium of Cape Supergroup rocks (Gresse et al., 2006).

The study area is divided into two embayments by a hard rock promontory extending from Dana Bay in the west to Cape St. Blaize in the east (Figure 2-4). The coastal caves extending westwards along the headland from Cape St. Blaize have been incised into the southern, south facing, limb of a large northward-directed asymmetrical anticline, with a fold axis trending WSW-ENE. The lithologies outcropping in this region were deposited between the Silurian and Neogene periods. All pre-Cretaceous strata were subjected to severe north-south oriented compressive stresses producing the CFB, with more resistant strata forming the prominent geomorphological terrain trending east-west. Overturning is common and reverse and thrust faults are present in places (Toerien, 1979). Also present are normal faults, largely Cretaceous in age, with down-throws to the south and associated with the extensional break-up of Gondwana. Caves incised into the Mossel Bay hard rock promontory at Pinnacle Point contain anthropogenic sediments, ancient dune and beach deposits and cave carbonate layers consisting of pure speleothem and impure tufa (Bar-Matthews et al., 2010; Pickering et al., 2013).

The South Coast continental shelf-slope break shoals from a depth of 200 m below Mean Sea Level (BMSL) offshore of Cape Agulhas to 140 m BMSL off Port Elizabeth (Figure 2-4; Martin and Flemming, 1986). The southern margin of South Africa was shaped by the middle Jurassic to early Cretaceous rift and subsequent drift phases that accompanied the fragmentation of the supercontinent Gondwana (Brown et al., 1995). The Pletmos Basin (Figure 2-3) lies on the continental shelf between Mossel Bay and Cape St. Francis and is one of five sub-basins of the larger Outeniqua Basin (Broad et al., 2012). The Pletmos Basin is bound to the west and east by basement highs of the Infanta and St. Francis Arches respectively and the northern boundary is defined by an approximately coast-parallel fault. The Pletmos Basin covers ~18 000 km^2 (Broad et al., 2006) and is the offshore extension of smaller onshore basins filled with coarse continental clastic deposits extending from Worcester past Robertson, Swellendam, Heidelberg and Mossel Bay (Viljoen and Malan, 1993; Visser, 1998).

The Pletmos Basin is composed of a series of fault bounded (Plettenberg, Superior, Pletmos Faults) graben-hosted sequences and extends seaward to a water depth of 200 m BMSL (Brown et al., 1995; Broad et al., 2006). The arcuate trend of the basin-bounding fault systems in this region is most likely related to the structural grain of the underlying orogenic CFB (De Swardt and McLachlan, 1982). The onshore Mesozoic basins near Mossel Bay host deposits of the Uitenhage Group, preserved in two fining-upward successions grading from conglomerates and sandstones into mudstone and tuff through the Robberg, Enon and Kirkwood Formations respectively, and are overlain by conglomerates of the Buffelskloof Formation and Hartenbos Formation sandstones and mudstones (Viljoen and Malan, 1993, Malan and Viljoen, 2008).

The unconsolidated sediments of the Agulhas Bank are underlain by Cretaceous, Palaeogene and Neogene strata that are interpreted to have infilled the Outeniqua sedimentary basin (Figure 2-3; Martin and Flemming, 1986). These sedimentary units dip seaward such that the early Cretaceous units outcrop on the inner shelf, with Cenozoic sediments outcropping on the outer shelf (Martin, 1985). Cretaceous deposits on the inner shelf are extensively folded and faulted (Dingle et al., 1983). The Cretaceous/Palaeogene boundary is suggested to be easily identifiable on shallow seismic profiles in the Mossel Bay area (Martin, 1985). The bulk of the basal Cenozoic deposits of the Agulhas Bank seems to be Mio-Pliocene sediments composed of moderately to loosely consolidated limestones and cemented phosphates, deposited after the major Oligocene regression (Dingle et al., 1983).

The Cenozoic deposits of the onshore region constitute the Bredasdorp Group (Malan, 1990), and include the basal early Pliocene marine calcarenites of the De Hoopvlei Formation, calcified aeolianites of the late Pliocene Wankoe Formation, middle Pleistocene beach deposits of the Klein Brak Formation, aeolianites of the Upper Pleistocene Waenhuiskrans Formation and unconsolidated sediments - of the Holocene Strandveld Formation (Maud and Botha, 2000; Roberts et al., 2006).

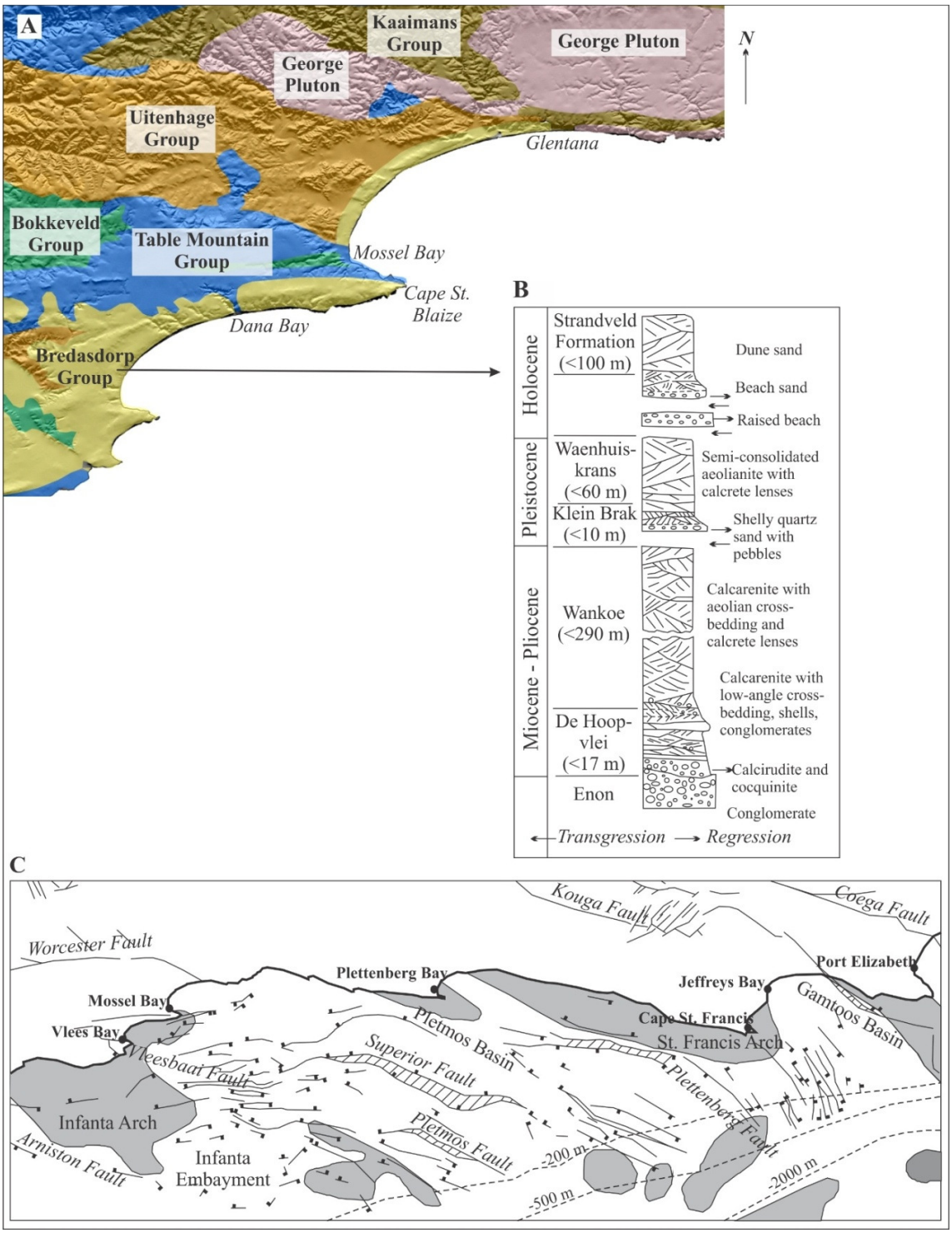

Figure 2-4. A. Digital Elevation Model with draped 1:250 000 scale geology showing the distribution and morphology of stratigraphic units in the vicinity of Mossel Bay. B. Generalised composite stratigraphic column of the Cenozoic Bredasdorp Group (modified from Roberts et al., 2006). C. Onshore-offshore structural features of Mossel Bay, compiled with datasets from du Toit (1976), Broad et al. (2006) and information provided by C.H. de Beer (Council for Geoscience). The shaded areas represent basement highs.

2.3.2 The Wilderness Embayment

The Wilderness Embayment (Figure 1-2; Figure 2-5) is a prominent physiographic feature within the coastal plain of the Southern Cape, South Africa. It, along with Nature's Valley to the east, are unusual embayments compared to the general trend observed on the South Coast, in that the cliff lines are eroded into less resistant strata rather than Mesozoic half-grabens. Within the embayment are a series of large, approximately shore-parallel ridges, which are also referred to as cordon dunes (*sensu* Illenberger, 1996) or coastal barriers. These aeolian deposits comprise unconsolidated sand to heavily lithified aeolianite and they are separated by several back-barrier lakes. Four shore-parallel barriers were originally identified by Martin (1962), termed (from landward to seaward) I, II, III and IV. Illenberger (1996) condensed these to three units by combining the most seaward barriers (III and IV) and referring to them as the seaward, middle and landward barriers (Figure 2-5). While lithification of the aeolian sediments has rendered them relatively resistant to erosion, the barriers have been breached in places by rivers (e.g. the middle barrier by the Swartvlei River). The seaward and middle barriers are the most prominent features. The landward barrier often lacks clear geomorphic expression and its distribution is seemingly constrained by hardrock geology in some locations. The modern seaward barrier is being eroded by the sea forming sea cliffs in excess of 180 m. The current chronological framework suggests that the Wilderness barriers have been constructed over at least two glacial-interglacial cycles and possibly as far back as MIS 11 (Illenberger, 1996; Bateman et al., 2011). Notable phases of construction have been constrained to between 241 - 221 ka, 159 - 143 ka, 130 - 120 ka, 92 - 87 ka and post 6 ka based on luminescence ages. These appear to be associated with regressive phases subsequent to sea-level highstands (Bateman et al., 2011).

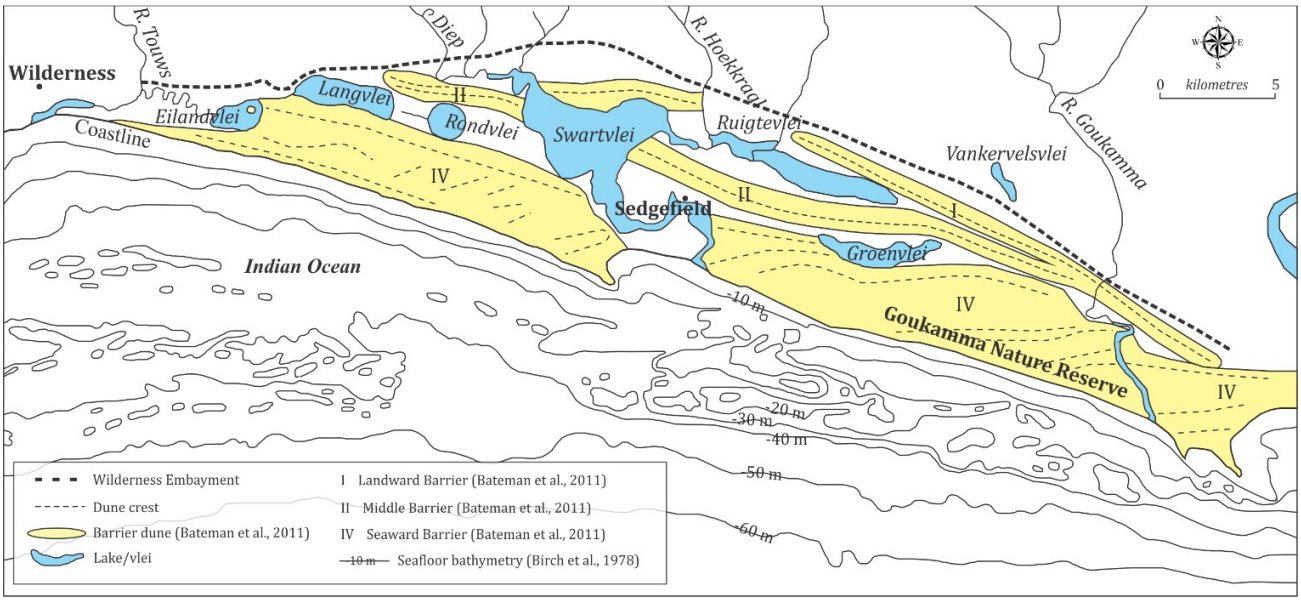

Figure 2-5. Features of the Wilderness Embayment, characterised by Quaternary palaeodune ridges and coastal barrier lakes. Numerous rivers drain the area. These are displayed with the prefix '*R.*'

2.4 Holocene sedimentation

Unconsolidated Holocene sediments along the coast form deposits of Recent sand accreted as beaches and dunes, along a narrow coastal belt (Roberts et al., 2006) and are more significantly developed in geomorphic coastal embayments. The origins and age of onshore South Coast sediment accumulations, episodes of dune building, the accumulation of sand sheets and their association with sea-level fluctuations during the Quaternary have been investigated in some detail during the last decade (Illenberger, 1996; Bateman et al., 2004; Marker and Holmes, 2005; Carr et al., 2007; Holmes et al., 2007; Bateman et al., 2008; Roberts et al., 2008; Carr et al., 2010; Marker and Holmes, 2010; Bateman et al., 2011).

A relatively thin veneer of modern unconsolidated sediment reflects the most recent sedimentation on the continental shelf (Martin and Flemming, 1986). Their 'Holocene sediment wedge' extends approximately 1500 km along the South African shelf from the East to the South Coast. Flemming (1981) sub-divided the offshore Holocene succession into two components: initially a basal biogenic conglomerate, which formed during the Holocene transgression (the outer shelf relict carbonate facies) and superimposed onto this sand-depleted gravel pavement, is an inner shelf modern terrigenous facies forming the inshore sediment wedge. As sediments tend to shift onshore during summer, they fill coves and build beaches, and when they shift seawards during the winter months, they expose the gravel pavements and basement outcrops (Flemming, 1978). This general model is supported on the South Coast by the earlier work of Rogers (1971), which showed the outer shelf to be dominated by sediments composed of relict shell fragments that vary in texture from muddy sands to gravelly sands, and the sediments of the inner and middle shelf to a maximum water depth of 120 m BMSL that are characterised chiefly by quartz in the coarse fraction (Figure 2-6).

The South Coast receives fluvial sediment from several rivers. Thus, the delivery of sediment to the coast, and ultimately the Holocene sediment wedge, is strongly influenced by the catchment size and geological substrate within the river catchments. The Gouritz and Breede rivers are the main sediment source for the continental shelf between Cape Agulhas and Cape Seal (Birch, 1980). It is argued that a significant portion of the bedload of fluvial systems are lost through aeolian processes as coarse sediments are trapped in the littoral zone by wave action, resulting in the subsequent formation of the extensive coastal dune fields. Nearly half of total bedload sediments offshore of the South Coast are located between Wilderness and Plettenberg Bay (Birch, 1980), trapped in the Wilderness Embayment and a submerged spit off Cape Seal/Plettenberg Bay (De Decker, 1983). The spit defines the termination of an eastwards-trending longshore drift system from Cape Agulhas (Birch, 1980; Martin and Flemming, 1986).

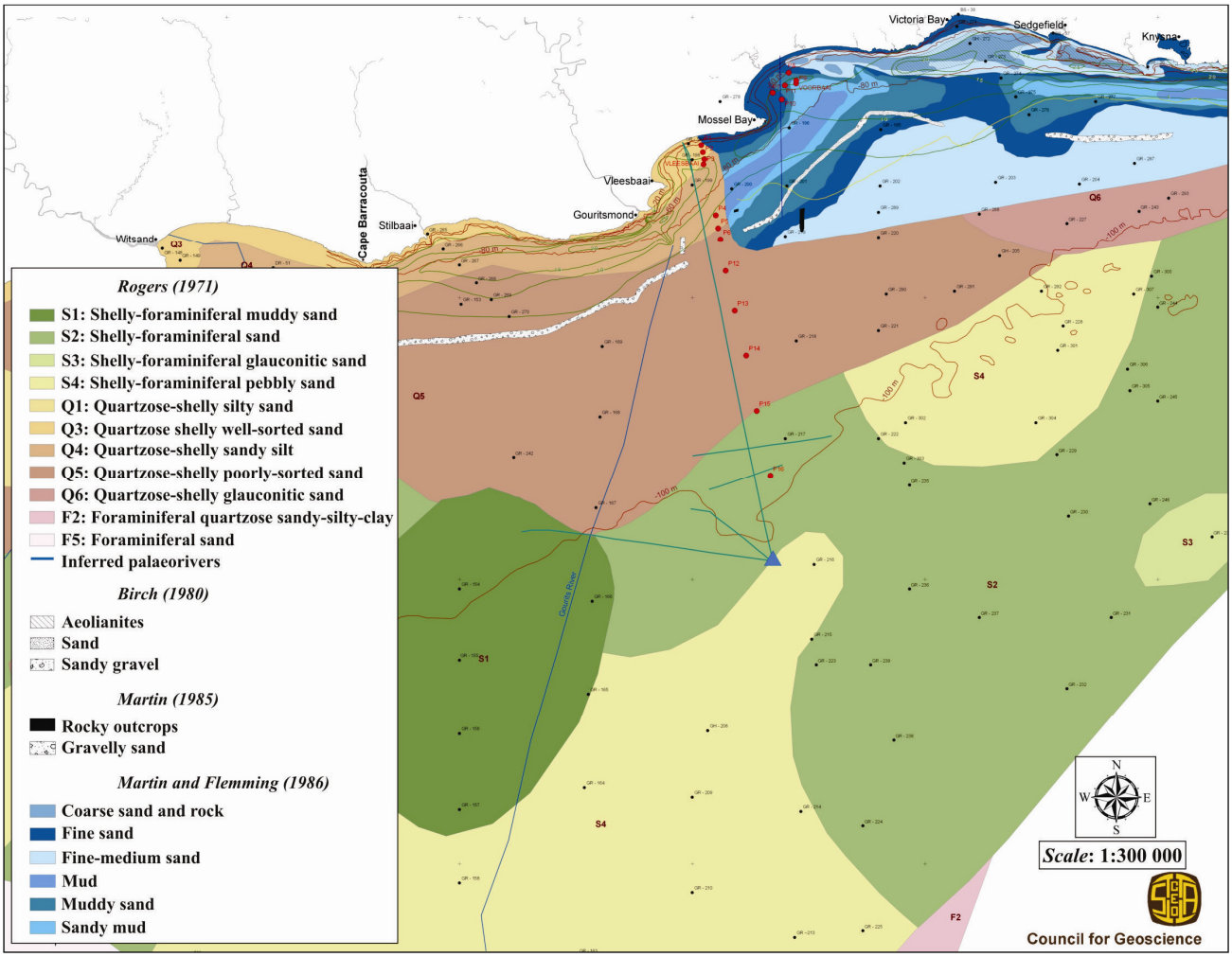

Figure 2-6. Sediment compartments of the South Coast (after Rogers, 1971; Birch, 1980; Martin, 1985; Martin and Flemming, 1986).

2.5 Climate, vegetation and hydrodynamic environment

The trajectory of the southwestward-flowing geostrophic Agulhas Current closely follows the continental shelf break (Lutjeharms, 1981, 2006) (Figure 2-7) and hence migrates away from the coastline south of Port Elizabeth where the shelf broadens (Martin and Flemming, 1986). Localised eddies and waves caused from shear edge effects, such as deflection of the Agulhas Current around the Alphard Rise, result in inshore currents on the Agulhas Bank (Rogers, 1971; Martin and Flemming, 1986). This system is characterised by the eastward-flowing Agulhas counter current, with a reported surface velocity of ~50 cm/sec (Rogers, 1971). The coastal currents have a strong westerly dominance in summer (Rogers, 1971; Birch, 1980). The western sector of the South Coast is also influenced by the convergence with waters of the cold Benguela upwelling system, leading to greater complexity to oceanographic systems in this region. Quaternary perturbations vary in relative strength of these systems influenced climatic patterns related to sea surface temperature and upwelling (Walker, 1990;

Cohen and Tyson, 1995). The confluence of warm and cold waters has contributed to a rich coastal and marine ecosystem, characterised by high density and diversity of marine and shellfish species along both rocky and sandy intertidal zones on the South Coast (Branch and Branch, 1992; Branch and Menge, 2001).

Coastal cut-off low-pressure systems associated with heavy rains in the spring and autumn months, occasionally cause flooding along the South Coast (Taljaard, 1996). In summer, moist air advected onto the coastal region by the Indian Ocean Anticyclone is generally the source of rainfall (Roberts et al., 2013). Winter rains are derived from the passage of cyclonic polar frontal systems linked to westerly winds which is the prevailing wind direction in Mossel Bay. The coast is, therefore, sensitive to orbitally driven meridional shifts in climate belts (Tyson 1999). The distribution of vegetation biomes in South Africa largely mirrors bedrock geology, although early burning, followed by agriculture, has commonly obscured the distribution of the original flora (Mucina et al., 2006; Compton, 2011). The poorly developed, nutrient-poor quartzose soils of the CFB are dominated by the fine and waxy leafed vegetation of the sandstone Fynbos ecoregion ("Lowland Fynbos"). The shale Renosterveld biome occurs where Bokkeveld Group shale sediments dominate landward of the coastal plain. Seaward of the shale Renosterveld vegetation, the coastal plain is dominated by a mixture of limestone Fynbos and strandveld biomes which grow on the sediments of the Bredasdorp Group limestones. Former strandlines extend up to tens of kilometres inland along the South Coast, and are associated with corresponding palaeo-dunefields (Roberts et al. 2006). The Holocene, largely unvegetated, Alexandria dunefield situated in Port Elizabeth (Figure 1-2) is the largest along the South African coast (Roberts et al., 2013). It extends for about 64 km parallel to the coast and penetrates up to 2.6 km inland. Prevailing wind regimes along the South African coast are dominantly bimodal: W/E on the South Coast, compared to S/NW on the west coast, and SW/NE on the east coast (Carr and Botha, 2012)

The South Coast is a wave-dominated coastline with a micro- to meso-tidal range, with spring tides exhibiting a vertical range of less than 2 m, or 2 – 4 m, respectively (Davies, 1980). The spring tidal range for much of the coastline lies between 1.8 and 2.0 m with neap tidal ranges between 0.6 and 0.8 m (Cooper, 2001). The prevailing wave direction on the Southern African coastline is from the southwest (Davies, 1980; Heydorn and Tinley, 1980), resulting in a net eastward littoral drift and the associated long fetch means that the coastline is dominated by swell waves. The South Coast generally experiences the high open water wave heights (Cooper, 2001), with median wave heights near to Knysna ~2.5 m (Whitfield et al., 1983).

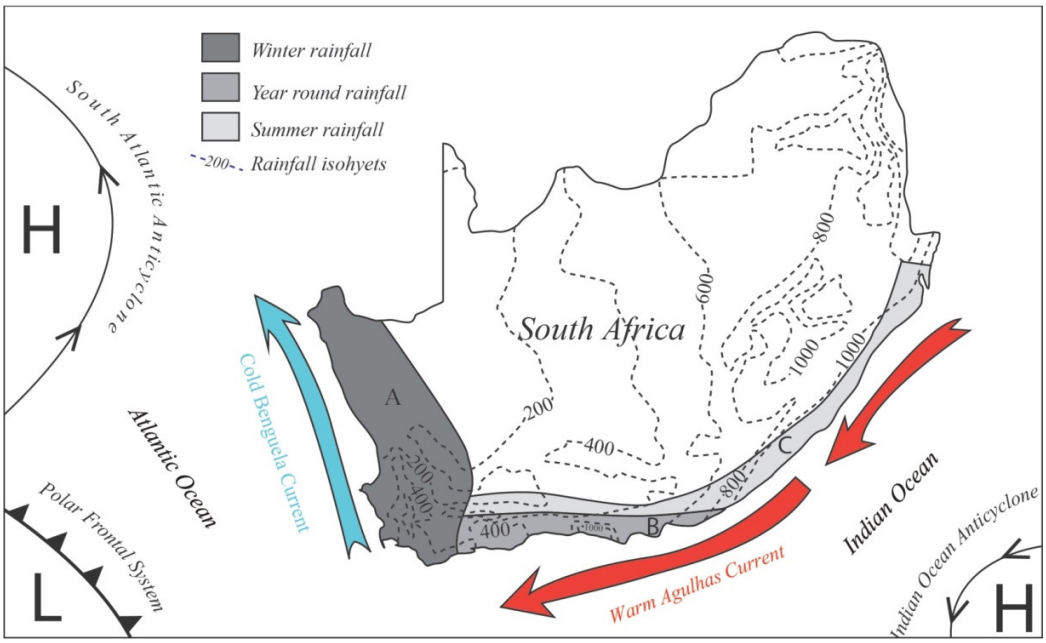

Figure 2-7. Oceanographic circulation dominated by the path of the Agulhas Current and notable climatic information for the South Coast. Modified from Roberts et al. (2013).

2.6 The South Coast archaeological record and palaeoclimate models

The archaeological and fossil record indicates that anatomically modern *Homo sapiens* appeared near 195 – 160 ka in Africa (White et al. 2003; McDougall et al. 2005; Smith et al. 2007) and evolutionary genetics suggest that the origin point for the modern human lineage lies between 200 and 100 ka (Ingman et al. 2000; Tishkoff et al. 2007; Gonder et al. 2007; Fagundes et al. 2007; Behar et al. 2008). Modern humans have very low genetic diversity relative to other animals that is best explained by one or more population bottlenecks late in the evolution of the lineage. One such bottleneck may have occurred during MIS 6, a long and cold glacial period (Fagundes et al., 2007; Gonder et al., 2007). The South African archaeological record remains the most well-known and documented of the Middle Stone Age records in Africa (Marean and Assefa, 2005) and additionally provides the world's earliest and richest record for the origins and evolution of the coastal adaptation (Marean et al., 2007) and cultural complexity. Many of these sites are situated along the coastline (e.g. Die Kelders Cave 1, Blombos, Pinnacle Point 13B, Nelson Bay Cave, and Klasies River; Figure 1-2) that contain sedimentary and archaeological sequences spanning the late Middle Pleistocene into the Holocene. Evidence for symbolic behaviour commencing at ~100 ka has been documented in the form of engraved ochre from Blombos (Henshilwood et al., 2002) and Klein Kliphuis (Mackay and Welz, 2008), engraved ostrich eggshell from Diepkloof (Texier et al., 2010), shell beads from Blombos (Henshilwood et al. 2004), and ochre mixing palettes from Blombos (Henshilwood et al., 2011). Until recently, the Middle Stone Age record was restricted to sites that postdate the MIS 5e sea-level highstand (~123 ka) but at Cave PP 13B, the elusive MIS 6 *Homo sapiens*

population has been intercepted because the cave lies 15 metres AMSL, and at around 167 ka the coast transgressed sufficiently to make the cave attractive to coastal foragers (Marean et al. 2007; Fisher et al., 2010). The Pinnacle Point record has thus provided evidence for symbolic behaviour at significantly earlier times compared to the other South Coast sites (Marean 2010, 2011). Collection of sea-shells has been established at ~110 ka (Jerardino and Marean, 2010), and worked ochre has been documented at ~162 ka (Marean et al., 2007). Evidence for complex cognition has been documented in the form of an understanding of lunar phases for maximum return associated with shellfish harvesting by ~110 ka and perhaps as early as 162 ka (Marean et al., 2007). Brown et al. (2009) showed the earliest evidence of stone tool heat treatment (~162 ka), a complex chain technology. Brown et al. (2012) also presented the origins of microlithic technology at ~71 ka, previously rarely found before 40 ka.

The last million years have been characterised by two major patterns of global climate change: an increase in the amplitude of temperature change between glacial and interglacial phases and the periodicity of glacial-interglacial cycles. Northern Hemisphere temperature changes were in the order of 8–16°C (North Greenland Ice Core Project Members, 2004) while the Antarctic ice core record suggests less extreme temperature changes for the Southern Hemisphere (1 – 3°C; EPICA Community Members, 2006). For the majority of the middle to late Pleistocene, the world's climate was highly variable and much of the human occupation of the South Coast preserved at the cave sites at Pinnacle Point occurred when the world was in a glacial phase.

The global palaeoclimate record shows that MIS 6 was for the most part cold (EPICA community members 2004) and that overall Africa was considerably drier than at present (Dupont et al. 2000), which is consistent with conditions during the more recent LGM. The MIS 6 PP 13B record shows predominantly grassland faunas alongside the more typical Cape Floral Region faunal elements and this is most likely associated with the exposed Agulhas Bank and adjacent shelf (Marean, 2011). The combination of grazing ungulates, predictable coastal foods associated with relative stability of oceanographic elements and carbohydrates from geophytes has been hypothesised by Marean (2010) to provide the ideal resource base to support human populations on the South Coast. Assuming people focused on the coastal zone (Marean, 2010), evidence of their occupation is now under water. At PP 13B the site was occupied intermittently from ~160 to 90 ka when close to the coast. When the coastline was near, occupation intensities were high and people lived at the cave, yet when sea level retreated the site was generally abandoned (Marean et al., 2007). Through much of MIS 6 the coastline was distant from the South Coast sites, excluding 167 - 160 ka ago, when a short warm phase brought sea-level to within 10 km of the present PP 13B (van Andel, 1989; Fisher et al., 2010).

The boundary between the winter and summer rainfall in Southern Africa is known to have shifted in response to glacials, yet the dominant trends remain debated. Van Zinderen Bakker (1976) predicted that during glacial phases the winter rainfall zone would be displaced north of the CFB, extending into Namibia on the coast and

protruding inward over the Great Karoo. Summer rains would thus dominate the South Coast and expand onto the west coast. The models of Heine (1982) and Cockcroft et al. (1987) proposed an expansion of the amount of winter rain eastward and northward, differing in amount and magnitude during the LGM, but remaining stable on the west coast. However, the model of Chase and Meadows (2007) favours glacial winter rainfall expansion models. An isotope curve generated from speleothem at Pinnacle Point dating from 90 - 53 ka shows significant changes in $\delta^{18}O$ and $\delta^{13}C$ both at long and short time scales (Bar-Matthews et al. 2010) suggesting an increase in summer rain and C4 grasses during the glacial of MIS 4. There is therefore some evidence to suggest that summer rains from the east may have expanded onto the South Coast during glacials, which is associated with greater changes in flora and fauna than on the West Coast, likely representing a reflection of the shifting winter/bimodal rainfall boundary (Bar-Matthews et al., 2010). Micromammals from Pinnacle Point dating from MIS 6 through MIS 5 showed subtle variations, but reflect no indication of significant changes in precipitation (Matthews et al., 2011). Cave speleothems grew continuously (Bar-Matthews et al., 2010). Pulses of dune deposition along the South Coast seem to be driven more by sea-level changes than by aridity (Bateman et al. 2011). The Holocene is characterised by a comparatively stable climate at the global scale relative to the Pleistocene and the loss of the widespread Agulhas plain with marine flooding and the adjustment of the shoreline to its present elevation.

2.7 Quaternary sea-level fluctuations

Marine isotope ratio ($\delta^{18}O$) records (Lisiecki and Raymo, 2005) indicate that major Northern Hemisphere glaciations started to occur from about 2.7 Ma ago as a result of late Pliocene climate cooling (Raymo, 1994; Lear et al., 2000; Lawrence et al., 2006). Earth's climate underwent a significant change between 1.25 and 0.7 Ma, at the Mid-Pleistocene Transition (MPT) (Clark and Pollard., 1998; Clark et al., 2006; Huybers, 2007), when the prevailing periodicity of climate cycles changed from 41 kyr to 100 kyr. Elderfield et al. (2012) suggested that the MPT was initiated by an abrupt increase in Antarctic ice volume at 0.9 Ma. The growth and decay of Northern Hemisphere ice sheets over the past million years is dominated by an approximately 100 kyr year periodicity and a 'sawtooth' pattern (characterised by slow growth and a rapid termination) (Hays et al., 1976; Clark et al., 2009). Milankovitch theory proposed that summer insolation at high Northern Hemisphere latitudes drives the glacial cycles, and statistical tests have demonstrated that the glacial cycles are indeed linked to eccentricity, obliquity and precession cycles (Lisiecki, 2010). It is argued by Abe-Ouchi et al. (2013) that insolation alone cannot explain the strong 100 kyr cycle, suggesting internal climatic feedbacks. Previous models showed that glacial terminations are associated with the build-up of Northern Hemisphere ice sheets (e.g. Bintanja and van de Wal, 2008), but the dominant mechanism behind the 100 kyr cycle has most recently been argued to relate to lithosphere–asthenosphere processes associated with continental rebound at the North American ice sheet (Abe-Ouchi et al., 2013). According to this model, the larger the ice sheet becomes and as it

extends southward into lower latitudes, the smaller is the insolation required to make the mass balance negative. Once a large ice sheet exists, a moderate increase in insolation is enough to initiate a negative mass balance, leading to an almost complete retreat of the ice sheet within several thousand years. The geometry of North America and the long response time of isostatic adjustment are, therefore, considered the predominant agents that control the 19, 23 and 41 kyr orbital variations within the 100 kyr responses (Marshall, 2013). The origin of the periodic sea level changes of the Quaternary have thus been shaped by altering the configuration of oceans and ocean currents and palaeo pCO_2, coupled with orbital variations and isostatic rebound. Benthic isotope data indicate that these changes lowered global sea level by an average of 125 – 130 m during the glacial periods (e.g. Waelbroeck et al., 2002). Southern Africa has been considered one of the reliable regions to study palaeo sea-level proxies as it is situated beyond the area influenced by glacio-isostatic effects, typically located adjacent to ice sheets (Fleming et al., 1998; Woodroffe and Horton, 2005). In the case of the Holocene maximum sea level, the greatest offset between the Southern African sea-level record (Compton, 2001; 2006) occurs between 6.5 and 5.5 ka, and by 3 ka the curves overlap. The recorded sea-level record for Southern Africa is, therefore, generally considered similar to that predicted for continental margins by glacio-hydro-eustatic models (Fleming et al., 1998; Peltier, 1998). Relative tectonic stability also, however, suggests that onshore records will likely be biased toward preservation of the highest highstand deposits as a result of extensive reworking in the marginal marine environment during transgressions. The preservation of lower elevation deposits may therefore be incomplete (Murray-Wallace et al., 2001).

This study uses a compilation of the most recently published and most widely accepted Quaternary glacio-eustatic sea-level curves to build interpretations based on the models presented in Figure 2-8A, as opposed to the comparatively fragmentary, albeit reliable, local sea-level models shown in Figure 2-8B which show a similar trend to the global studies. The terminology of Marine Isotope Stages (prefix MIS) is utilised in the definition and timing of Quaternary glacial/interglacial cycles in accordance with the protocol of the International Commission on Stratigraphy. This definition is derived from the benthic stack LR04 of Lisiecki and Raymo (2005) conditions (Table 2-1). Stages with even numbers are indicative of high levels of oxygen-18, representing cold glacial periods; while odd-numbered stages with low oxygen-18 values represent warm interglacial periods.

Table 2-1. Nomenclature and start dates of the Lisiecki and Raymo (2005) Quaternary Marine Isotope Stages referred to in this study.

Stage	Sub-stage	Start date	Comments
MIS 1		14 ka	From the end of the Younger Dryas (start of the Holocene) to the present
MIS 2		29 ka	Near the Last Glacial Maximum (LGM)
MIS 3		57 ka	

MIS 4		71 ka	
MIS 5		130 ka	Includes the Eemian, subdivided into a-e
	MIS 5a	82 ka	
	MIS 5b	87 ka	
	MIS 5c	96 ka	
	MIS 5d	109 ka	
	MIS 5e	123 ka	
MIS 6		191 ka	
MIS 7		243 ka	
MIS 8		300 ka	
MIS 9		337 ka	
MIS 10		374 ka	
MIS 11		424 ka	Considered most comparable to MIS 1
MIS 12		478 ka	
MIS 13		533 ka	
MIS 14		563 ka	
MIS 15		621 ka	

2.7.1 Glacio-eustatic (global) sea-level models

This study mainly draws on the middle to late Quaternary glacio-eustatic sea-level records of Waelbroeck et al., 2002; Bintanja et al., 2005; Clark et al., 2009 and Rohling et al., 2009 (Figure 2-8A). These records were derived from marine $\delta^{18}O$ and from benthic foraminifera data since 3 Ma (Bintanja et al., 2005), 450 ka (Waelbroeck et al., 2002) and 520 ka from the Red Sea (Rohling et al., 2009), as well as from coral records (Clark et al., 2009). The uncertainty within these sea-level records generally shows within their ages (~1 – 10 kyr) and amplitudes (~6 – 15 m; Compton, 2011) and broadly illustrate full interglacials/peak warming with maximum sea-levels, and full glacials/peak cooling with minimum sea-levels, separated by terminations. The sea-level tract between the full glacials and interglacials is interrupted by stadials, or periods of lower temperature during a dominant interglacial, and interstadials, or periods of higher temperature during a dominant glacial which typically last less than 10 kyr. Notable stadials include the Older Dryas (18 – 14.5 ka), the Younger Dryas (12.8 – 11.5 ka) and the Little Ice Age (~400 - 200 years BP). A noteworthy interstadial is the Bølling-Allerød Interstadial, which persisted from 14.7 to 12.7 ka (Cronin, 1999). Ice cores from Greenland have revealed 25 specific records of rapid climate fluctuations referred to as Dansgaard-Oescher events (Dansgaard et al., 1993) from 85 – 11 ka, associated with the retreat of sea level from the peak of the Last Interglacial towards the Last Glacial Maximum (LGM). Although the processes behind the timing and amplitude of Dansgaard-Oescher events remains debated (Schulz, 2002; Stocker and Johnsen, 2003), these take the form of rapid warming episodes followed by a gradual

cooling and their effects have been documented globally (Voelker, 2002). In the North Atlantic marine sediments, Dansgaard-Oescher events are grouped into composite Bond cycles that terminate with ice-rafted detritus horizons called Heinrich events from substantial ice breakouts originating in the Labrador Sea (Bond et al., 1993). Six Bond Cycles are recorded and they are rapid, each lasting approximately 0.75 kyr (Maslin et al., 2001).

Glacial periods terminate relatively rapidly with the melting of Northern Hemisphere ice sheets, followed by an abrupt rise in sea level. Based on relative sea level (RSL) data, the LGM occurred between 26.5 and 19.0 ka (Lambeck and Chappell, 2001; Cutler et al., 2003; Peltier and Fairbanks, 2006) and the peak fall in sea-level was 130 m lower than present sea-level. By 26.5 ka almost all ice sheets had attained their maximum thickness, representing the onset of the LGM (Clark et al., 2009).

To date, the most complete record of the Post-glacial Marine Transition (PMT) is based on reef cores drilled at Barbados, which is characterised by two periods of accelerated sea-level rise: meltwater pulses (MWP) 1A and 1B that occurred at 14 and 11.3 ka, respectively (Bard et al., 1990; Peltier and Fairbanks, 2006). During each MWP event, sea level was said to rise by several meters per century, likely impacting the ocean circulation (e.g Weaver et al., 2003). MWP 1A represents a rapid 10 m rise in sea-level from the LGM lowstand originated in the Northern Hemisphere ice sheets (Clark et al., 2009). The time interval of MWP 1B occurs within a gap of approximately one millennium (12.1 – 11.1 cal yr BP) (Edwards et al., 1993; Cutler et al., 2003), but MWP 1B generally remains contested Bard et al. (2010). Between the Bølling-Allerød Interstadial and the Older Dryas events MWP 1A is expressed in the West Antarctica record between 13.9 and 15.2 ka (Clark et al., 2009) and corresponds to a maximum rise in sea-level at 14.5 ka (Steig et al., 1998; Clark et al., 2009) by up to 20 m in this time (Stanford et al., 2006). These two MWPs represent a massive influx of freshwater into the oceans and induced extensive ocean and climate changes at these times (Weaver et al., 2003; Clark et al., 2004).

2.7.2 Local sea-level models

Late Quaternary sea-level curves for South Africa have been compiled by Ramsay and Cooper (2002), Compton and Wiltshire (2009) and Carr et al. (2010) for the Pleistocene, and Ramsay (1995) and Compton (2001, 2006) for the Holocene (Figure 2-8B). Pleistocene models show that since MIS 11 (~440 ka), four glacial/interglacial cycles are identified from sedimentological and biological proxies. Maximum Quaternary sea levels of +5 m were attained during the Last Interglacial (MIS 5e), at ~125 ka (Ramsay and Cooper, 2002; Compton and Wiltshire, 2009; Carr et al., 2010). Between 90 and 12 ka, sea level dropped beyond the shelf break before rapidly rising from this eustatic low (the LGM). The Holocene Transgression (commencing during MIS 2) extensively eroded the pre-existing shelf and coastal plain sediments until stabilising at its present elevation

between 7 and 6 ka (Ramsay, 1995; Compton, 2001; 2006). According to the East Coast model of Ramsay (1995) sea level then rose by a further 2.75 m for 2.5 ka until culminating in the Holocene highstand of 4.5 ka. The Ramsay (1995) model proposes that sea-level returned to the current elevation at 0.9 ka. In contrast, Compton (2001, 2006) proposed, based on work on the Southern African West Coast that the peak of the Holocene highstand was reached between 7.3 and 5.9 ka and that sea-level re-attained its present elevation at 5.5 ka. Compton argues that sea-level has oscillated near 0 m with notable lowstands at 4.5 ka, 1.8 ka and 0.7 ka during the intervening period to present and that the gradual increase in sea level from 5.5 to 3 ka for Southern Africa is consistent with the 3 – 5 m rise in eustatic sea level between 7 and 6 ka from continued melting of ice sheets. There is good evidence from the South African West- and South coasts (Reddering, 1988; Marker and Miller, 1993; Compton, 2001; Compton, 2006) for a mid-Holocene highstand from ~7.3 - 5.9 ka on the order of ~3 m above present MSL, and a significantly later mid-Holocene highstand documented for the South African east coast suggested by Ramsay (1995).

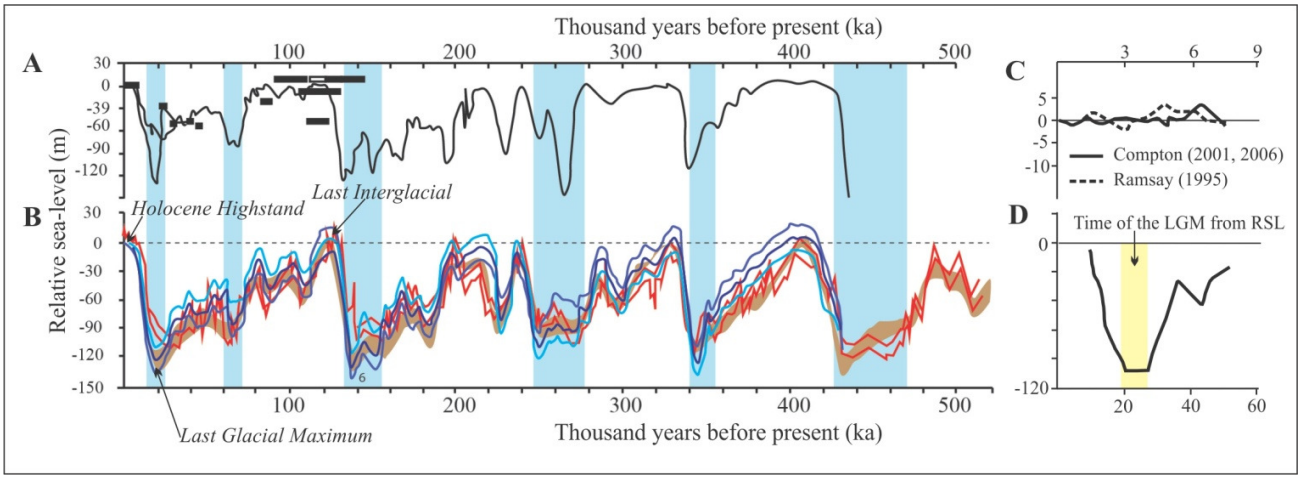

Figure 2-8. A. Sea-level records from Southern Africa (Ramsay and Cooper, 2002; Compton and Wiltshire, 2009; Carr et al., 2010). B. Glacio-eustatic sea-level curves of Waelbroeck et al. (2002) in blue, Bintanja et al. (2005) in brown, Rohling et al. (2009) in red. C. Local Holocene sea-level curves (Ramsay, 1995; Compton, 2001; 2006) D. Late Pleistocene and Holocene sea-level of Clark et al. (2009). A and B are modified from Compton (2011).

3 METHODS

3.1 Marine geophysical surveys

Four separate geophysical surveys were undertaken for this project (Figure 3-1) using three vessels (Figure 3-2), two different positioning systems (one of which is appropriate for hydrographic/multibeam echosounder surveys: Table 3-1, Figure 3-2) and the suite of CGS equipment (Figure 3-6). The most appropriate techniques were applied, as required, to address the objectives of this study. The selection was based on desired depth of penetration as a function of water depth in the case of seismic surveys and for surficial geophysics, as guided by the anticipated geological and sedimentological substrate identified by previous South Coast studies. In addition to the data collected exclusively for this project, PetroSA provided supplementary geophysical data, which were collected for a Mossel Bay pipeline survey done at the end of 2010. The coverage of this dataset is shown on Figure 3-1. All datasets were integrated in their raw form and processed together for consistency to produce the maps presented in this thesis. All geophysical data are archived at the CGS.

During data collection surveys, vessel speed was dependent on wind conditions and line azimuth, but was generally optimised between 3.5 and 5 knots. Line planning was carried out in Hypack software. For the Mossel Bay multibeam echosounder and side-scan sonar survey, line spacing was calculated according to the required spacing of side-scan sonar. However, side-scan sonar and multibeam bathymetric data were acquired simultaneously. The area of greatest interest was surveyed with side-scan sonar seafloor coverage of more than 100 %, providing 20 % overlap between adjacent lines. The line spacing was calculated as 137 m in water depths shallower than 20 m BMSL and 260 m in depths exceeding 20 m BMSL. The scan ranges applied were 75 m and 150 m respectively. Data coverage achieved during the survey is illustrated in the track chart displayed in Figure 3-1A, with additional multibeam infill shown in Figure 3-1B. For areas of geological outcrop, multibeam echosounder data were collected as ‘infill’ areas to achieve seamless coverage over prominent features. The lateral swath coverage of a fan of sonar projected from the multibeam transmitter is proportional to the depth in any given area, hence the line spacing in this case was determined by the specified overlap, minimum and maximum depths on each path, and predetermined angular beam width settings. The seismic lines offshore of Mossel Bay (Figure 3-1C) and for the South Coast survey (Figure 3-1D) were designed to intercept features and areas of interest, but were arranged on both coast-parallel and coast-perpendicular orientations. In Swartvlei, (Figure 3-1E) evenly spaced 100 m grids were surveyed, also oriented parallel and perpendicular to the coastline.

The geodetic parameters applied to the data presented in this thesis were produced in the Universal Transverse Mercator (UTM) projection of zone 34 south [World Geodetic System (WGS) 1984 ellipsoid]. The central

meridian for Zone 34S is 21°. Projected distortion increases toward a zone's peripheries, but the scaling factor and false eastings used in the UTM system minimize distortion up to 500 km buffer on either side of the central meridian (Fenna, 2006). All depths reported are reduced to Mean Sea Level (MSL). Where elevations above this datum are quoted, they are referred to as above Mean Sea Level (AMSL) and depths below abbreviated to below Mean Sea Level (BMSL).

Table 3-1. Details of the four geophysical surveys undertaken for this project. Abbreviations are as follows: km – kilometres, S/V – survey vessel, M/V – marine vessel.

Survey (listed in chronologically)	**Region**	**Coverage (line km)**	**Geophysical techniques applied**	**GPS/Positioning**	**Vessel**
1 (April – May 2011)	Mossel Bay	1822	Multibeam bathymetry, side-scan sonar	C-Nav differential GPS	S/V *Geo Manzi*
2 (June 2011)	Mossel Bay	328	Boomer & pinger sub-bottom profiling	CSI Wireless differential GPS	S/V *Geo Manzi*
3 (September 2011)	Wilderness (Swartvlei)	127	Single beam bathymetry, pinger sub-bottom profiling	CSI Wireless differential GPS	SAN Parks
4 (February 2012)	South Coast (Buffels Bay to Still Bay)	420	Pinger sub-bottom profiling	CSI Wireless differential GPS	M/V *Princess Lee*

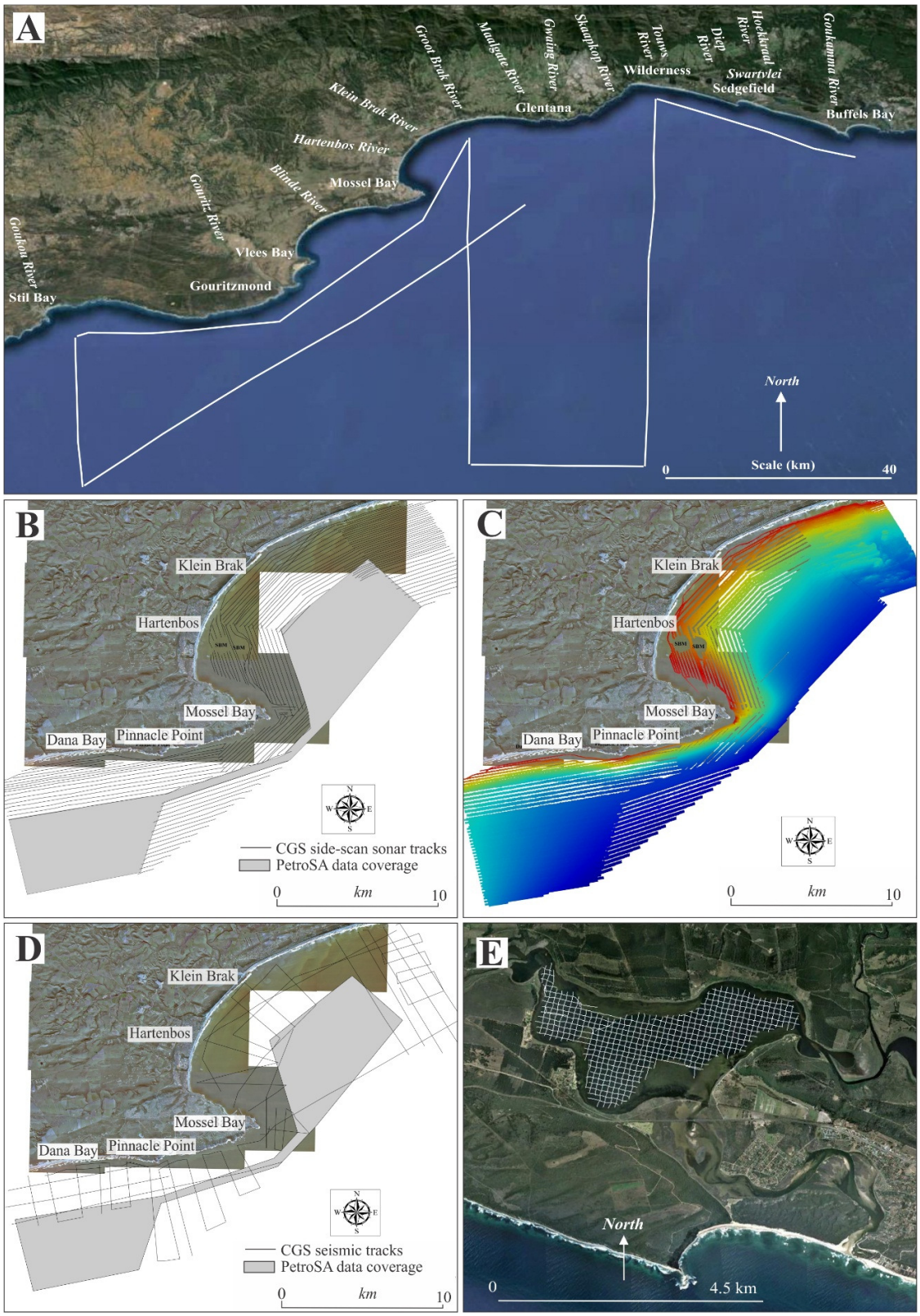

Figure 3-1. Ship track navigation along lines collected during the four marine geophysical surveys for this study. A. Track chart indicating coverage of seismic data acquired for the South Coast regional survey by the CGS

MGU. B. Track chart indicating coverage of side-scan sonar data acquired in Mossel Bay by the CGS MGU. C. PetroSA multibeam bathymetric data and the multibeam bathymetric data acquired by the CGS. Areas of rocky outcrop were surveyed with 100 % overlap between swaths but the low-gradient sections of seafloor characterised by shelf sand were not. Gridding algorithms had not been applied to these areas in the map presented here, but for interpretive purposes were extrapolated as seen in later data presentation. Abbreviation: SBM – Single Buoy Mooring (within a restricted zone defined by a 1 km radius). D. Track chart indicating coverage of seismic data acquired in Mossel Bay by the CGS MGU. E. Seismic track charts within Swartvlei by the CGS MGU.

3.1.1 Survey vessels

The nearshore vessel S/V *Geo Manzi* (Figure 3-2Ai) was used for the collection of all geophysical and hydrographic data in Mossel Bay by the CGS. S/V *Geo Manzi* is an 8.5 m custom-built aluminium technicraft catamaran, powered by two 175 Suzuki four-stroke outboard motors. Due to the shallow draft of approximately 0.6 m, S/V *Geo Manzi* is able to safely navigate into shallow water of the surf zone (swell permitting), to maximise data acquisition and area coverage. A 3.5 m South African National Parks (SAN Parks) vessel was used for the collection of bathymetric and seismic data in Swartvlei, Wilderness. This vessel has a draft of less than 0.5 m, making it appropriate for collecting data in a shallow coastal lake. The mounted pinger transducers were tethered to the port gunwale and towed adjacent to the vessel. The nearshore vessel M/V *Princess Lee* (Figure 3-2Aiii) was used for the collection of the regional South Coast seismic profiles. M/V *Princess Lee* is a 15 m charter boat, registered to work to a maximum distance of 40 nautical miles offshore. The sub-bottom profiler was not hull-mounted to reduce the cavitation effects. Towing the float was found to provide a clearer, unobscured acoustic signal. An outrigger was constructed off the starboard gunwale of the vessel to minimise noise from the propeller wash.

3.1.2 Positioning/navigational equipment

The navigation system for the Mossel Bay multibeam echosounder and side-scan sonar survey consisted of a C&C Technologies C-Nav 2050 RTG differential GPS (dGPS) system capable of decimetre accuracy, interfaced as an auxiliary GPS input into an Applanix POS MV 320 system to provide highly precise positioning (7 cm accuracy). The C-Nav 2050 Sensor (Figure 3-2Bi) consists of a 10-channel dual frequency precision GPS receiver, two additional channels for receiving Satellite Based Augmentation System (SABS) signals and an L-Band demodulator for reception of the StarFire Network APS correction service. With the C-Nav 2050 interfaced to the POS-MV (Figure 3-2Bii), high precision navigation data were output to the QINSy navigational software package at an update rate of 50 Hz. A CSI Wireless dGPS Max (Figure 3-2Biii) was used for the

seismic profiling surveys. This is a high-accuracy GPS receiver that incorporates internal sensors capable of receiving corrections from Space Based Augmentation Systems (SBAS), the worldwide OmniSTAR service and dGPS beacon stations. When using any of these services, the dGPS MAX provides sub-metre accuracy at position update rates of up to five times per second (5 Hz). The NPA beacon reference service dGPS correction was used for this survey to provide sub-metre positioning.

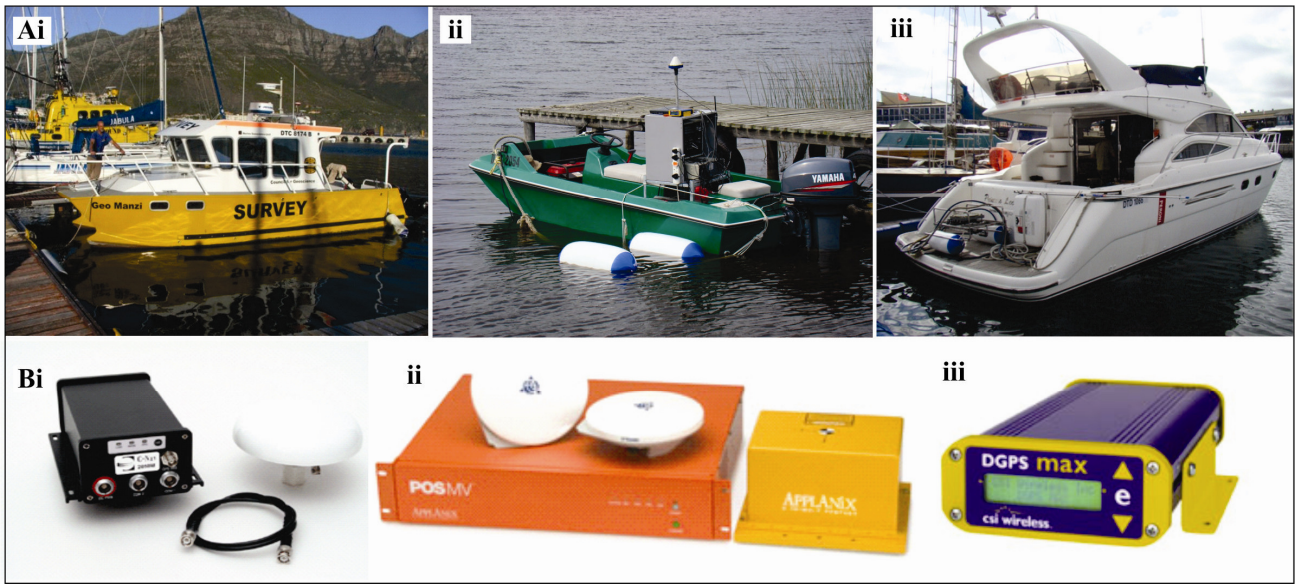

Figure 3-2. A. Vessels used. i. The CGS inshore survey vessel S/V *Geo Manzi* used for Mossel Bay surveys. Photograph taken in Hout Bay by Dr John Rogers. ii. SAN Parks vessel used in the Swartvlei survey. iii. Vessel M/V *Princess Lee* used in the regional South Coast survey. B. i. C-Nav 2050 RTG system ii: Applanix POS MV inertial motion reference unit. iii. CSI Wireless dGPS Max navigational system.

3.1.3 Multibeam bathymetry

Echosounders determine the travel time of an acoustic pulse by detecting the sharp leading edge of the return echo, providing a depth to seafloor (Mayer and Hughes-Clarke, 1995). Acquisition of sonar swath bathymetry using a multibeam echosounder encompasses the principle of a three-dimensional fan shape of acoustic energy, subjected to pitch, roll, yaw and vessel oscillation (Parkinson, 2001). The array transmits pulses triggered at known intervals to insonify an area of seafloor normal to the ship's track. High-resolution motion reference units compensate for the inherent motion in the data acquired (Jones, 1999). The angular coverage sector of beam angles varies with depth, allowing accurate bathymetric determination from a relatively small number of passes across a deeper area (Parkinson, 2001).

The Mossel Bay continental shelf was surveyed between depths of 5 m and 55 m BMSL using a 400 kHz Reson Seabat 7125 multibeam echosounder. This ultrahigh-resolution system uses 512 dynamically focused receive beams at 0.5° across-track beam width separations to form a swath 128° wide at an operating frequency of 400 kHz. The SeaBat 7125 multibeam echosounder was interfaced to an Applanix POS MV 320 motion reference unit with L1/L2 RTK capability to adjust the sonar beams for motion of the vessel (Figure 3-2Bii). As an integrated GPS/inertial reference system, the POS MV outputs all motion variables at high rates of up to 200 Hz even in the presence of GPS dropouts or degraded differential GPS corrections. The data output variables include RTK positioning and elevation, velocity, 3D attitude (roll, pitch and true heading), heave (and true heave), acceleration vectors and angular rate vectors. The survey was navigated using QPS QINSy software. Sound velocity profiles were collected daily within the survey area to correct the multibeam echosounder data for changes in the velocity of sound through the water column.

3.1.4 Side-scan sonar

Side-scan sonars project two beams are formed by transducers along the flanks of a towfish and propagate outwards, angled 5º below the horizontal (Jones, 1999; Parkinson, 2001). Most energy reaching the seafloor is scattered; a small proportion is lost in the ground and a small proportion is returned to the sonar which is amplified and recorded. This return signal is referred to as backscatter. The time between the transmission and reception is directly proportional to the composition of the substrate and the distance between the sensor and the target. This intensity is plotted in shades of greyscale with dark hues representing “hard” objects and light hues representing “soft” objects. White record represents zones of acoustic shadow on a grayscale view. Side-scan sonar data thus provides an acoustic map of a desired section of seafloor and when these sequential profiles are merged, 2-D maps of the seafloor’s acoustic backscatter can be produced. Depths are not derived from side-scan sonar.

Mossel Bay and the surrounding shelf area were imaged using a dual-frequency (500/100 kHz) Klein 3000 side-scan sonar with scan range of 75 – 150 m to produce a surficial acoustic texture map/mosaic. This system is based on transducer technology and advanced circuitry developed for the Klein multi-beam focused side-scan sonar. Acquisition was accomplished using Klein's SonarPro PC based software.

3.1.5 Processing of multibeam bathymetric data

A series of parallel survey lines were collected over a rocky ledge in the vicinity of the Groot Brak River (Figure 1-2) during the geophysical survey to conduct a ‘patch test’ on the data. A patch test is used to calibrate multibeam echosounder installations for bias in time, roll, pitch, and heading. Specific combinations of these

survey line data were processed within QINSy editor (the Validator function) to measure and correct for the inherent misalignments. The results of the patch test offsets implemented in the sonar data are listed and indicated graphically in Figure 3-3. A real-time multi-layered sounding grid was shown in the navigation display during the marine survey which is populated with corrected depth soundings as they are received. Once data collection was complete, the data were replayed through the QINSy processing manager to update the navigation surface (dynamic grid) and apply the patch test to the QPDs (raw sounding files). In addition to patch test calibration, 30 second tidal data obtained from the South African Navy Hydrographic Office and true heave data were applied to the soundings. True heave (achieved with the POS-MV motion reference unit) allowed for effective improvement in heave precision. True heave is based on an advanced multibeam processing algorithm, which uses both past and present vertical motion data to compute a significantly improved heave estimate. The data were imported into the QINSy Qloud utility to create a binned sounding grid (where a cell size of 0.5 m was specified). Data cleaning involved filtering, clipping filters for anomalous points in space and the application de-spiking methods. Finally, the cleaned, filtered dataset was exported to QINSy as a cleaned sounding grid and in the Sounding Grid Editor, output GEOTIFF files, grids for ArcGIS and individual points were produced. An interpolation to fill in areas of missing data on the grid was run.

Various datasets on different resolutions were produced and the area sub-divided into blocks according to density of line coverage and geological interest. The blocks defined were based on the orientation of lines acquired and include: Groot Brak, Mossel Bay, Cape St. Blaize, Dana Bay, Mossel Bay Deep and PetroSA. These were gridded separately in Surfer and the resultant grids mosaiced. A 1x1 m digital elevation model (DEM) of the Groot Brak was produced from QINSy and exported as a GEOTIFF. Using Surfer software, the various mosaics were stitched together to allow for the combination of different resolution datasets on one grid. The grid was filtered using Low Pass filters, Spline Smoothed and blanked. Isobaths were generated from the same grid and smoothed (Figure 3-4).

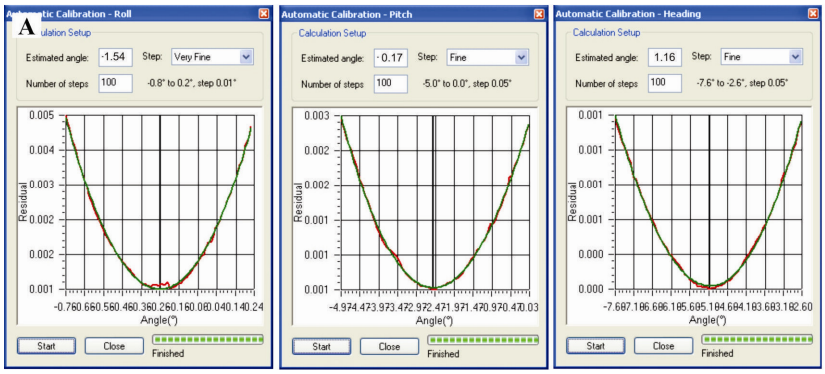

B

Correction	Angular offset
Roll	-1.54°
Pitch	-0.17°
Yaw	1.16°

Figure 3-3. A. Curves derived for roll, pitch and heading (yaw) for the hydrographic survey offshore of Mossel Bay. B. Patch test values for the survey configuration.

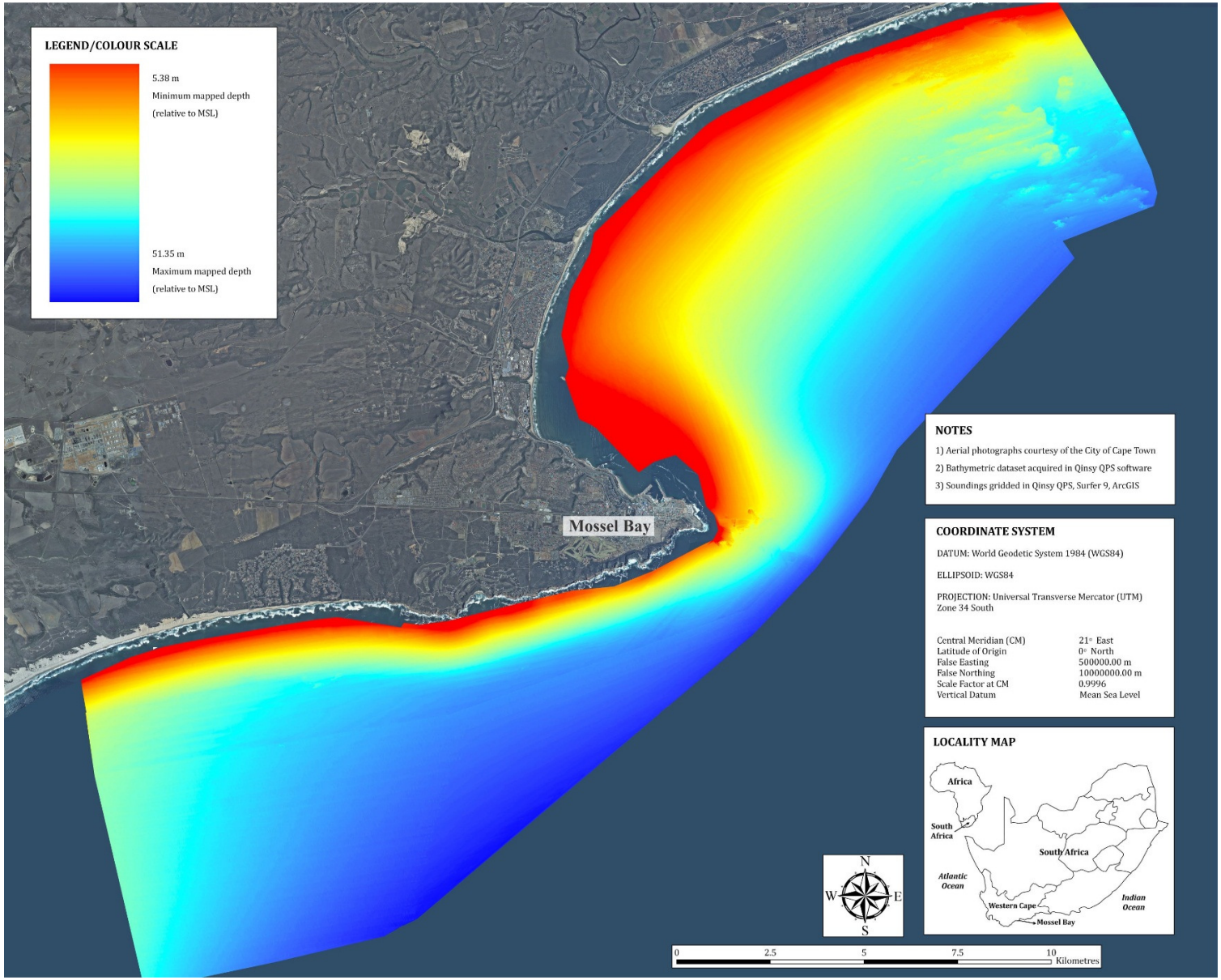

Figure 3-4. Multibeam bathymetric chart for Mossel Bay, showing a range of depths from 5 – 55 m BMSL.

3.1.6 Processing of side-scan sonar data

The 500 kHz port and starboard channels were used in side-scan sonar data processing and corrected lines were processed with 25 % overlap. Slant range distortion and anomalous navigational points caused by dGPS drift were edited out of each line prior to the correction of tow-fish layback behind the dGPS antennae and bottom tracking corrected. The side-scan sonar data were converted from Klein's SDF format to Q-MIPS format using Navlog Systems software. This software converts the composite SDF file into a 100 kHz (or 500 kHz) Q-MIPS sonar file, down-samples each channel to 1024 data points, applies automatic time varied gain (ATVG), and bottom tracking for slant range correction and calculates the towfish position based on the cable layback criteria in the trace headers. The embedded navigation is then extracted out of the Q-MIPS sonar files, edited and filtered for dGPS aerial movements. The layback correct navigation is then re-integrated into the sonar files. The generation of 8 separate side-scan sonar mosaics was carried out in ER Mapper software. Due to the large extent of the geographic area mapped, the division into 8 mosaics was necessitated and these were later merged in ArcGIS software (Figure 3-5).

The 500 kHz side-scan sonar mosaic GEOTIFF was imported into AutoCAD for digitising the various features identified from the side-scan sonar mosaic. Discrete polygons reflecting the spatial distribution for each of the identified acoustic seafloor facies were prepared and combined to form an interpreted seafloor map. The resultant polygons were “cleaned” in AutoCAD prior to the production of the final maps.

3.1.7 Manipulation of the multibeam echosounder and side-scan sonar datasets

The primary goal was to use these data to address the geomorphological features and geological deposits on the seafloor by a visual inspection of the datasets. Multibeam bathymetry was used in conjunction with the geophysical data, notably side-scan sonar, to delineate topographic features at high resolution. The interpretations are built on the assumption that the regional oceanographic conditions (wave regime, tidal range) were comparable to the present situation. Thus, it is inferred, that the palaeocoastlines on the shelf can be identified according to the modern analogue of the existing shoreline of the Mossel Bay embayment. If features were preserved on the shelf and currently exposed on the seafloor then they were visible on the multibeam echosounder and side-scan sonar datasets in the form of distinct linear features or breaks in slope.

Figure 3-5. Composite side-scan sonar mosaic for the Mossel Bay area. The lines are individual processed tracks.

3.1.8 Boomer sub-bottom profiling

Boomers are low frequency seismic profilers, characterised by a broadband frequency spectrum and high peak intensity (Parkinson, 2001). Seismic energy is derived from a bank of capacitors, discharged into an electromagnetic coil and providing a clear pulse and resolvability of seismic return. Boomer sub-bottom profilers are considered medium-penetrating seismic systems and allow an insight into upper continental shelf stratigraphy.

A Design Projects high frequency boomer was used to collect medium penetration seismic profiling data in the Mossel Bay survey area. An Applied Acoustic Engineering CSP1000 power supply that produces a maximum energy output of 1000 Js^{-1} was used to power the boomer plate and a Design Projects 20 element hydrophone array was used in conjunction with an Octopus 760 seismic processor to acquire and store the seismic data in SEG-Y format. The boomer system was triggered every 250 ms at an energy level of 1000 J and the reflected seismic data were acquired by the hydrophone array and recorded at the Octopus seismic processor, using a sampling rate of 24 kHz and a sweep period of 75 ms. The Octopus 760 was used for real-time processing, digital recording and as a post-processing workstation. Onboard processing facilities include swell filtering, stacking, water column blanking, time varied band pass filtering, time varied gain, and automatic bottom tracking.

3.1.9 Pinger sub-bottom profiling

The pinger sub-bottom profiler uses pulsed energy at a fixed frequency, similar in principle to an echosounder but with a lower output frequency and boosted power for penetration beyond the seafloor. Pingers use a piezoelectric transducer to generate power within an acoustic frequency range of 4 – 12 kHz and are useful for mapping of shallow shelf deposits.

Resolution of Quaternary features is considered optimal with a pinger system on the South Coast (Cawthra, 2011 a, b). A combination GeoAcoustics/Octopus 760 system (Figure 3-6) was used to collect pinger seismic profiles. The seismic profiling system consists of a GeoAcoustics Model 5430A transmitter, an Octopus 760 seismic processor and an over the side mounted array of four Massa transducers. Pulse length cycles were selected to improve efficiency of the transducers and to reduce “ringing”. The pinger system was triggered every 125 ms with a sweep period of 200 ms using a sampling rate of 24 kHz. The Octopus 760 was used to apply band pass filtering of pinger data in the range from 2000 - 8000 Hz.

Figure 3-6. Components of the pinger sub-bottom profiling system. A. Massa array transducers in float. B. GeoAcoustics signal transmitter. C. Coda Octopus 760 (topside receiver).

3.1.10 Processing and manipulation of seismic data

The pinger and boomer sub-bottom profiling data were processed using the seismic processing module of Navlog Systems software. Stacking, filters and TVG were applied to enhance the seismic records. Post-processing of the reflection seismic data involved the application of time-varied gain, a bandpass filter generally optimised between 900 and 8000 Hz, swell filter and seafloor tracking. Sound velocity through the water column was set at 1500 ms^{-1} to constrain time-depth conversions. This value was based on average sound velocity readings taken in this area for the numerous geophysical surveys. The navigational information embedded in the source data as eastings and northings of the points along seismic lines is accurate to within 0.5 m in the horizontal.

All vertical thicknesses were computed with a constant nominal two-way speed of sound of 1650 ms^{-1} and bottom tracking information was used for computing isopach distance where applicable. For the generation of the isopach surface, the basal reflector was digitised and these ASCII data exported as text files. The ASCII data were gridded in Surfer 9 software. For general interpretation and visualisation, compressed seismic data images were produced in Navlog software to show the general features of long sections of logged data in a practical space. The degree of compression was selected and exported as Bitmap files which were stitched in Corel Draw 15 software. Seismic data were interpreted and utilised in the development of the sequence stratigraphic model.

3.2 Geological observations of structures at the Pinnacle Point cave complex

Structural geological features and detailed lithology of the bedrock substrate of the basement rocks on the Pinnacle Point coastline were documented during July 2011. The purpose of recording these observations was to understand why the coastal caves incised where they did, and to identify a possible trend. The Pinnacle Point

area was traversed and each significant cave, or cluster of caves, was studied. Dip and strike measurements of bedding was recorded, orientations of faults and joint sets were measured, and cave dimensions recorded.

3.3 Geological mapping and sampling of shoreline Quaternary rocks

The Mossel Bay rocky intertidal zone was mapped during spring low-tide cycles from December 2010 to May 2011. The distribution of sedimentological facies within Quaternary calcarenite deposits along the rocky shoreline of Mossel Bay was carefully recorded in the highest possible resolution onto aerial photographs. A total of 78 rock samples were obtained (details listed in Appendix I), dip and strike measurements were recorded on bedding surfaces and lineations, and facies descriptions recorded. Unconsolidated sediment reference samples were also taken from the beach environment during this time from transverse sections oriented perpendicular to the modern beach profile. Specific zones of interest included modern facies from the upper shoreface (sampled by swimming to the appropriate area), the swash zone, foreshore, berm, backshore, dune, and fluvial sandbanks and washover deposits.

3.4 Geological mapping of seafloor units

Offshore rock and marine sediment samples were collected during two 'ground-truth'/seafloor sampling surveys between March and May 2013. The diving surveys facilitated physical underwater observations of the geology and geological features of the seafloor and correlation to acoustic facies identified on the side-scan sonar mosaic which could be extrapolated along strike according to the backscatter/geophysical textural characteristics.

3.4.1 Scuba diving surveys

Sampling off Mossel Bay is challenging as this area is internationally recognised as a year-round centre of abundance for Great White sharks (*Carcharodon carcharias*) (Bonfil et al., 2005; Johnson and Kock, 2006) where they have been studied since 2001 and monitored by a commercial cage-diving operator since 1995 (Johnson et al., 2009). The two main patrol areas for the white sharks include Seal Island and the area offshore of the Groot Brak River (Johnson et al., 2009; Ryklief, 2012). As such, certain unusual precautions had to be taken in the scuba diving operations and a 3-person shark cage was utilised and transverse dives across vast tracts of seafloor were not a possibility.

Two vessels were used for dive sampling. The CGS inflatable *Tethys* was the dive boat and platform for sediment sampling, and the Oceans Research catamaran *Cheetah* housed the precautionary 3-man winch-operated shark cage. Key sites were selected on the side-scan sonar mosaic and positioning was fixed using the CSI Wireless dGPS described above. Navigation was constrained in Hypack navigational software housed on

Tethys. Near each site, a marked target was used to guide the vessel to the point with an accuracy defined by the dGPS (typically in the range of 50 cm in the horizontal plane).

During diving operations a 3-person shark cage remained suspended at 5 m, tethered to vessel *Cheetah*. A shot line running from *Cheetah* to the seafloor was weighted with dive weights and the 15 pound sledge hammer used for sampling. Divers, in teams of 2 to 4 people, descended down the shot line to the seafloor and upon reaching the target outcrop below the boats; photographs were taken of the locality (Figure 3-7). Rock samples were hammered with a selection of appropriate tools including a 4 pound mallet, sharpened chisels, a crowbar and a 15 pound sledge hammer. If the rock samples were too large to swim up, they were placed into a net shackled to a lift bag rated to carry 100 kg and sent to the surface. Safety stops at 5 m, a necessity for decompression, were carried out in the shark cage. In addition to photographic evidence, additional GoPro video footage was obtained for most of the dives. The sample database presented in Appendix I lists locations of all rock samples obtained and used for this study.

A total of 41 dives were achieved in Mossel Bay (Figure 3-8), which consisted of exploratory dives near the Cape St. Blaize area and geological sampling in the northeast section of the study area between the mouths of the Klein- and Groot Brak Rivers where significant outcrops exist. A total of 28 geological samples were obtained from offshore by scuba diving (Figure 3-9), ranging in depths from 12 – 45 m BMSL (Figure 3-8). A total of 11 of these 28 samples were submitted for geochronological analysis, with one additional shoreline sample. The selected samples represent dominant seafloor units which can be traced along strike on the geophysical datasets according to characteristic textures and features. These units were considered critical in gaining an understanding of the Quaternary evolution of this part of the continental shelf. The selection criteria for geochronology additionally considered a representative range in depth, including samples from various bathymetric zones between the shoreline and mid-shelf.

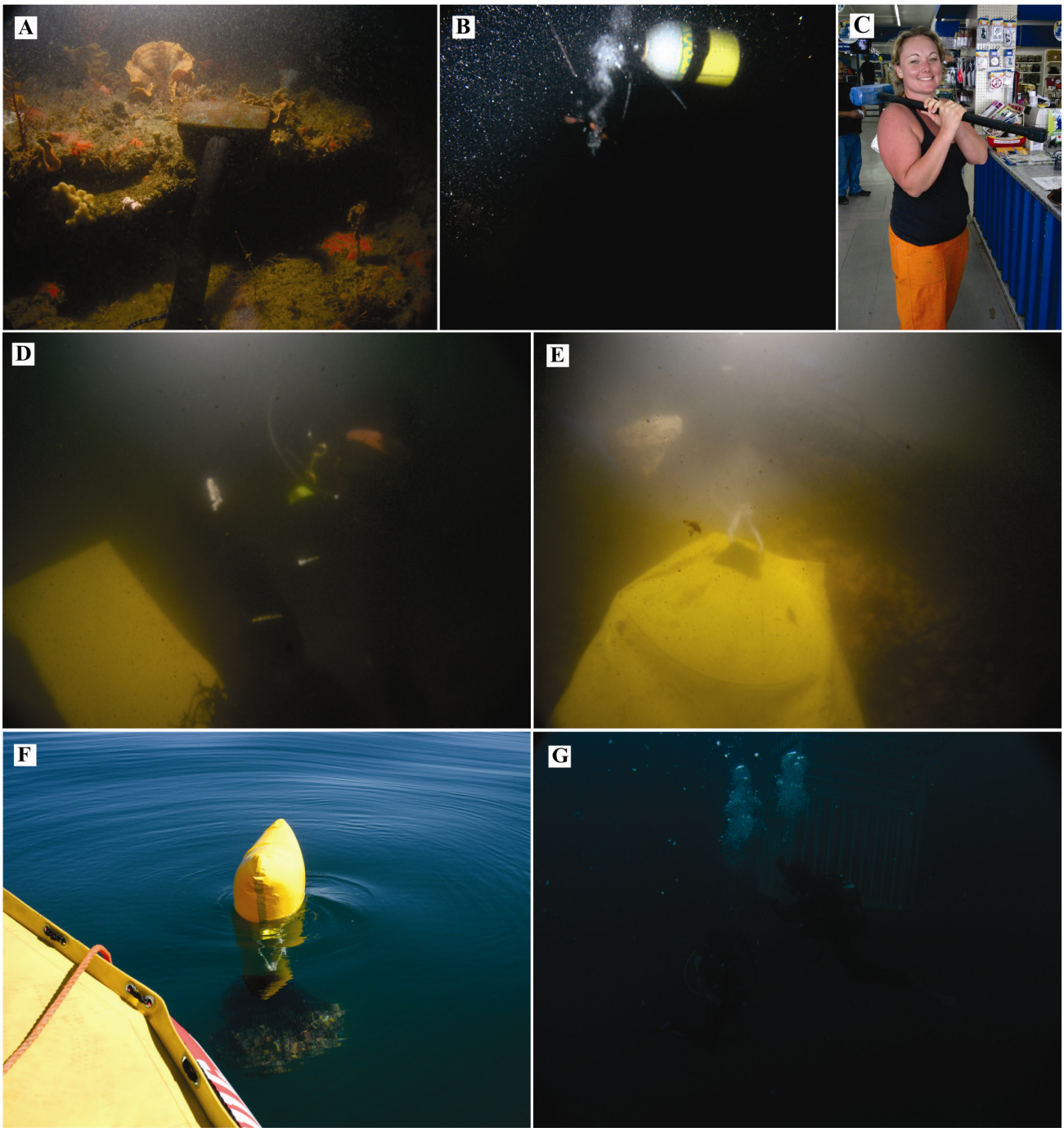

Figure 3-7. A-C: Diver tools for geological sampling on the seafloor. D, E: Underwater photos of a diver placing a rock sample into a net to be sent to the surface in an inflatable lift bag. F: The lift bag with rock sample on the surface, to be collected by *Tethys*. G. Divers at the -5 m safety stop.

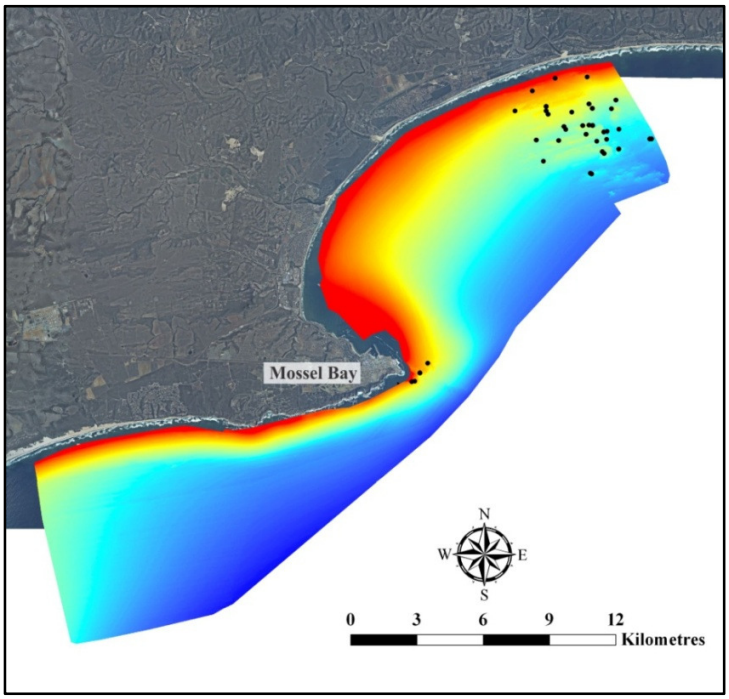

Figure 3-8. Dive localities in the Mossel Bay area (black dots), offshore of Groot Brak and the Cape St. Blaize point shown on the multibeam bathymetric chart. The depths range from a minimum of 5 m BMSL (red) to maximum of 55 m BMSL (blue).

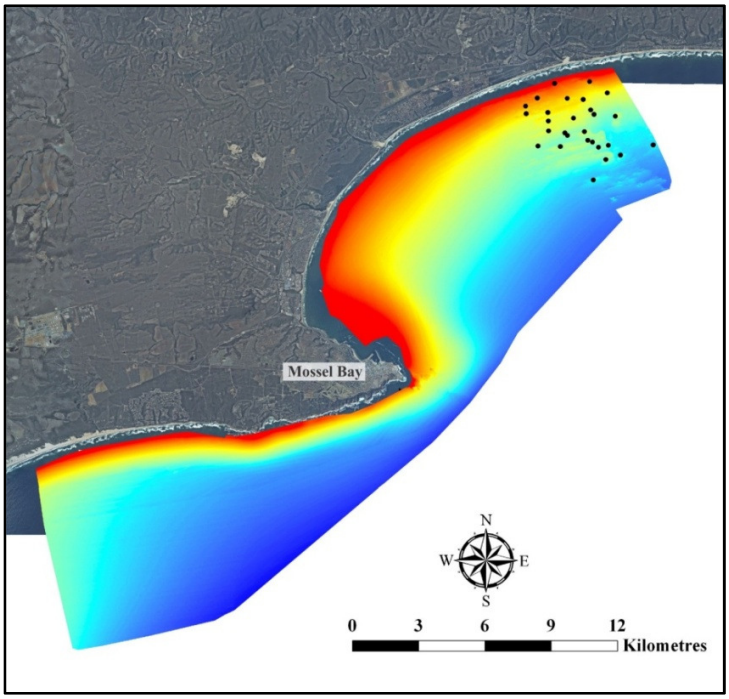

Figure 3-9. Location of the 28 offshore calcarenite samples obtained during scuba diving surveys (black dots) shown on the multibeam bathymetric chart. The depths range from a minimum of 5 m BMSL (red) to maximum of 55 m BMSL (blue).

3.4.2 Ship-based sediment grab sampling

A total of 118 surficial sediment samples were obtained from the Mossel Bay seafloor. A van Veen grab sampler was used to retrieve all unconsolidated sediment samples (Figure 3-10). The equipment comprises a stainless steel clamshell bucket that samples up to 0.1 m^2 of marine sediment, penetrating up to 20 cm into seafloor sediments. Two levers are locked into position and these unlock as the bucket hits the seafloor. As the rope is pulled upward, the buckets close, containing the sampled material. The sediment sampling was carried out from *Tethys*, positioned using the CSI Wireless dGPS, and navigated with Hypack software. The van Veen grab was tethered to 80 m of rope and fastened with additional diving weights to avoid either closing on the way down in the strong current, or not closing as it reached the seafloor. Once the operator felt the grab had hit the seafloor, it was retrieved and the sediment samples bottled in 250 ml plastic jars on the boat.

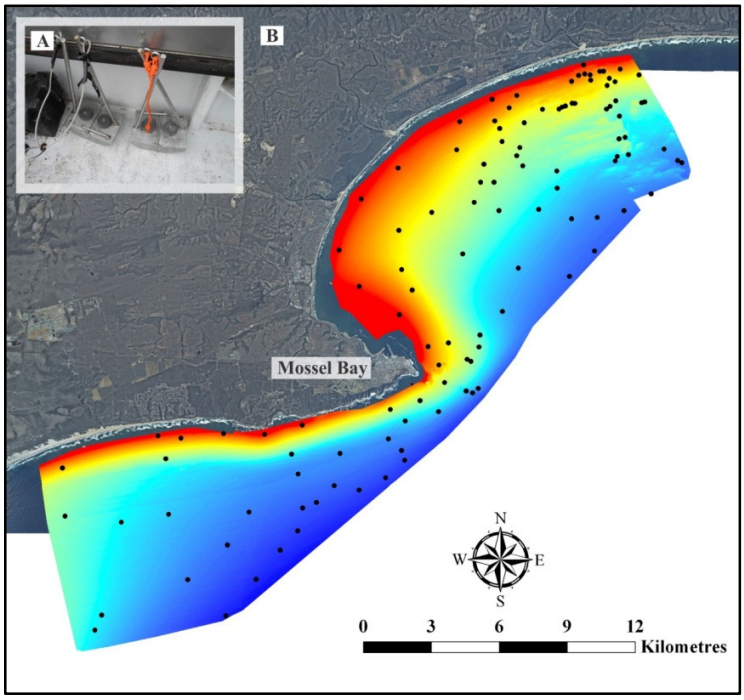

Figure 3-10. A. van Veen grab sampler. B. Sediment sample sites (black dots) shown on the multibeam bathymetric chart. The depths range from a minimum of 5 m BMSL (red) to maximum of 55 m BMSL (blue).

3.5 Carbonate content determination

Carbonate content was determined for the 118 sediment samples obtained from the continental shelf, 106 crushed rock samples from the shoreline and continental shelf and an additional 19 sediment samples that were obtained from the beaches extending from the Hartenbos River to the Groot Brak River in June 2011, after storms and during fair weather conditions, as reference samples or analogues for the cemented Quaternary deposits. In the case of rock samples, small (~25 g) sub-samples of all 106 calcarenite samples were crushed

with a pestle and mortar for sedimentological analysis. Carbonate content was determined by the carbonate bomb method, based on the technique initially described by Schink et al. (1979). This procedure relates the amount of CO_2 liberated from the dissolution of $CaCO_3$ by dilute Hydrochloric (HCl) acid to a carbonate percentage. The pressure increase that occurs in a closed system during this reaction is directly related to the mass of carbonate in the sample. The accuracy of this test is higher than 3 % with a precision of 2 % for concentrations <5 % $CaCO_3$ (Birch, 1979a). The samples were reproducible to within 3 %. Results of the carbonate analysis are presented in Appendix III.

3.6 Thin sections

Petrographic analysis of 120 thin sections from rock samples from both the shoreline and continental shelf was undertaken using transmitted light microscopy. The thin sections were prepared on the Quaternary calcarenites and back-barrier sedimentary rocks from the area surrounding Groot Brak, as well as one calcrete palaeosol from Vlees Bay and three quartz arenites from bedrock outcrops on the seafloor offshore of Cape St. Blaize. Observation of the thin sections was conducted under a Leica binocular microscope to quantify grain size and sedimentary characteristics of the clasts (sorting, roundness), composition of the samples and primary and secondary structures. Secondly, the thin sections were observed under a Nikon Petrographic microscope at magnifications of 5x, 10x and 20x to study the carbonate cements and diagenetic phases. Photographs were taken and these are presented in Chapters 4 and 7, shown under plane polarised light, as well as under crossed polarisers to enhance features within the carbonate cements.

3.7 Scanning electron microscope analyses

A total of 16 selected sub-samples of rocks were glued to aluminium stubs with carbon glue, coated with a carbon conductor and observed and measured under a Scanning Electron Microscope (SEM), allowing a close investigation of the carbonate cements. The Nova NanoSEM, housed at the University of Cape Town, is a high resolution Field Emission SEM, combining low kV imaging and analytical capabilities with unique low vacuum performance. The chemical composition of carbonate phases was analysed using Element Dispersive Spectrography (EDS) (Appendix IV). Weight percentages of Mg were converted to mole percent $MgCO_3$ but because they all fell within a common classification (Low Magnesium Calcite/LMC). As such, the numerical values are not presented in this thesis.

3.8 Geochronology

3.8.1 Samples and sampling procedure

A total of 12 selected geological samples (Table 3-2), spatially distributed from the present intertidal zone to a depth of 42 m BMSL, were dated by using Optically Stimulated Luminescence (OSL) at the Department of Earth Sciences, University of Wollongong, Australia, by Dr Zenobia Jacobs. Large sample blocks were collected from suitable lithological units during specialised geochronological sampling by scuba diving. Drilled cores from the thickest part of each sample were extracted to ensure a fresh and homogenous sample. The cores were labelled and sealed and packed for transport to the OSL dating laboratory at the University of Wollongong in Australia where it was opened under subdued red light. Here the sample was cut into at least two slices, one for luminescence dating and the other for laboratory dosimetry measurements.

Table 3-2. Selected samples submitted for luminescence dating to the University of Wollongong, Australia. The sample numbers with prefix 'HC' were labelled specifically for OSL and the prefix 'O' relates to the nomenclature of geological samples listed in Appendix I.

Sample number	**Depth (metres relative to MSL)**	**Easting**	**Northing**
HC_37 (O37)	-12	613841	6229915
HC_30 (O30)	-34	616251	6227111
HC_26 (O26)	-33	614071	6227063
HC_35 (O35)	-30	615157	6227757
HC_36 (O36)	-30	615620	6228543
HC_SH (SH)	0 (shoreline)	608760	6228710
HC_29 (O29)	-35	616795	6227038
HC_40 (O40)	-26	616195	6229492
HC_32 (O32)	-17	615402	6230000
HC_39 (O39)	-25	615101	6229193
HC_24 (O24)	-38	615613	6225541
HC_6 (O6)	-33	614300	6227685

In addition to the samples obtained and dated exclusively for this study, the interpretations presented in this study incorporate a further 44 OSL dates, analysed on aeolianite and coastal dunes for the SACP4 programme from the area surrounding Pinnacle Point. These data were provided by Prof Curtis Marean and Dr Zenobia Jacobs and were dated at the same laboratory, using the same technique (Appendix II).

3.8.2 Sample preparation

All sample preparation and measurements were performed in dim red light to prevent light exposure that leads to zeroing of the luminescence signal. The surface layer of the samples that had been exposed to sunlight was

discarded. The outer diameter and length of each core were measured and the core was traced before being submerged in concentrated HCl. The HCl dissolved the carbonates which resulted in the disintegration of the core. The core was measured at frequent intervals until ~0.5 cm was removed on all sides. This indicated that there were no remaining light-exposed grains left. Once a light-safe core of the sediments was obtained, the rest of the sample was dissolved in 10% HCl which completely dissolved the carbonates. All organic matter was oxidised in 30 vol H_2O_2. Mechanical dry sieving separated the 180-212 μm diameter grain size fractions for all the samples. Quartz was obtained from the 180 - 212 μm fraction through density separation using a sodium polytungstate solution of specific gravity 2.62 to reduce the potassium feldspar content and specific gravity 2.70 to remove heavy minerals. The separated quartz fraction was etched in 48% HF for 40 minutes to destroy any remaining feldspars and then washed with concentrated HCl for 45 minutes to remove fluorides. The purified quartz grains were then re-sieved, using the lower sieve size (180 μm).

3.8.3 Luminescence measurements

All single aliquot and single grain measurements were carried out using an automated Risø TL/OSL reader. Optical stimulation of all single aliquots was with blue light emitting diodes (LEDs) with peak emission at 470 nm, with 5 clusters of 6 LEDs directed at the sample disc. In front of each cluster, a green long-pass filter (Schott GG420) was fitted to attenuate the short wavelength tail of the LED emission. Optical stimulation of all single grains (for samples HC-32) was with a green laser (532 nm) focused onto a ~3 μm diameter spot on each grain. In addition, infrared LEDs at 875 nm were included in the reader. The OSL was measured with an EMI 9635Q photomultiplier tube through three 3 mm Hoya U-340 filters, one of which has a ZrO/SiO_2 coating to reduce transmission in the red. Beta irradiation was with a calibrated $^{90}Sr/^{90}Y$ sources.

3.8.4 Dose rate measurements

Estimates of U and Th on bulk sediment samples were obtained using three Daybreak 583 thick source alpha counters. Sample material was placed in an 'alpha thick' (>1 mm) layer on top of the ZnS screen. All potassium (K) measurements in this study were calculated from the difference between data obtained with the TSAC and GM-25-5 beta counting results. A laboratory-based Risø GM-25-5 beta counter was used to obtain a measurement of the beta dose rate for each sample.

3.8.5 Internal dose rate

In this study the U and Th concentrations internal to the grains was not measured. Instead, values of 0.169 ppm U and 0.586 ppm Th, obtained previously by Jacobs (2004) on South African quartz grains, were used. Using an

alpha efficiency value of 0.04±0.01 Gy/ka (Rees-Jones, 1995) an internal alpha dose rate of 0.033 Gy/ka was determined and applied to each samples in this study.

3.8.6 Measurement of the beta dose rates

Beta counting using the low level Risø beta counter (GM-25-5) involved measurement of the beta emission from a mineral sample containing a natural mixture of U, Th and K. To convert the count rates (counts per minute), a standard was measured in one of the five positions during every measurement cycle. At the same time a blank was measured to determine the background count rate. The standard used was a Nussi standard, prepared in the same way as the samples i.e. filling up the pot. The beta dose rate of the Nussi standard was estimated at 1.4874 Gy/ka. The blank measured was magnesium oxide (MgO) with an average count rate of 0.17 counts per minute. The beta dose rate for each sample was calculated using the average count rate from 24 hours of counting time from three sub-samples of each sample. Firstly, the background count rate was subtracted from the count rate of the sub-samples and the standard. Secondly, the corrected count rate was then divided by the corrected count rate from the standard and multiplied by the known beta dose rate of the standard.

In this study, grains of quartz were etched in the laboratory with hydrofluoric acid (HF) to remove the external alpha contribution to the grains. The values used for correction of the dose rate due to attenuation were those provided by Bell (1979), and for the effects of HF etching based on Bell and Zimmerman (1978).

3.8.7 Measurement of the gamma dose rates

Measurements of U and Th external to the quartz grains were determined using Thick Source Alpha Counting (TSAC). This method measures the total combined contribution from all of the alpha particles from the U and Th decay chains and provides a measure of the Th activity in the sample by recording all successive alpha decays of ^{220}Rn to ^{216}Po (half-life = 0.145 s), both daughter products of ^{232}Th, that occur in pairs. It is known that in the Th decay chain about 3% of the counts occur in pairs. The pairs rate is therefore a measure of the Th activity in the sample. The numbers of pairs counted, compared with the total number of alpha particles counted, are used to determine the Th and U concentrations in the sample (Huntley and Wintle, 1981; Aitken, 1985).

A background count was always measured by placing two ZnS screens face to face in the perspex sample container (counting area = 19.8 square cm) and counting for 24 hours, immediately prior to measurement of the sample (the background count rate for each screen is half the measured value). This measurement procedure prevented contamination of the ZnS screen from radon in the air and allows one to obtain a background-subtracted 'true' count rate for the sample. All sample material was dried and ground in a ball mill to less than

20 µm in diameter to obtain full measurement of the alpha activity due to the limited alpha particle range. The samples were counted as unsealed samples until at least 2000 counts had been measured, providing a statistical error of ± 3%.

Measurements of K were obtained using the difference between TSAC and GM-25-5 beta counting. In order for the values of U, Th and K to be used, the radioelement concentrations (ppm and %) needed to be converted to gamma dose rates (Gy/ka). These conversion factors are based on nuclear data tables assuming an infinite matrix where the rate of energy absorption is equal to the rate of energy emission in a volume that has proportions greater than the ranges of the radiations. This implies that there is uniformity in the radioactive content and in the absorption coefficient. Gamma dose rates were calculated using the conversion factors calculated by Guerin et al. (2011).

3.8.8 Moisture content correction

Samples were selected from a range of different sedimentary units from very different localities. Moisture contents (expressed herein % dry weight) were measured in the laboratory. These measured moisture contents are almost certainly not representative of long term moisture content. To get a better estimate of the long-term average moisture content of the sample, an additional measurement was made. A saturated moisture content was obtained to determine the upper level, in other words what is the wettest this sample can be. This was dependent on the porosity of the sample and considering that the majority of samples were cemented, the porosity would have been largely unchanged. Generous error margins (33 %) were applied to further encompass a large number of possibilities of changes through time.

3.8.9 Dose recovery tests

Dose recovery tests were performed for one of the samples (HC-40). A dose recovery test involves zeroing of the natural luminescence signal using a light source (natural sunlight), followed by application of a known laboratory dose that are of similar magnitude to the D_e expected from the natural sample. The aliquots are then treated in an identical way to those aliquots used to obtain D_e to see if that given dose can be recovered. The dose recovery test does not completely reflect the determination of the natural dose, because of a number of differences between doses accumulated in nature and those given in the laboratory. However, if a laboratory experiment like this does not work, it is unlikely that the SAR measurement of the D_e of a natural sample will be accurate. An accurate result from a dose recovery test should thus be a minimum requirement, since it will at least display the appropriateness of the SAR protocol for the laboratory regenerated measurements that make up the sensitivity-corrected dose response curve.

Six aliquots from sample HC-6 were bleached in natural sunlight for at least 4 sunny days and given a beta dose close to the expected D_e (~100 Gy). A preheat of 240 °C/10s and a cutheat of 160 °C/10 s were applied. The measured over given dose ratios for all 6 aliquots measured resulted in a weighted mean of 1.02 ± 0.03, consistent with the desired unity value of 1.00. This indicates that the conditions used are appropriate for these samples.

3.8.10 Measurement conditions for samples

The measurement conditions for all 12 samples were kept constant. For all samples, optical stimulation was made at an elevated temperature (125ºC), using a heating rate of 5ºC/s to reach this temperature. Optical stimulation was for 40 s using blue LEDs at a constant power (90 % of full power) to obtain the OSL and test dose measurements. A preheat temperature of 240ºC for 10 s was applied and a cutheat (prior to measurement of the test dose) of 160ºC for 10 s was applied to all samples. Individual dose response curves were constructed for each individual aliquot using a range of regeneration doses and a test dose. For all the samples at least 24 aliquots using a 3 mm mask size, containing ~100 grains, was measured to obtain 24 individual estimates of the D_e. A further 1000 individual grains were measured for the sample HC-32.

3.8.11 Estimate of the cosmic radiation

The contribution from cosmic rays to the environmental dose rate was variable for the samples measured in this study, because of the varying depth of sedimentary and water overburden. Due to the burial depth of these samples and the overburden (sedimentary + water), the cosmic-ray component responsible for the radiation dose is the so-called 'hard' component; this consists of muons that are absorbed much less readily and can be observed to quite substantial depths, but with decreasing intensity with increasing depth (Prescott and Hutton, 1994).

To estimate the cosmic dose rate, the effect of depth below overburden (sediment + water) and latitude and altitude effects were taken into account. The average sediment overburden density was based on a value of 2.5 g/cm^3 for all the consolidated rock samples and an average water overburden density was based on a value of 1.025 g/cm^3. This difference in density between water and sediment is important since energy loss per gm/sq cm is greater in water than in rock by a factor of 1.23. Calculations were made using the standard procedures as described in Prescott and Hutton (1994). An uncertainty of 15 % was used for all estimates of the overburden depth.

3.8.12 Derivation of the age model in this study

Given inherent uncertainties in OSL, the accuracy of the ages obtained is presented within an error range (Table 3-2; Appendix II). For the interpretations to follow in this thesis, in order to constrain the likely timing of deposition of a specific geological unit, a series of factors were considered to describe the most likely scenario. First, the sedimentary facies were used to derive the environment of deposition on the beach profile relative to sea level at the time of deposition (e.g. intertidal facies versus sedimentation in the dune environment). Second, the OSL age was considered within its error. Third, these were jointly considered in terms of placing the deposit in context using glacio-eustatic sea-level curves to constrain the timing of the event. This is shown graphically in Chapter 6, where applicable.

4 MARINE GEOLOGY OF MOSSEL BAY

4.1 Introduction

This chapter provides a description of the coastal and offshore geomorphic features and mapped geological deposits along the coastal plain and on the adjacent continental shelf. The intertidal and offshore Quaternary rocks described here were defined and described for the first time in this study. The geophysical datasets utilised in this section include multibeam bathymetry and side-scan sonar; sub-bottom profiling results are presented in Chapter 5. This chapter deals specifically with the Mossel Bay section of the study area, which was mapped in high resolution, with full surficial coverage (for details, see Chapter 3). Geological deposits described include the Table Mountain- and Uitenhage Group sandstones and associated incision of coastal caves, the relatively younger Bredasdorp Group Quaternary calcarenites which were mapped from the present shoreline to the mid-shelf, and the youngest unconsolidated sediments that blanket all underlying lithologies. This chapter, in addition to the sedimentology and geology, includes details on carbonate diagenesis and erosional events, which modified the pre-existing features subsequent to their formation.

This study builds on numerous prior South Coast investigations on Quaternary stratigraphy, which have all been carried out above the high water mark (e.g. Malan, 1990; Viljoen and Malan, 1993; Bateman et al., 2004; Carr et al., 2007; Roberts et al., 2008; Bateman et al., 2011; Roberts et al., 2012). Prior to the work presented in this thesis, no recent, high-resolution and non-commercial studies had been conducted offshore of Mossel Bay besides several regional South Coast continental shelf investigations carried out four decades ago (e.g. Birch et al., 1978; Flemming et al., 1983). Geomorphological, stratigraphic and sedimentological models of the shelf have, therefore, remained relatively outdated for the South Coast shelf. Numerous geophysical studies carried out in the South African offshore environment on the West Coast (e.g. de Decker, 1987; Woodborne, 1991; Wigley, 2004; MacHutchon, 2012) and on the East Coast (Ramsay, 1996; Bosman et al., 2005; Cawthra et al., 2012a; Green et al., 2012; Bosman, 2012) have documented marine geological evolution of the South African margin. The methodology for mapping shelf sequences, therefore, becomes increasingly detailed and refined. This study builds on this methodology and is the first within a South African context to examine and stress the significance of these geomorphological elements of the continental shelf in terms of its periodic exposure as a terrestrial landscape.

4.2 Seafloor features from multibeam bathymetry

The bathymetry in the mapped area is seen to range from a minimum of 5 m BMSL to a maximum depth of 55 m BMSL. The morphology is relatively flat and smooth in the two embayments of Vlees Bay in the west and Mossel Bay in the east, punctuated by features of noteworthy relief, but the inner shelf narrows significantly in the region adjacent to the Pinnacle Point coastline (Figure 4-1). Analysis of the bathymetric data has allowed the delineation of two distinct morphological zones of the mapped shelf that are separated by a terrace/break in slope (Figure 4-2). The inner shelf is characterised by a relatively steep gradient (averaging 0.86°) and a concentration of geological and sedimentological deposits. The mid shelf, extending seaward of the -45 m isobath, is comparatively featureless for the most part and the gradient is significantly lower (averaging 0.05° in the mapped area). The seafloor morphology, evident from the DEM, consists of flat and sloping zones, crests, depressions and breaks of slope. Therefore, the present Mossel Bay shoreline is flanked by a relatively wide (up to 8 km) bathymetrically-defined inner continental shelf terminated by a terrace defined by a nick-point at 45 m BMSL. The drop-off defines the start of the mid shelf at a depth of 45 m BMSL. The surficial geophysical dataset mapped with multibeam bathymetry does not extend as far as the outer shelf.

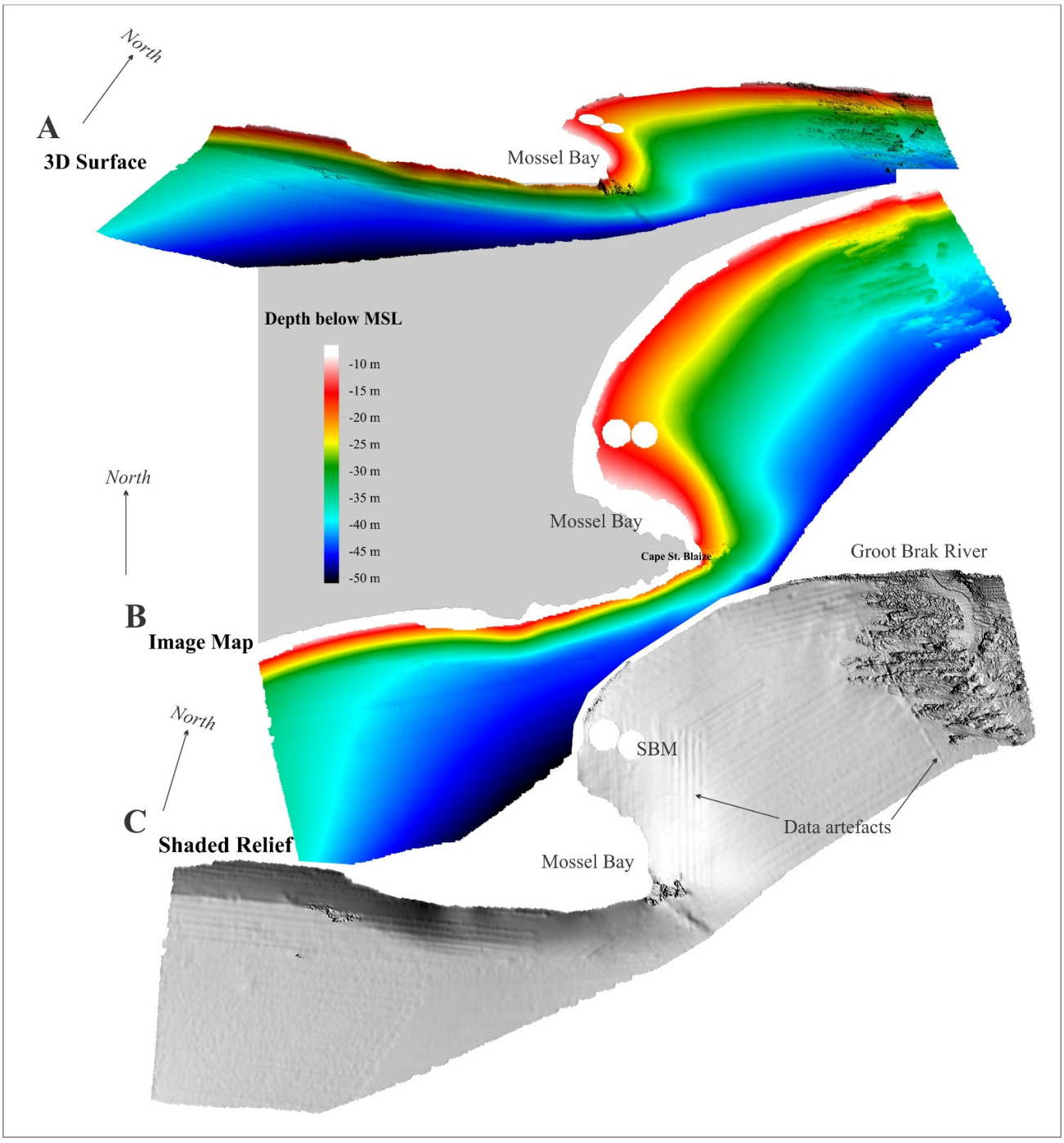

Figure 4-1. Seafloor morphology shown by multibeam bathymetric data acquired for this study. Abbreviation: SBM – Single Buoy Mooring (restricted zone, denoted by white circles). A represents a 3D surface of multibeam bathymetry. B is an image map from above, C presents a hillshade plot to highlight shadow associated with geological outcrop and changes in gradient on the seafloor.

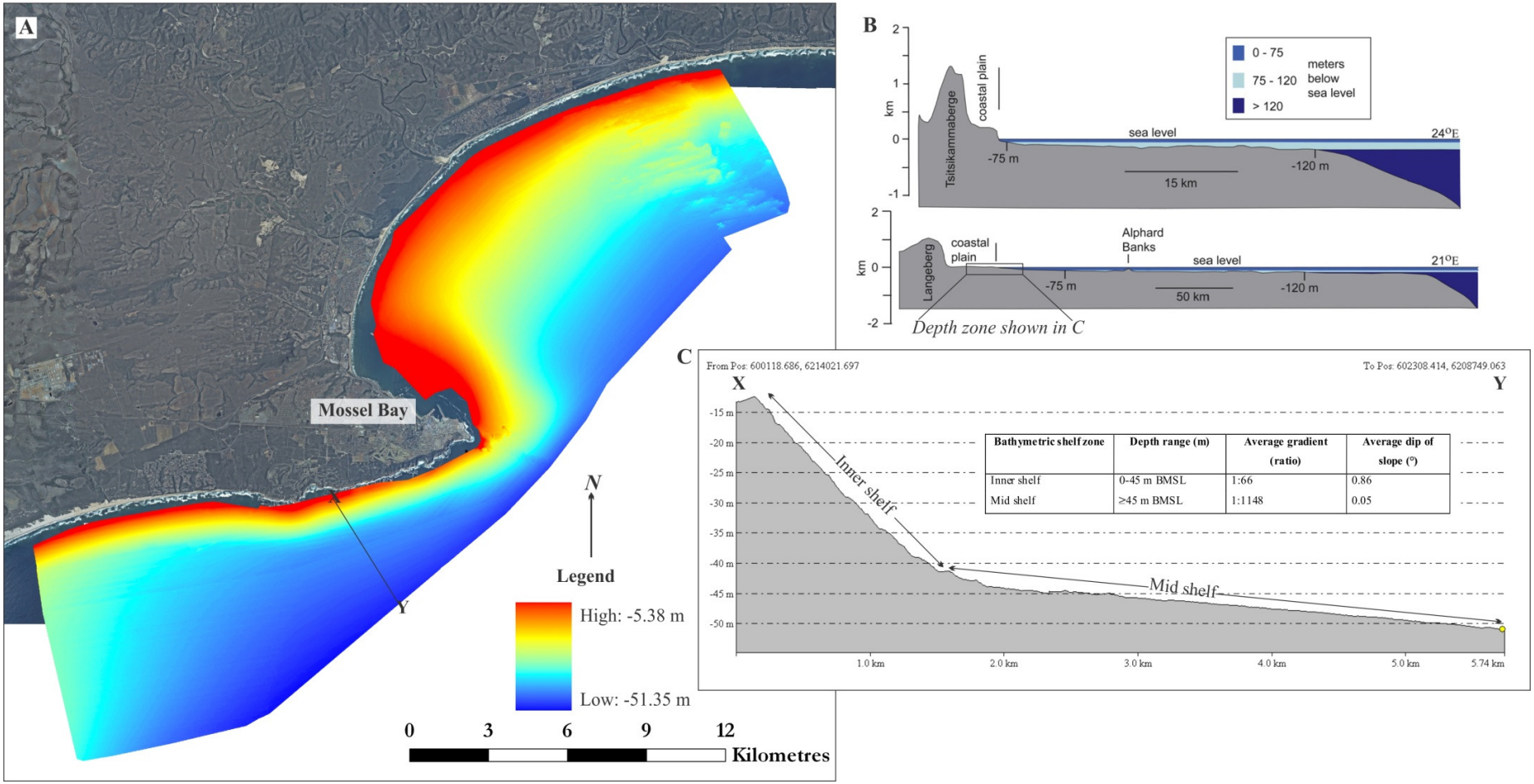

Bathymetric shelf zone	Depth range (m)	Average gradient (ratio)	Average dip of slope (°)
Inner shelf	0-45 m BMSL	1:66	0.86
Mid shelf	>45 m BMSL	1:1148	0.05

Figure 4-2. Details of the inner- and mid-shelf zones, defined by the block mapped with multibeam bathymetry in this study. A. Multibeam bathymetry of Mossel Bay. B. South Coast shelf profiles from Compton (2011) extending to the shelf break of Tsitsikamma (above) and the Breede River region (below). C. Cross section X – Y illustrating the 45 m BMSL nick point. The vertical exaggeration on the bathymetric profile is 8x.

4.3 Side-scan sonar acoustic facies

Surficial texture was classified by the analysis of side-scan sonar data (Figure 3-5). Seven discrete acoustic facies were identified. A distinct cluster of acoustic facies comprising silicified sandstone and calcarenites extend offshore of Cape St. Blaize and dominate the northeastern area of the mapped seafloor respectively. These, in composite, represent Acoustic Facies a. Facies b is closely associated with Facies a. Facies c lies adjacent to Facies a and b, generally in close association with these geological outcrops. Facies c, however, also crops out on low gradient, current-swept, areas of shelf sediment. Facies d is most prevalent in the Vlees Bay and Mossel Bay embayments and volumetrically dominates the study area. Facies e lies adjacent to the cliffed coast. Facies f and g were mapped mostly in the northeast part of the study area.

Table 4-1. A summary of the acoustic facies and their relative distributions in the study area.

Geophysical/ acoustic facies	**Description**	**Percentage of the mapped area**	**Area occupied (km^2)**
a	Speckled, highly reflective, even-toned to mottled sonar facies, with minor acoustic shadows.	6 %	18.3
b	Highly reflective, mottled acoustic facies with a granular appearance and minor or no acoustic shadows present. Closely associated/interspersed with low to moderately reflective, even-toned to occasionally granular acoustic facies.	2.9 %	10.3
c	Moderate to highly reflective, granular and even-toned acoustic facies, often exhibiting small scale alternating bands of weak reflectance with a more even-toned acoustic reflectance. Complex bedforms abundant. In places associated with Facies a and b.	5.5 %	6.6
d	Low to moderately reflective, smooth, even toned acoustic facies.	76.8 %	206.9
e	Low to moderately reflective, smooth, even toned acoustic facies with characteristic shore-parallel oriented bedforms.	1 %	1.1
f	Non-reflective, smooth acoustic facies. Crops out in the vicinity of the mouth of the Groot Brak River in the eastern section of the study area.	6.5 %	7.6
g	Moderate reflectivity, mottled acoustic facies.	1.3 %	2.4

Figure 4-3. A. Close-up views of acoustic facies characterising the seafloor of Mossel Bay, labelled a-g. B. Complete mosaic, though the resolution at this scale does not allow detail to be discernable.

4.3.1 Interpretation of the surficial acoustic facies from side-scan sonar

The intensity and texture of the image created by the backscattered acoustic pulse (see Chapter 3) is determined by the seafloor composition, allowing the identification of various features or facies types. These are illustrated in Figure 4-3 and described in Table 4-1. Subsequent 'ground-truthing' by scuba diving surveys and seafloor sediment grab sampling (Chapter 3) allowed a classification of acoustic facies according to distinctive textural characteristics. Figure 4-4 shows the distribution of these surficial facies.

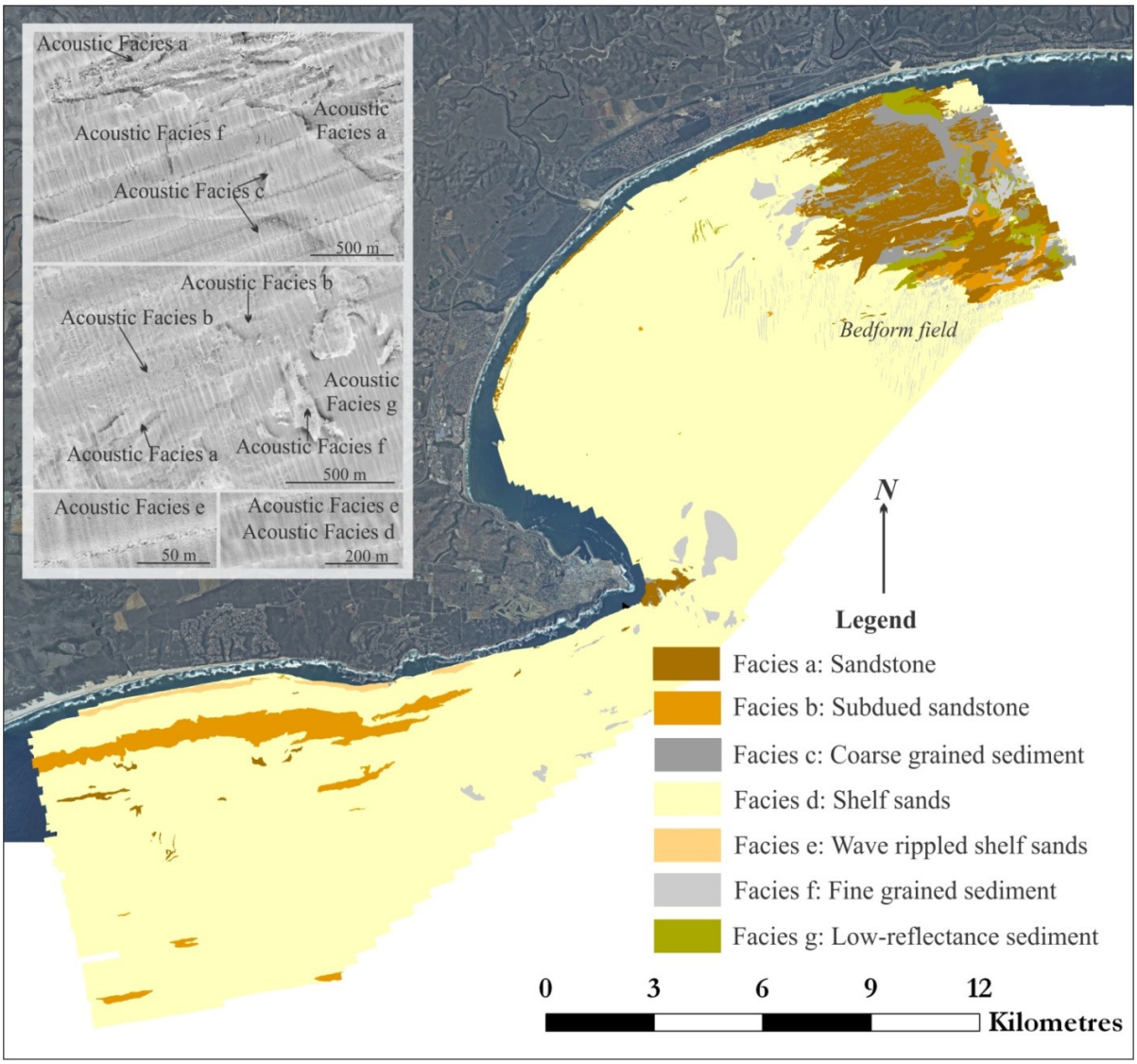

Figure 4-4. Distribution of interpreted acoustic facies characterising the seafloor of Mossel Bay, labelled a-g. The greyscale insets show the characteristics of the uninterpreted side-scan sonar mosaic for each acoustic facies.

Table 4-2. Geological classification of the acoustic facies, facilitated by the seafloor sampling programme.

Geophysical/ acoustic facies	Geological Classification
a	Silicified sandstone and calcarenite seafloor outcrops
b	Subdued morphology/eroded outcrops of Acoustic Facies a
c	Coarse grained bioclastic sediment
d	Planar shelf sands
e	Wave rippled shelf sands
f	Fine grained sediment: silty mud
g	Low reflectance, fine-grained sediment: mud

4.4 Geomorphic features of the seafloor: elements of a submerged landscape defined from multibeam echosounder and side-scan sonar data

Geomorphic features were identified in ArcGIS based on a combination of the bathymetric grid produced with a resolution of 2 m (Figure 4-2) and acoustic textures derived from the side-scan sonar mosaic (Figure 4-3). Features were mapped by digitisation of polygons representing composite units, or as linear demarcations for breaks in slope on the shelf. Complex inner shelf geomorphology is defined by seafloor outcrops separated by troughs and fluvially incised valleys, in an area generally dominated by shelf sands.

4.4.1 Terraces

Along the South Coast, the 45 m BMSL isobath separates the inner- from the mid-shelf (Figure 4-2). This bathymetric zone is distinct and forms a shelf terrace, or break in the dominant gradient that extends seaward of the 45 m nick-point. Heap and Harris (2008) define terraces as relatively flat areas of regional extent, bordered by steeper margins. The marked change in gradient at this depth has been described by Martin and Flemming (1987) as one of the four prominent South Coast nick points at 105 - 100 m, 80 - 75 m, 55 - 50 m and ~40 m water depths, the latter equivalent to the 45 m BMSL terrace described in this study.

4.4.2 Sea cliffs

Offshore of Cape St. Blaize, the hard rock geological substrate that characterises the Point coastline extends offshore for a further 2 km towards the east (Figure 4-5). From the base at 23 m BMSL the submerged sea cliffs rise 20 m off the seafloor and this outcrop correlates to the Skurweberg and Robberg Formations of Acoustic Facies a (Table 4-1). The seaward margin of the outcrop is defined by incised caves and overhangs, as confirmed on scuba diving investigations, and is eroded into an embayment comparable in size and form to the presently exposed coastal cliffs at Pinnacle Point and Cape St. Blaize (Figure 4-5). Therefore, these submerged sea cliffs are a lowstand expression of a continuous coastal promontory.

4.4.3 Shelf banks/shoals

A shelf bank/shoal is considered to be an area of seafloor characterised by widely spaced isobaths at the base, intercepted by areas of relief and incision (Heap and Harris, 2008). Numerous ridges with prominent relief compared to the surrounding seafloor occur at water depths of 35 - 55 m BMSL in the eastern study area offshore the Groot Brak River (Figure 4-2, Figure 4-6). The ridges are typically separated by depressions; hence their classification as shoals, but in places they coalesce, bifurcate and can be grouped into distinct clusters. The ridges reach a maximum relief of 8 m. The most significant linear features generally trend E-W and individual ridges reach maximum widths of up to 400 m. Within clusters, the individual ridges are closely stacked down the depositional profile of the shelf. In the study area the shoals extend for 6.5 km along strike and likely continue to crop out to the east beyond the extent of the mapped zone. These features are classed within Acoustic Facies a.

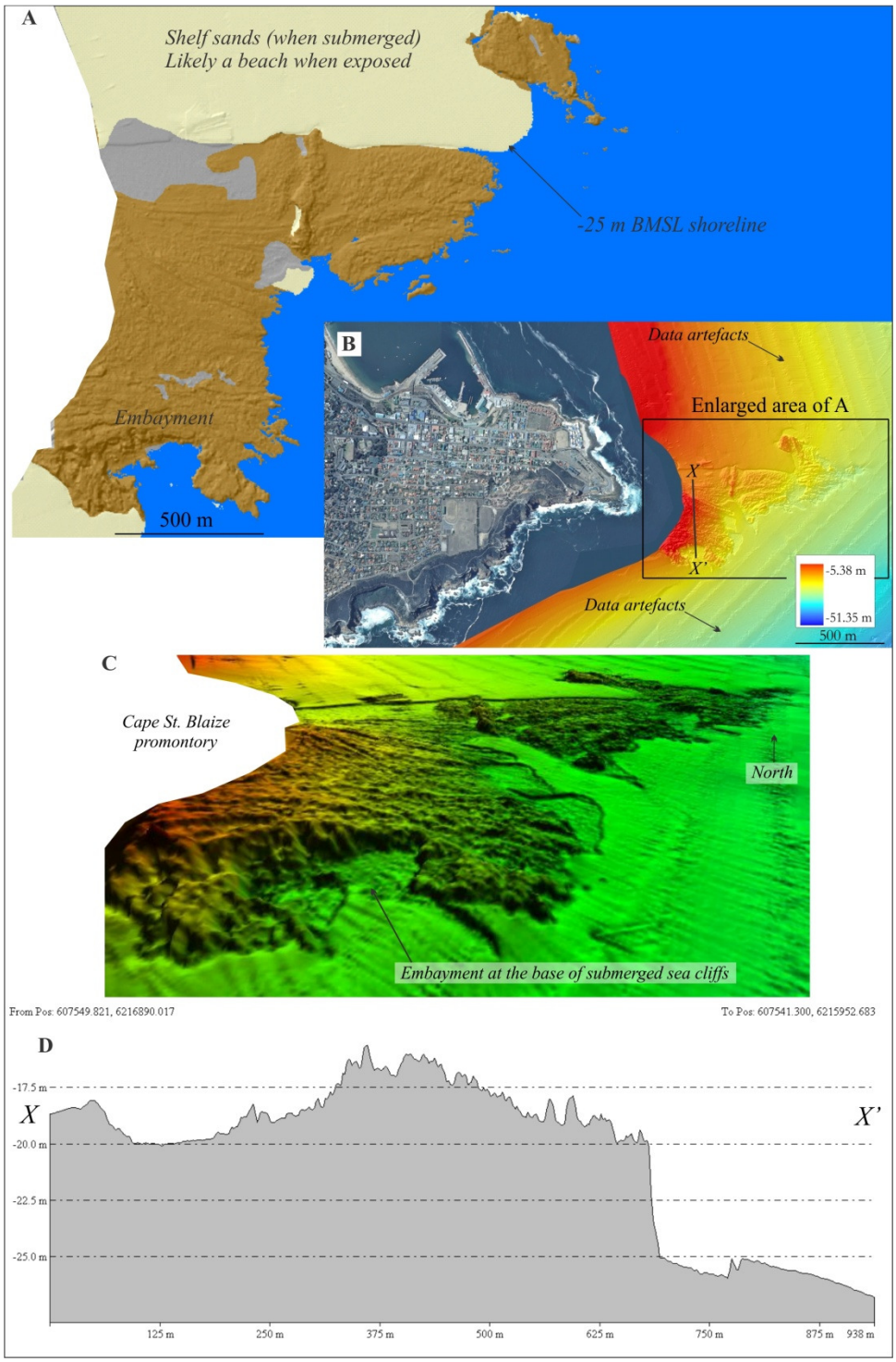

Figure 4-5. Submerged sea cliffs offshore Cape St. Blaize. The sea cliffs are incised into embayments within the hard-rock coastal promontory shown here from above. A. Interpreted acoustic facies draped over multibeam bathymetry and showing a 25 m BMSL shoreline. B. The present cliffed coast of Pinnacle Point and Cape St. Blaize adjacent to the offshore bathymetry. C. 3-Dimensional view of the submerged system, derived from multibeam bathymetry. D. Cross section X – X' (for location, please refer to B).

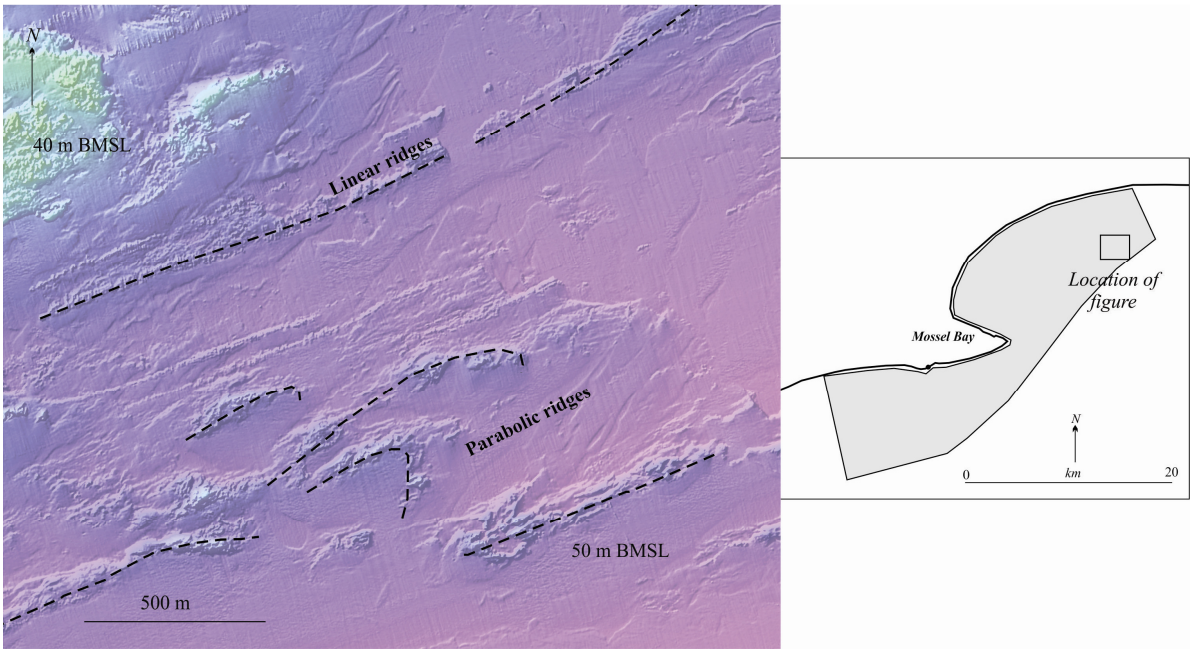

Figure 4-6. Multibeam bathymetry showing shoals on the mid-shelf of the Mossel Bay study area.

Numerous sub-aerially exposed superimposed retrogressive barrier systems have been described along the wave-dominated South Coast (Bateman et al., 2004; Carr et al., 2010; Bateman et al., 2011); offshore on the east coast (Bosman et al., 2005; Green et al., 2012; Cawthra et al., 2012a); and recently off the South Coast (this study). The morphology and relief of the shelf banks/shoals on the shelf of Mossel Bay (Figure 4-6) suggest that they represent submerged coastal dunes (barriers). The previously studied barriers (see Chapter 2) on the South African coastal plain and continental shelf are dominated by aeolian facies. Mobile dunes on a coastal plain are commonly linear in form, trending vaguely parallel to the coastline. Parabolic dunes (Pye, 1983; Tinley, 1985) are also observed along the South African coastline. Parabolic dunes are 'u' shaped with the leeward nose of sediment transport oriented in a downwind direction. Resulting trailing arms lengthen as the dunefields migrate and extend. The u-shaped features annotated on the multibeam bathymetry in Figure 4-6 are interpreted to be parabolic dunes and indicate a SW prevailing wind direction.

4.4.4 Low-relief ridges

Narrow, slightly elevated sections of seafloor with characteristic elongate, tightly spaced, contours of decreasing depth, were observed in the northeast region of the mapped area (Figure 4-7). These ridges (part of Acoustic Facies b) are commonly expressed as shore-parallel oriented linear outcrops on the seafloor and reach a maximum relief of only 1.5 m. They are interpreted to be submerged palaeoshorelines, based on the orientation, lateral dimensions and relief. The palaeoshorelines are relatively open and linear, similar to the modern Mossel Bay coastline.

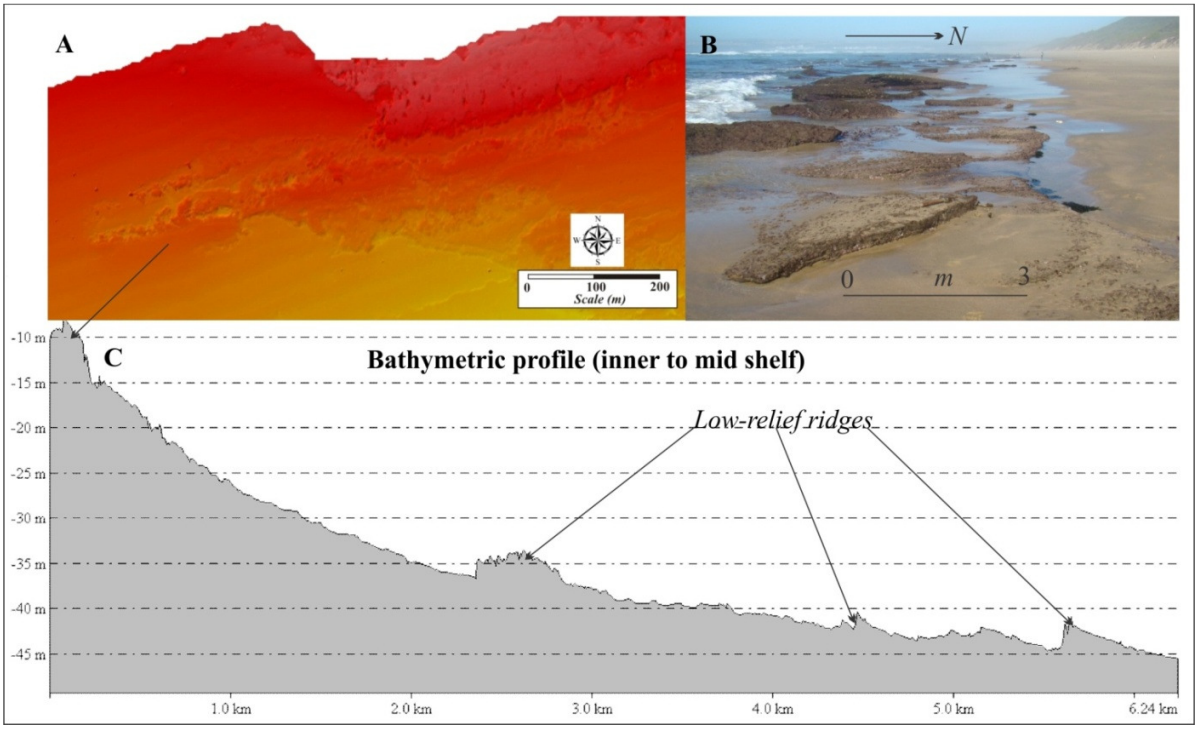

Figure 4-7. A. Multibeam bathymetry showing an example of a low-relief ridge in the Mossel Bay study area. B. Modern analogue environment is the present rocky shoreline of the Mossel Bay embayment. C. Vertically-exaggerated (8x) bathymetric cross section oriented perpendicularly to the coast.

4.4.5 Incised valleys

Although described in detail in Chapter 5, one prominent incised valley on the Mossel Bay shelf is also exposed at the seafloor surface and is observed on the DEM and facies interpretation of the side-scan sonar mosaic (Figure 4-3, Figure 4-8). The offshore terrain in the vicinity of the Groot Brak River indicates a meandering and migrating river system in this section of the fluvial profile with associated bank and levee deposits. The incision, as well as the subsequent sedimentary infill, (Acoustic Facies f and g) are recognised surficially as the Groot Brak River palaeochannel. The incised channel is asymmetrical (Figure 4-8).

In the case of a meandering river (after Miall, 1997), the dominant flow of the channel is directed away from the bank (e.g. on the inside of a meander) and as surface flow impinges onto the outer bank, the result is cutbank erosion. Return-flow passes obliquely up the bed of the inner bank and substantial sedimentation occurs as the bank accretes. Interpreted features of bank accretion are visible on Figure 4-9. Sediment removed from the cutbank is incorporated into the sediment load of the river and large blocks deposited form a channel lag with the fines being deposited into bedforms and bars. These features are also visible on the resolution provided by the multibeam bathymetric dataset in Figure 4-8. The width to depth ratio of the Groot Brak channel (500:4.5 m) at a

depth of 35 m BMSL is 111, which is considered 'moderate' after Schumm (1985). In this case, rivers tend from meandering toward braided form and may be associated with alluvial fan distribution (Miall, 1997).

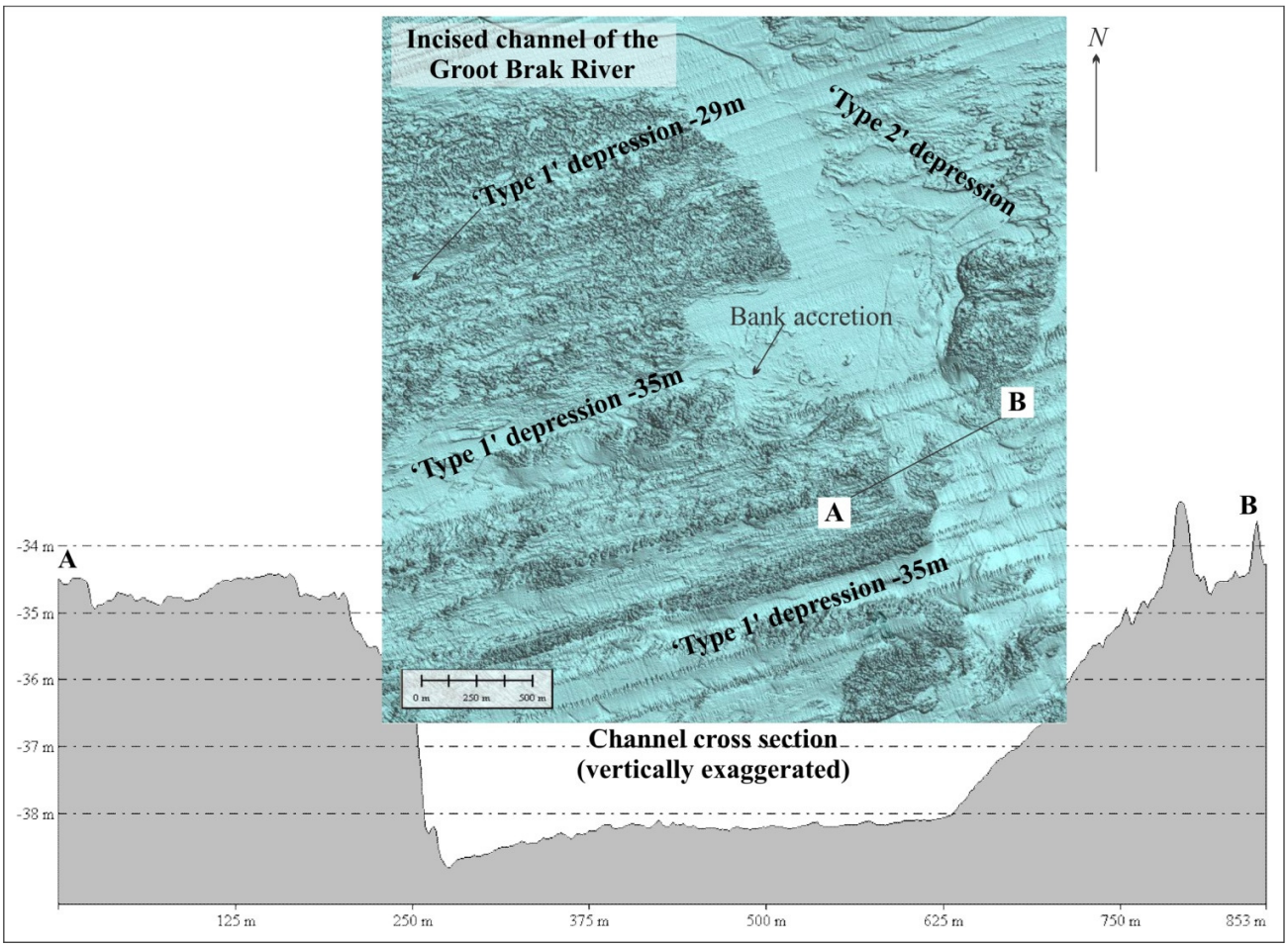

Figure 4-8. DEM showing the drowned palaeochannel of the Groot Brak River offshore Mossel Bay. The smooth sediment infilling the incised channel has a smooth texture compared to the adjacent rocky seafloor. The depth range is 30 – 36 m BMSL. A-B shows a vertically exaggerated (8x) cross section through the bathymetry.

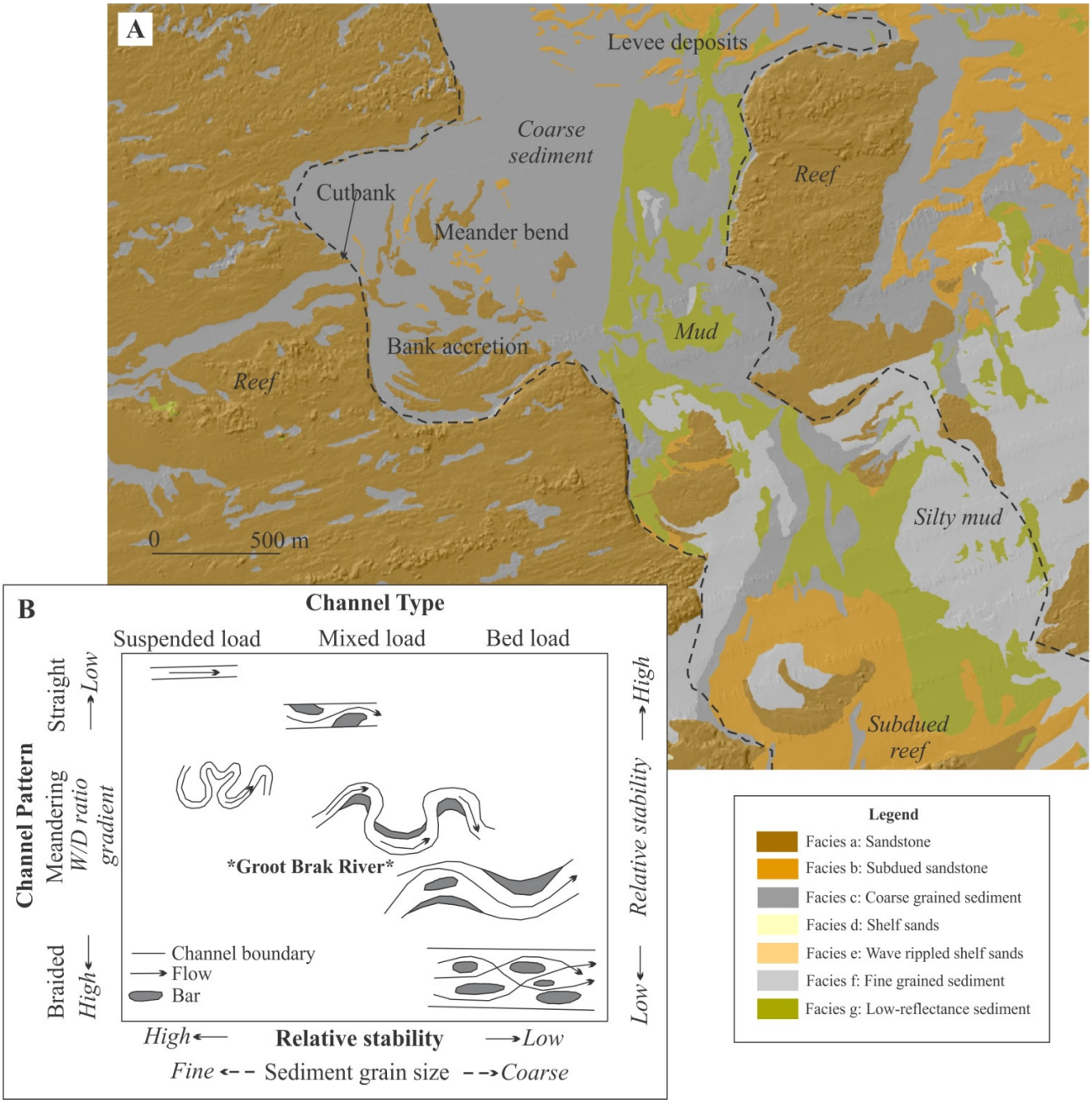

Figure 4-9. A. Notable fluvial features observed within the palaeochannel of the Groot Brak River, plotted on the interpreted side-scan sonar mosaic and showing association of Acoustic Facies. B. Model for the river channel form (modified from Schumm, 1985 and Miall, 1997).

4.4.6 Seafloor depressions

Two different forms of seafloor depression were mapped in the study area, named here as 'type 1' and 'type 2' for clarity. Adjacent to the incised valley off the Groot Brak River, three 'type 1' depressions on the western side

of the multibeam bathymetric inset of Figure 4-8 are elongate, coast-parallel oriented features of 1400 x 150 m, 2500 x 400 m and 850 x 150 m in dimension from the most landward, to the most seaward. These depressions occur at depths of 29 m and 35 m BMSL respectively, with both seaward features lying at the same elevation, and they are bounded at their landward and seaward margins by low-relief ridges and a shelf banks or shoals. In the west the features terminate where they shallow, and in the east, they terminate against the incised valley of the Groot Brak. The close association of these 'type 1' depressions and the shelf banks/shoals allowed these systems to be interpreted to represent drowned coastal barrier systems, with the depression being reminiscent of the low-energy back-barrier area of sedimentation. The Wilderness Embayment back-barrier lagoons are bounded by mid- to late Quaternary barriers (Bateman et al., 2004; 2011). In Still Bay the present coastal plain is characterised by a comparable model of sedimentation, though the barriers are volumetrically smaller than at Wilderness and the lagoons are absent (Roberts et al., 2008). These two locations provide suitable analogues for the submerged back-barrier environments offshore of the Groot Brak River.

The occurrence of 'type 2' depressions is associated with a sediment bedform field identified both on the DEM and side-scan sonar mosaic (labelled on Figure 4-3) and is characterised by elongate areas of coarse sediment (Acoustic Facies c) exposed in an area dominated by smooth shelf sands (Acoustic Facies d). The exposed sediment ribbons (classed according to the nomenclature of Ashley, 1990) are oriented vaguely perpendicular to the dominant swell and wave direction, and facies associations suggest that they expose a basal surface underlying the shelf sands. The surface of the 'type 2' depression is up to 0.6 m lower than the surrounding shelf sands and the elongate exposed sections reach up to 700 m in length with an average width of 50 m. The measured orientation of the sediment ribbons is NNW-SSE within the 'bedform field' labelled on Figure 4-3. East of the incised channel of the Groot Brak River (Figure 4-8), is an exposed 'type 2' depression trends E-W and NE-SW.

4.4.7 Shelf Sediments

The smooth nature of the inner shelf (Figure 4-1) supports the presence of sedimentary deposits. The sediment is rippled (Acoustic Facies e) adjacent to the cliffed coast. Where developed, these ripples are oriented coast-parallel and reach amplitudes of 0.5 m with a typical wavelength of approximately 3 m. These ripples generally display a symmetrical form and are interpreted to be shaped by wave action, following the Ashley (1990) classification of sedimentary bedforms.

4.5 Contemporary seafloor sediments

4.5.1 Characteristics of the sediments

The sediments in the mapped area were classed into five acoustic facies from side-scan sonar data and four sedimentary units as defined by samples obtained for the seafloor sampling programme (Figure 4-3, Table 4-1). These discrete facies include: coarse grained bioclastic sediment, medium-sand dominated shelf sands (in areas, wave rippled), silty mud and mud. As a composite group they constitute the Holocene sediment wedge (after Martin and Flemming, 1986). The distribution of carbonate within the offshore sediments is closely linked to the association with seafloor geological outcrops and modern river mouths where maximum carbonate reached 57 % (Figure 4-10; Appendix III). Vlees Bay is undernourished with respect to carbonate in comparison with the Mossel Bay embayment. Carbonate distribution is highest around the river mouths, which contrasts to the West Coast, where carbonate content tends to exhibit low values around river mouths due to dilution by quartz sand (Compton and Franceschini, 2005). The relatively low carbonate content in the marine sediments, despite high biological productivity in this region (Branch and Branch, 1992) may be attributed to these sands being dominantly relict and the carbonate largely leached during lowstands by meteoric waters.

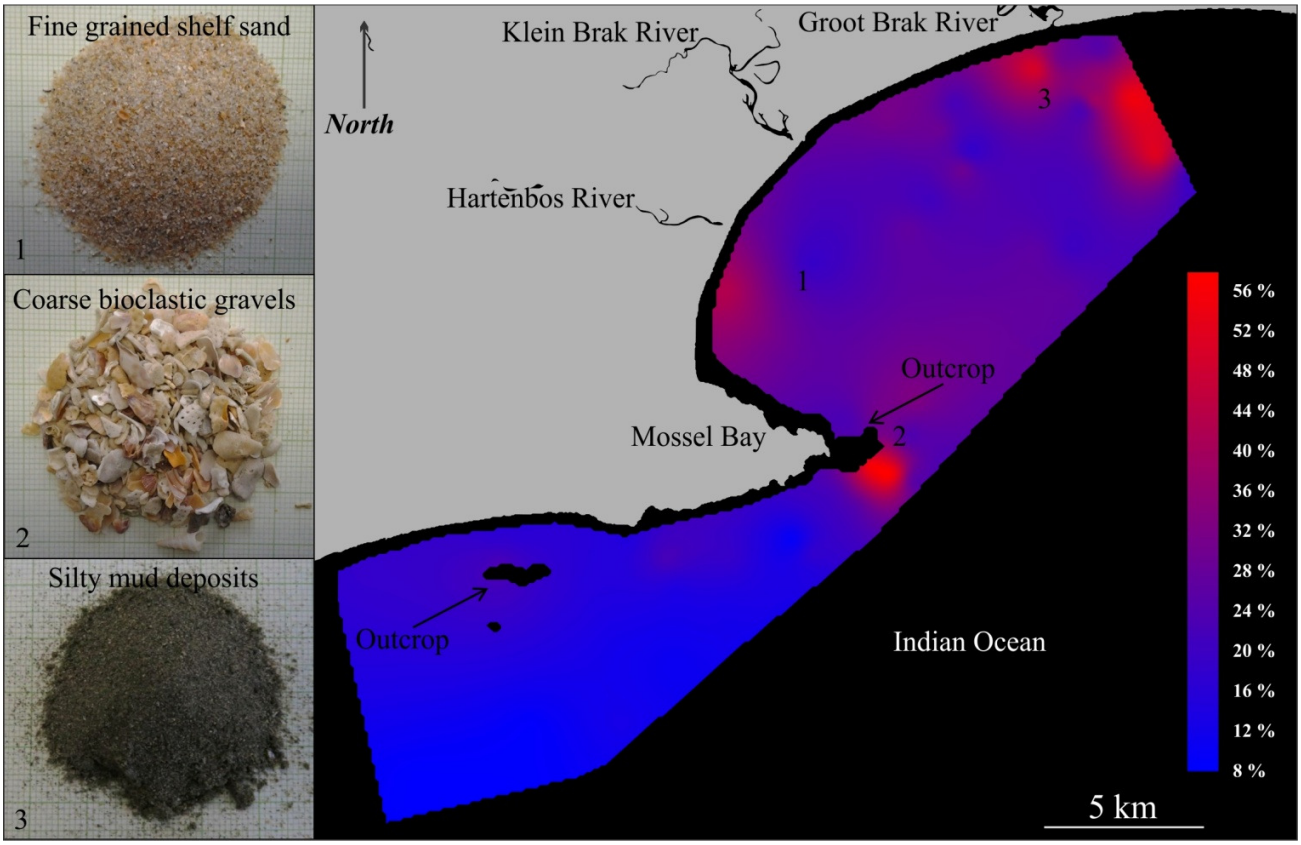

Figure 4-10. Carbonate distribution within the modern seafloor sediments of Mossel Bay. The three dominant types of seafloor sediments are shown on the left and their sample locations indicated on the map.

4.5.2 Discussion: seafloor sediments

Sediments of the South Coast generally tend to be trapped in the nearshore zone, forming an elongated sediment prism (De Decker, 1983). The general lack of terrigenous sediments on the South Coast shelf is attributed, in part, to the relative lack of fluvial input in the area (small rivers) as well as to winnowing of the fine fraction during Pleistocene eustatic sea-level fluctuations (Rogers, 1971), indicating that relict sediments dominate the South Coast middle and outer shelf (De Decker, 1983). From the textural characteristics of the side-scan sonar and multibeam echosounder datasets, this margin can be classed as sediment starved. The unconsolidated sediment deposits on the shelf are a likely source of beach and dune material to facilitate substantial beaches during lowstand conditions, so the available sediment is an important consideration. The thin drape of relatively coarse sediment is thought to be either a result of sediment starvation, or a lack of accommodation space. Wigley and Compton (2006) argue for Pliocene uplift on the West Coast that has contributed to reduced accommodation space and erosion on the margin, but the South Coast is generally said to have experienced normal uplift and erosion through the Neogene (Erlanger et al., 2012), so a relative lack of mobile sediment is proposed to explain the distribution of unconsolidated sediments in this study.

4.6 Cemented Quaternary units

For this study, consolidated Quaternary deposits cropping out along the Mossel Bay rocky intertidal zone and continental shelf were mapped in detail. Where luminescence dates were not obtained, the relative ages were derived from field relationships to the samples dated for this work and to the raised Roberts et al. (2012) MIS 11 sequence exposed in Mossel Bay landward of this study area and at an elevation of ~13 m AMSL. The shoreline and offshore deposits are treated seamlessly in this thesis, with the exception of the gap between the shoreline and inner continental shelf that is the surf zone. This section describes the facies, diagenesis and chronology and these are finally combined to enable interpretation of the Quaternary evolution of shoreline-associated units. The geological evolution of specific units in this area is presented chronologically in Chapter 6.

Five fundamental, yet different, elements are considered in the analysis of Quaternary deposits in this chapter. These include: (1) sedimentary facies, defined according to diagnostic sedimentological characteristics; (2) the carbonate cements that are responsible for the consolidation of the deposits; (3) geological units, consisting of cemented sedimentary facies contextualised in space and in time; (4) palaeoshorelines, expressed as one-dimensional, linear features; and (5) palaeo-coastal zones, constituting the area of active sedimentation associated with a palaeoshoreline and extending landward of that shoreline along a band of unchanged gradient.

4.7 Facies of Quaternary calcarenites deposited on ancient littoral zones

Eleven sedimentary facies (abbreviation: Sed. F.) of clastic shorelines are identified in the area and classified into discrete geological units depending on their relative ages and distribution.

1) Sed. F. 1

This facies (Figure 4-12A) typically consists of relatively high-angle planar cross beds. Foresets range in thickness from 2 – 10 cm and dip at the angle of repose of medium sand, from 16° to 37°, averaging approximately 20°. The constituent clasts of facies 1 comprise well-rounded, well sorted, fine- to medium grained sand of quartzose-feldspathic, and carbonate composition (Figure 4-14A). In places, thin layers of coarse material containing a biofabric of imbricated shell fragments lie conformably with the bedding. There is evidence for minor surficial dissolution on outcrops and sections of Sed. F.1 deposits are slightly rubified.

2) Sed. F. 2

Sed. F. 2 is characterised by trough cross-stratified, well rounded sediments dominated by gravels and interbedded sandy laminae, and containing a high percentage of imbricated calcareous bioclasts (Figure 4-12B; Figure 4-14B). The hummocky bedding indicates a seaward–landward oriented direction of palaeocurrent flow and internal stratification is convex-upward.

3) Sed. F. 3

Sed. F. 3 is (Figure 4-12C) interpreted as a well-layered, cobble-supported polymict conglomerate indicating no clear imbrication/preferred orientation of clasts. The lithoclasts are extraformational and were possibly derived from the underlying Mesozoic deposits in the area. The pebbles and cobbles consist of sub- to well-rounded Table Mountain Group Sandstone and vein quartz, as well as well-rounded Kaaimans Formation shale. Within the sandstone matrix, the particles are very coarse sand to granule sized and angular shell fragments are imbricated (Figure 4-14C).

4) Sed. F. 4

Tightly packed, crudely stratified beds of boulders, cobbles and pebbles of the same lithoclasts which constitute the cobble conglomerate (Sed. F. 3) fill eroded potholes along the intertidal zone (Figure 4-12D). This unit, in places, is preserved above the surface elevation of the substrate when the pothole rims have been eroded and the perched infill facies remains.

5) Sed. F. 5

Sed. F. 5 forms a massive deposit of medium- to coarse sand (Figure 4-12E). Constituent clasts are generally moderately sorted and are composed predominantly of quartz, with marine molluscs and minor feldspar (Figure

4-14D). Thick bands and thinner laminations of heavy minerals characterise this facies and intense bioturbation is observed in the stratigraphically lower sections. Stratification is evident where layers are distinct from under- and overlying strata with respect to texture. Distinct boundary planes separate these zones. The parallel beds range in thickness from ~5 – 25 cm and dip seaward between 2° and 12°.

6) Sed. F. 6

Sed. F. 6 (Figure 4-12F; Figure 4-14E) consists of tabular seaward-dipping pebble- and cobble matrix supported conglomerates with a well-sorted matrix of medium- to coarse sand. Layering within the primary structure is planar and beds dip gently seaward. The clasts comprise the same materials as Sed. F. 3, but also including a dominance of calcarenite lithoclasts. The planar beds range from 20 – 30 cm in thickness and there is no distinct contact to differentiate between Sed. F. 5 and Sed. F. 6; the two have a gradational contact.

7) Sed. F. 7

Intraclasts of aeolianite (Figure 4-13A) derived from nearby outcrops reach dimensions of up to 2.5 m along the long axis, are generally oriented seaward, and scatter the region surrounding the western side of the Klein Brak River mouth. These deposits are blanketed in a cemented coarse-sand/gravel matrix (Figure 4-13B) and are interpreted to be indicative of storm-wave erosion. The matrix of Sed. F. 7 consists of large, angular bivalves and a coarse lag of other shell debris among well rounded pebbles within a moderately sorted matrix of quartz and feldspar-rich sand.

8) Sed. F. 8

This facies of bivalves in a sandy matrix is welded onto the underlying aeolianite and upper shoreface deposits in distinct clusters (Figure 4-13C) which reach a diameter of 60 – 80 cm with a thickness of up to 40 cm. The dominant species is thought to be *Ostrea atherstonei* based on the length and form of these bivalves.

9) Sed. F. 9

Sed. F. 9 (Figure 4-13D) consists of clasts of coarse- to very coarse sand and granules. This facies is very poorly sorted and contains a high percentage (~40 %) of imbricated shell fragments. The grain morphology ranges from well-rounded to angular and bed thicknesses from 30 – 70 cm. Tabular beds dip gently seaward (5° to 8°) and the deposits have subdued topography and low-relief.

10) Sed. F. 10

These finely bedded planar units consist of poorly sorted coarse sand and compositionally variable bedding (Figure 4-13E). Pebbles, large shell fragments and other carbonate/skeletal grains, as well as very coarse sand form layered beds but the constituent clasts are not imbricated, and show little evidence of a preferred

orientation. Sed. F. 10 fills erosional gullies and drapes aeolianite and other basal lithologies with a sharp contact.

11) Sed. F. 11

Sed. F. 11 (Figure 4-13F) crops out on the western bank of the mouth of the Klein Brak River (~3 m AMSL) and on the seafloor at a depth of 35 m BMSL. The onshore locality is presently situated within the trough of an active dune and, as a result, the facies is mostly buried. These poorly sorted deposits are composed of organic and sedimentary material with a high percentage of imbricated bioclasts (Figure 4-14F; Figure 4-14F). Sed. F. 11 is generally partly consolidated.

4.7.1 Interpretation of the sedimentological facies

The broad classifications of beach environments of Elliott (1986), Coe and Church (2003) and Nichols (2009), summarised in Figure 4-11, were combined to create what the author felt was the most appropriate representative profile for Mossel Bay and this was applied throughout the interpretations in this study. For specific further classification of the samples obtained in the study area, reference samples were collected from the modern beach of Reebok (Figure 1-2; Appendix I) to compare the sedimentology of crushed rock samples and constrain the most accurate possible environments of deposition for this part of the coast.

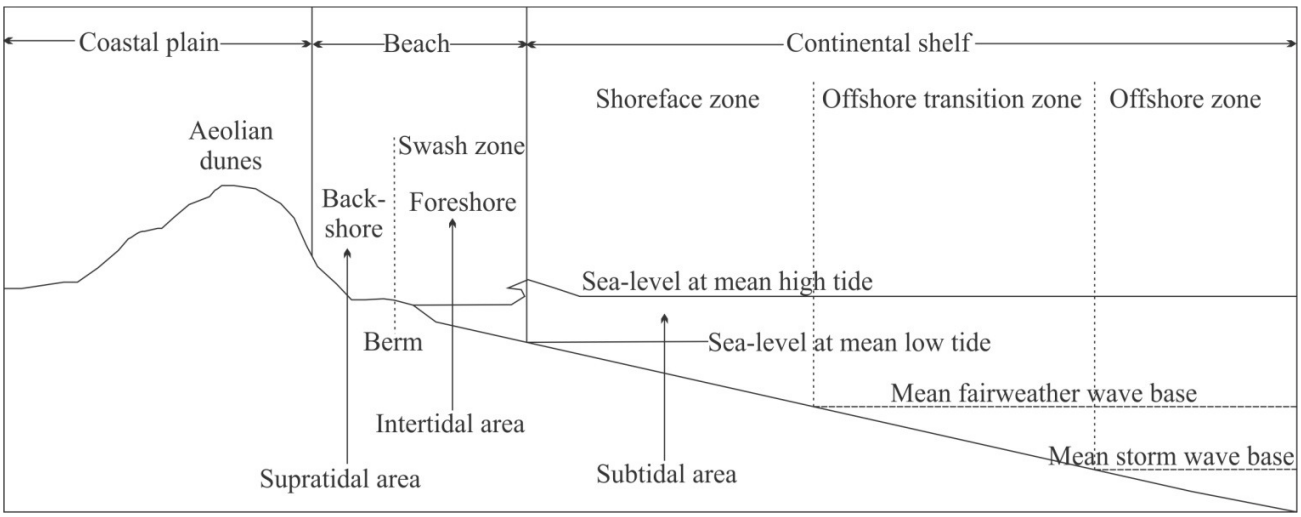

Figure 4-11. Classification of the sedimentological zones of a typical clastic shoreline. Synthesised and modified from Elliott (1986), Coe and Church (2003) and Nichols (2009).

The 11 lithofacies identified in this study are correlated to environments of deposition associated with sedimentation on the littoral zone (Table 4-3). A sedimentary facies is defined as a package of sedimentary material characterised by a specific combination of lithology, sedimentary characteristics, physical and

sometimes biological features which is distinguishable from other sedimentary units (Walker, 1992). For the purposes of this thesis, the sedimentary facies divisions are established based on lithology, colour, sediment constituents, particle size and structures. The spatial and temporal recurrence of discrete sedimentary units that possess many of these characteristics in common facilitated the subsequent division of the stratigraphic record into geological units. From a sedimentological viewpoint and based on compositional analysis, dominant grain size, modal abundance of constituent grains and presence of interstitial carbonate in these deposits, all facies can be classified as calcarenite (as per the definition of Grabau, 1904).

Table 4-3. Interpreted environments of deposition for the sedimentological facies described above.

Sedimentological facies	**Facies interpretation**	**Characteristics**
Sed. F. 1	Aeolianite	High-angle planar cross beds, well sorted, fine- to medium grained sand.
Sed. F. 2	Upper shoreface	Trough cross-stratified, well rounded sediments dominated by gravels and interbedded sandy laminae, high percentage of imbricated calcareous bioclasts.
Sed. F. 3	Cobble conglomerate	Well-layered, cobble-supported polymict conglomerate, lithoclasts are extraformational.
Sed. F. 4	Palaeo-pothole fill associated stratigraphically with the cobble conglomerate	Tightly packed, crudely stratified beds of boulders, cobbles and pebbles.
Sed. F. 5	Foreshore	Massive deposit of medium- to coarse sand, moderately sorted, thick bands and thinner laminations of heavy minerals.
Sed. F. 6	Cobble conglomerates associated stratigraphically with the foreshore	Tabular seaward-dipping pebble- and cobble matrix supported conglomerates, well-sorted matrix of medium- to coarse sand.
Sed. F. 7	Storm deposits	Intraclasts of aeolianite, cemented coarse-sand/gravel matrix.
Sed. F. 8	*In situ* subtidal oyster beds	Bivalves in a sandy matrix.
Sed. F. 9	Beachrock	Coarse- to very coarse sand and granules, very poorly sorted, imbricated shell fragments.
Sed. F. 10	Beach deposits: swash/shallow nearshore	Finely bedded planar units, poorly sorted coarse sand, compositionally variable bedding.
Sed. F. 11	Back-barrier deposits	Poorly sorted deposits, of organic and sedimentary material.

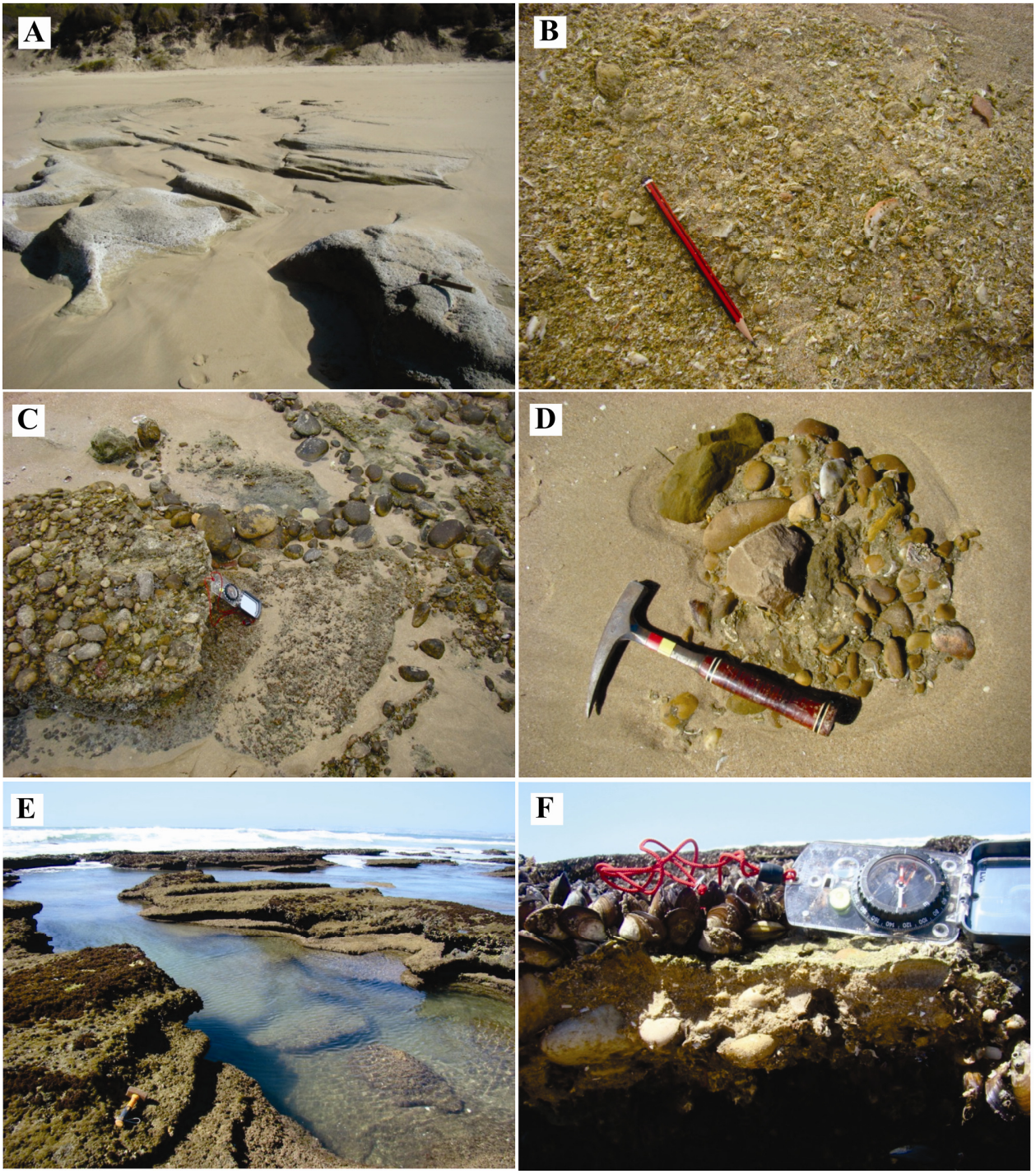

Figure 4-12. Sedimentary facies 1 - 6 – examples from the Mossel Bay shoreline. A. Aeolianite/ Sed. F. 1. B. Upper shoreface deposits/ Sed. F. 2. C. Cobble conglomerate/ Sed. F. 3. D. Palaeo pothole-fill/ Sed. F. 4. E. Foreshore deposits/ Sed. F. 5. F. Foreshore cobble conglomerate/ Sed. F. 6.

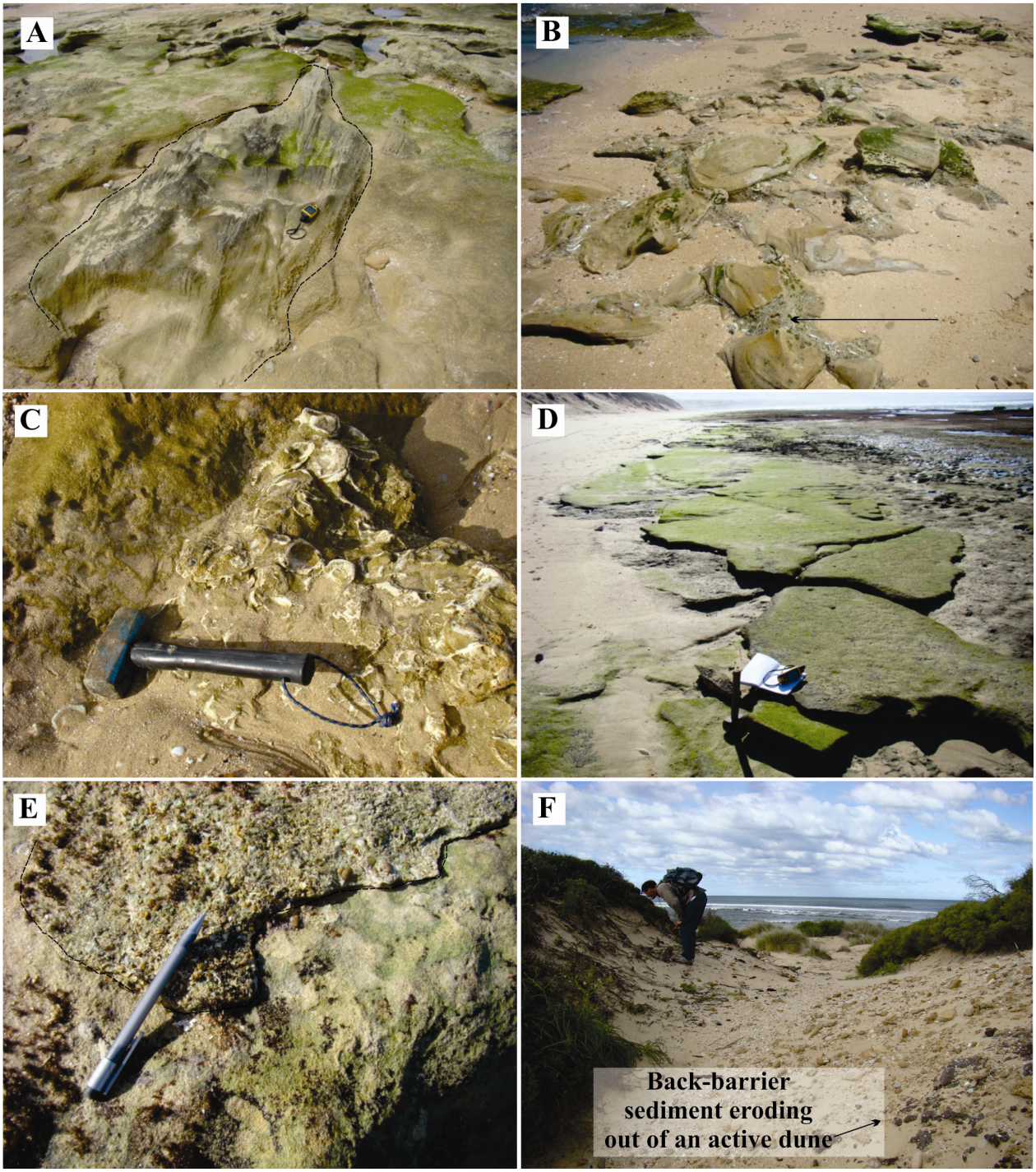

Figure 4-13. Sedimentary facies 7 - 11 – examples from the Mossel Bay shoreline. A. Storm-derived blocks (marked by the stippled line). B. Associated storm lag deposits/ Sed. F. 7 denoted by the arrow. C. In situ palaeo oyster beds/ Sed. F. 8. D. Beachrock/ Sed. F. 9. E. Coarse-grained swash deposit/ Sed. F. 10 (marked by the stippled line). F. Back barrier deposits/ Sed. F. 11.

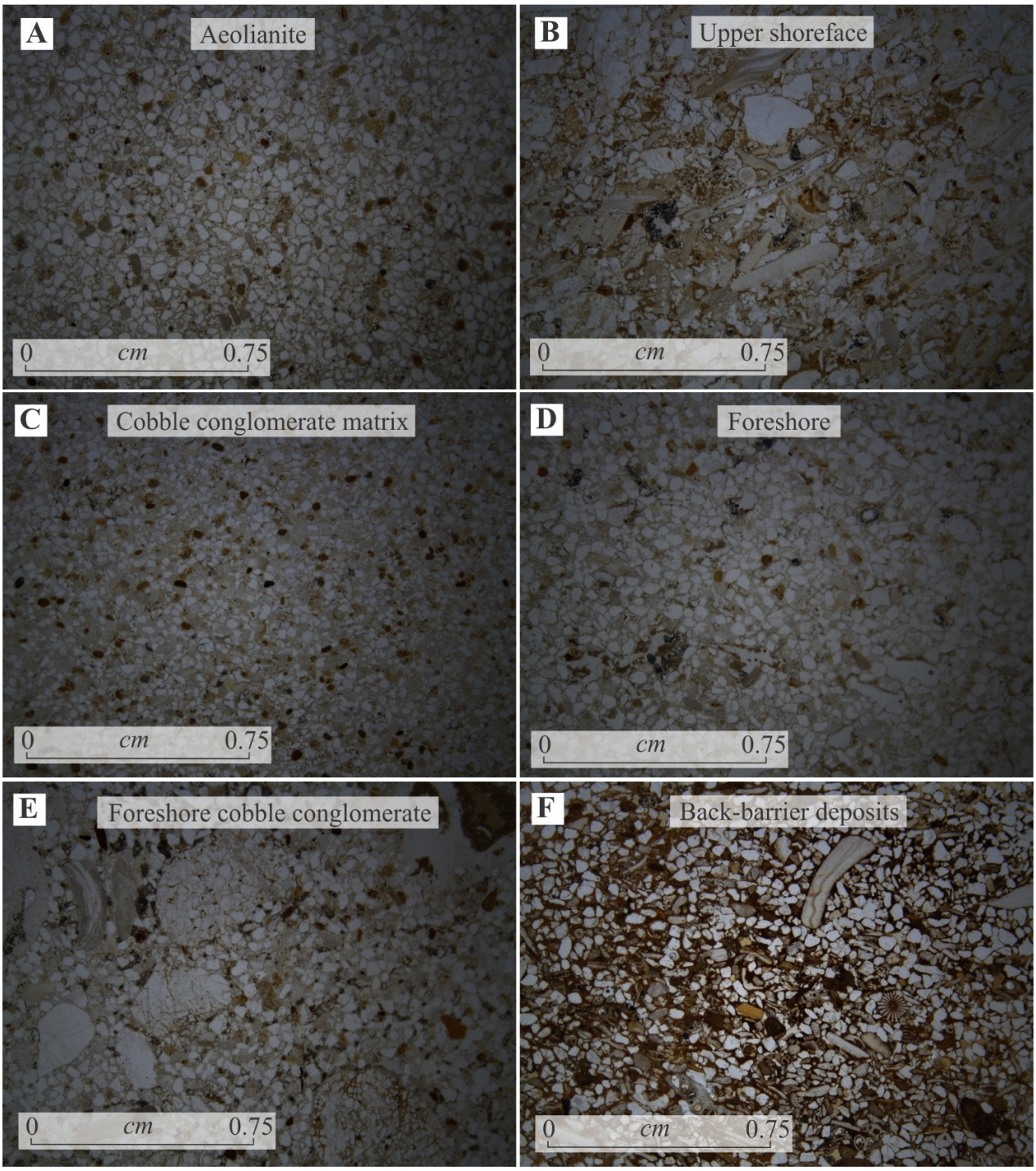

Figure 4-14. Photomicrographs showing the matrix characteristics of selected sedimentary facies (Sed. F. 1, 2, 3, 5, 6, 11) under a binocular microscope.

4.8 Carbonate diagenesis

4.8.1 Diagenetic features

The carbonate cements within the Quaternary deposits are composed exclusively of LMC, as revealed by SEM-EDS analysis (Figure 4-15). The LMC cements occur in six main morphologies, namely: (1) cryptocrystalline coatings, (2) isopachous prismatic rims, (3) dogtooth spar, (4) microspar mosaics, (5) pseudo-pelloidal aggregates, (6) radial aggregates (Figure 4-16; Figure 4-17). Other cements include authigenic clays, occurring in two forms, and a mixed carbonate-organic matrix. The physical arrangement of constituent clasts, including texture and structure (e.g. Figure 4-14), forms a primary sedimentary fabric that has in many cases influenced the subsequent diagenesis of these deposits. The diagenetic cements comprise three general types: (1) envelopes surrounding grain boundaries in the form of microcrystalline crystals forming meniscus layers or occurring as replacement in the groundmass filling voids (Figure 4-16), (2) cements consisting of crystals growing from a substrate into a pore space (e.g. fibrous, dogtooth forms) (Figure 4-16) and (3) pore filling cements characterised by crystals increasing in size toward the centre of the void (e.g. blocky calcite spar) (Figure 4-17).

1) Cryptocrystalline coatings

These high-reflectance rims form a thin carbonate band lining grain boundaries and lack discernible structure under transmitted light microscopy. This cement also presents as a meniscus cement, connecting adjacent grains and rounding off pore spaces (Figure 4-16B). This facies is directly precipitated around grain boundaries of both carbonate and siliciclastic clasts and is interpreted to be micrite, characterised by a crypto- to micro-crystalline texture (after Folk, 1959). These coatings were classified under high magnification transmitted light petrography and SEM. The cryptocrystalline coatings are most abundant in beach deposits near the land-sea interface and likely formed in the marine-vadose environment.

2) Isopachous microcrystalline cement (micrite) rims

These rims are developed around grain boundaries but are more visibly defined than the cryptocrystalline rims in terms of textural characteristics. Under transmitted light, a dominantly prismatic crystal form can be identified (Figure 4-16C, D). This cement phase is thought to be indicative of precipitation in the marine vadose environment.

3) Fibrous cement rims

Interpreted to have initially precipitated as aragonite needles, fibrous cements surround grain boundaries of rounded litho- and bioclasts and line pre-existing grain coating cements in the study area (Figure 4-16E, F). The long axes of crystals generally propagate perpendicular to grain surfaces. In the fibrous cement, crystals form a network of needles. Precipitation most likely occurred in the marine phreatic zone and more specifically, the

upper subtidal or lower intertidal zones. Partially dissolved aragonite needles seen under SEM indicate the likelihood of a later influence of fresh water. These generally represent the first generation of marine cement where identified and have been subsequently replaced by LMC.

4) Dogtooth calcite

The crystal boundaries of dogtooth calcite rims are clearly defined and there is a sharp contact between calcite spar and grain boundaries (Figure 4-16G, H). The crystal form is generally scalenohedral and elongate rhombohedral with blunt edges and a length:width ratio of ~3:1. Dogtooth cement is not strictly indicative of meteoric conditions because it has also been recorded in marine-phreatic zones by Reinhold (1999). The composition is LMC and no evidence for alteration was observed.

5) Calcite spar infill

A drusy to blocky equant calcite spar mosaic, here referred to as calcite spar, represents pore infilling in intergranular and interskeletal pores (Figure 4-17C, D). This cement is also associated with geopetal infilling of shell chambers. Crystal size increases towards the centre of the void, suggesting a drusiform crystal habit. In the meteoric phreatic zone, below the water table, pores are filled with water and large crystals dominate the cement (Flügel, 2004). This cement therefore suggests near-surface meteoric environments.

6) Microspar mosaics

This microcrystalline or micrite cement refers to a fine grained calcite matrix and with closer inspection (through SEM) is seen to be characterised by uniform size distribution. As a groundmass in these samples, the microspar has a fine grained texture and the crystal form is equant. This diagenetic feature is distributed in irregular masses in pore spaces (Figure 4-17E, F).

7) Authigenic smectite

Authigenic clays (Figure 4-17A, B) occur in two dominant diagenetic phases in the study area. Firstly, the alteration of rims at grain boundaries is generally associated with feldspar and lithic clasts in the deposits and was noted in select geological units. The mechanism for formation is interpreted to be the breakdown of the actual grain surfaces and subsequent alteration into authigenic clay minerals. These rims are displayed as a brown layer under plane polarised light and almost isotropic under crossed polarisers. These discontinuous envelopes are variable in thickness and where present, occur as the earliest diagenetic phase. Secondly, authigenic smectite is also associated with widespread pore-filling. In this case, the abundance is strictly related to the geographic location of the sample within a geological unit rather than being preferentially associated with a specific type of deposit or sedimentological lithofacies. SEM-EDS analysis indicated the composition of this

material to likely be smectite, as peaks of Si, Al, Mg and Fe were noted with additional Ti in select samples (Figure 4-15).

8) Carbonate-organic mixed matrix

This cement (Figure 4-17G, H) consists of carbonate, siliciclastic mud and organic material mixed in different proportions. In plane-polarised light, this material presents a brown colour, while under crossed polarisers, evenly dispersed points of high birefringence colours occur in an almost opaque mass.

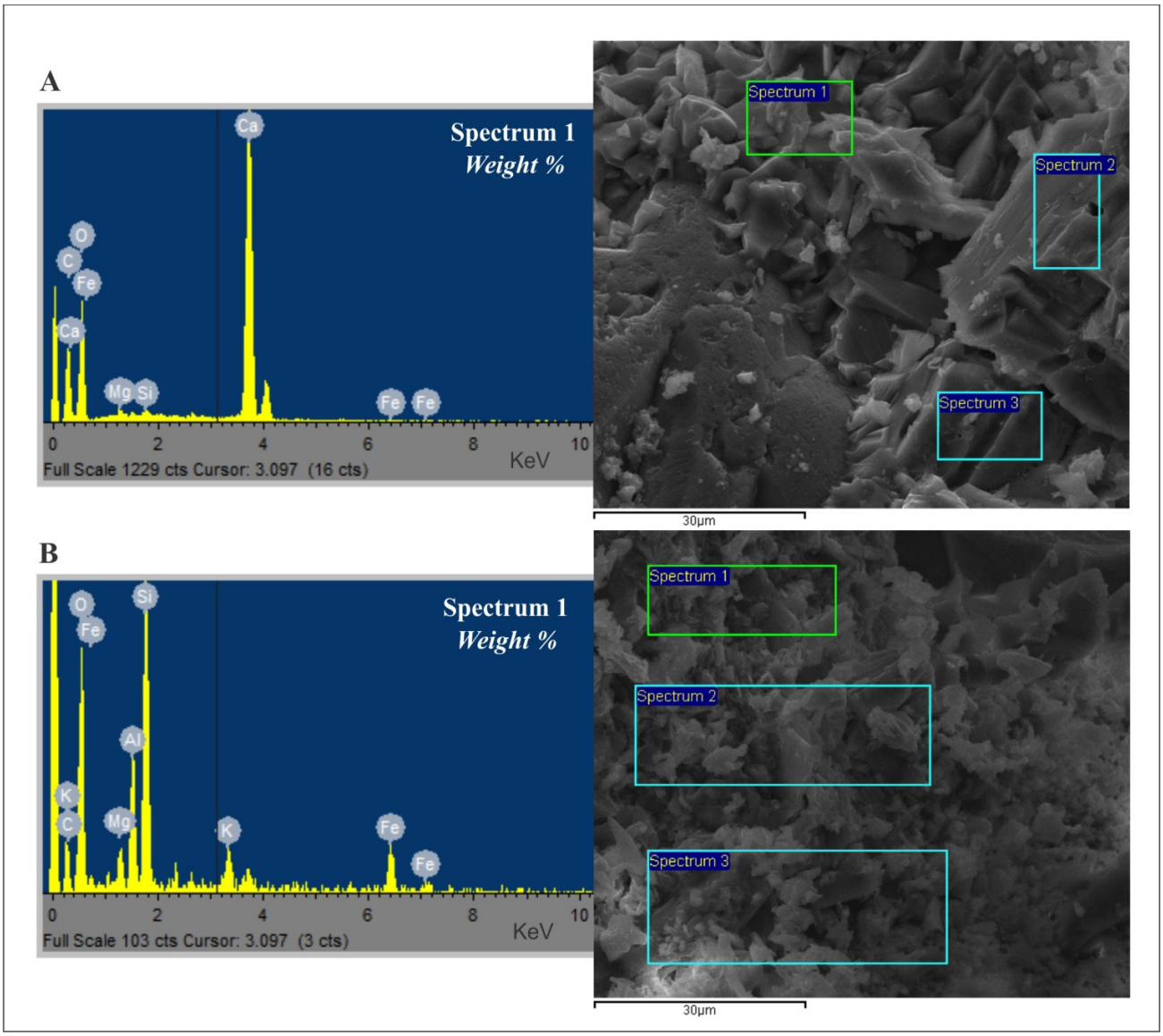

Figure 4-15. SEM-EDS plots showing elements present and relative distribution as a weight percent. A. LMC isopachous rim cement. B. Authigenic smectite dominated matrix.

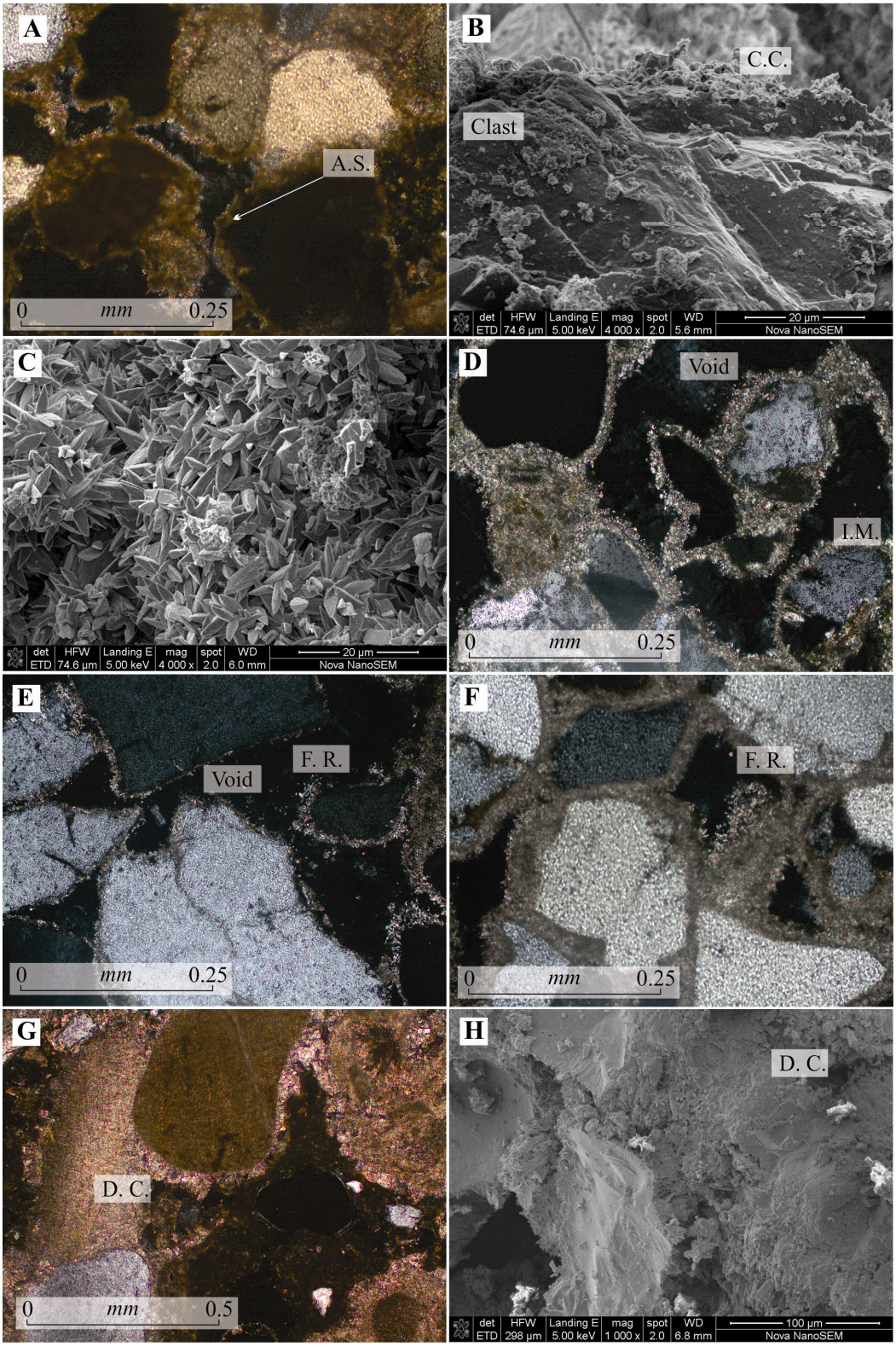

Figure 4-16. Transmitted light- and SEM microscopy showing the grain boundary diagenetic cements of the Mossel Bay deposits. A. Authigenic smectite (A.S.) rims. B. Cryptocrystalline coatings (C.C.) on a grain boundary. C, D. Isopachous micrite (I.M.) rims. E, F. Fibrous rims (F.R.). G, H. Dogtooth calcite (D.C.) rims.

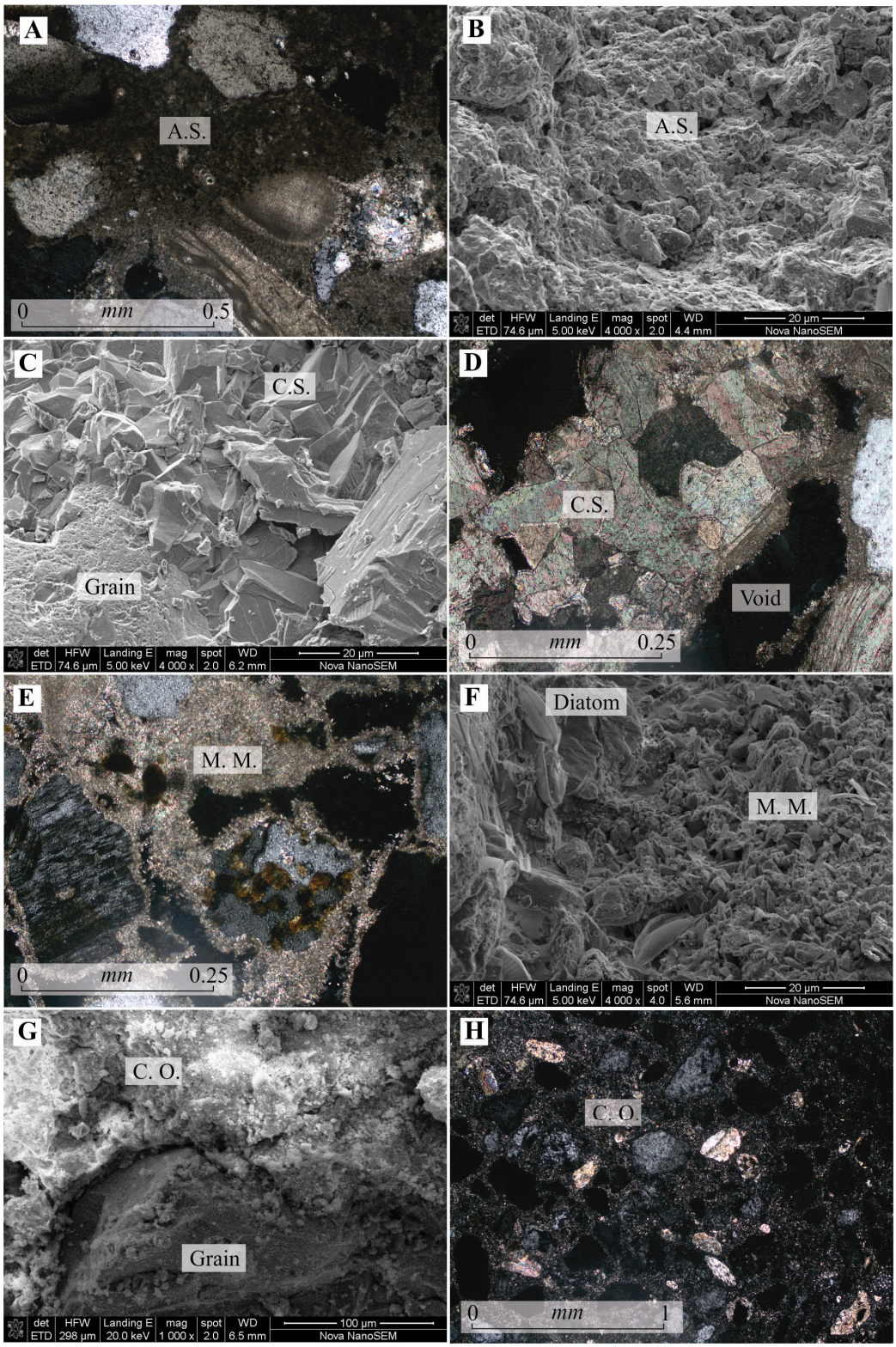

Figure 4-17. Transmitted light- and SEM microscopy showing the pore infilling diagenetic cements of the Mossel Bay deposits. A, B. Authigenic smectite (A.S.) infill. C, D. Blocky calcite spar (C.S.) infill. E, F. Microspar mosaics (M.M.). G, H. Carbonate-organic (C.O.) mixed matrix.

4.8.2 Carbonate minerals

The carbonate minerals forming the cements in the Quaternary deposits were identified under transmitted light microscopy and SEM-EDS, where relative abundances of mineral phases were determined in selected representative samples.

1) Aragonite

Complete or partial aragonite moulds have subsequently been filled with calcite cement or transformed to LMC by simultaneous volume-for-volume dissolution of aragonite and precipitation of calcite. Skeletal aragonite is indicative of a near-surface, fresh water, diagenetic process (Flügel, 2004).

2) The lack of Mg-calcite (HMC)

Modern marine inorganic Mg-calcite cements form mainly in warm low-latitude waters, supersaturated with respect to calcium carbonate (Flügel, 2004). No diagenetic phases in the study area contain HMC. As the Mg/Ca ratio of Mg calcites varies according to the Mg^{2+}/Ca^{2+} ratio and water temperature, with colder water carbonates generally having less Mg. HMC is rarely preserved in the geological record as exposure of HMC to meteoric water leads to rapid dissolution and eventual complete replacement by stable LMC. This has been calculated to take in the order of hundreds to thousands of years (Richter, 1979 in Flügel, 2004). Therefore with the dominance of relatively old Quaternary deposits in Mossel Bay, and the prevalence of cold seawater, it is not unexpected that this carbonate mineral is not present.

3) Calcite (LMC)

Low-Mg calcite is considered a stable carbonate phase with little tendency to alter, but dissolution-cementation processes do occur (Flügel, 2004; Figure 4-15). Low Mg/Ca ratios of meteoric water facilitate the precipitation of LMC in meteoric environments. LMC is shown in Figure 4-20A.

4.8.3 Available carbonate in the system

When compared to the modern reference samples analysed for this work, the carbonate abundance during MIS 5 seemed most comparable to the modern situation with a net loss of carbonate suggested for MIS 11 and a net abundance of carbonate during this system during MIS 6 (Table 4-4). In general, the South Coast exhibits a relatively low carbonate environment when compared to the East Coast (Cooper and Flores, 1991; Cawthra and Uken, 2012; Bosman, 2012), yet the South Coast samples contain more biogenic carbonate.

Table 4-4. Carbonate percentages derived for the geological samples, compared to modern reference material.

Geological unit	Facies	Age	Percentage carbonate	Modern reference sample	Percentage carbonate
H 2	Back-barrier deposit	MIS 1	57.4 %	-	-
H 1	Aeolianite	MIS 1	59.8 %	Ref 1 (dune)	21.64 %
Pu 13	Aeolianite	MIS 3	-	Ref 1 (dune)	21.64 %
Pu 12	Back-barrier deposit	MIS 3	-	-	-
Pu 11	Back-barrier deposit	MIS 3	49.6 %	-	-
Pu 10	Aeolianite	MIS 5a	-	Ref 1 (dune)	21.64 %
Pu 9	Beachrock	MIS 5a	-	Mean of Ref, 4 Ref 5, Ref 7 (swash zone)	47.20 %
Pu 8	Aeolianite	MIS 4	31.9 %	Ref 1 (dune)	21.64 %
Pu 7	Aeolianite	MIS 5a	-	Ref 1 (dune)	21.64 %
Pu 6	Foreshore	MIS 5c	39.8 % (mean of 3 samples)	Ref 3 (foreshore)	33.25 %
Pu 5	Aeolianite	MIS 5d	35.2 % (mean of 3 samples)	Ref 1 (dune)	21.64 %
Pu 4	Upper shoreface	MIS 5e	42.9 % (mean of 5 samples)	Ref 15 (surf zone)	94.41 %
Pu 3	Foreshore	MIS 5e	59.3 % (mean of 3 samples)	Ref 3 (foreshore)	33.25 %
Pu 2	Aeolianite	MIS 5e	45.7 % (mean of 4 samples)	Ref 1 (dune)	21.64 %
Pu 1	Foreshore	MIS 5e	37.8 % (mean of 16 samples)	Ref 3 (foreshore)	33.25 %
Pu 1	Foreshore: conglomerate facies	MIS 5e	27.6 % (mean of 3 samples)	Mean of Ref 8, Ref 9 (beach cusp)	61.56 %
Pu 1	Foreshore: swash facies	MIS 5e	40.0 % (mean of 6 samples)	Mean of Ref, 4 Ref 5, Ref 7 (swash zone)	47.20 %
Pm 18	Beachrock	MIS 5e	43.8 % (mean of 2 samples)	Mean of Ref, 4 Ref 5, Ref 7 (swash zone)	47.20 %
Pm 17	Aeolianite	MIS 6	52.1 %	Ref 1 (dune)	21.64 %
Pm 16	Aeolianite	MIS 6	-	Ref 1 (dune)	21.64 %
Pm 15	Aeolianite	MIS 6	45.8 % (mean of 4 samples)	Ref 1 (dune)	21.64 %
Pm 14	Foreshore	MIS 6	48.3 %	Ref 3 (foreshore)	33.25 %
Pm 13	Aeolianite	MIS 6	56.50 % (mean of 2 samples)	Ref 1 (dune)	21.64 %
Pm 12	Foreshore	MIS 6	69.40 %	Ref 3 (foreshore)	33.25 %
Pm 11	Aeolianite	MIS 6	39.2 %	Ref 1 (dune)	21.64 %
Pm 10	Foreshore	MIS 6	-	Ref 3 (foreshore)	33.25 %
Pm 9	Upper shoreface	MIS 7	29.9 %	Ref 15 (surf zone)	94.41 %
Pm 8	Aeolianite	MIS 7	-	Ref 1 (dune)	21.64 %
Pm 7	Aeolianite	MIS 11	36.0 % (mean of 5 samples)	Ref 1 (dune)	21.64 %
Pm 6	Conglomerate	MIS 11	42.2 % (mean of 4 samples)	Ref 6 (swash conglomerate)	47.62 %
Pm 5	Storm deposits	MIS 11	49.2 % (mean of 3 samples)	Ref 13	58.76 %
Pm 4	Subtidal oyster bed	MIS 11	-	-	-
Pm 3	Upper shoreface	MIS 11	48.2 % (mean of 9 samples)	Ref 15 (surf zone)	94.41 %

Pm 2	Aeolianite	MIS 15	36.0 % (mean of 7 samples)	Ref 1 (dune)	21.64 %
Pm 1	Foreshore	MIS 15	47.7 %	Ref 12 (foreshore adjacent to Klein Brak River)	40.48 %

4.8.4 Association of organic matter and coastal deposits

'Black lithoclasts' is the name given to distinctive blackened carbonate clasts present as depositional microfacies, which are described in Holocene, and Pleistocene deposits in Florida, Bermuda, the Persian Gulf and the Great Barrier Reef by Beach and Ginsburg (1980) and Montenat (1981). In this study they are recorded in rocks deposited in intertidal and subtidal environments and are believed to form in laterally migrating tidal channels or sub-aerial mudbanks near the coast. They are therefore associated with organic muds (Figure 4-18; Table 4-5).

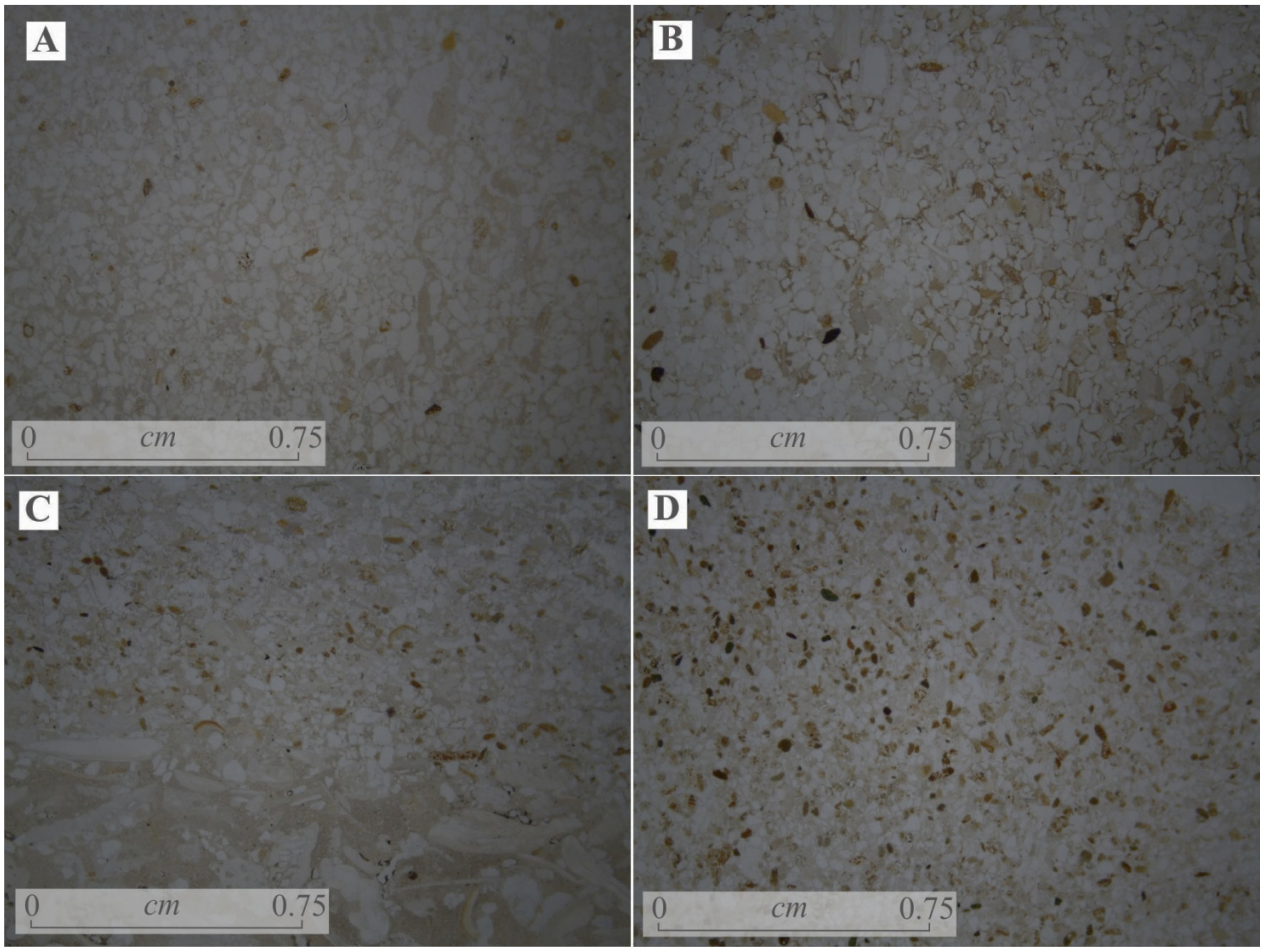

Figure 4-18. Black lithoclasts shown under a binocular microscope, according to relative abundance, and distribution along the Mossel Bay coastline. A. None present. B. Minor occurrence (<5 %). C. Moderate occurrence (5 - 20 %). D. Abundant occurrence (≥20 %).

Table 4-5. Summary of the distribution of geological facies in the study area according to elevation above, or depth below, MSL. 0 MSL indicates the present intertidal zone. The relative abundance of black lithoclasts listed is based on a minor abundance being <5 %, moderate abundance 5 - 20 % and abundant being ≥20 %.

Geological unit	**Sedimentary facies/depositional environment**	**Present elevation of occurrence**	**Presence and abundance of black lithoclasts**
H 2	Back-barrier deposit	~3 m AMSL	Abundant
H 1	Aeolianite	~3 m AMSL	Abundant
Pu 13	Aeolianite	?	Unit not seen in thin section
Pu 12	Back-barrier deposit	29 m BMSL	Unit not seen in thin section
Pu 11	Back-barrier deposit	35 m BMSL	Absent
Pu 10	Aeolianite	?	Unit not seen in thin section
Pu 9	Beachrock	?	Unit not seen in thin section
Pu 8	Aeolianite	38 m BMSL	Absent
Pu 7	Aeolianite	?	Unit not seen in thin section
Pu 6	Foreshore	25 m BMSL	Minor
Pu 5	Aeolianite	35 m BMSL	Minor
Pu 4	Upper shoreface	17 m BMSL	Moderate to abundant
Pu 3	Foreshore	26 m BMSL	Minor
Pu 2	Aeolianite	0 MSL	Abundant near the Klein Brak River mouth, decreases to being absent from 2 km to the west
Pu 1	Foreshore	0 m MSL	Abundant near the Klein Brak River mouth, absent from 1 km to the east until 2 km west of the Groot Brak River where present again in minor concentrations, grading eastward into moderate
Pu 1	Foreshore: conglomerate facies	0 m MSL	Minor
Pu 1	Foreshore: swash facies	0 m MSL	Minor
Pm 18	Beachrock	0 m MSL	Absent
Pm 17	Aeolianite	30 m BMSL	Minor or absent
Pm 16	Aeolianite	?	Unit not seen in thin section
Pm 15	Aeolianite	30 m BMSL	Absent
Pm 14	Foreshore	30 m BMSL	Moderate to abundant
Pm 13	Aeolianite	32 m BMSL	Moderate to abundant
Pm 12	Foreshore	36 m BMSL	Moderate to abundant
Pm 11	Aeolianite	34 m BMSL	Moderate to abundant
Pm 10	Foreshore	?	Unit not seen in thin section
Pm 9	Upper shoreface	12 m BMSL	Moderate
Pm 8	Aeolianite	?	Unit not seen in thin section
Pm 7	Aeolianite	0 - 10 m AMSL	Minor; absent in most samples
Pm 6	Conglomerate	0 m MSL	Absent
Pm 5	Storm deposits	0 m MSL	Minor
Pm 4	Subtidal oyster bed	0 m MSL	Unit not seen in thin section
Pm 3	Upper shoreface	0 - 10 m AMSL	Minor
Pm 2	Aeolianite	0 m MSL	Abundant near the Klein Brak

			River mouth, minor or absent at all other localities
Pm 1	Foreshore	0 m MSL	Minor

4.8.5 Interpreted diagenetic environments

Analysis of the sampled consolidated Quaternary deposits in thin section indicate deposition in aeolian, transitional marginal marine (shorelines) and shallow marine environments with subsequent cementation in the meteoric and vadose diagenetic zones (Figure 4-19). The precipitation of carbonate minerals and biogenic materials has occurred in primary and secondary pores. In the study area, the carbonate diagenesis that took place in the dune environment and along the shoreline is not always contemporaneous with the deposition of the sediments. Samples tend to indicate multiple phases of cementation, as the units were exposed to repeated fluctuation of Pleistocene sea level. SEM-EDS investigations revealed the prevalence of only one carbonate mineral (calcite), present in the low-Mg calcite (LMC) form. Low Mg and high Mg calcite are generally separated by a value of 1.5 – 7.8 mol % $MgCO_3$ (Gunatilaka and Till, 1971). For this study, the values were converted from weight percent (as derived from SEM-EDS) to mole percent to determine the type of calcite present. In addition to cementation by calcite, red/brown material interpreted to be alteration of authigenic clays forms a prominent matrix incorporated with carbonate. One studied unit from a back-barrier environment is characterised by a dominantly organic matrix. Carbonate diagenesis is dependent on various factors, including the lower and upper tidal elevations on the shoreline, the depth of wave base, occurrence of thermoclines, salinity, and photic zones of biological productivity (Flügel, 2004). The Mossel Bay Quaternary deposits generally typify burial diagenesis in the shallow burial zone (i.e. the first few metres below the surface). No evidence for deep burial was detected in this study.

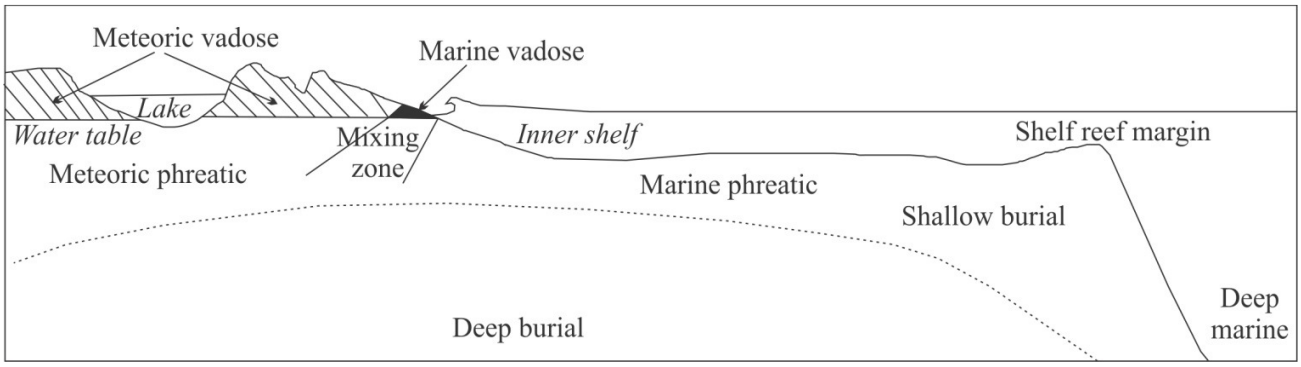

Figure 4-19. Diagenetic environments applied to the interpretations in this study (modified from Flügel, 2004).

1) Meteoric (freshwater) diagenesis

Meteoric diagenesis commences with the loss of Mg from HMC, followed by the replacement of aragonite by calcite. This process occurs in the meteoric vadose zone, the meteoric phreatic zone and the shallow sub-surface (Figure 4-19), and is characterised by the mixing of fresh and salt water. In the vadose zone, water is concentrated at grain contacts and in the phreatic zone water fills the pores (Flügel, 2004). Meteoric cements are therefore generally characterised by LMC and dissolution of biogenic carbonate as well as formerly beach-precipitated cements. Blocky and granular mosaic fabrics completely fill voids.

2) Mixing zone (marine vadose environment) diagenesis

The interaction of waters with different chemistries occurs in this diagenetic zone and this generally takes place on beaches and in the shoreface (Flügel, 2004). The resulting cementation is the precipitation of aragonite. Cementation is rapid and beachrocks commonly originate. In addition to the precipitation of these cements, the mixing zone is also responsible for the subsequent dissolution of carbonate rocks on coasts. Marine-vadose cements in this study are characterised by fibrous relict textures.

4.8.6 General diagenetic sequence observed in Mossel Bay

The sedimentary deposits in the study commonly exhibit a complex diagenetic history, related to post-depositional sea-level fluctuations. Specific timing of the precipitation of the cements described here is considered in further detail in Chapter 6, but a general sequence can be traced. The cements can be classed into early (grain bound) diagenetic features and later (pore-filling) diagenetic features, associated with precipitation in both beach and dune littoral environments. As a general rule, the alteration of select grain boundaries into authigenic clay minerals was the first diagenetic event. This suggests significant exposure of the deposits prior to the onset of diagenesis and cementation. If present, cryptocrystalline coatings at grain boundaries were the second diagenetic event to occur in the general sequence. The cementation of deposits in Mossel Bay and on the adjacent shelf that occurred along a shoreline can be subdivided further into two diagnostic environments: within a beach-barrier island-lagoon system, and a beach-strandplain setting (after the models of Reinson, 1984 and Tucker and Wright, 1990). Most carbonate cemented deposits in the latter environment are dominated by skeletal grainstones (beachrock and aeolianite) where the lagoonal sediments, which are sites of fine-grained sediment deposition, are characterised by mudstone/packstone clasts. Constituent clasts of the beach-strandplain deposits tend to be initially cemented at the grain boundaries, followed by subsequent pore infilling.

1) Aeolianite

The palaeodune deposits of aeolianite, associated with initial cementation in the meteoric diagenetic environment, show a strong association with rims of dogtooth calcite (Figure 4-16G) and extensive pore infilling

by blocky calcite spar (Figure 4-17C, D), which in places infill the voids directly from the grain boundaries. The infiltration of authigenic smectite may have been contemporaneous with the precipitation of the calcite spar infill, depending on the source of overlying material, as the authigenic smectite is interpreted to have co-precipitated with the calcite. Late-stage dissolution of the existing pore-infilling cements resulted in the occurrence of microspar mosaics.

2) Foreshore and nearshore (beach environment)

The general diagenetic sequence of foreshore, intertidal and nearshore deposits commenced with an initial isopachous or fibrous micrite rim cement (Figure 4-16E) with later void infilling characterised by the presence of authigenic smectite, blocky calcite spar and microspar mosaics as described above.

3) Back-barrier, low energy environment

The precipitation of carbonate minerals is controlled by physiochemical conditions in the system and is accelerated by biological factors (e.g. organic matter) present in the carbonate cements (Leinfelder, 1987). Organic matter has been found on grain surfaces and in pores and was identified here primarily in back-barrier deposits. In addition to the cementation by mixed carbonate with existing organic matter, the offshore back-barrier deposit contains isopachous micrite, dogtooth calcite rims coating grain boundaries and late stage microspar mosaics overprinting the dominant carbonate-organic cement. The onshore back-barrier deposit, lying adjacent to the mouth of the Klein Brak River (Figure 4-17H), is characterised by an early diagenetic phase of micrite rims.

4.8.7 Discussion: carbonate diagenesis

The most commonly documented cements of beach deposits are isopachous rims of aragonite needles and/or micritic Mg calcite (e.g., Ginsburg, 1953; Alexandersson, 1972; Vieira and de Ros, 2006) and in a South African context, these have been described throughout the Late Quaternary and Holocene by Cooper and Flores (1991), Cawthra and Uken (2012) and Bosman (2012). Meteoric diagenesis is relatively well constrained (Flügel, 2004) but despite decades of debate, the mechanisms controlling the mineralogy and crystalline habit of marine carbonate cements remains poorly understood (Vieira and de Ros, 2006). The variability has been ascribed to parameters including the concentration of Mg^{2+} (Folk, 1974), temperature (Morse and Mackenzie, 1990), salinity (Zhong and Mucci, 1989), partial pressure of CO_2 (Burton and Walter, 1991), presence of organic compounds (Kitano and Hood, 1965; Berner et al., 1978), and the participation of bacteria (Neumeier, 1999).

The cements generated in this study area are characterised by freshwater LMC (dogtooth calcite spar, blocky caltcite spar; Figure 4-15, Figure 4-16, Figure 4-17) and marine phreatic micrite and aragonite (isopachous and

fibrous rims, microspar mosaics) later altered to LMC by diagenesis upon exposure. It is proposed that marine phreatic diagenesis in Mossel Bay was initially associated with HMC but that this phase is poorly represented as a result of most of it being recrystallized as LMC over time. The remaining crystal forms are thus indicative of micrite phases, but the compositional analysis derived from SEM-EDS attest to the subsequent alteration to LMC. A change from vadose to marine phreatic conditions facilitated the precipitation of aragonite cement in the cases where micrite rims are followed by fibrous cement. Because aragonite is metastable and susceptible to diagenesis it has, in all cases observed here, been replaced by LMC (Flügel, 2004). The stability of marine carbonates has been summarised into a generalised ranking as follows: dolomite > calcite > Mg-calcite (<12 mole % $MgCO_3$) > aragonite > very high Mg Calcite (>12 mole % $MgCO_3$) and for meteorically influenced carbonates: calcite > aragonite > High-Mg calcite (Flügel, 2004). In this area all carbonates are of the LMC form, typical of a cool temperate environment (Flügel, 2004).

The microspar mosaics originate from recrystallisation of existing micrite in the vadose zone (Flügel, 2004). Microspar can be precipitated in a variety of littoral settings, including intertidal beachrocks and shallow seafloor environments and consequently is not a particularly reliable sea-level indicator. It is proposed that the *in situ* 'recrystallisation' that took place was from the calcite spar matrix cements.

Porosity is a prerequisite for diagenesis but the relative dominance of samples containing interparticle unfilled voids (Figure 4-20E) attests to a relatively low carbonate abundance in this system in comparison with studies on similar deposits at comparable elevations on the east coast (Cooper and Flores, 1991; Cawthra and Uken, 2012; Cawthra et al., 2012a; Bosman, 2012) where unfilled voids are uncommon compared to these Mossel Bay samples. This is thought to be associated with the amount of available carbonate in the system and a difference in climate and seawater temperature. Undersaturation of pore fluids with respect to carbonate has resulted in minor dissolution along boundaries of skeletal materials in these Mossel Bay samples, a phenomenon which is known to be effective in shallow and near-surface meteoric environments (Flügel, 2004).

The red colouration in the fine grained matrix of the authigenic smectite diagenetic phase is interpreted to be caused by small percentages of iron, likely Fe^{3+}, derived from hinterland weathering. The Fe^{3+} can be present as colloids or preserved on clay minerals, or associated with organic matter (Flügel, 2004). The proposed introduction of this material into the littoral zone may relate to transport via solution phases associated with compaction, as the coastal sediments in this area are characterised by common inter-granular voids. The mixing of clay minerals with carbonate is likely in the study area, given the prevalence of rubified palaeosols in the region (Figure 4-20G, H), which are notably preserved in the modern dunes at Suiderkruis on the western bank of the Groot Brak River mouth and in Vlees Bay to the west (Figure 1-2).

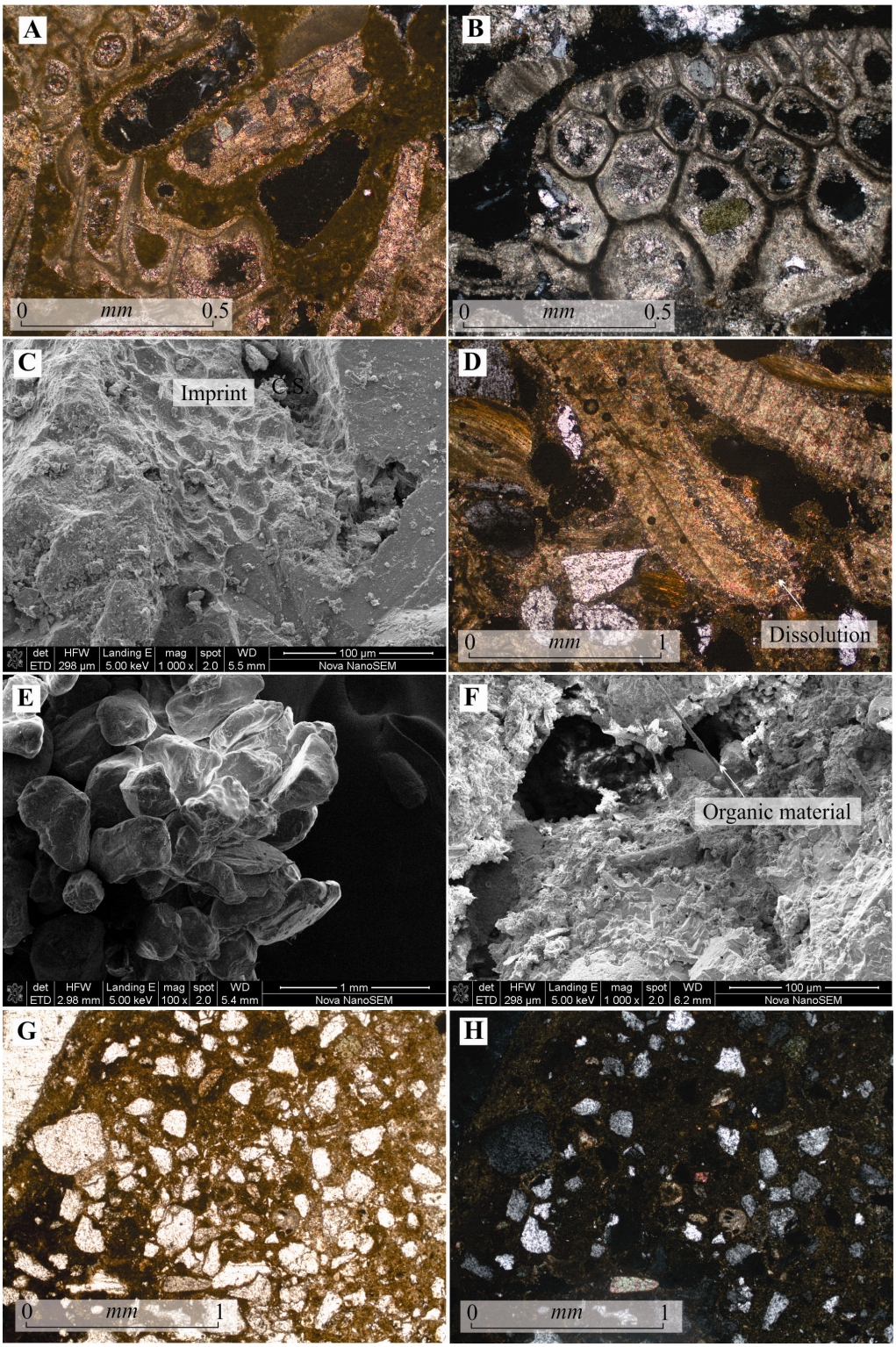

Figure 4-20. Select diagenetic features. A, B. Calcite infilling of shell chambers. C. Imprint of biological material imaged on SEM. D. Dissolution along the margin of a shell fragment. E. Cemented clasts showing the prevalence of voids. F. Organic filament in cement. G, H. Onshore coastal dune palaeosol sample seen under transmitted light as a reference to the palaeo record.

4.9 Geochronology and stratigraphic units

The 12 samples dated by OSL (Table 4-6; Figure 4-22) show a distribution in ages ranging from MIS 6 – MIS 3. The 11 sedimentary facies mapped and 8 diagnostic cements identified are used to define 33 geological units (Pm 1 – 18; Pu 1 – 13; H 1 - 2) according to field relationships, geochronological control, and correlations with existing onshore published work and stratigraphic datasets. The results are presented in Table 4-8 (an enlarged fold-out version is available in Appendix V) and a detailed spreadsheet of geochronological data is provided in Appendix II. These deposits are represented in Figure 4-22 and can be correlated with the Klein Brak- and Waenhuiskrans Formations of the Bredasdorp Group which dominate the Cenozoic geological record of the South Coast coastal plain (described in detail in Chapter 2). Units that were not dated are interpreted relative to the ones with geochronological control based on stratigraphic/field associations.

In approximate accordance with the nomenclature of the protocol of the CGS and the South African Commission for Lithostratigraphy (SACS), the geological units in this study are named with the prefix Pm *x* and Pu *x*, denoting Middle Pleistocene (*x* representing the numbered geological unit) and Upper Pleistocene (*x* representing the numbered geological unit). Prefix H indicates Holocene. The temporal divisions are based on the geological time scale of Haq (2007), which defines the Early – Middle Pleistocene boundary at 781 ka, the Middle – Late Pleistocene subdivision at 126 ka and the Late Pleistocene – Holocene boundary at 11.7 ka. Although the most detailed published CGS maps are generally presented on a scale of 1:50 000 and mapped on a scale of 1:10 000, the nature of this study necessitates the highest possible resolution level of detail to link facies and units to complex Quaternary sea level fluctuations.

Table 4-6. Results from luminescence dating. The 'refined age from the age model used' may be the same as the OSL age but considers the error range in conjunction with sedimentary environment of deposition and glacio-eustatic sea level. The uncertainy is defined by the sea level data.

Sample number	**Depth (metres relative to MSL)**	**OSL age (ka)**	**Depositional environment**	**Refined age from the age model used (ka)**
HC_37 (O37)	-12	206 ± 19	Upper shoreface	210± 15
HC_30 (O30)	-34	142 ± 12	Dune	142± 5
HC_26 (O26)	-33	138± 14	Dune	138± 5
HC_35 (O35)	-30	134 ± 13	Dune	134± 5
HC_36 (O36)	-30	125 ± 12	Dune	130± 5
HC_SH (SH)	0 (shoreline)	122 ± 15	Foreshore	122± 10
HC_29 (O29)	-35	122 ± 10	Dune	114± 8
HC_40 (O40)	-26	117 ± 11	Foreshore	118± 10
HC_32 (O32)	-17	115 ± 9	Upper shoreface	116± 10

HC_39 (O39)	-25	103 ± 8	Foreshore	98± 10
HC_24 (O24)	-38	87 ± 9	Dune	80± 5
HC_6 (O6)	-33	59 ± 6	Foreshore	62± 10

1) Sub-aerially exposed/shoreline units

Aeolianites

Four units of aeolianite are preserved along the shoreline of Mossel Bay (Units Pm 2, Pm 7, Pu 2 and H 1) (Figure 4-23). These, based on field relations to regionally dated outcrops and geochronological analysis (Table 4-8), are interpreted to have been deposited during MIS 15, 11, 5e and 1, respectively. The deposition of these aeolianites is associated with sea-level still-stands which periodically prevailed, allowing the available sediment of the coastal zone to mobilise into dunes on the palaeocoastlines. Although now only relatively small cores remain, these may reflect the relics of extensive dune systems on a now partially submerged coastal plain: the inner continental shelf. Units Pm 2 and Pm 7 are extensively planed by subsequent erosion by multiple post-depositional sea-level transgressions. The South Coast palaeowind vectors measured for this study on shoreline outcrops of aeolianite point to a dominance of northeasterly winds during MIS 15 and prevailing westerlies during MIS 11 and MIS 5e (Figure 4-21).

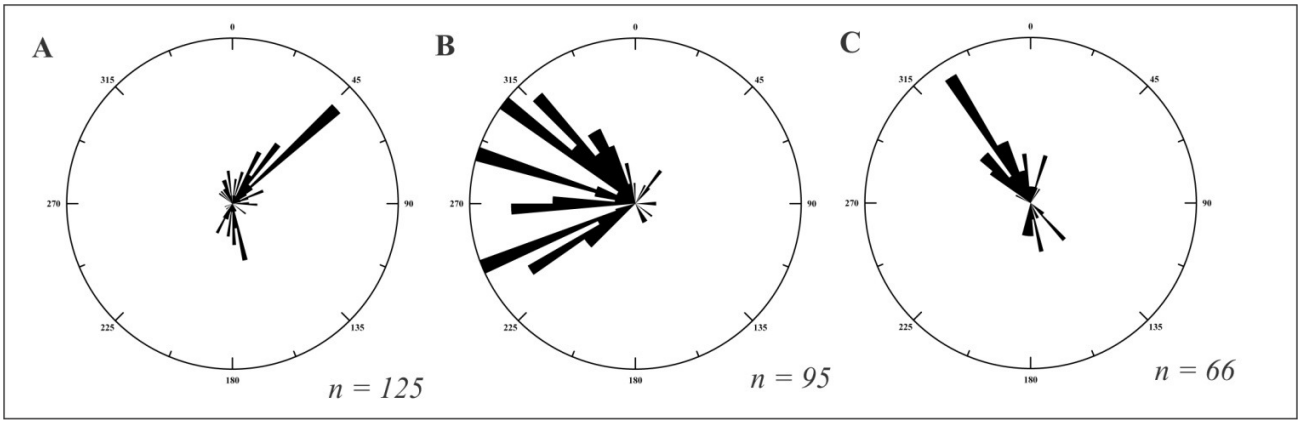

Figure 4-21. Wind roses constructed from strike readings obtained from the shoreline aeolianite units. A. Pm 2 (MIS 15 aeolianite). B. Pm 7 (MIS 11 aeolianite). C. Pu 2 (MIS 5e aeolianite). The strike readings were corrected to plot the direction from which the wind was blowing when the foresets were deposited. *n* signifies the number of readings taken for each unit.

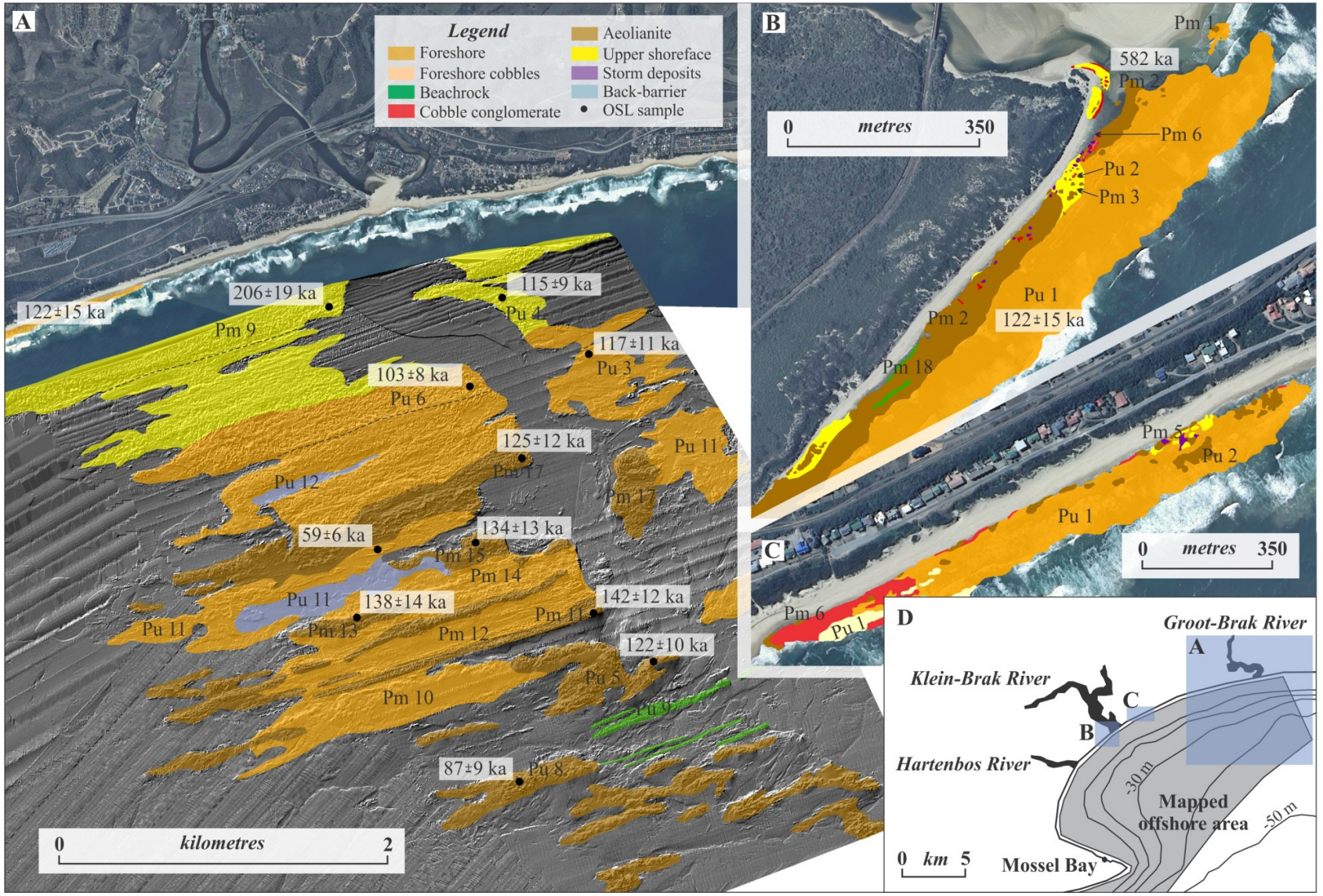

Figure 4-22. Spatial distribution of representative Pleistocene geological units on the Mossel Bay shoreline and adjacent continental shelf. These units are preserved only in the northeast section of the study area and at present shoreline elevation, only within the Mossel Bay embayment.

Beach deposits

Units Pm 1, Pm 5, Pm 6, Pm 9 and Pu 1 (Figure 4-22; Figure 4-23) were deposited on beaches, in the foreshore, and along swash zones. Some of these units (Pm 1, Pu 1) have been dated in the laboratory to MIS 15 and MIS 5e, respectively, whereas relative ages for the remaining ones are based on stratigraphic associations in the depositional record. Pm 1 and Pu 1 are foreshore deposits, characterised by a seaward-dipping profile. Sedimentological analyses suggest that the palaeo-beach environment at their times of deposition was comparable to the beach morphology seen today and consisted of a relatively gently sloping beach on a wave-dominated coastline. The resultant broad surf zone left behind a substantial foreshore deposit. In the vicinity of the Klein Brak River mouth (Pm 1) the foreshore rocks have thick accumulations of heavy minerals, possibly introduced and concentrated by the palaeo-drainage of this river system. The cobble conglomerate of Pm 5 suggests deposition in a high-energy environment and field relations suggest a likely provenance to be a regressive surface associated with the retreat of sea level from the transition from MIS 11 to MIS 10. Pm 6 (storm deposits) is thought to be associated with this sea-level regression and overprint pre-existing lithologies. Pm 18 is a unit of beachrock, deposited in an intertidal zone. This is interpreted to be remnant of the early MIS 5e sea-level transgression. A high-energy progradational shoreline constituting the Pu 1 foreshore facies and interfingering cobble conglomerate can be considered to be localised sections of the foreshore, comprising coarse deposits associated with high-energy cusps. The matrix-supported cobble conglomerate of Pu 1 thus laterally and stratigraphically correlates with the foreshore of MIS 5e. In addition, Pu 1 is associated with a facies interpreted to reflect deposition in a swash zone. This facies of unit Pu 1 is stratigraphically associated with the foreshore and no distinct contact allowed the separation of these facies. The swash deposits are composed of coarse-grained clasts and a high percentage of shell material. This part of the unit drapes underlying stratigraphy and fills existing erosional depressions, much like the tendency of the present swash-deposited sands in Mossel Bay.

Nearshore deposits

Units Pm 3 and Pm 4 (Figure 4-23) were deposited in the shallow nearshore. Pm 3 reflects sedimentation in the upper shoreface and Pm 4, subtidal oyster beds of *Ostrea atherstonei.* Pm 3 dips seaward and can be traced up the Klein Brak River to correlate with dated MIS 11 raised beach deposits dated by Roberts et al. (2012). Relative occurrence of Pm 4 allowed the inference of the MIS 11 age for this unit.

Back-barrier deposits

One back-barrier deposit (Unit H 2), interpreted to be remnant of the Holocene highstand, was mapped along the present coastal plain of Mossel Bay. H 2 crops out adjacent to the mouth of the Klein Brak River and lies at an elevation of approximately 3 – 4 m AMSL.

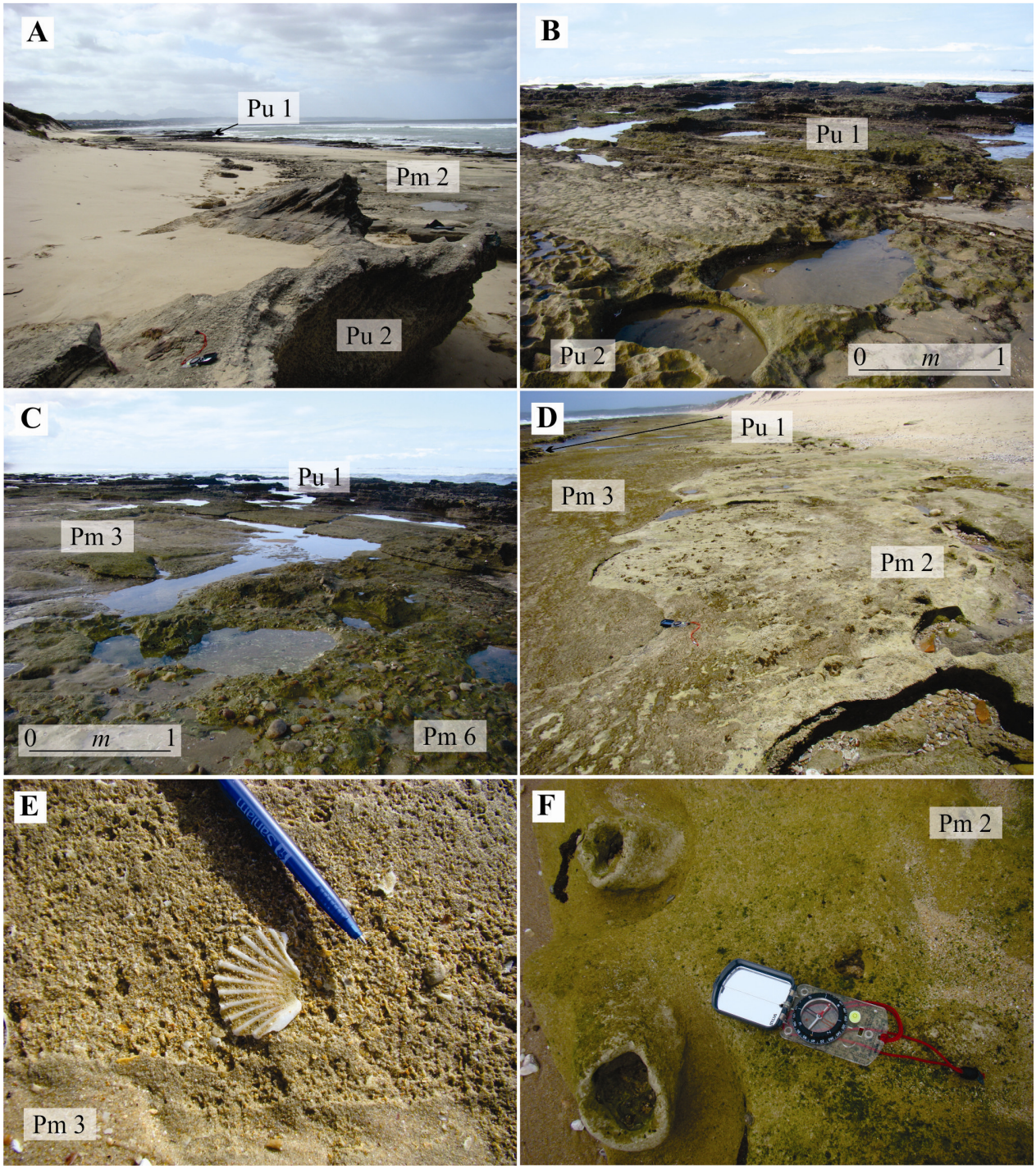

Figure 4-23. Photographs of shoreline units. A. Pm 2 (basal MIS 15 aeolianite), Pu 1 (MIS 5e foreshore deposits) and Pu 2 (MIS 5e aeolianite). B. Pu 1 (MIS 5e foreshore deposits) and overlying Pu 2 (MIS 5e aeolianite). C. Pm 3 (MIS 11 upper shoreface unit) overlain by Pm 6 (MIS 11 cobble conglomerate) and Pu 1 (MIS 5e foreshore deposits). D. Pm 2 (basal MIS 15 aeolianite), Pm 3 (MIS 11 upper shoreface unit) and uppermost Pu 1 (MIS 5e foreshore deposits). E. Bivalve in Pm 3 (MIS 11 upper shoreface deposit). F. Solution pipes in Pm 2 (MIS 15 aeolianite).

2) Submerged/offshore units

Although the offshore units appear more homogenous than those on the shoreline, this is likely a function of the detail allowed by scuba dive sampling at limited locations only. For the offshore area, representative samples and the associated geophysical signature recognised were utilised in the along-strike extrapolation of geological units.

Aeolianites

Units Pm 11, Pm 13, Pm 15, Pm 17, Pu 5 and Pu 8 (Figure 4-24) are aeolianites. Sedimentology of the deposits, carbonate diagenesis, and primary structures, allowed these units to be interpreted as palaeodune ridges. The aeolianites on the shelf range in age from ~142 – 87 ka and were deposited on both regressive and transgressive sea-level cycles.

Beach deposits

Sedimentary characteristics and morphological structure suggests that Units Pu 3, Pu 6, Pu 11, Pu 9 and the composite group Pm 10 – 14 were deposited on beaches, in the foreshore and swash zones (Figure 4-25). The dated units suggest (1) deposition during the transgression from MIS 6 – 5e (for the latter middle Pleistocene units); and (2) deposition on a retreating sea-level from the peak of the Last Interglacial (referring to the former group, consisting of upper Pleistocene deposits). The beachrock of Unit Pu 9 adjoins the dune system of Unit Pu 8. The dominance of this unit across the palaeochannel of the Groot Brak River confirms that the cemented palaeocoastline has not been exposed to another regressive sea-level cycle since the time of deposition and preservation. Therefore, Unit Pu 9 is inferred to be the youngest consolidated geological unit preserved on the continental shelf.

Nearshore deposits

Units Pu 4 and Pm 9 (Figure 4-25) were deposited in the shallow nearshore; likely the upper shoreface environment. Additionally, unconsolidated cobbles on the inner shelf overlying the substrate of older Pleistocene units on the planation between palaeo-coastal zones 3 and 4 (Figure 4-26) are suggested to represent the landward shift of the Holocene shoreface. Luminescence ages confirmed that Pm 9 was deposited during the fall of sea-level from MIS 7c – 7a. Pu 4, also representing the upper shoreface environment, was deposited on the regression of sea-level from the peak of the Last Interglacial.

Back-barrier deposits

Two back-barrier systems were mapped offshore (Pu 12 and Pu 11) (Figure 4-25). These units lie at depths of 29 m and 35 m BMSL, respectively, and are bounded by cemented Pleistocene lithologies. The back-barrier deposits themselves were unfortunately not dated, although one sample was obtained. The inferred ages are

based on field relationships, the association of Pm 11 with its adjacent beach, and the likely response to sea-level fluctuations according to the seismic stratigraphic analogue coastal plain study of the Wilderness Embayment for this study as an analogue for a transgressive barrier system.

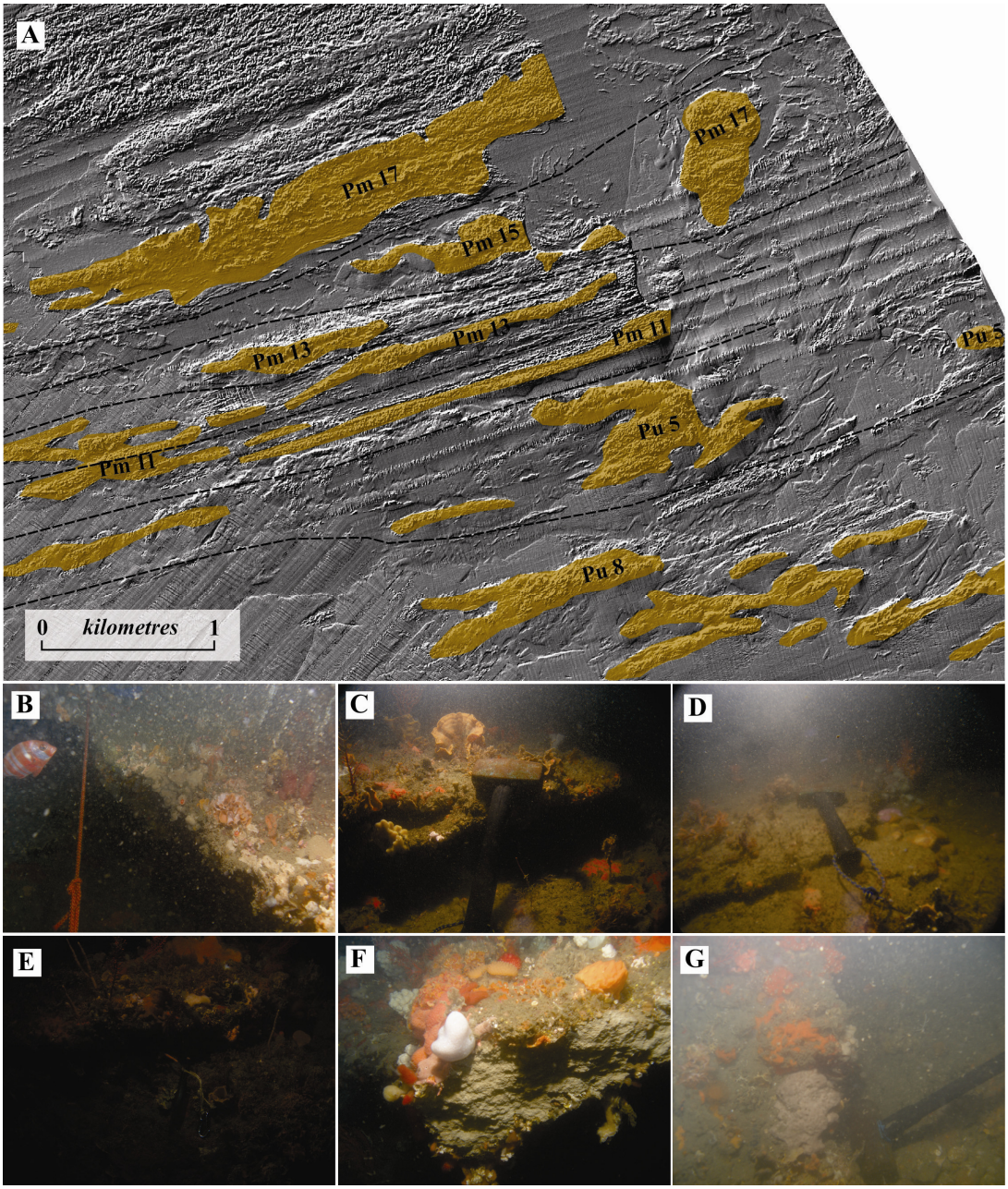

Figure 4-24. Submerged aeolianites. A. Distribution of aeolianites on the shelf – the basal dataset is multibeam bathymetry, showing the morphological features of these outcrops and the stippled line separates discrete units. The dotted line groups units B. Underwater photograph of Unit Pm 17 (31 m BMSL). C and D. Underwater photographs of Unit Pm 15 (33 m BMSL). E. Underwater photograph of Unit Pm 13 (34 m BMSL). F. Underwater photograph of Unit Pm 11 (36 m BMSL). G. Underwater photograph of Unit Pu 8 (42 m BMSL).

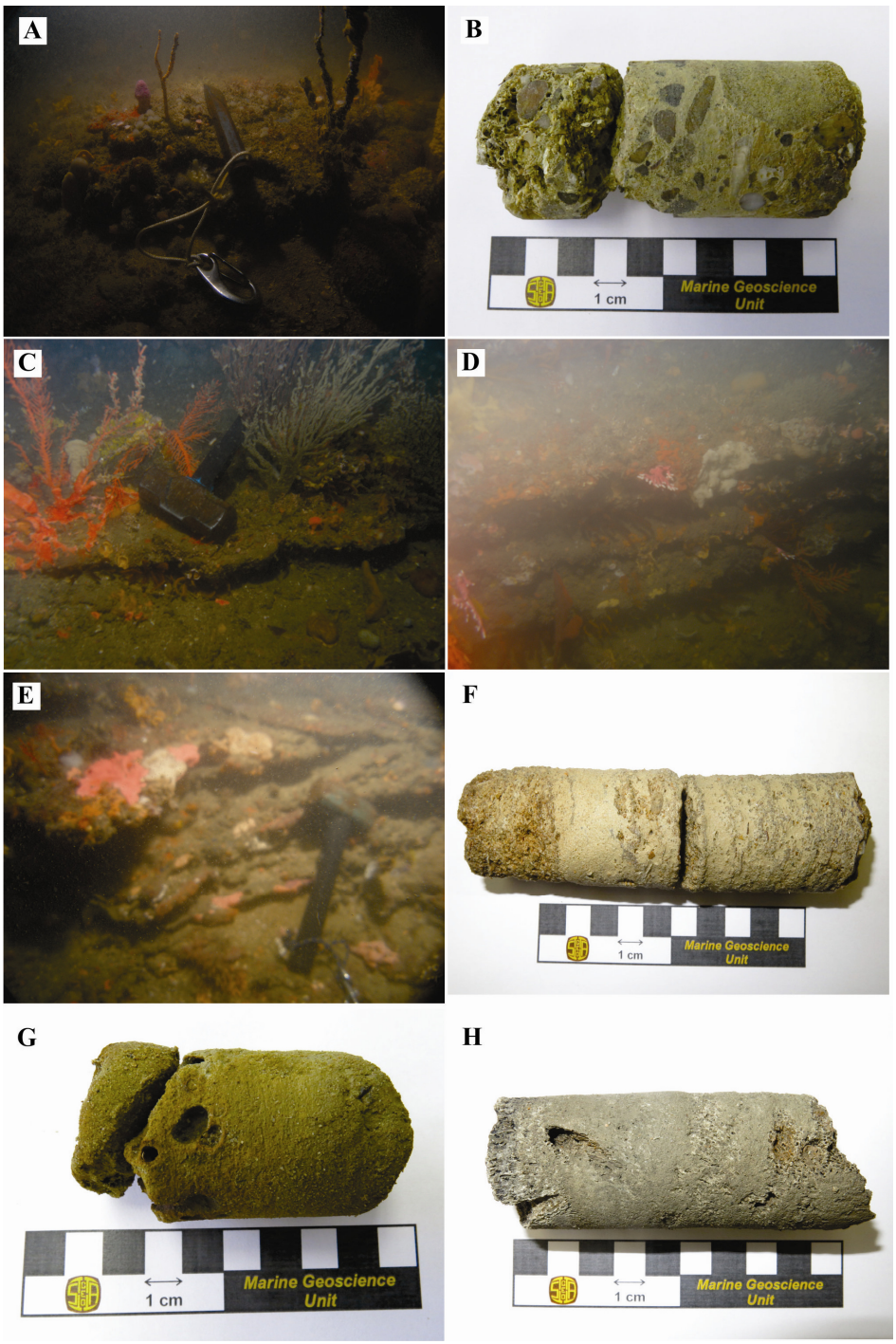

Figure 4-25. Submerged beach, nearshore and back-barrier deposits. A. Underwater photograph of Unit Pu 4 (23 m BMSL).B. Core sub-sample obtained from Pm 9 (14 m BMSL). C. Underwater photograph of Unit Pm 14 (31 m BMSL). D. Underwater photograph of Unit Pm 12 (33 m BMSL). E. Underwater photograph of Unit Pu 3 (20 m BMSL). F. Core sub-sample obtained from Pu 6 (22 m BMSL). G. Core sub-sample obtained from Pu 11 (28 m BMSL). H. Core sub-sample obtained from Pu 11 (35 m BMSL).

4.9.1 Correlation to previous studies on Quaternary highstand deposits in Mossel Bay

The Mossel Bay Quaternary stratigraphy has most recently been investigated by Jacobs et al. (2011) and Roberts et al. (2012), who documented shallow marine and aeolian deposits dated to MIS 11. This stratigraphy, exposed up the Klein Brak River and landward of the study area described in this thesis, formed a basis for relative ages of the shoreline units mapped in this study and presented in Table 4-8, as the upper shoreface unit from the raised succession dips seaward and can be correlated to the near-basal shoreline stratigraphy. The MIS 11 interglacial was probably the longest (~ 423,000 to 362,000 years ago) and warmest of the entire Quaternary Period (see Chapter 2). Roberts et al. (2012) determined a precise maximum elevation of 13 m AMSL from an unambiguous sea-level indicator: the interface between subtidal and intertidal deposits. These authors also documented sea-level fluctuations during MIS 11, including an earlier (lower) highstand close to present sea-level, much like the pattern during MIS 1 and the Holocene highstand, though the MIS 11 initial highstand was longer than the Holocene highstand.

4.9.2 Summary of geological units in Mossel Bay

The facies interpretation, carbonate diagenesis, geomorphology and geochronology allowed geological units to be defined. These are displayed in Figure 4-22 and all information tabulated in Table 4-8. The geological units are placed within a chronological evolutionary framework in Chapter 6.

Units Pm 1 and Pm 2 (Table 4-8) were deposited during MIS 15 and represent foreshore and dune deposits respectively. These deposits are preserved on the shoreline. The shoreline and raised MIS 11 deposits of Pm 3 – Pm 7 reflect a regressive sedimentary sequence associated with the MIS 11 sea-level highstand. Aeolianite of Pm 8 is interpreted to indicate progradation on a sea-level highstand. Pm 9, dated to 206 ± 19 ka for this study (Figure 4-22, Table 4-6, Table 4-8), is an upper shoreface deposit presently croppingout at a depth of 8 – 12 m BMSL and is argued to have been deposited on a forced regressive sea-level cycle. Pm 10 – Pm 15 (Figure 4-22, Table 4-8) represent a sequence of transgressive barrier migration on the mid shelf, ranging from depths of 36 – 33 m BMSL. These units are composed of both dune and beach deposits. The aeolianites of Pm 16 and Pm 17 crop out along the shoreline and offshore at a depth of 30 – 32 m BMSL. Pm 17 was dated for this study and yielded an OSL age of 125 ± 12 ka (Figure 4-22, Table 4-6, Table 4-8). The sub-aerially exposed beachrock of Pm 18 (Figure 4-22) is interpreted according to field relationships to represent a sea level stillstand on an ensuing transgression and Pu 1 has been dated to 122 ± 15 ka, indicative of the Last Interglacial high sea level. These foreshore and swash facies preserved on the Mossel Bay shoreline are associated with beach progradation during this event. Normal regression from the sea-level highstand resulted in the deposition of Pu 2 aeolianite. Pu 3 foreshore deposits (Figure 4-22) which crop out at on the seafloor at a depth of 26 – 28 m BMSL are 117 ± 11 ka in age (Table 4-6, Table 4-8). This forced regression also resulted in the deposition of Pu 4 upper

shoreface sediments, now preserved 12 – 22 m BMSL. This deposit is 115 ± 9 ka in age (Figure 4-22). Pu 5 aeolianite, exposed at a depth of 35 – 38 m BMSL, is indicative of regressive barrier migration and yielded an OSL age of 122 ± 10 ka. Pu 6 (Figure 4-22, Table 4-6) is an extensive unit of sedimentary rocks deposited in the foreshore environment at depths from 15 – 26 m BMSL. This deposit was dated and is 103 ± 8 ka in age. Aeolianites of Pu 7 (exposed sub-aerially) and Pu 8 (on the seafloor, at a depth of 40 m BMSL; Figure 4-22) represent regressive barriers. Pu 9 beachrock, mapped at a depth of 40 – 41 m BMSL, was assigned a relative age of 80 kabased on the association with Pu 7 and Pu 8. Unit Pu 10 aeolianite (73 ka, Table 4-8) is only exposed sub-aerially. Pu 11 consists of a foreshore and associated back-barrier deposit. These units crop out on the inner shelf at a depth of 32 – 35 m BMSL and were dated for this study. The age is 59 ± 6 ka (Figure 4-22; Table 4-6, Table 4-8). This composite system is interpreted to represent landward migration of a transgressive barrier. Pu 12, which was mapped 29 m BMSL, is also interpreted to represent a transgressive back-barrier deposit based on sedimentlogy and field relationships to Pu 11. Pu 13 is a unit of aeolianite preserved sub-aerially. This 52 ka aeolianite (Table 4-8) is interpreted to reflect sedimentation on a sea level stillstand. Units H 1 and H 2 are inferred to be Holocene in age. These cemented dunes (H 1) and organic-rich back-barrier sediments (H 2) lie 1 m AMSL and are suggested to have been deposited on the Holocene highstand. These relative ages were determined predominantly by the carbonate cementation in thin sections.

4.10 Palaeoshorelines and palaeo-coastal zones

The ‘palaeoshoreline’ is defined here as a linear definition of past sea level. The offshore palaeoshorelines are typically expressed along a single isobath at the most seaward extent of that particular (now submerged) coast; and in this area may represent shorelines associated with either rising, or falling, sea level. Bridging the interface of the ocean and terrestrial landscape, shorelines are inherently dynamic environments. This depositional complexity shows in the palaeo record of Mossel Bay, as the consolidated facies of rocky shorelines are stacked and juxtaposed as sea-level periodically returns to the elevations/depths at which they lie, yet with time the amalgamation of geological units becomes eroded to a uniform elevation. Small fragments of depositional units remain along rocky shorelines and facies are typically discontinuous along strike. In addition to the depositional characteristics of rocky shorelines, intertidal zones are extensively eroded along the wave-dominated coast of Mossel Bay. Seismically the palaeoshoreline is indicative of a sea-level stillstand, and they are commonly defined by stepped interruptions in the shelf bathymetric profile/terraces or more minor erosional notches where they are more poorly defined. Where present, these erosional terraces/notches represent the seaward limit of the palaeoshoreline. Palaeoshorelines in this study are thus classified according to geomorphology/prevalence along an isobath or contour as they can be dominated by either one, or more, pre-existing geological unit(s) and facies.

The geological units described previously (shown in Figure 4-22) represent deposition along an active coastal environment, encompassing the area extending from the shallow nearshore to the coastal dunes (as per Figure 4-11). At the time of each palaeoshoreline representing base-level, however, with all landward-lying deposits on the shelf being sub-aerially exposed, the coastal strip of *active* sedimentation can be far broader than the shoreline alone and is defined by gradient of the substrate, identified as zones along bathymetric profiles. These are referred to here as palaeo-coastal zones. The presence of several laterally continuous offshore ridges in the Mossel Bay embayment, supplemented with geochronological data to constrain ages of selected seafloor outcrops, allowed an onshore-offshore palaeocoastline model to be inferred. These palaeo-coastal zones represent a composite collection of the geomorphic features 'shelf banks/shoals' (Figure 4-6) interpreted to represent palaeodune ridges, 'low-relief ridges' (Figure 4-7) interpreted to represent rocky shorelines and 'type 1' depressions interpreted to represent back-barrier deposits (Figure 4-8). Eleven palaeoshorelines/palaeo-coastal zones are identified in this study and they are sequentially numbered down the depositional profile from 1 at the shoreline to 11 on the outermost mid-shelf at a depth of 50 m BMSL. In this study area, the palaeoshorelines and palaeo-coastal zones are defined in the offshore area near the Groot Brak River from the well preserved Pleistocene stratigraphy, but can be extended across isobaths for the whole of the Mossel Bay study area.

Planation surfaces commonly interlink palaeoshorelines and/or palaeo-coastal zones, interpreted in this study to have been eroded mainly on transgressive sea-level cycles with the landward migration of a high-energy, wave-dominated, shoreface. Depositional evidence of this erosive shoreface is preserved as unconsolidated cobbles on the inner shelf between shorelines 3 and 4. The planation surfaces are interpreted to represent a steady rate of sea-level rise, not punctuated by stillstands.

Table 4-7. Elevations and horizontal extents of the eleven palaeoshorelines/palaeo-coastal zones and their interlinking planation surfaces in Mossel Bay. These zonations represent the coasts of active sediment deposition and the actual shoreline elevation (representing sea-level) is indicated in bold. The distances are taken along one representative bathymetric profile constructed normal to the modern shoreline (shown in Figure 4-26). The erosional notches are shore platforms.

Palaeoshoreline	**Elevation relative to present MSL**	**Distance from the present shoreline**	**Geological units along palaeoshoreline**
1	**0** m MSL	N/A	Pm 1 - 8, Pm 18; Pu 1 - 2, H 1 - 2
Unmapped area below the breaker zone			
2	8 – **12** m BMSL	560 – 720 m	Pm 9
Minor erosional notch: 10 m BMSL			
3	12 – **15** m BMSL	720 – 840 m	Pu 4
Planation surface	15 – 23 m BMSL	840 – 1500 m	Pu 4
Minor erosional notches: 17 m BMSL, 18 m BMSL, 21 m BMSL			
4	23 – **25** m BMSL	1500 – 1860 m	Pu 4, Pu 6
Planation surface	25 – 26 m BMSL	1860 – 2060 m	Pu 3
5	26 – **27** m BMSL	2060 – 2310 m	Pu 3, Pu 12
Planation surface	27 – 29 m BMSL	2310 – 2460 m	Pu 3
Minor erosional notch: 28 m BMSL			
6	**29** m BMSL	2460 – 2660 m	Pu 3, Pm 17
Erosional notch	29 – 30 m BMSL	2660 – 2735 m	Pm 17
7	30 – **33** m BMSL	2735 – 3510 m	Pm 17, Pu 11, Pm 15
Erosional notch	33 m BMSL	3510 – 3540 m	Pm 14
8	33 – **34** m BMSL	3540 – 4310 m	Pm 11, Pm 12, Pm 13
Erosional notch	34 m BMSL	4310 – 4460 m	Pm 10
9	34 – **38** m BMSL	4460 – 5160 m	Pu 5
Minor erosional notch: 35 m BMSL			
Planation surface	38 – 40 m BMSL	5160 – 5260 m	Pm 11
10	**40** m BMSL	5260 – 5360 m	Pu 9
Planation surface	40 – 41 m BMSL	5360 – 5410 m	?
11	41 – **44** m BMSL	5410 – 6840 m	Pu 8, Pu 9
Planation surface	44 – 47 m BMSL	6840 – 7110 m	Pu 8
Minor erosional notch: 45 m BMSL			

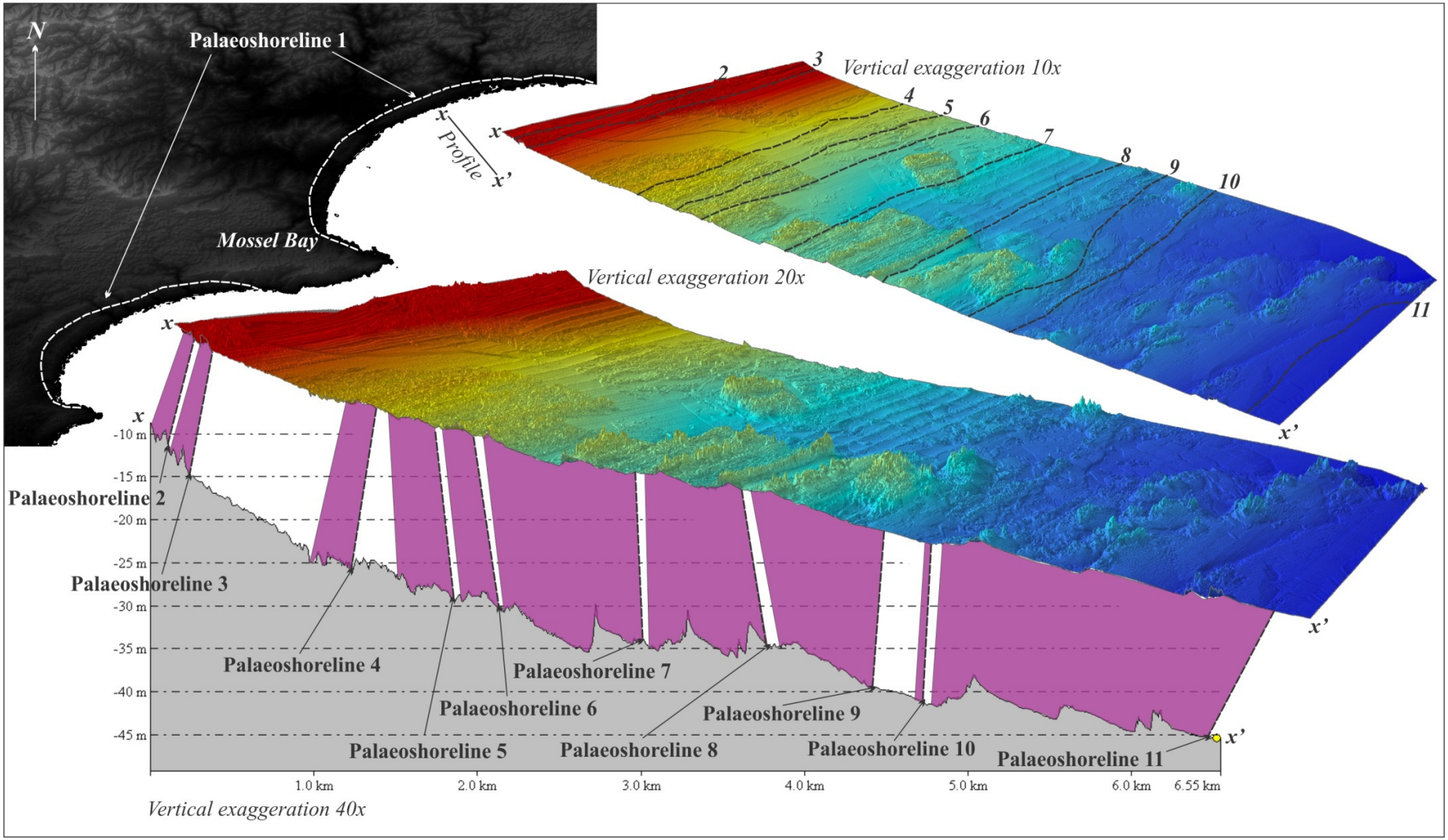

Figure 4-26. The eleven dominant palaeocoastlines identified in this study, extending from the present intertidal zone to the mid-shelf.

Table 4-8. An overview of identified geological units in the study area and their associated palaeoshorelines. Where radiometric dates were not obtained, relative ages are assigned stratigraphically based on field relations. Where the maximum relief is unknown, this is listed with a question mark. Where thin sections were not available for geological units, or units were not samples offshore, N/A is listed in the relevant columns. Although not strictly indicative of meteoric diagenesis, dogtooth calcite is considered to have precipitated in a meteoric environment in this area. A separate A3 fold-out version of this table is available in Appendix V.

Geological unit	**Palaeo shoreline**	**Elevation /depth**	**Max. relief**	**Age (TT-OSL/OSL) (ka)**	**Sedimentary facies**	**Relationship to underlying units**	**Sea-level association**	**Authi-genic clay rims**	**Meteoric cements**	**Marine cements**	**Un-filled voids**	**No. of thin sections along strike and sample numbers**
H 2	1	Present coastal plain (shore-line: 0-1 m AMSL & dunes (up to 20 m AMSL)	1 m (buried by modern dune)	Relative age: Holocene highstand	Back-barrier deposit	Not discernible	Sea-level highstand	Yes	None	Micro-crystalline rims	Yes	1 (D2)
H 1			1 m (buried by modern dune)	Relative age: Holocene highstand	Aeolianite	Not discernible	Sea-level highstand; prograda-tion	Yes	Dogtooth calcite rims	None	Yes	1 (D1)
Pu 13	?		?	52 (grouped average)	Aeolianite	?	Sea-level stillstand on forced regression	N/A	N/A	N/A	N/A	0
Pu 12	5	29 m BMSL	0 m	Relative age:	Back-barrier deposit	?	Transgressive barrier	N/A	N/A	N/A	N/A	0
Pu 11	7	34 – 35 m BMSL	0 m	Relative age	Back-barrier deposit	?	Transgressive barrier	No	Carbonate-organic mixed matrix, dogtooth	Isopachous micro-crystalline calcite, microspar	No	1 (O27)

									calcite rims	mosaics		
		32 – 35 m BMSL	1 m	59 ± 6	Foreshore	?	Transgressive barrier	No	Carbonate-organic mixed matrix , authigenic clay	Micro-crystalline rims	No	1 (O6)
Pu 10	?		?	73 (grouped average)	Aeolianite	?	Sea-level stillstand on forced regression	N/A	N/A	N/A	N/A	0
Pu 9	10, 11	40 - 41 m BMSL	1 m	Relative age ~80	Beachrock	?	Regressive barrier	N/A	N/A	N/A	N/A	0
Pu 8	11	40 m BMSL	5 m	87 ± 9	Aeolianite	?	Regressive barrier	No	Dogtooth calcite rims, blocky calcite spar infill	None	Yes	1 (O24)
Pu 7	?		?	91 (grouped average)	Aeolianite	?	Sea-level stillstand on forced regression	N/A	N/A	N/A	N/A	0
Pu 6	Planation 3 - 4	15 - 26 m BMSL	1.6 m	103 ± 8	Foreshore	?	Normal regression; progradation on stillstand	No	Blocky calcite spar infill	Isopachous micro-crystalline calcite, fibrous rim cements, microspar mosaics	Yes	2 (O23, O39)
Pu 5	9	35 – 38 m BMSL	4 m	122 ± 10	Aeolianite	?	Regressive barrier migration	Yes	Dogtooth calcite rims , blocky calcite spar infill, minor authigenic clay	Micro-crystalline rims, microspar mosaics (in places)	Yes	3 (O28, O29, O9)
Pu 4	3	12-22 m BMSL	3 m	115 ± 9	Upper shoreface	?	Forced regressive deposition	Yes	Authigenic clay, blocky calcite spar infill	Isopachous micro-crystalline calcite	Yes	4 (O22, O32, O41, O42)

Pu 3	4	26-28 m BMSL	1.6 m	117 ± 11	Foreshore	?	Forced regressive deposition	No	Blocky calcite spar infill	Isopachous micro-crystalline calcite, fibrous rim cements, microspar mosaics	Yes	3 (O11, O40, O43)
Pu 2	1		1.5 m	Relative age: MIS 5e	Aeolianite	Angular unconformity over Pm 6, sharp contact where overlies Pm 3	Prograding beaches and associated seaward shifting dunes: normal regression from sea-level highstand	No	Dogtooth calcite rims, authigenic clay, blocky calcite spar infill	Minor microspar mosaics	Yes	4 (G1, J5, K2, L1)
			>1 m	Relative age: MIS 5e	Palaeosol	Stratigraphically associated with MIS 5e aeolianite		No	Authigenic clay, blocky calcite spar infill	Microspar mosaics	No	1 (B1)
Pu 1			1 m	122 ± 15	Foreshore	Conformably overlies Pm 6; gradational contact with the associated conglomerates (below)	Progradation of barrier beach system on sea-level highstand, followed by normal regressive sedimentation	Yes	Authigenic clay, blocky calcite spar infill	Fibrous rim cements	Yes	16 (E2, E3, E5, E7, E9, F6, G3, I1, J7, R11, S1, T1, T3, T8, U1, V3)
			0.6 m	Relative age: MIS 5e	Foreshore – matrix-supported pebble conglomerate facies	Grades into foreshore deposits, occurs in laterally discontinuous lenses		Yes	Dogtooth calcite rims, authigenic clay, blocky calcite spar infill	Microspar mosaics	Yes	3 (F1, F2, F4)
			<0.3 m	Relative age: MIS 5e	Foreshore swash facies	Coarse fraction associated with		No	Dogtooth calcite rims, authigenic clay	Fibrous rim cements, microspar mosaics	Yes	6 (K1_2, R3, R7, R8, R9,

						foreshore deposits. Drapes pre-existing deposits and infills erosional features						R10)
Pm 18			0.5 m	Relative age: early MIS 5e	Beachrock	Sharp, unconform-able contact with underlying Pm 1	Stillstand on ensuing trans-gression	No	Blocky calcite spar infill	Fibrous rim cements, microspar mosaics	Yes	2 (K3, L3)
Pm 17	6, 7	30 – 32 m BMSL	2 m	125 ± 12	Aeolianite	?	Transgress -ive barrier	No	Dogtooth calcite rims, authigenic clay, blocky calcite spar infill	None	No	4 (O36, O38, O44, O46)
Pm 16	1		1.5 m	127 (grouped average)	Aeolianite	?	Transgress -ive barrier		N/A	N/A	N/A	0
Pm 15	7	32 – 33 m BMSL	5 m	134 ± 13	Aeolianite	?	Transgress -ive barrier migration of a composite beach-dune system	No	Dogtooth calcite rims, minor authigenic clay, blocky calcite spar infill	Isopachous micro-crystalline calcite	Yes	3 (O7, O35, O45)
Pm 14	9	33 – 34 m BMSL	1.2 m	Relative age	Foreshore	?		No	Blocky calcite spar infill, minor authigenic clay	Micro-crystalline rims, isopachous micro-crystalline calcite	Yes	1 (O33)
Pm 13		32 - 34 m BMSL	3 m	138 ± 14	Aeolianite	?		No	Dogtooth calcite rims, blocky calcite spar infill,	Micro-crystalline rims	Yes	2 (O4, O26)

									authigenic clay			
Pm 12		33 – 34 m BMSL	1.2 m	Relative age	Foreshore	?		No	Blocky calcite spar infill, minor authigenic clay	Micro-crystalline rims, isopachous micro-crystalline calcite	Yes	1 (O3)
Pm 11		35 – 36 m BMSL	2 m	142 ± 12	Aeolianite	?		Yes	Dogtooth calcite rims, authigenic clay, blocky calcite spar infill	None	Yes	1 (O30)
Pm 10		33 – 34 m BMSL	1.2 m	Relative age	Foreshore	?		N/A	N/A	N/A	N/A	0
Pm 9	2	8-12 m BMSL	3 m	206 ± 19	Upper shoreface	?	Regressive sedimentation on forced regression	Yes	Authigenic clay, blocky calcite spar infill	Isopachous micro-crystalline calcite, microspar mosaics	Yes	1 (O37)
Pm 8	?		?	250 (grouped average)	Aeolianite	?	Progradation on sea-level highstand	N/A	N/A	N/A	N/A	0
Pm 7	1		4 m	400 (grouped average)	Aeolianite	Sharp contact with underlying Pm 5 and Pm 3	Regressive sequence – normal regression associated with a sea-level highstand	Yes	Authigenic clay, blocky calcite spar infill	Micro-crystalline rims, fibrous rim cements	No	5 (E1, E6, E8, I3, L2)
Pm 6			0.4 m	Relative age: MIS 11	Cobble conglomerate/gravel lag	Sharp contact with Pm 3 & Pm 2		Yes	Blocky calcite spar infill, authigenic clay	Isopachous micro-crystalline calcite	No	4 (F5, Q1, R4, R5)
Pm 5			0.3 m	Relative age: MIS 11	Storm deposits	Sharp basal contact with Pm 2, erosional basal contact		No	Dogtooth calcite rims, blocky calcite spar, authigenic	Isopachous micro-crystalline calcite, microspar	Yes	3 (J9, K4, T2)

						where overlies Pm 3			clay	mosaics, fibrous rim cements		
Pm 4			0.2 m	Relative age: MIS 11	Subtidal oyster beds	Sharp contact with Pm 2		N/A	N/A	N/A	N/A	0
Pm 3			1 m	Relative age: MIS 11	Upper shoreface	Separated from Pm 2 with an angular unconform-ity; sharp contact		No	Dogtooth calcite rims, authigenic clay, blocky calcite spar infill	Isopachous micro-crystalline calcite, fibrous rim cements	Yes	8 (I4, J2, J3, F7, J8, P1, R6, T5)
Pm 2			0.6 m	582	Aeolianite	Dissolution on the surface, conformably overlies Pm 1	Regressive sequence – normal regression associated with a sea-level highstand	Yes	Dogtooth calcite rims, authigenic clay, blocky calcite spar infill	Fibrous rim cements, isopachous micro-crystalline calcite	Yes	9 (I5, J6, M1, N2A, N2B, R1, T4, V1, V2)
Pm 1			1 m	Relative age: MIS 15	Foreshore	N/A		Yes	Authigenic clay (poorly developed), blocky calcite spar infill	Isopachous micro-crystalline calcite, Microspar mosaics	Yes	1 (G2)

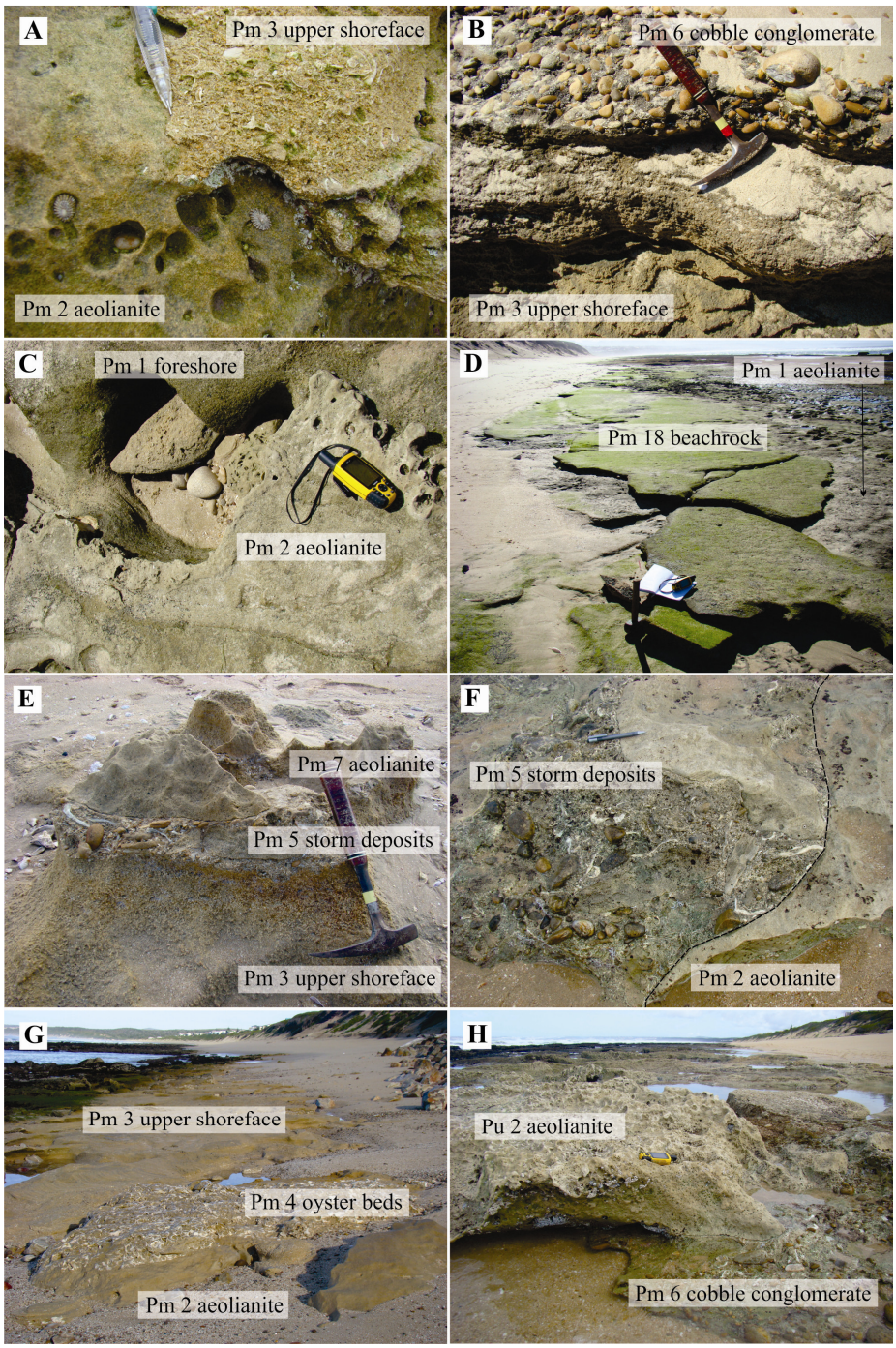

Figure 4-27. The nature of contacts between geological units mapped along the shoreline of Mossel Bay. A. Angular unconformity between stratified beds of Pm 3 overlying Pm 2. B. Sharp contact between Pm 6 and underlying Pm 3. C. Sharp contact between Pm 1 and overlying Pm 2. D. Pm 18 unconformably overlying Pm 1. E. Sharp contact of Pm 7 overlying Pm 5 and erosional contact between Pm 5 and the basal Pm 3. F. Sharp contact between Pm 5 and underlying Pm 2. G. Pm 4 unconformably overlying both Pm 3 and Pm 2. G. Angular unconformity between Pu 2 and underlying Pm 6.

4.11 Factors which determined the preservation of geological deposits on the Mossel Bay shelf

4.11.1 Dunes

Sedimentary barriers (i.e. sand dunes) are interpreted to have shifted across the shelf in a shore-perpendicular sense as sea levels fluctuated (see Chapter 6). Where stillstands ensued on relatively low gradient areas and cementation of deposits was facilitated, the sedimentation at these localities developed in an alongshore orientation, preserving the linear features that now remain in the offshore environment.

The results from this study and from the Wilderness Embayment to the east (e.g. Bateman et al., 2011) have demonstrated a clear link between components of barrier systems: aeolianite, back-barrier environments and incised channels. These features are, in the seismic record, stacked vertically in response to fluctuating sea levels. Along the South Coast, rivers provide a plentiful source for the coarser grade of sediment required to build coastal dune systems and physical processes causing sediment movement are a direct consequence of the coupling between fluid dynamics and morphology of depositional features (e.g. after Cowell and Thom, 1994).

Parabolic dunes (Pye, 1983; Tinley, 1985) are observed along the South African coastline where accommodation space allows for their accretion. Based on the poor development (or preservation) of the trailing arms on the Mossel Bay shelf associated with Unit Pu 8, these dunes are likely relatively young. This is confirmed by the luminescence date of Unit Pu 8 of ~87 ka (Table 4-8). When compared to the oldest Cenozoic dune system of the South Coast, the Wankoe Formation, the magnitude of older dune deposits suggest a significantly greater sediment volume than supplied during the Quaternary. The Wankoe Formation extends for a distance of up to 15 km inland and individual barriers reach a maximum elevation of 70 m (Roberts et al., 2013). The reasons for the preservation of these features is attributed to a low-relief coastal plain incised into weakly cemented Mesozoic or easily erodible Palaeozoic bedrock, repeated Cenozoic marine transgressions providing accommodation space for dune construction, strong regional winds, and a noteworthy sediment supply from the Goukou and Gouritz Rivers during this time as the Bokkeveld Group shales were significantly eroded. The preservation potential was likely enhanced by the successive late Cenozoic sea-level highstands declining in elevation through time (Roberts et al., 2011). The distribution of sedimentary and aeolian deposits on the shelf at MIS 5e illustrate increasing dune sedimentation from the lowstand of MIS 6 reaching a maximum when sea level was highest during MIS 5e at 130 - 120 ka. The MIS 3 parabolic dunes suggest continued deposition by dominantly westerlies. The Holocene was a time of intense aeolian activity, as the ‘modern’ dunefields and the seaward barrier of the Wilderness Embayment developed.

Where broad, low-relief coastal plains are developed from repeated planation during Cenozoic sea-level fluctuations, former shorelines may penetrate up to tens of kilometres inland and so do the corresponding palaeo-

dunefields along these coastal plains (Roberts et al. 2006; Pether et al. 2000). The dune systems of the South Coast are associated with log-spiral bays, greater vegetation cover and a tendency to accrete vertically but on lowstands laterally extensive dunefields develop (Figure 4-28). Seasonality on the South Coast is less intense than on the West and East Coasts of South Africa as the South Coast straddles these inherently different climatic systems and lies at the confluence of two major ocean currents.

Tankard and Schweitzer (1974), Dingle and Rogers (1972) and Tinley (1985) suggested that the offshore dunes were formed during marine regressions, and Bateman et al. (2004) and Carr et al. (2007) both suggested that aeolian depositional ages appear to be controlled by interglacial and subsequent interstadial sea-level high stands and that aeolian deposition appears to be episodic. This work has, however, shown no distinct preference and dunes were deposited on both sea-level regressions and transgressions on the shelf. The inability to map below water before this study is proposed to explain the preference for the sub-aerial/highstand model.

Dune sediment reaching the present shoreline was seemingly not influenced by sea-level retreat towards the LGM as anticipated by Roberts et al. (2013). Roberts et al. (2013) predict that these winds may have been capable of transporting sediment from the shelf or reworked older dunes from the present shoreline, but no evidence of South Coast dune sedimentation was previously reported for the period ~50 - 40 ka prior to this study. From this work it is apparent that active deposition was taking place in palaeo-coastal zones on the continental shelf, distal compared to the previous studies undertaken on the South Coast highstand deposits.

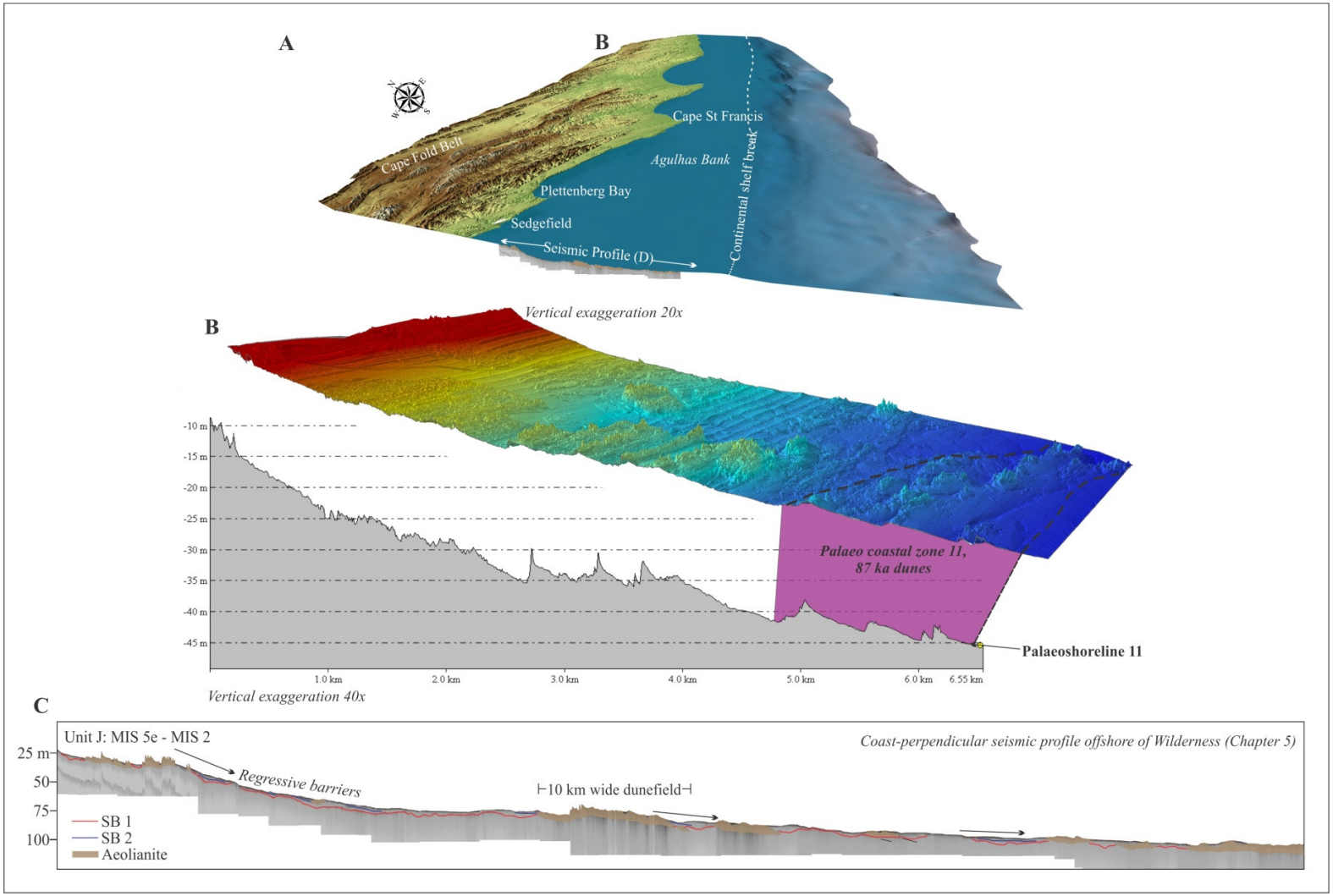

Figure 4-28. The tendency for dune plumes to accrete on this shelf during periods of lowered sea-level. A. DEM offshore of Wilderness, showing the location of the seismic profile displayed in (C). B. Mossel Bay multibeam bathymetric data illustrating the breadth of dunefields associated with palaeo-coastal zone and palaeoshoreline 11 and Unit Pm 8. C. Seismic profile offshore of Wilderness illustrating the character of laterally extensive aeolian deposits when accommodation space on a low gradient shelf allows for this sort of accretion.

4.12 Coastal caves

Coastal caves and rock shelters along the west- and south coasts of South Africa hold some of the richest Middle Stone Age archaeological deposits worldwide. Understanding the geological mechanism behind cave incision by past high sea levels was considered in this study. The Pinnacle Point cave complex holds 29 mapped and sequentially numbered separate cave/overhangs within a ~2 km stretch of coast (e.g. Figure 1-2, Figure 4-34). These caves are denoted with the prefix 'PP' and the incisions generally occur within two dominant bands of elevation: 3 – 7 m AMSL and 12 – 15 m AMSL (Fisher et al., 2010).

Structural features associated with compression (thrusts, reverse faults, tension/a-c fractures, shortening, foliation, fracture cleavage) and with an extensional regime (normal faults, joints, conjugate joints, offset veins) were documented in this study in the vicinity of Pinnacle Point for this study to investigate the susceptibility of the strata to cave formation (Figure 4-29). Four general criteria are identified by grouping the above structural features, thought to represent zones of pre-existing weakness and the incision of coastal caves during higher sea levels. The most important features are interpreted to be, in decreasing order of importance, lithology, faults, degree of silicification and joints.

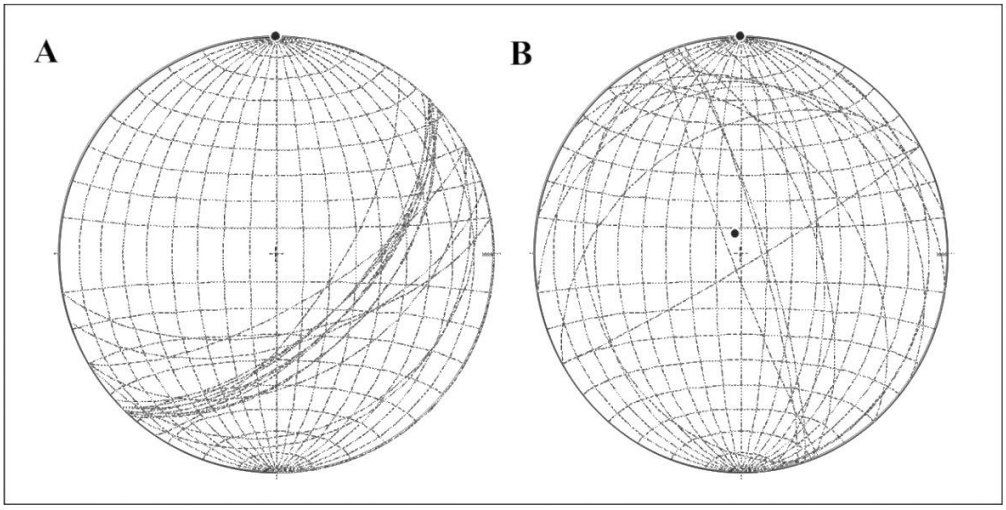

Figure 4-29. Examples of stereonet plots for structural measurements taken near Pinnacle Point. A. Dip and strike of beds. B. Joints. These stereonets were plotted in Stereonet 9 software.

Structural observations on the quartz arenite sea cliffs at Pinnacle Point for this study showed that folding, accompanied by brecciation and local thrusts, are common features and bedding planes exhibit a regional east-west oriented strike (Figure 4-34A). Measured dip and strike (n = 126) for the stretch of coast studied showed the average dip of beds to be 46º and the strike is generally toward 046. Thrust fault planes, in line with bedding, trend at approximately 60/048º and the orientation of normal faults averaged a trend of 190/010. Where fault

breccia outcrops, the fault plane has either (1) crushed the marginal deposits of both the hanging wall and the footwall, particularly in the case of the low-angle thrust and listric faults along tilted bedding planes, or (2) created resilient zones by the process of silicification by silica-rich fluids (Figure 4-30) that would have been present during the shortening event. Small iron and manganese deposits were observed near PP 5/6 (Figure 4-30). These may occur as leached ferricretes on an erosional palaeo-surface, or may be associated with faults and fluid mobilisation (e.g. as described by McGregor, 2013).

4.12.1 Interpretation of geological structures

Maximum compressive stress (σ_1) of the D1 compression is interpreted to represent the Cape Orogeny and is expressed by the reverse and thrust faults. The compression, in accordance with regional studies, and has a north-south orientation. Features associated with shortening include reverse faults, sigmoidal tension fissures, fracture cleavage and veins. Low angle faults, often listric in character, show a reverse sense of movement. Decollement/glide plane horizons between the thrust faults resulted in some strata resembling gentle folds. Shearing is parallel to layer boundaries, as the sedimentary strata have a well-developed plane-parallel stratification and this inherent weakness in the rocks will control the deformation (shown in Figure 4-31A). The individual rock layers are flexed and the outermost layers slip over the inner layers towards the hinge zones. Planar structures such as bedding surfaces (S_0) strike east-west, other than where normal fault blocks have disrupted the common orientation. Fracture cleavage in the massive quartzites can be poorly defined, but is clear in the thrust zones. The most intense strain is developed closest to fold hinges and is concentrated along the bonding zones of competent layers (Figure 4-31E). At Pinnacle Point, the shearing associated with low-angle reverse faults was mostly homogenous, but in places tension fissures became sigmoidally oriented (Figure 4-31B). These feature in the present mapped area as parallel- and perpendicularly-oriented planar quartz-fill fractures (Figure 4-31D). Some lie at right angles to the fracture cleavage of S_1 and others are obliquely inclined. Veins have a lenticular form in places (pinching in at the ends) showing the a-c tension fissures. The quartz fracture cleavage forms a-b fractures because it forms in the a-b fabric plane of the fold (Figure 4-31C). Near Staircase Cave, there is further evidence of compressional features, such as quartz- and calcite veins that indicate shortening.

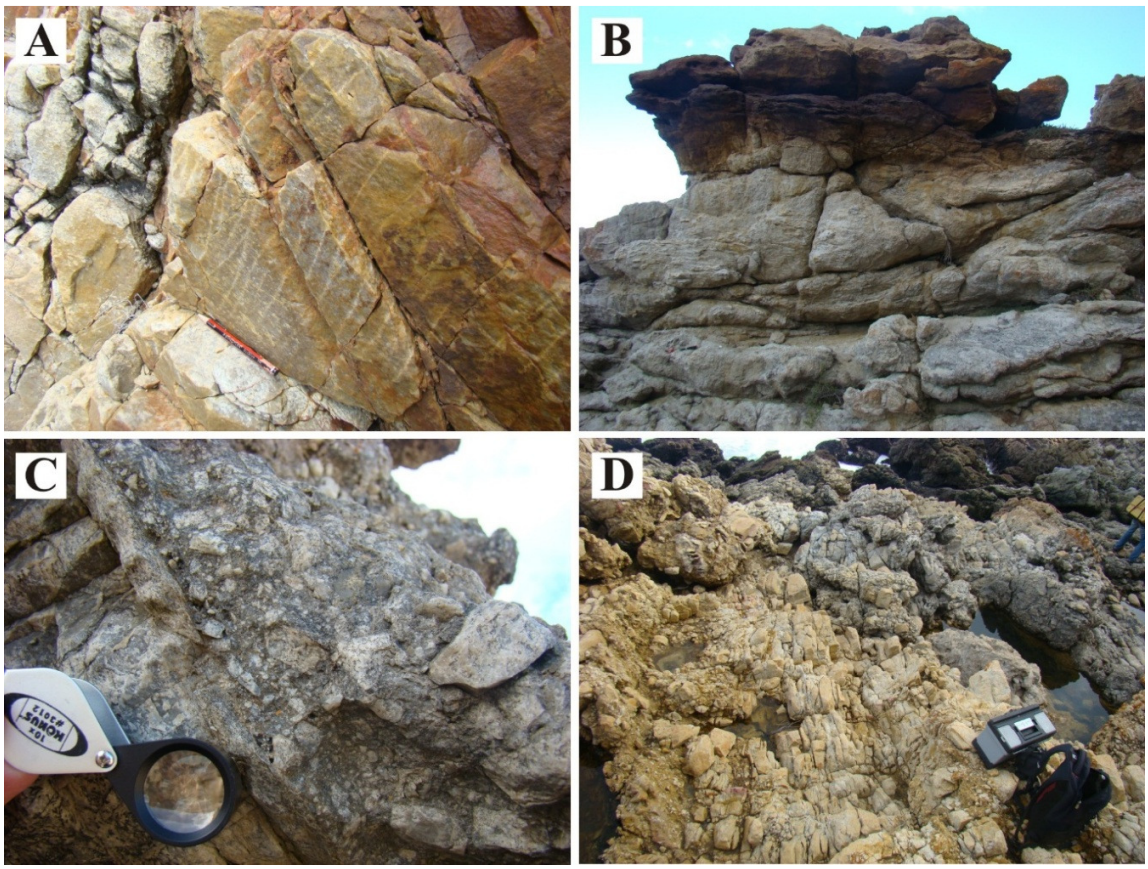

Figure 4-30. A: Primary sedimentary structures (cross-bedding). The pencil indicates the way up orientation of these overturned beds. B: Leached iron/manganese deposits near PP 5/6. C and D: Silicified fault breccia between PP 1 and North Beach.

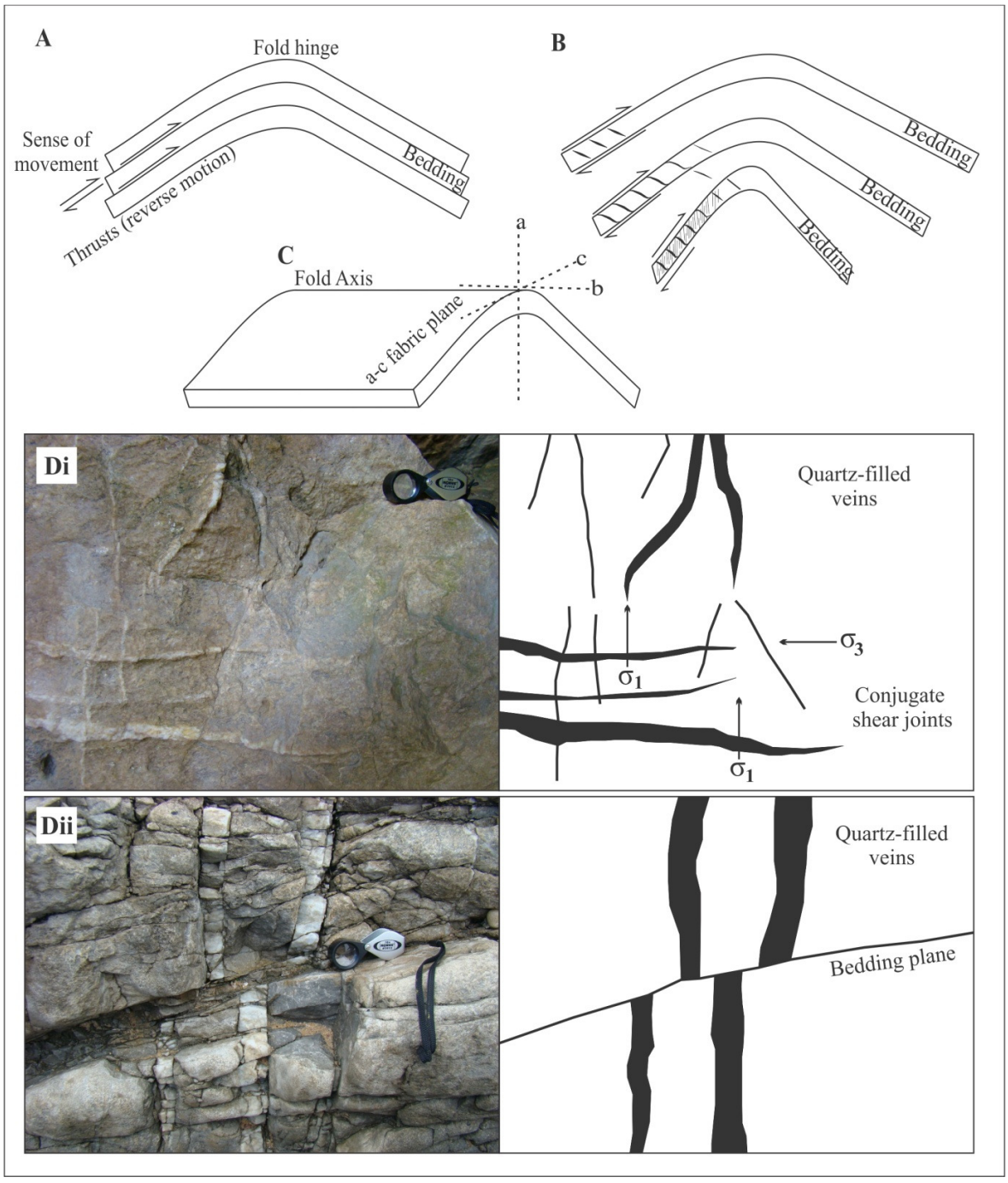

Figure 4-31. Features associated with compression, correlated to the D1 deformation event. A. Schematic image showing the proposed mechanism for development of reverse thrust faults along bedding planes at Pinnacle Point. B. Progressive development of sigmoidal tension fissures (thicker lines) and fracture cleavage (fine lines normal to the sense of movement) at Pinnacle Point. C. Schematic image showing the a-b plane of a fold. D. i: Joint sets and conjugate joints in a cave between Staircase Cave and the PP 13 complex. Sigmoidal (rotational) structures show the stress orientations. ii: a-c quartz-filled veins. The opening of the fractures and infilling by SiO_2 –rich fluids are simultaneous.

The extensional event D2 is most likely associated with the fragmentation of Gondwana. Here, maximum compressive stress is vertical (normal faulting) (Figure 4-29B). Features of brittle deformation associated with extension/stretching include joints, normal faults and fractures. Joints incorporate master joints, perpendicular joint sets and conjugate joint sets. At PP 1 a normal fault has displaced the strata. Fractures with no relative displacement, commonly infilled by vein quartz and fractures with incipient rotation (offset veins) obliquely inclined to the foliation. (Figure 4-32). Silicification and quartz recrystallisation from pressure solution can produce localised competent zones surrounding fault planes. The silica is mobilised and may dissolve the most soluble parts of a rock mass leaving behind discrete insoluble residues in irregular planar zones that define the cleavage/"armouring".

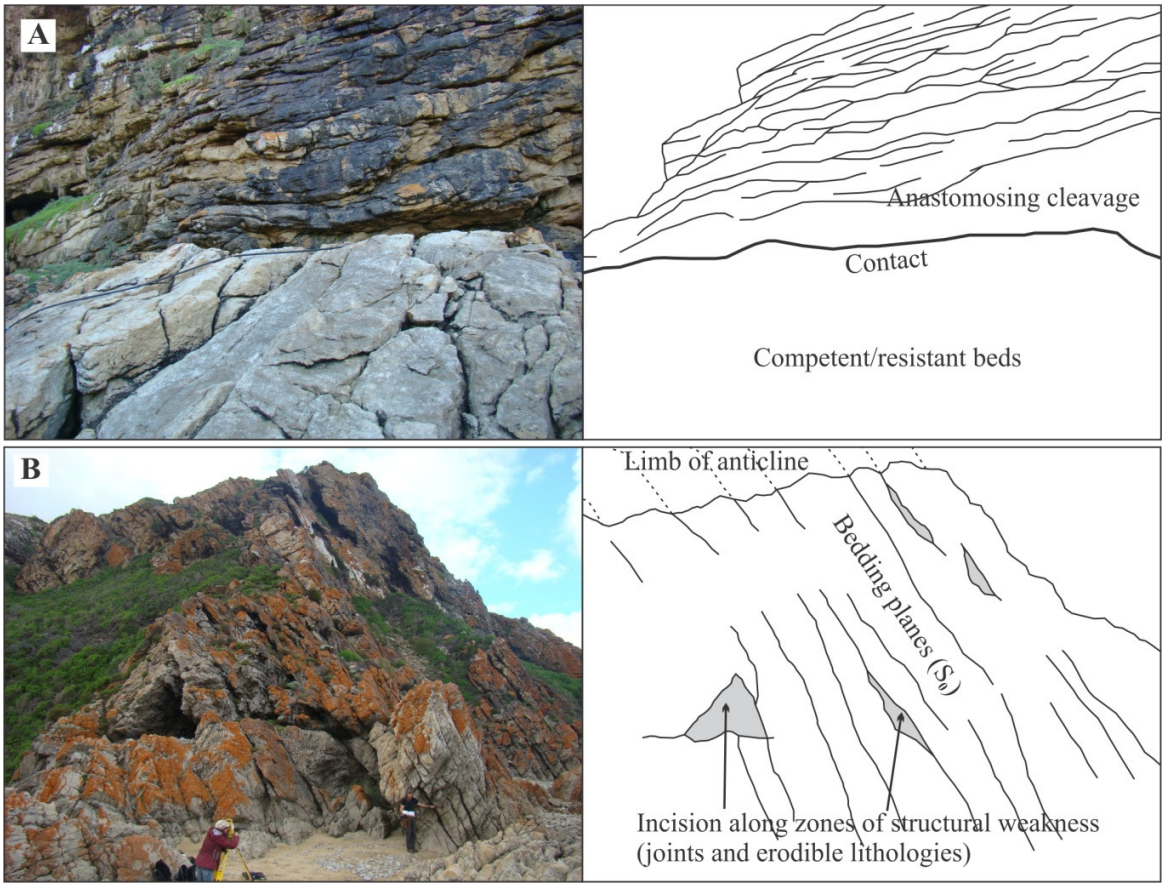

Figure 4-32. A. Anastomosing cleavage and the base of a contact to the east of Crevice Cave. B. Orientation of bedding planes adjacent to PP 1. Black surfaces in A are Mn oxides and orange in B are lichens.

4.12.2 Origin of the Pinnacle Point caves

PP 1 has been incised into a large-scale normal fault. Thrust faults at and above PP 5/6) are listric in morphology, probably as a result of mostly lithological control. Silty deposits associated with the thrust have

been milled/crushed to form mylonite in places. These mylonites remain unconsolidated for the most part. Crevice Cave (Figure 4-33) is incised into the base of a fault, which is seen in profile at PP 5/6 and above PP 5/6 (Figure 4-33) where there is a prominent overhang. Relatively more erodible strata within the horizontal bedding have been carved out in the region of Opera House Cave. The base of Opera House Cave lies along strike (towards the west) of the same thrust fault that Crevice was notched into. This indicates lithological control. The PP 9 complex displays a complicated arrangement of a deeply incised thrust fault at the base, cross-cutting (conjugate) joints and faults. There is also evidence of less competent strata that have been preferentially incised. Listric thrust faults and zones of silicification versus zones of non-silicification seem to have influenced formation of the Staircase Cave and surrounds (Figure 4-33). These beds consist of milled siltstone along a bedding plane, but an adjacent area along strike may be silicified and therefore more competent. Iron leaching along the thrust plane has resulted in the orange coloured outcrops, which are different to orange lichens. The base of the lower PP 13 caves and the roof of PP 13B are incised into thrust faults, originating at the Staircase complex. It is thought, however, that the incision of the PP 13 complex is largely based on lithology as the uppermost Skurweberg Formation may contain increased feldspar as it grades into the overlying Baviaanskloof Formation which has since eroded away. Traced along strike, these lithologies correlate to the adjacent embayment area and possibly also to cave PP 29.

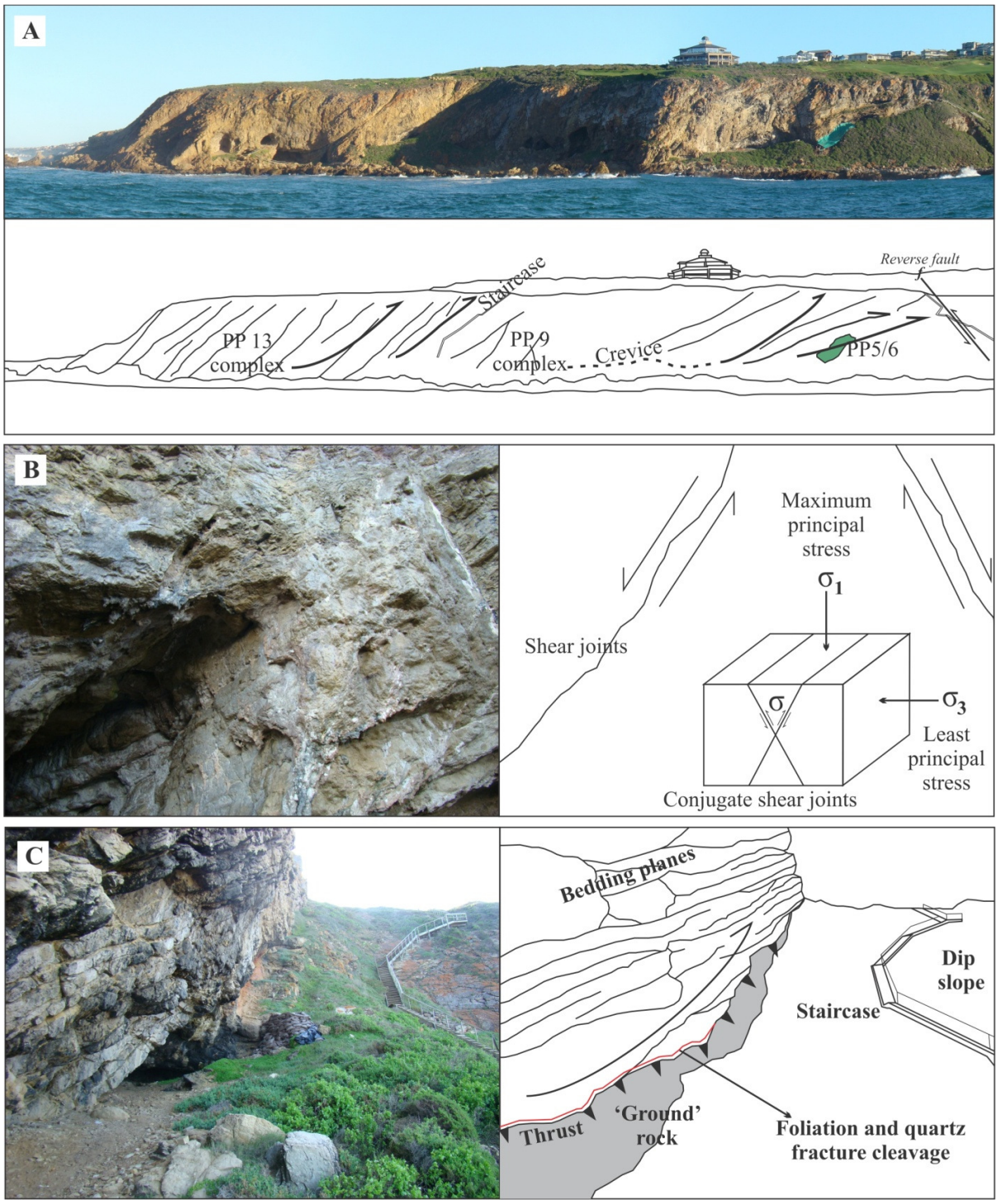

Figure 4-33. A. Reverse thrust faults along bedding planes from PP 5/6 to the PP 13 complex. Crevice Cave is incised along the base of a contact associated with foliation and fracture cleavage. The flat surface on top of the cliffs is a subsequent feature of erosion. B. Conjugate joint set in the PP 9 complex. C. Staircase Cave (incised into fault breccia of a reverse thrust fault). The orange coloured sediment is from the precipitation of Fe in percolating fluids. The primary control is interpreted to be lithological as determined by structure.

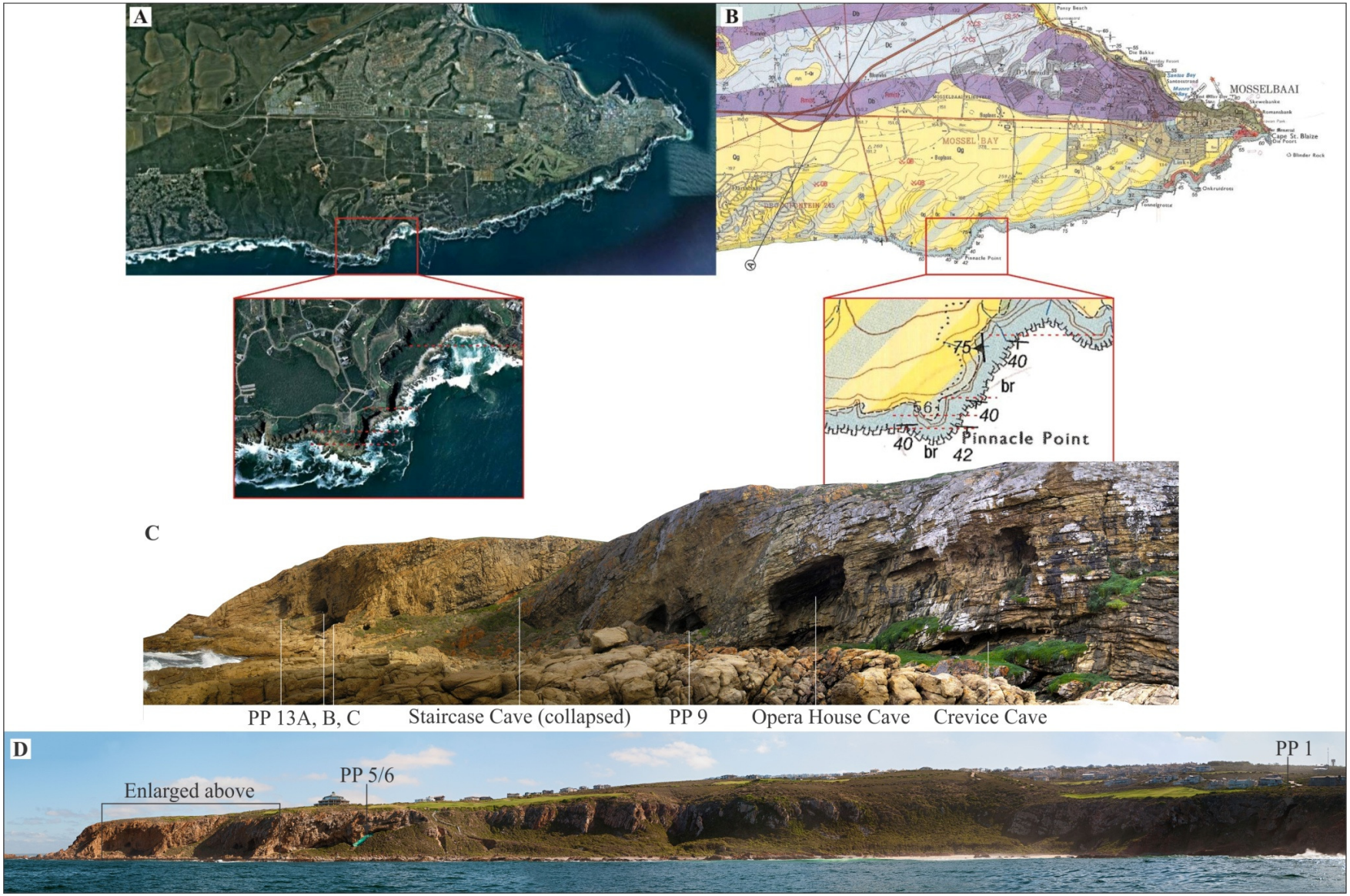

Figure 4-34. A. Google Earth Image and B: 1:50 000 geological map of Mossel Bay (Viljoen and Malan, 1993) showing the dominant east-west strike of the deposits forming the Pinnacle Point area (dotted red lines). C and D. Cave nomenclature along the Pinnacle Point coast. Abbreviation: PP – Pinnacle Point.

4.12.3 Discussion: coastal cave incision

The rocks at Pinnacle Point specifically consist of folded Skurweberg Formation (Nardouw Subgroup) quartz arenites of the Table Mountain Group, overlain to the north by the basal units of the shale-rich, argillaceous Bokkeveld Group such as the Gydo Formation (*Db*; Figure 4-34). The Skurweberg Formation (*Ss*) comprises cross-bedded whitish weathering quartz arenites, medium- to coarse grained highly quartzose units, with a higher percentage of feldspar near top of the succession, and subordinate shale. This is overlain by less resistant feldspathic, thinner-bedded sandstones of the Baviaanskloof Formation (Toerien, 1979; Viljoen and Malan, 1993). The cross section in Figure 4-34 indicates that the southern limb of the anticline in the area of interest exposed the uppermost Skurweberg Formation (being further south), and probably the transition into the overlying Baviaanskloof Formation, which itself, had been eroded away. Because Pinnacle Point protrudes further into the Indian Ocean than the bulk of the cliffed coastline from Cape St. Blaize to Dana Bay (Figure 4-34), it is suggested that the PP 13 complex erodibility has been increased by the overlying less resistant rocks. Caves could therefore form more easily at Pinnacle Point that along the adjoining coastline.

4.13 Discussion of the stratigraphy of Mossel Bay

4.13.1 Quaternary deposits

This chapter has shown that deposition of prominent geological units has occurred across facies of the littoral zone, ranging from dunes, to beaches, and onto the shallow nearshore, and that the units were deposited and preserved on both regressive sea-level cycles of MIS 11, MIS 7, MIS 1, and transgressive cycles of MIS 6 – 5e, MIS 2 – 1. The cementation of these deposits is indicative of both sub-aqueous and sub-aerial precipitation and this was not always contemporaneous with deposition. Subsequent sea-level oscillations resulted in recrystallisation of carbonate, now presenting as multiple generations of interstitial cement.

Although the present shoreline of Mossel Bay is log-spiral in form, the palaeocoastlines preserved in the Quaternary rock record are generally linear. These non-protected, potentially high wave energy shorelines could therefore be expected to have been vulnerable to the effects of storms and evidence of storm deposits remains preserved in the rock record to support this hypothesis. As an example, the numerous pebble and cobble layers in the foreshore facies (Sed. F. 5) may indicate alternating storm and fairweather conditions. The planed trough cross-beds in the upper shoreface facies (Sed. F. 2) could be assigned to the repeated interruption of fairweather deposits by storms resulting in erosion surfaces. Flood events and storms are considered important in the construction of the stratigraphic record (Ager, 1993). Many sedimentary units accumulate as a result of short intervals of sedimentation separated by long periods of non-deposition or low rates of deposition.

Geological evidence for Pleistocene sea-level highstands along the South Coast, in the form of both sedimentary deposits and erosional features, have been postulated for almost a century (Krige, 1927) and documented over at least the last five decades with the first detailed investigations having been those of Martin (1962) and Marker (1987). More recent studies based on luminescence techniques have provided chronological constraints for at least two major sea-level highstands at 13 m AMSL and 6 – 8 m AMSL during the middle to late Quaternary (Bateman et al., 2004; Jacobs and Roberts, 2009; Carr et al., 2010; Roberts et al., 2012). The numerical age data have confirmed that these events correspond to the interglacial periods MIS 11 (~440 ka) and MIS 5e (~125 ka), respectively. Evidence for Holocene sea-level fluctuations in this region have been described near Knysna (Marker and Miller, 1993) and indicate a middle Holocene highstand of 2 – 3 m AMSL, consistent with the Southern African records of Compton (2001, 2006) and Ramsay (1995) from the west and east coasts. Geological evidence for Quaternary sea-level lowstands along the South Coast continental shelf was first recognised by Birch et al. (1978) and Martin and Flemming (1986, 1987) in the form of offshore cemented palaeodunes (aeolianite). Although the depths of occurrence of aeolianite ridges were documented, no geochronological investigations were carried out. Bateman et al. (2011) presented palaeocoastline reconstructions based on relatively coarse resolution satellite data and showed how spatial variations in offshore topography potentially had a profound effect on sediment delivery and construction of these barriers. Until now, the submerged expression of Quaternary deposits on the South Coast had not been investigated with modern geophysical techniques.

The presence of alteration rims of authigenic feldspar at grain boundaries is used tentatively to consider carbonate productivity, as prolonged exposure without rapid diagenesis is suggested to have allowed alteration on grain boundaries. In this case, low carbonate productivity is suggested for MIS 15. In the case of MIS 11 cementation was relatively rapid, as alteration rims were not observed in these deposits. A carbonate-producing environment is therefore suggested for the MIS 11 interglacial. Authigenic rims are present, in relatively low abundance, at MIS 7c and are less prevalent in the MIS 6 deposits, suggesting increased carbonate towards MIS 6 and on the ensuing transgression to the Last Interglacial. Succeeding the peak of MIS 5e, authigenic rims reappear in the rock record until MIS 4, potentially indicating a temporary decrease in productivity for this time interglacial termination.

Diagenesis in this study is dominated by post-depositional cements, including late-stage presence of organic matter in a reducing environment interpreted to be associated with an abundance of water seeping through the unconsolidated sediments of the shelf, as well as the likelihood for dissolved material from overlying palaeosols. Tannin rich waters may result in organic matter included in calcite cements. Meteoric diagenesis generally showed that in the vadose zone, water was concentrated at grain contacts and in the phreatic zone water filled the pores.

4.13.2 Incision of coastal caves

The presence of steep rocky cliffs on the trailing edge, passive margin is a remnant feature of irregular erosion as a function of lithological substrate discussed above. Coastal cliff retreat on marine transgressions has shaped the Pinnacle Point shoreline and incised the coastal caves between Cape St. Blaize and Dana Bay. The preferred zones of weakness are generally represented by faults within the Skurweberg Formation in the vicinity of Pinnacle Point. A minimum age of incision, derived from cave deposits, places cave formation at 1000 - 1100 ka (Pickering et al., 2013) but the highest elevation caves (~30 m AMSL) attest to a longer history of erosion by high sea-levels, likely associated with the Pliocene high sea-level.

Mechanical weathering by wave action is considered the primary erosional agent in most storm-wave and swell-wave settings (Griggs and Trenhaile, 1994) and the pressure exerted on coastal cliffs by standing, breaking and broken waves are highest at, and slightly above, still water level (Trenhaile, 1987). The zones of maximum wave pressure and greatest erosion are therefore considered here to be the area above the neap high tide level in this microtidal environment. The raised elevation of incised caves, notches and planations suggest that the transgressive incision of this coastline has prevailed since before the onset of the mid- to late Quaternary glacial-interglacial cycles as the highest incisions lie approximately 30 m AMSL. When reaching comparable elevations at the lower levels, reactivated erosion has likely occurred on ensuing transgressive cycles, resulting in the two dominant erosional bands at ~15 m AMSL and ~5 m AMSL at Pinnacle Point.

Although initially incised by wave action, the sea cliffs are also shaped by mass wasting processes Accumulations of rock debris at the base of the sub-aerially and submerged cliffs at Mossel Bay and the complete collapse of Staircase Cave, suggest evidence for mass wasting which is probably likely to occur in highly fractured geological terranes such as this study area. Waves can, in addition, work boulders on the cave floors to act as erosive agents to enhance rate of erosion.

In addition to geological structure, lithology is also considered a major factor in the incision of coastal cliffs along the Pinnacle Point coast, where zones of weakness (structural or lithological) have provided zones of accelerated wave erosion on sea-level transgressional cycles. During sea-level highstands the absence of an adjacent protective beach facilitates this process. The adjacent nearshore environment of Pinnacle Point generally lacks topographic barriers to dissipate wave energy as observed in the seismic record. Cliff retreat in this region is therefore considered to be episodic, coinciding with high sea level and a high-energy migrating shoreline, terminating against the base of these sea cliffs.

Scharf et al. (2013) suggested that the extremely slow denudation rates calculated for the CFB are predominantly a function of lithology. In the case of the Pinnacle Point coast, the incision of caves still preserved at the

shoreline may be ancient and subjected to only minor cliff retreat. A preliminary calculation attempted here from the geological cross section of Viljoen and Malan (1993), comparing the thickness of the Skurweberg Formation anticlinal seaward and landward limbs which exhibit a difference in thickness of ~10 m, suggests that cliff retreat on the seaward limb of the anticline may have taken place for at least 1 Myr using an average erosion rate of 10 m/Myr after Tinker et al. (2008a) or 3.3 Myr using the denudation rate of 3.3 m/Myr as suggested by Scarf et al. (2013) . These values bracket minimum and maximum estimates for the amount of overall erosion of this coast and is supported by the age of cemented deposits on the inner walls of caves PP 13G and Opera House Cave dated to 1000 - 1100 ka (Pickering et al., 2013). This rather preliminary calculation is, however, based on natural denudation calculated for the *interior* of the CFB and the rates do not take into account erosion by coastal processes at the shoreline, which are very likely to have been accelerated when located at sea level. It also assumes a uniform compressive stress applied in the folding of the strata.

5 SEISMIC AND SEQUENCE STRATIGRAPHY OF THE SOUTH COAST

5.1 Introduction

Recent seismic stratigraphic studies on the South Coast have concentrated on continental margin processes (Uenzelmann-Neben and Huhn, 2009), or the continental slope in pursuit of oil and gas (PASA, 2012). Such studies rely on lower resolution data generated by deeper penetrating seismic systems than the data produced by the sub-bottom profilers used in this study. Deep structure of the continental shelf and Mesozoic to Early Cenozoic stratigraphy are outlined in detail by Dingle et al. (1983), and summarised in Brown (1995) and Broad et al. (2006, 2012) from a hydrocarbon perspective. The last non-commercial published shelf surveys conducted on the South Coast using shallow penetrating seismic systems aimed to understand the distribution of the Holocene sediment wedge (Birch, 1981; Martin and Flemming, 1986).

This chapter considers the broad-scale evolution of the South Coast shelf and coastal plain from a seismic stratigraphic perspective, with most emphasis placed on the Quaternary record. Interpretation of selected representative profiles from the three datasets with high resolution coverage in Mossel Bay and Swartvlei, as well as regionally spaced continental shelf seismic transects offshore of Still Bay, Mossel Bay and Wilderness (see Chapter 3 for details) are treated holistically for the purposes of this study. Detailed interpretation of the sesmic stratigraphy is presented in Chapter 6.

Sequence stratigraphic procedures have been developed and refined by Mitchum and Vail (1977), Vail (1987), Posamentier and Vail (1988) and recently summarised by Coe and Church (2003) and Catuneanu (2006). The nomenclature and associations presented here are based on the proposed standardised terminology of Catuneanu et al. (2009). Despite this work having been questioned by Helland-Hansen (2009) and Zecchin (2010), the sequence stratigraphic terminology of Catuneanu et al. (2009) arguably remains the most consistent, and accordingly is utilised in this chapter. The interpretations in this work recognise four systems tracts in each complete sequence (as per Coe and Church, 2003; Catuneanu et al., 2009): the falling stage systems tract (FSST), the lowstand systems tract (LST), the transgressive systems tract (TST) and the highstand systems tract (HST). Within these classification schemes, a systems tract refers to the subdivisions of sequences that consist of discrete depositional units differing in geometry from other systems tracts and which have distinct boundaries (Coe and Church, 2003).

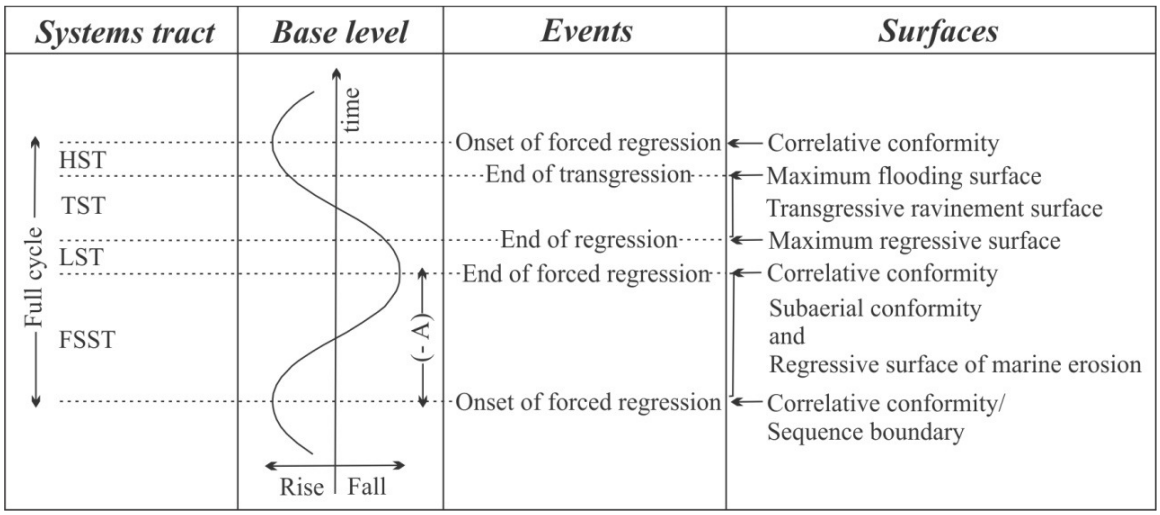

Figure 5-1. The relationship between the seven surfaces identified in sequence stratigraphy and the four phases of the base level cycle. Abbreviations are as follows: (–A) – negative accommodation space.

5.2 The basis for sequence stratigraphic interpretations

5.2.1 Sequence boundaries

With a relative fall in sea level, no sediment is deposited in the proximal section of the depositional profile and a zone of sediment by-pass (unconformity) is created (Coe and Church, 2003). Where marking the commencement of new sequences in the South Coast depositional record, these erosional/non-depositional features are interpreted to represent sequence boundaries. Three sequence boundaries were mapped in this study, indicative of erosional truncation and resultant sediment by-pass associated with a forced regression. Marine erosion of existing sediments occurred as currents and waves impinged lower down the depositional profile and the re-deposition of these eroded sediments is interpreted to become progressively distal.

5.2.2 Unconformities and correlative sub-aerial conformities (regressive surfaces of marine erosion)

Sub-aerial conformities are erosional surfaces that form throughout the cycle of base level fall (Catuneanu et al., 2009). Surfaces that correlate laterally with sub-aerial unconformities are interpreted to be marine correlative conformities. Towards the termination of the FSST, with changes in the direction of base-level shift at the coastline independent of sediment supply (Catuneanu et al., 2009), the correlative conformity develops. This study takes the correlative conformity at the base of the FSST after Posamentier et al. (1988) and Posamentier and Allen (1999).

5.2.3 Falling stage systems tract deposits and structures

The FSST develops in response to forced regression, where accommodation space is decreased by a fall in sea level, independent of sediment supply (Hunt and Tucker, 1992; Coe and Church, 2003). Along the South Coast continental shelf, the deposits associated with the FSST shift basinward and accrete lower down the depositional profile.

5.2.4 Lowstand systems tract deposits

Subsequent to the FSST, with relative sea level having reached the minimum elevation on the depositional profile, sedimentary progradation eventually increases accommodation space (Coe and Church, 2003). These progradational and aggradational parasequence sets deposited at this time, between minimum relative sea-level and the distinct increase in accommodation space, represent the LST. The LST thus relies on significant sediment supply and these deposits were not observed at many locations on the South Coast as the maximum depth mapped in this study was 110 m BMSL, significantly shallower than the 130 m BMSL LGM lowstand.

5.2.5 Maximum regressive surface

Associated with the FSST and LST, a sub-aqueous erosional surface younging in a basinward direction and scoured by waves in a lower shoreface environment (after Plint, 1988), is interpreted to represent the maximum regressive surface.

5.2.6 Stillstand deposits

The basinward shift of the shoreline during stillstand is a function of 'normal' regression, where the rate of increase in accommodation space is exceeded by sediment supply (as per Coe and Church, 2003). The author proposes that the mechanism for this process on the South Coast shelf is dominated by significant sediment supply on an ensuing sea-level stillstand. The net effect is an infilling of accommodation space and the deposition of a regressive succession. Episodic fluctuations in sea level at the elevation of the stillstand (for instance, generated by storm events), is thought to influence the consistency in sediment supply and accounts for the subdivision of facies within the seismic units.

5.2.7 Wave ravinement surfaces

Long-term creation of accommodation space exceeds sediment supply and the resultant sea-level transgression forces sediment landward (Coe and Church, 2003). The retrogradational parasequence sets are underlain by a transgressive surface or wave ravinement surface (WRS). On the South Coast, a prominent surface has been

mapped, interpreted to represent the shift of the shoreface and foreshore sediments. This occurs from the time of the LST towards the end of TST, pre-deposition of the HST sediments. Transgressive ravinement surfaces (Nummedal and Swift, 1987; Nordfjord et al., 2009) refer to erosional surfaces that form in response to wave or tidal scouring during transgression in coastal or upper shoreface settings. The recognition of erosional shoreface retreat by Swift et al. (1972) was of particular importance. This process redistributes sediments from the shoreline to the shelf during transgression. Erosional shoreface retreat generates a regionally transgressive ravinement surface and commonly has great influence on the shaping of the shelf topography. The ravinement surface is a significant marker forming the base of the TST on the south coast.

5.2.8 Transgressive systems tract deposits

The TST is deposited when the increase in accommodation space is greater than the rate of sediment supply (Coe and Church, 2003; Catuneanu et al., 2009). The dominant sediment deposition occurs proximally, associated with the rise in sea level and parasequences retrograde.

5.2.9 Maximum flooding surfaces and deposits

As distal portions of the depositional profile become starved of sediment with an increased rate of sea-level rise, these drowned areas commonly form condensed horizons representing marine unconformities or thin marine deposits (Coe and Church, 2003). On the low gradient South Coast shelf, the rise in the water table due to maximum flooding may promote the formation of swamps/marshes/flooded areas, particularly in the vicinity of existing rivers.

5.2.10 Highstand systems tract deposits

As sea level rises and accommodation space is created, aggradational stacking of parasequences occurs (Coe and Church, 2003). As the rate of sea-level rise is outpaced by sediment supply, in proximal areas, depositional parasequences are forced to prograde into the basin. The HST is deposited between the maximum rate of sea-level rise and maximum relative sea level and is associated with a regime of normal regression.

5.3 Seismic units and facies

The seismic stratigraphic investigation of the South Coast has revealed seventeen seismic units in the region (A – Q) (Figures 5-2 – 5-10), some of which are further sub-divided into constituent seismic facies (SFi – iii; Table 5-1; and a larger A3 fold-out copy provided in Appendix V). The seismic facies are defined according to distinctive characteristics and these occur repeatedly in the record, at various stratigraphic levels. The 17 discrete

seismic units belong to 9 sequences and are bounded by 2 unconformities (U/C 1 and 2), 3 regional sequence boundaries (SB 1, 2 and 3) and 1 wave ravinement surface (WRS). Though numerous reflectors were observed, most are not interpreted to represent prominent bounding surfaces, and were therefore applied only in the geometric classification of clinoforms, where applicable. The three clinoforms (Reflectors *l, m* and *o*) considered to be traceable across strike or across facies were named and appear in Table 5-1 and Figures 5-2 – 5-10. In addition to seismic units and bounding surfaces, geological units from Chapter 4 are included in Table 5-1 for context. Where not directly correlated to the offshore record, these units are clearly demarcated.

Table 5-1. Seismic units and interpreted ages of the South Coast shelf deposits and Swartvlei sediments. Abbreviations are as follows: FSST- Falling stage systems tract, LST- Lowstand systems tract, TST- Transgressive systems tract, HST- Highstand systems tract, SB – Sequence Boundary, WRS – Wave Ravinement Surface. Abbreviations of representative regions (used only in this table): S – Still Bay, G – Gouritzmond, V – Vlees Bay, M – Mossel Bay, W – Wilderness, Se – Sedgefield, Sw – Swartvlei. A separate A3 fold-out version of this table is available in Appendix V.

Seismic unit	**Seismic facies**	**Stratal characteristics of clinoforms**	**Seismic facies interpretation**	**Interpreted environment of deposition**	**Systems tract**	**Thick ness**	**Interpreted age**	**Sequ ence**	**Present in region**	**Assoc-iated geologi-cal unit**
Q	N/A	Not observable	Basin infill	Low energy back-barrier basin infill	Stillstand	≤ 9 m	Recent	9	Sw	
P	N/A	Acoustically transparent; low-amplitude divergent reflectors	Basin infill, progradation	Back-barrier margin deposits (sandbanks) accreted since the fall from the Holocene highstand (Bredasdorp Group – Strandveld Formation)	FSST	≥ 5 m	Holocene Highstand to Recent		Sw	H 2
Sequence Boundary (SB) 3 - Erosional truncation of underlying surface associated with shoreline retreat – Holocene highstand to present										
O	SFO iii	Acoustically transparent, wedge, low amplitude divergent clinoforms	Sediment accumulation in response to rising sea-level	Sedimentary back edge margin in Swartvlei and development of coastal dunes (Bredasdorp Group – Strandveld Formation)	HST	≤ 12 m	Late Holocene	8	Sw	Marine sediment wedge
O	SFO ii	Acoustically transparent, wedge, low amplitude divergent clinoforms	Sediment accumulation in response to rising sea-level	Transgressive deposit/inner to outer shelf prograding Holocene sediment wedge (Bredasdorp Group – Strandveld Formation)	LST-TST	≤ 8 m	Post-LGM		S,G, V, M, Se	Marine sediment wedge
Reflector o – maximum regressive surface on the shelf - Late Holocene										
O	SFO i	Semi-transparent or acoustically transparent	Sediment accumulation in response to rising sea-level	Marine transgressive sediments, capping deposits of incised channels. Shoreface sediments	LST-TST	≥ 8 m	MIS 2-pre Holocene Highstand	8	G, V, M, W, Se, Sw	Marine sediment wedge
N	N/A	High to medium amplitude discontinuous, chaotic reflectors.	Aeolianite	Mobile sands on an active palaeoshoreline	TST	≥ 20 m	MIS 2 – pre-Holocene highstand		Sw	H 1
Wave Ravinement Surface (WRS) - Regional marine flooding event across the rapidly drowning continental shelf – latest Pleistocene, early to late Holocene										

M	SFM ii	Structureless, high acoustic impedance	Basin infill	Lagoonal or low energy coastal wetland environment. Can also be interdune deposits.	Maximum Flood-ing	≤ 4 m	Post-LGM	8	S, M, W	
Reflector m - separates lagoon facies – washover? Or storm lag?										
	SFM i	Acoustically transparent	Basin infill, progradation	Lagoonal or low energy coastal wetland environment. Can also be interdune deposits.	Stillstand/ maximum flooding	≤ 4 m	Post-LGM	8	M, W	
L	SFL ii	Low amplitude, horizontal clinoforms; semi transparent	Basin infill during stillstand	Low energy back-barrier basin infill. This low energy environment is protected by adjacent dune ridges	Stillstand (minor LST)	≤ 5 m	MIS 4 - 3		M, W	Pu 11
Reflector l - separates back-barrier facies – washover? Or storm lag?										
L	SFL i	Low- to medium amplitude discontinuous reflectors	Basin infill during stillstand	Base of back-barrier succession: lagoonal channel fill and floodplain facies	Stillstand (minor HST)	≤ 4 m	MIS 4 - 3	8	M	Pu 11
K	SFK ii	Semi-transparent deposits adjacent to SFK i	Progradation: high sediment supply	Flood plain or tidal flats deposits	LST	≤ 5 m	~55 m & ~95 m BMSL, MIS 5 d-c; 2 - 1		M, W	
K	SFK i	Parallel and sub-parallel chaotic reflectors infilling structural depressions, overlying SFG ii	Laterally discontinuous incised channel fill; onlapping clinoforms	Incised channel infill sequences (likely fluvial or estuarine or lacustrine regressive facies)	Stillstand	≤ 4 m	MIS 5e - 2		G, V, M, W, Se	
J	N/A	High to medium amplitude discontinuous, chaotic reflectors.	Aeolianite and beach deposits (stillstand palaeoshorelines) associated with SB 2	Mobile sands on an active palaeoshoreline	FSST	≤ 20 m	MIS 5e - 2		G, V, M, W, Se	Pu 5, 6, 8, 11
Sequence Boundary (SB) 2 - Erosional truncation of underlying surface; deposition/rubification/soil formation processes associated with shoreline retreat - MIS 5e-2										
I	N/A	Chaotic reflectors; rough texture	Aeolianite - stillstand palaeoshorelines	Mobile sands on an active palaeoshoreline (Bredasdorp Group – Waenhuiskrans Formation)	HST	≤ 10 m	Last Interglacial (MIS 5e)	7	Sw	Pu 16, 17
H	N/A	Acoustically	Marine	Coastal wetlands	Maximum	≤ 3 m	MIS 6 – 5e		V	

		transparent unit infilling depressions on SB 1	overprinting with rapid burial, associated with transgression		flooding					
G	SFG ii	Parallel and sub-parallel reflectors infilling structural depressions, can be acoustically transparent. Onlapping clinoforms	Channel infill by dominantly marine sediments	Incised channel infill sequence and shelf sedimentation on flat gradients	TST	≥ 6 m	MIS 6 – 5e		G, M. Se	
Maximum Flooding Surface (MFS)										
G	SFG i	Poorly defined high amplitude, chaotic reflectors, truncated against channel margins	Fluvial lag deposits	Incised channel infill sequences (likely fluvial or estuarine or lacustrine regressive facies)	FSST/LST/ HST	≤ 4 m	MIS 7 - 6	7	G, M. Se	
F	N/A	High to medium amplitude discontinuous, chaotic reflectors. Produces acoustic blanking of underlying strata	Aeolianite and barrier beach deposits (stillstand palaeoshorelines) associated with SB 1	Mobile sands on an active palaeoshoreline (Bredasdorp Group – Waenhuiskrans Formation)	FSST; TST	≤ 12 m	MIS 7; 6 – 5e		G, M, W	Pm 9, 11, 12, 13, 14, 15, 16, 17
Sequence Boundary (SB) 1 - Sub-aerial exposure and erosion of the substrate - Middle Miocene to Pleistocene, most recent reactivation along this surface: MIS 7 - 6										
E	N/A	Mid- to outer shelf deposits, aggradational to retrogradational parasequence	Extensively planed unit lacking clearly discernable reflectors.	Upward fining cycles of coarse sandstone grading into calcareous clay Cape St. Blaize Group. Correlated with regional stratigraphy	TST	>20 m	Palaeogene	3	W	
Unconformity (U/C) 2 - Unconformity/correlative conformity - Cretaceous -Tertiary boundary 22At1										
D	N/A	Mid-shelf aggradational to progradational parasequence	Moderate-amplitude oblique clinoforms dipping shallowly eastward	Transitional marine and prograding shelf deposits Uitenhage Group Buffelskloof and Hartenbos Formations	HST	>60 m	Early Cretaceous Valanginian – Aptian	2	M	
Unconformity (U/C) 1 - Major regressional hiatus - Early Cretaceous Synrift boundary 1At1										
C	N/A	Inner shelf retrograding parasequence;	Moderate-amplitude divergent	Fluvial and shallow marine facies deposited in response to rising sea-level	TST	>70 m	Late Jurassic - Early Cretaceous	1	V, M	

		subordinate incisions on upper boundary	clinoforms. Onlap and downlap.	Uitenhage Group Enon and Kirkwood Formations (Pletmos Basin)			Portlandian - Berriasian			
B	N/A	Acoustically impenetrable	Expressed as bedrock	Uitenhage Group Robberg Formation. Correlated with regional stratigraphy	Indeterminate	>20 m	Jurassic sandstone deposits		M	
A	N/A	Acoustically impenetrable	Expressed as bedrock	Table Mountain Group Skurweberg Formation (Infanta Arch). Correlated with regional stratigraphy	Indeterminate	N/A	Silurian sandstone deposits	Base - ment	S, G, V	

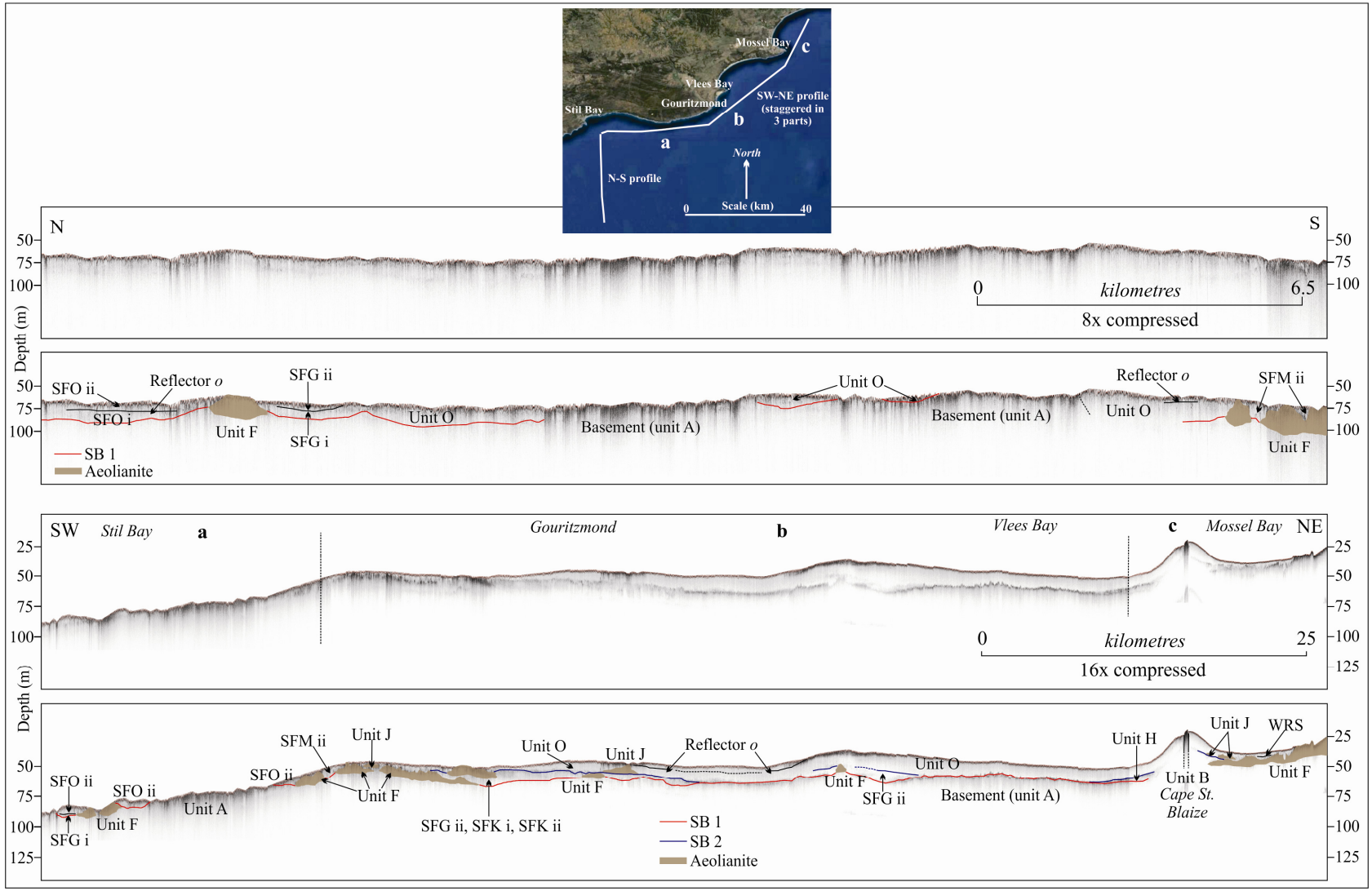

Figure 5-2. (Above) Westernmost (N-S) oriented seismic transect perpendicular to the coast offshore Still Bay (geographic region referred to Still Bay/S in Table 5-1). (Below) Composite coast-parallel oriented seismic transect from Still Bay (SW) to Mossel Bay (NE; geographic region referred to Gouritzmond/G in Table 5-1). Vertical exaggeration is 8x in A and B, and 16x in C and D.

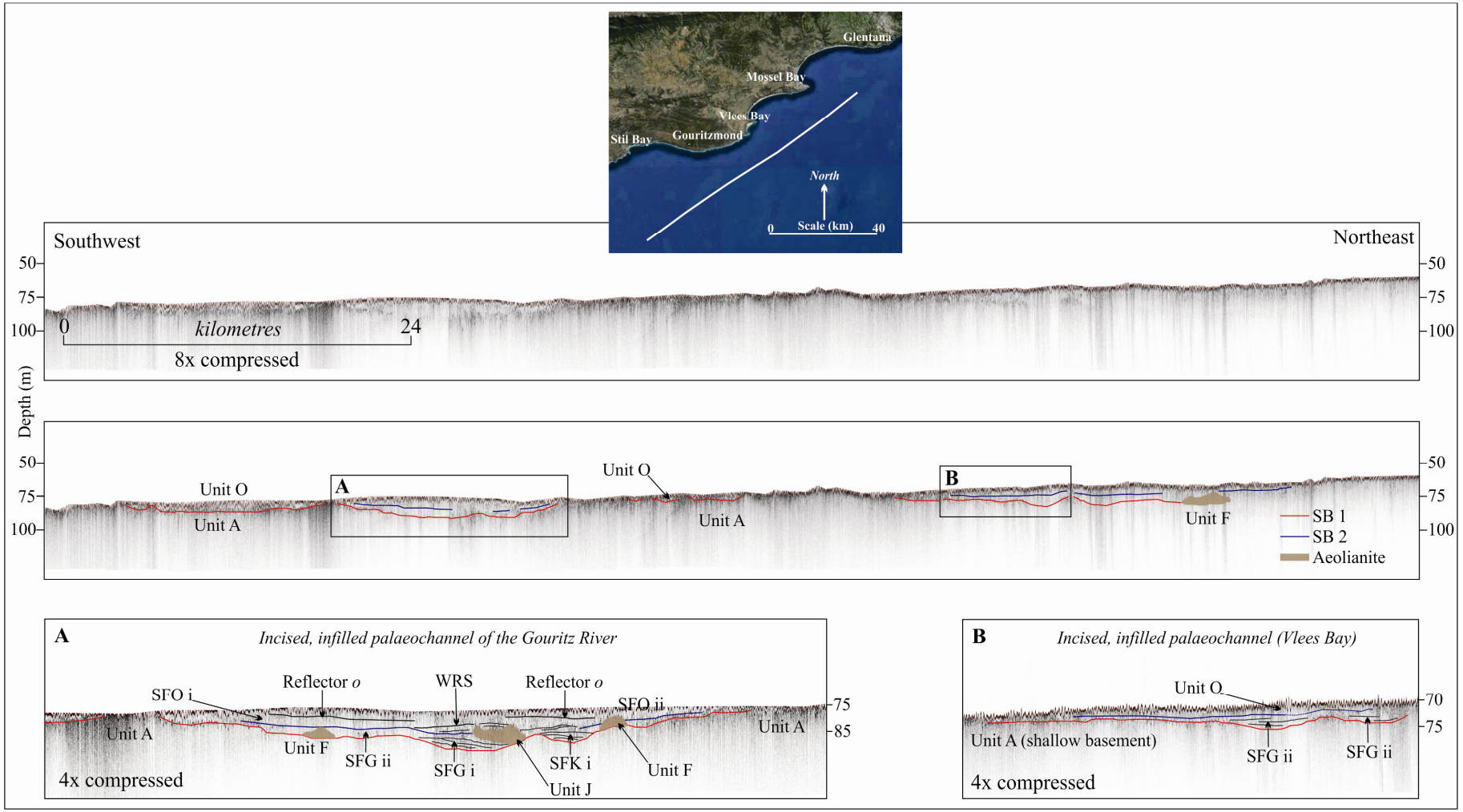

Figure 5-3. Obliquely-oriented transect from offshore Still Bay to Mossel Bay (geographic region referred to Gouritzmond/G in Table 5-1), with enlarged sections (A and B) showing two incised channels and their infill packages. Vertical exaggeration is 4x.

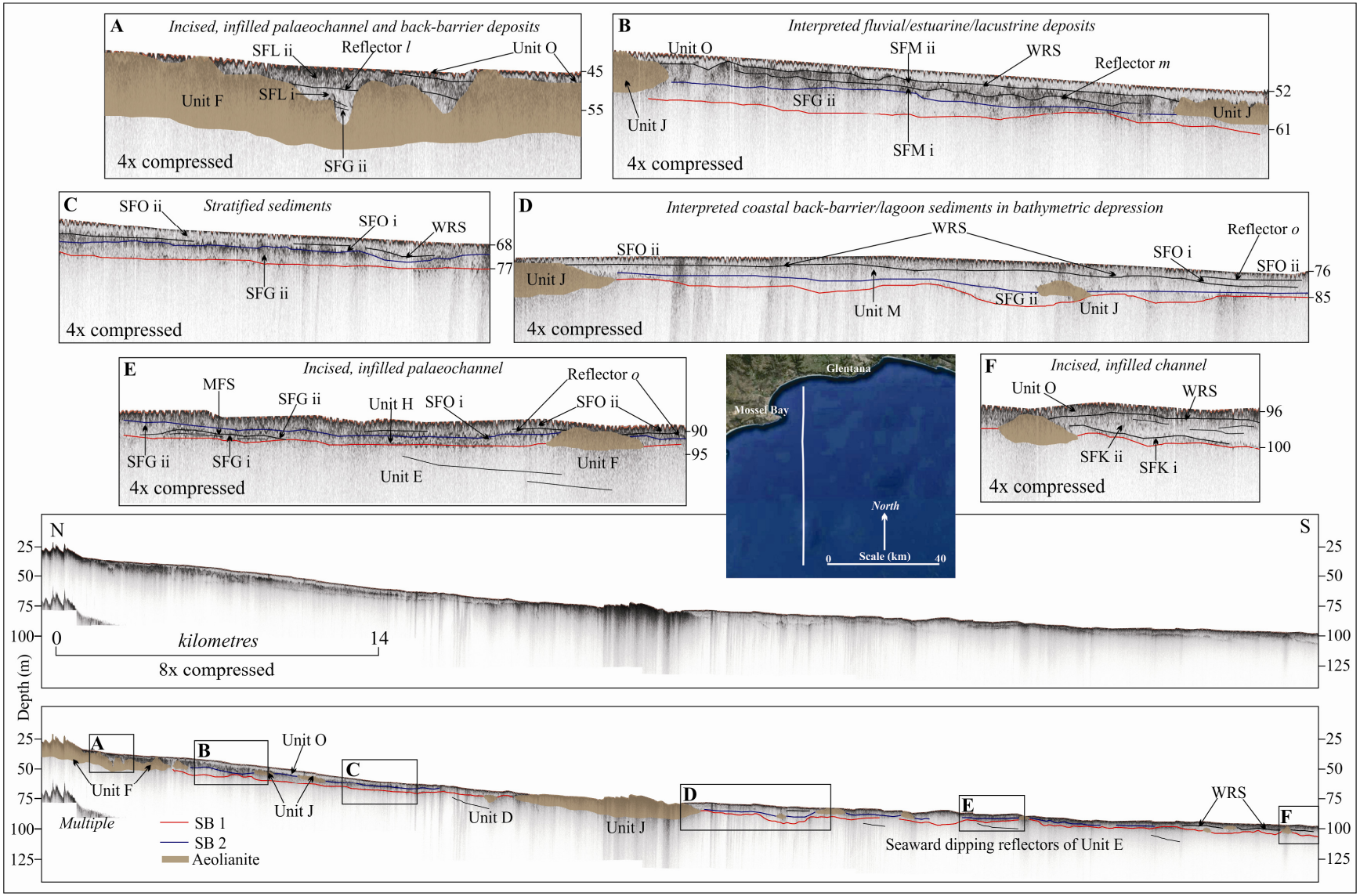

Figure 5-4. Seismic transect oriented perpendicular to the coast offshore Mossel Bay (geographic region referred to Mossel Bay/M in Table 5-1), with enlarged sections showing features of interest. Vertical exaggeration is 8x.

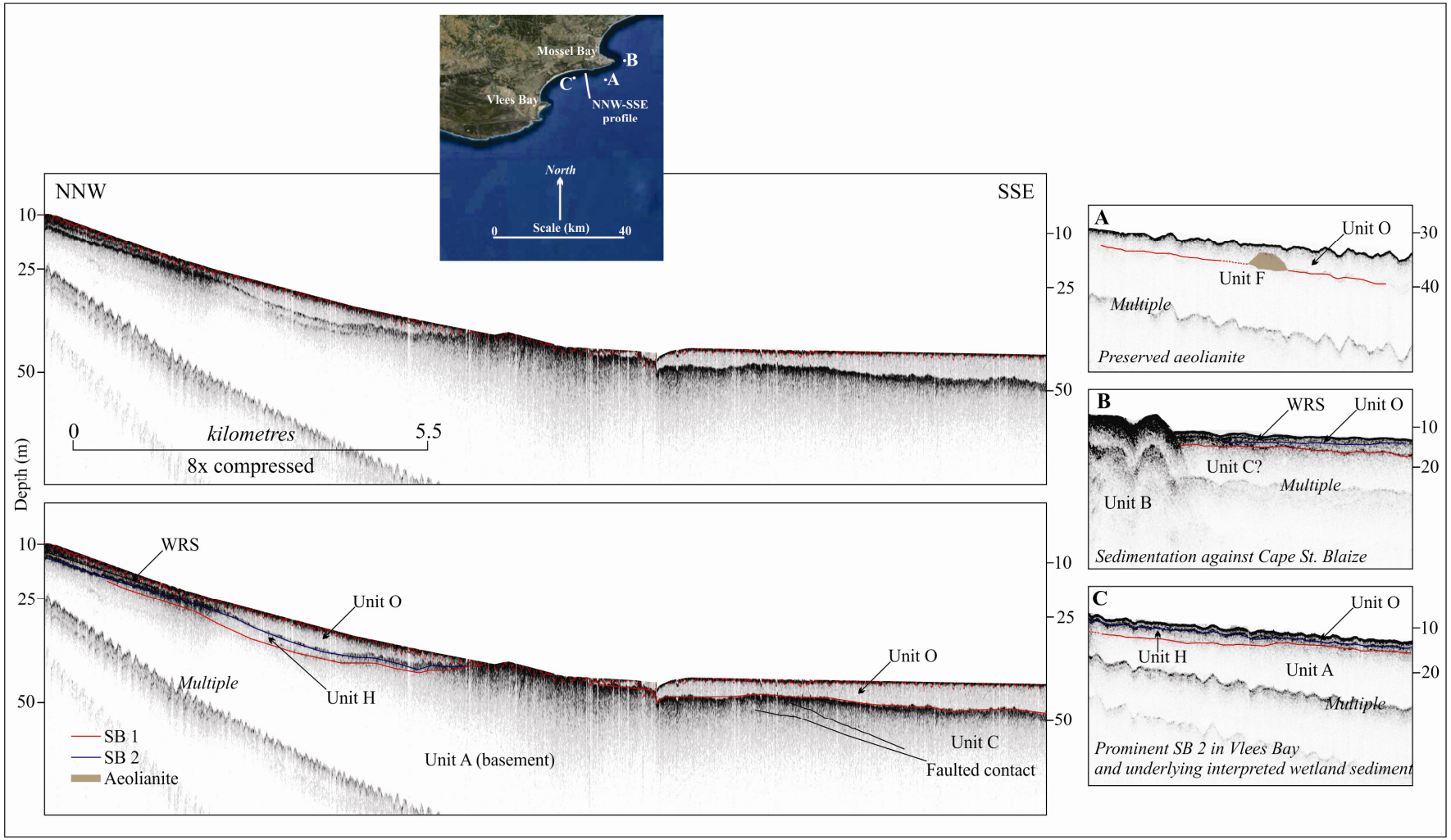

Figure 5-5. Various representative profiles from the Pinnacle Point inner- to mid-shelf study area (geographic region referred to Vlees Bay/V in Table 5-1). Vertical exaggeration is 8x.

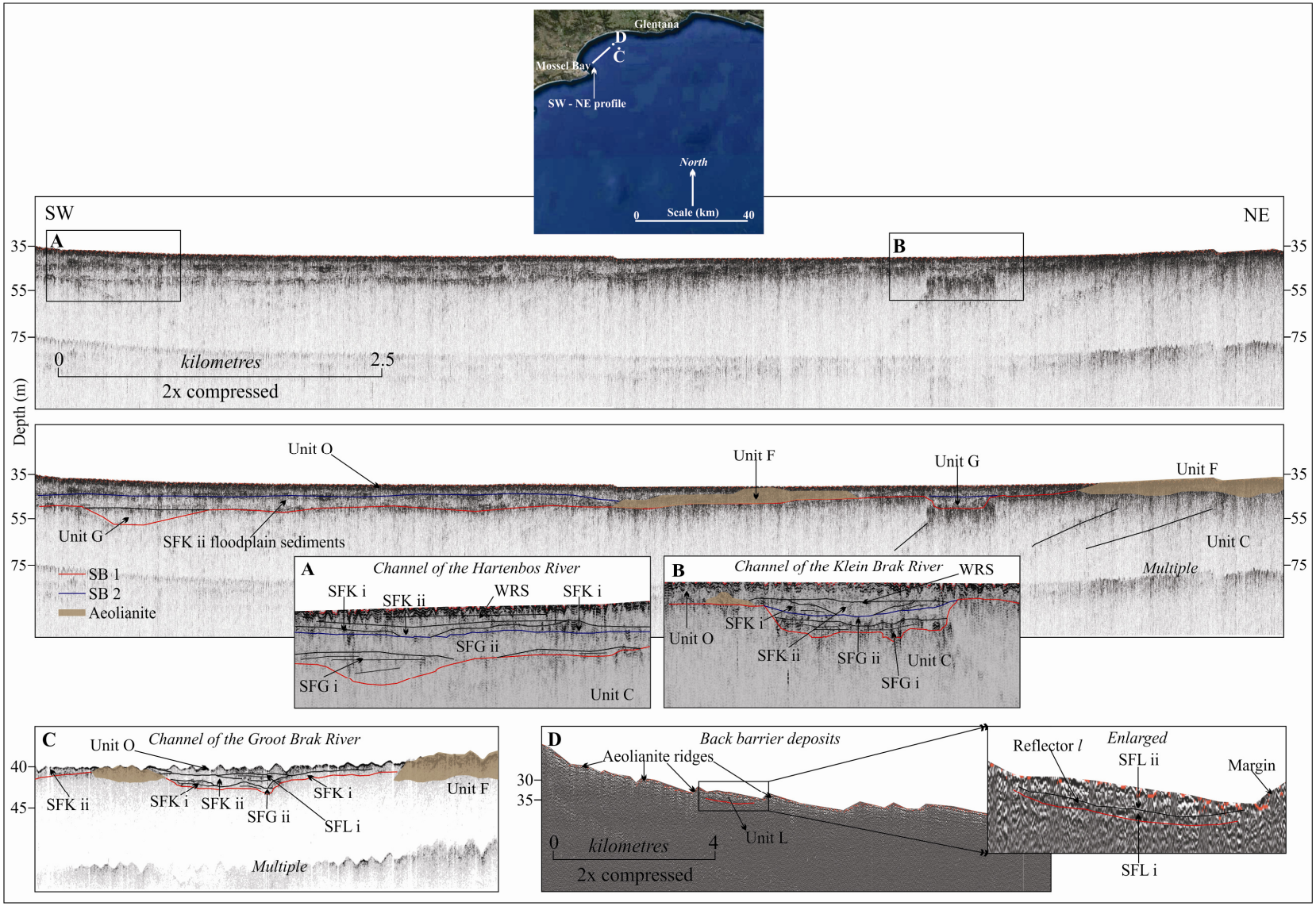

Figure 5-6. Various representative profiles from the Mossel Bay inner- to mid-shelf study area (geographic region referred to Mossel Bay/M in Table 5-1). Vertical exaggeration is 2x.

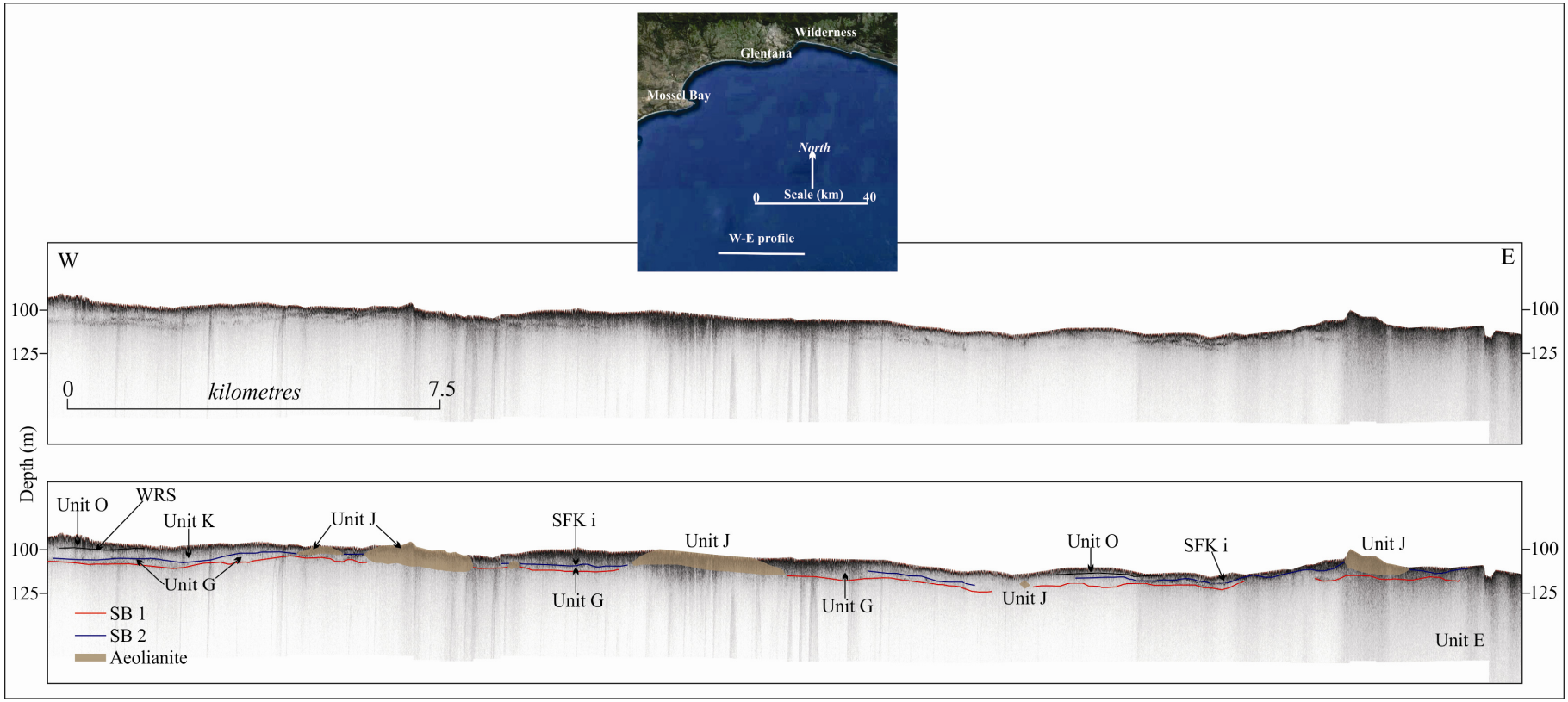

Figure 5-7. Coast-parallel oriented seismic transect from Mossel Bay to Wilderness near the LGM shoreline (geographic region referred to Mossel Bay/M in Table 5-1). Vertical exaggeration is 4x.

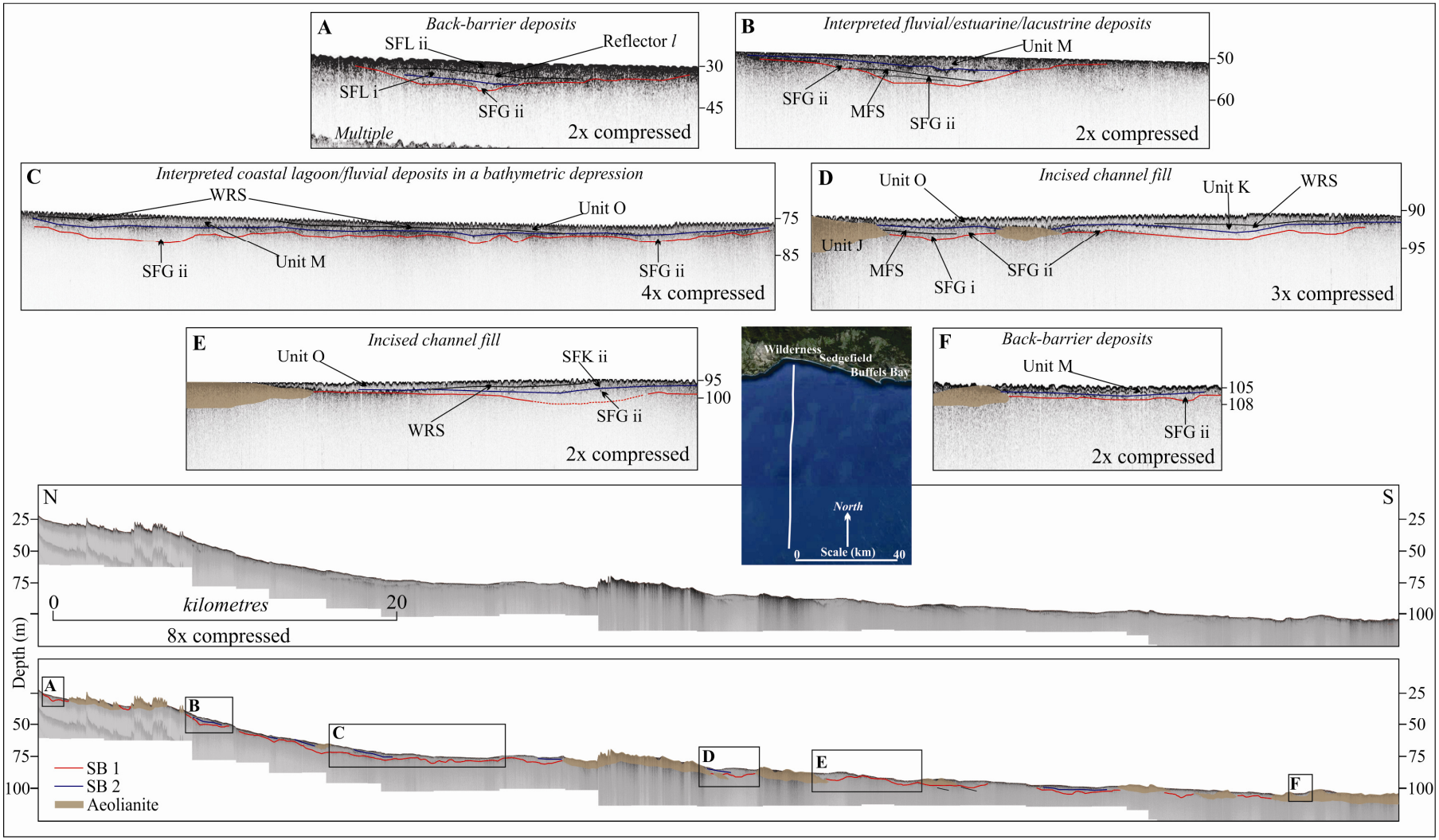

Figure 5-8. Seismic transect oriented perpendicular to the coast offshore Wilderness (geographic region referred to Wilderness/W in Table 5-1), with enlarged sections showing features of interest. Vertical exaggeration is 8x.

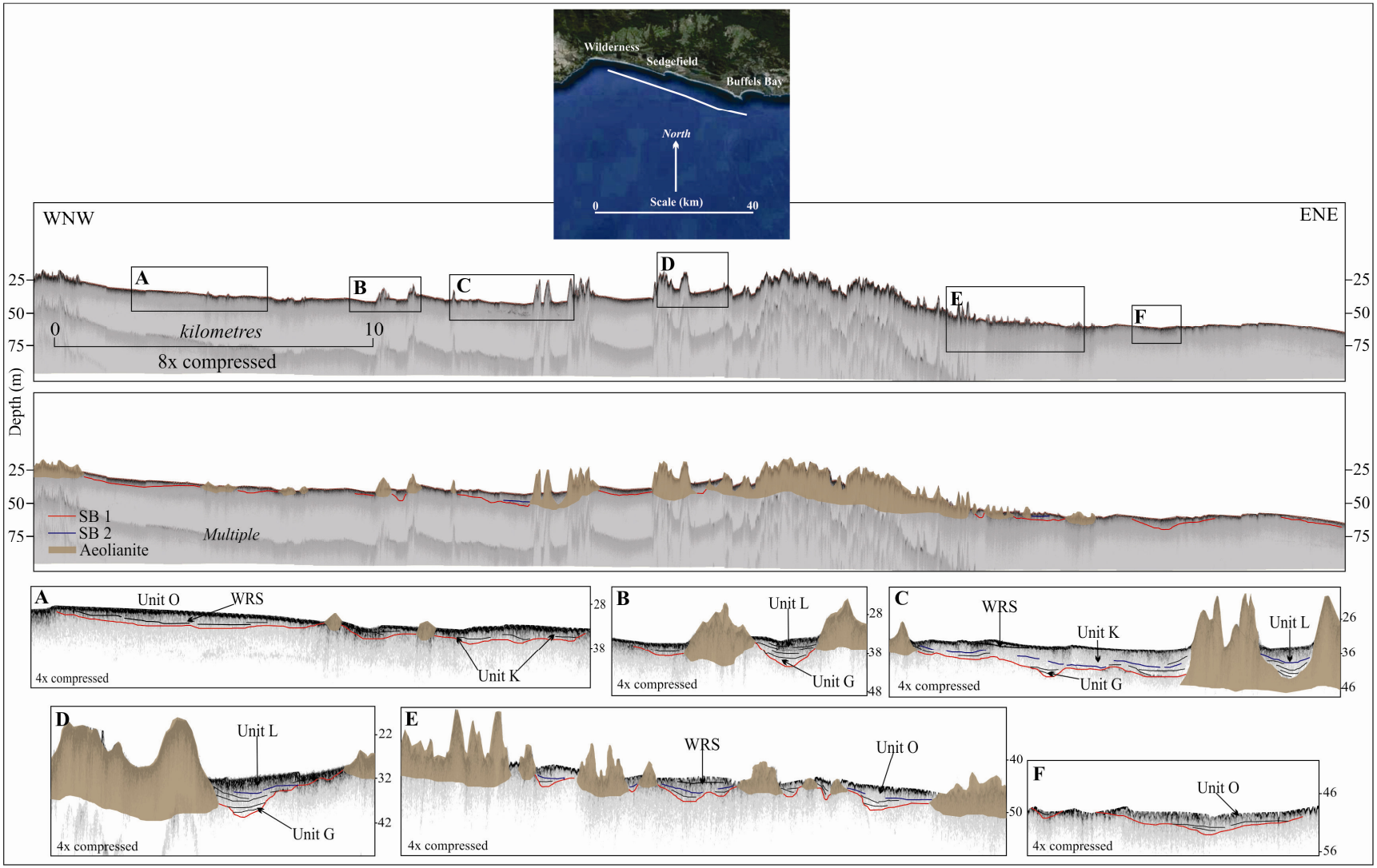

Figure 5-9. Easternmost coast-parallel oriented seismic transect from Wilderness to Buffels Bay (geographic region referred to Sedgefield/Se in Table 5-1), with enlarged incised channels intercepted along the profile. Vertical exaggeration is 8x.

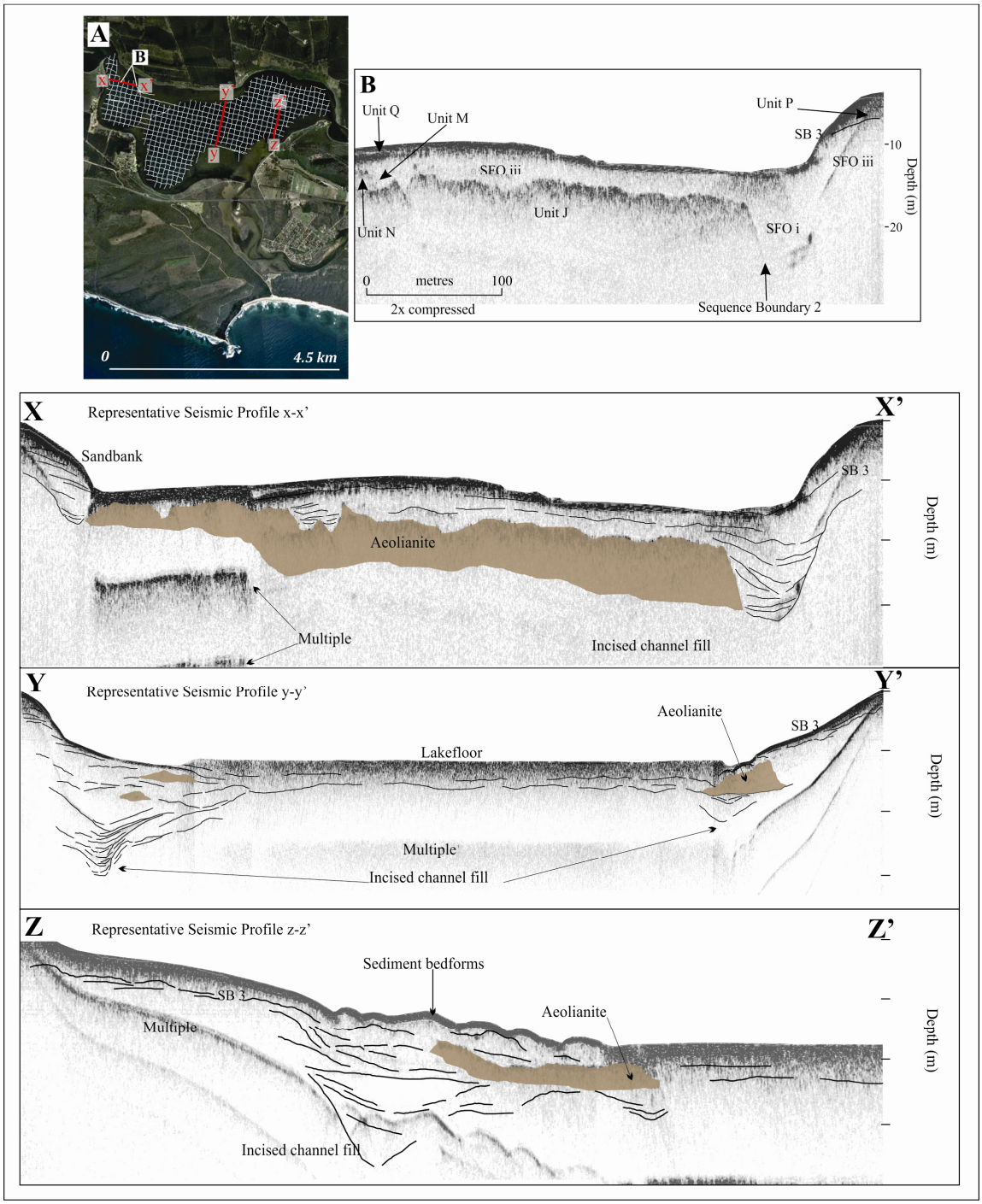

Figure 5-10. A. Navigational transects of selected seismic profiles from the Wilderness Embayment for context. B. Representative acoustic facies classed as seismic units in this study are displayed on a section of a profile within Swartvlei. Three Swartvlei seismic profiles are presented (X - X', Y - Y', Z - Z'), located on A, showing the relationship between incised channels on the lakefloor and the spatial distribution of aeolianite in the lake basin. Geographic region referred to Swartvlei/Sw in Table 5-1.

5.4 Seismic stratigraphic interpretation

From the continental shelf and Wilderness Embayment seismic stratigraphy, a broad sequence stratigraphic model of this system has been created by correlation with the well-documented regional stratigraphic successions in the area (Dingle et al., 1983; Viljoen and Malan, 1993; Broad et al., 2006; Bateman et al., 2011). The South Coast deposits are described in a detailed seismic, sedimentological and chronostratigraphic model in Chapter 6.

Unit A represents bedrock and is dominated in this region by the Silurian Table Mountain Group Skurweberg Formation arenites (Broad et al., 2006; 2012). Units B, C and D are associated with the Pletmos Basin stratigraphy (Broad et al., 2006), expressed onshore as the Cretaceous Uitenhage Group (Viljoen and Malan, 1993). Sequences 1 and 2 thus represent Synrift successions I and II, respectively (Figure 5-12, Figure 5-11). Unit E (Sequence 3) is interpreted as drift deposits, now exposed by extensive planation since the Neogene and forming the Agulhas Bank. The dominantly regressive sea-level movement from the Neogene into the Pleistocene (Figure 5-12; Miller et al., 2005a) accounts for non-deposition on the continental shelf that likely served as a zone of sediment by-pass and generated the hiatus that is expressed as SB 1. With the change in response of the Earth's internal feedback to the Milankovich cycles (Bradley, 1999) and consequent mid Pleistocene glacial – interglacials (e.g. Liesicki and Raymo, 2005), reactivation of existing surfaces left visible deposits in the seismic record with the onset of this climate pattern and relative tectonic stability in Southern Africa. Shelf sedimentation since at least MIS 7 and evolution of shifting shorelines now dominate the offshore and littoral zone record of the South Coast and stratigraphically form part of the Bredasdorp Group sedimentary record (after Malan, 1990). The high amplitude (130 m) 80 - 120 kyr glacial/interglacial cycles were initiated only by 0.9 Ma, with relatively steady 40 kyr, 20 - 80 m amplitude sea-level from 2.7 to 0.9 Ma. Thus, the impact of changes in sea-level underwent a major shift at 0.9 Ma and as a result much of what was deposited before that time was eroded away unless, like during the early Pliocene, it was deposited at high elevation of 25 m AMSL. Sequence 7, commencing with SB 1, preserves systems tracts providing insight into the depositional and erosional processes from MIS 7 to the Last Interglacial (MIS 5e). Sequence 8, the most complete sequence documented in this study, commenced with the retreat of sea-level from MIS 5e and extends to the Holocene highstand (MIS 1). Within Sequence 8, the response of sedimentation to stadial/interstadial cycles is documented in addition to the prevailing sedimentary processes to the overarching regressive and transgressive sea-level movement. Sequence 9 represents the ongoing evolution of the present shoreline within the Wilderness Embayment. This sequence commenced with the fall of sea level since the Holocene highstand.

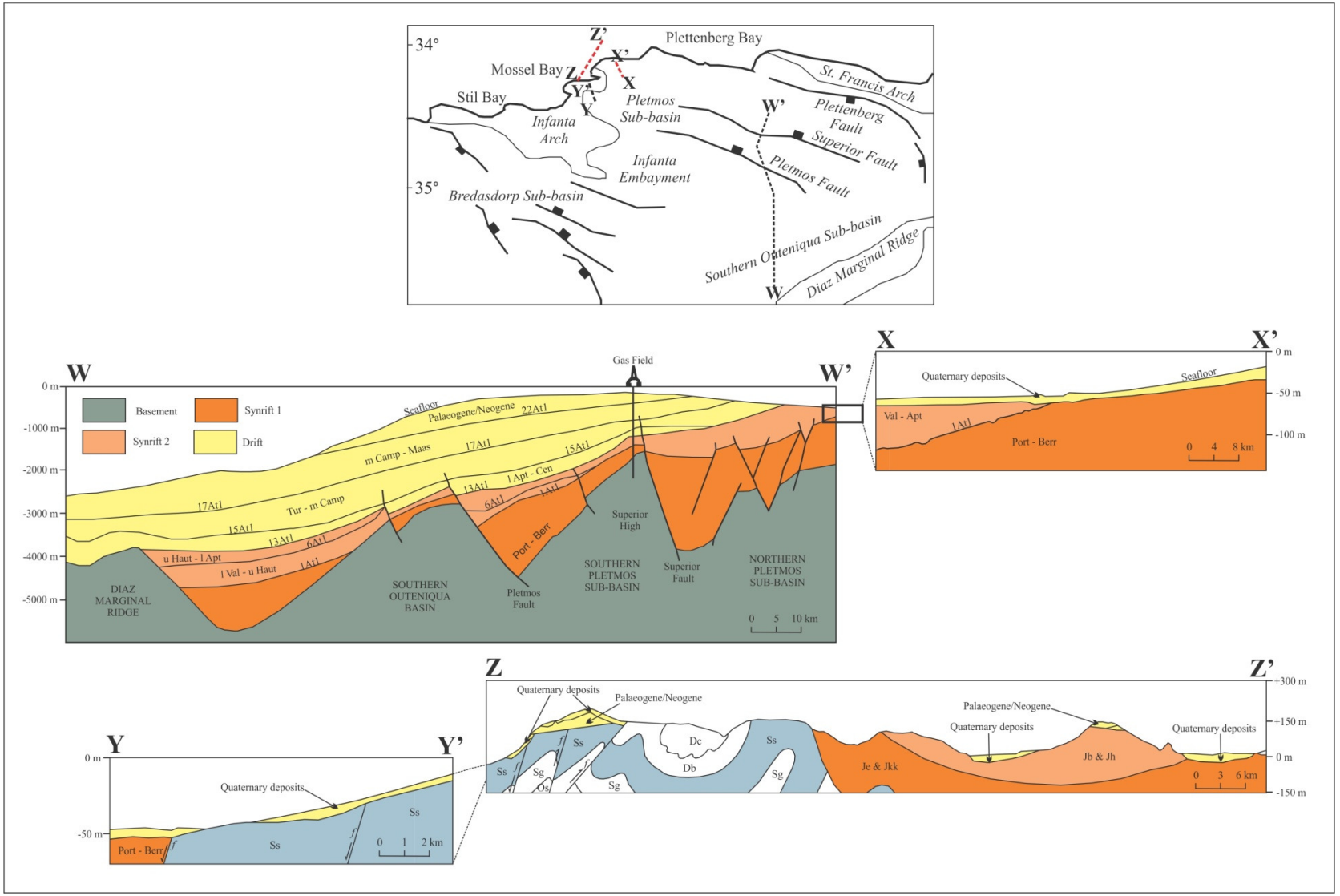

Figure 5-11. Correlated units (this study) to local and regional stratigraphy. A. Location of profiles, plotted on the structural geological setting (modified from Broad et al., 2006). B. Profile W - W' (deep offshore, modified from Broad et al., 2006), profile X - X' this study, profile Y - Y' this study, profile Z - Z' simplified from the CGS 1:50 000 geological map 3422AA (Mossel Bay) (Viljoen and Malan, 1993).

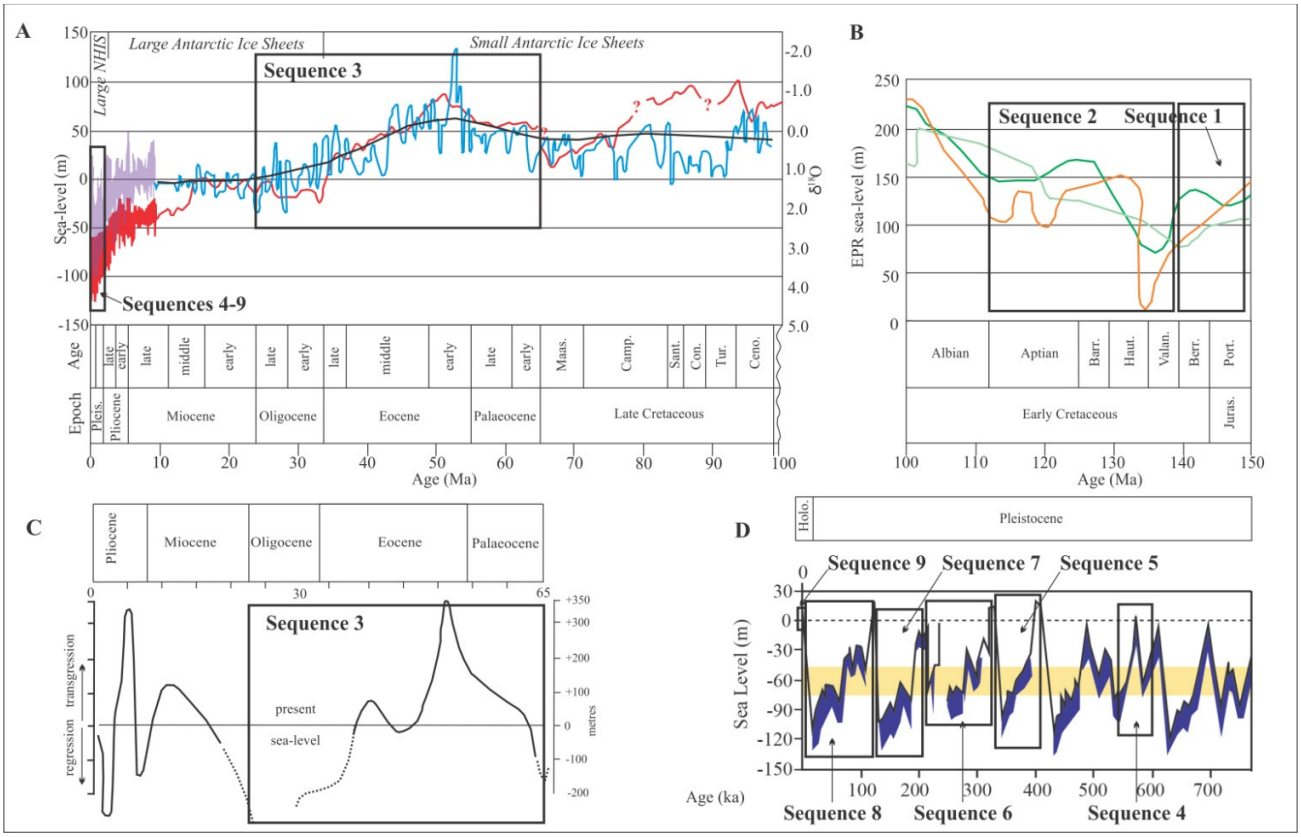

Figure 5-12. A. Global sea-level curves plotting the Cretaceous to Neogene deposits/sequences, after Miller et al. (2005b). For the Late Cretaceous – Pleistocene: global sea-level curve (blue) for the interval 7 to 100 Ma derived by backstripping data (van Sickel et al., 2004). Global sea-level (purple) for the interval 0 to 7 Ma derived from $\delta^{18}O$. Benthic foraminiferal $\delta^{18}O$ synthesis from 0 to 100 Ma shown in red. The portion of the $\delta^{18}O$ curve from 0 to 65 Ma from Miller et al. (1987). The $\delta^{18}O$ curve from 65 to 100 Ma is based on the data compiled by Miller et al. (2005a). The black line is the long-term fit to a backstripped curve. B. The Jurassic – Early Cretaceous shows Exxon Production Research data of Vail et al. (1977) (light green), Haq et al. (1987) (dark green), Haq and Al-Qahtani (2005) (orange). C. Local sea-level curve of Dingle et al. (1983). D. Quaternary glacio-eustatic sea-level curve of Bintanja and van de Wal (2008). Abbreviations are as follows: Holo. – Holocene, Pleis. – Pleistocene, Maas. – Maastrichtian, Camp. – Campanian, Sant. – Santonian, Con. – Coniacian, Tur. – Turonian, Ceno. – Cenomanian, Barr. – Barremian, Haut. – Hauterivian, Valan. – Valanginian, Berr. – Berriasian, Port. – Portlandian, Juras. – Jurassic.

5.5 Fluvial response to sea-level fluctuations

5.5.1 Palaeodrainage networks

A total of 16 incised channels of varying scales are identified on the South Coast shelf within the study area (Table 5-2; Figure 5-13). The bases of incised channels, typically represented by sequence boundaries, are generally concave-upward in form. In the westernmost section of the study area (Still Bay to Vlees Bay) the channels are extremely broad and shallowly incised in comparison with the eastern areas where the channels are still considerably broader and shallower than their onshore equivalents, but have a moderate width:depth ratio and tend more towards U and V shaped valleys. In general, it must be noted that all palaeochannels mapped on the mid- and outer shelf exhibit a vastly different character to their onshore and inner shelf geomorphic expressions. These systems are extensively broad and extremely shallowly incised and are likely associated with widespread lateral wetlands. The incised channels in the study area therefore consist either of: (1) broad and shallowly incised valleys; (2) narrow and relatively shallow incised valleys; or (3) shallow depressions.

A schematic representation of palaeodrainage networks incised on the continental shelf is provided in Figure 5-13. These inferences link interceptions of seismic channels from the profiles described above. The inferred channel courses shown in Figure 5-13 were constructed based on the distribution of rivers within the modern fluvial system, the antecedent geological substrate which governs the flow pattern, and the existence or absence of the dune barriers of the Wilderness Embayment in the case of the rivers in the east. Due to the regional nature of seismic data acquisition, it was not possible to generate an isopach surface showing continuous channel distribution. As such, thalweg borders were digitised and broad linkages drawn to create the drainage features as accurately as possible.

The channel geometry of incised systems on the South Coast shelf suggests that these drainage patterns were likely braided streams, referring to unstable low-sinuosity channel patterns and a wide shallow cross-section (Miall, 1997).

Within the Still Bay embayment, which ends at Gouritzmond, two channels characterise the incisions on the shelf. The westernmost channel is correlated to the Goukou River, which currently enters the Indian Ocean at Still Bay. A depression infilled with low acoustic impedance material was intercepted on two seismic profiles, and the palaeochannel of the Gouritz River spreads across a broad plain of approximately 18 km, with a channel ~4.5 km in width. The point of maximum vertical incision is merely 11.5 m (Table 5-2). The seismic profiles were collected in water depths greater than 50 m BMSL, so potentially relatively deeply incised landward channel forms on the inner shelf were not intercepted. The Infanta Arch extends as far east as Vlees Bay and here the Blinde River channel was mapped, having incised SB 2.

The Hartenbos and Klein Brak Rivers in Mossel Bay are currently buried on the shelf by the Holocene TST sediments, but seismic stratigraphy showed that they coalesce by the time the depositional profiles have reached the LGM shoreline. The Groot Brak channel is exposed surficially on the seafloor as it drained the eastern section of the Mossel Bay embayment where either erosion, or non-deposition, of younger sedimentation has occurred. A narrow, relatively deep, incision was mapped at the LGM, which is interpreted to be associated with the Maalgate River. The Gwaing, Skaapkop and Kaaimans Rivers are interpreted to have followed relatively straight courses onto the shelf and were obliquely intercepted on the coast-perpendicularly oriented seismic profile off Wilderness (Figure 5-13).

Topographic barriers in the Wilderness Embayment (Figure 5-13) in the east have been dissected in places by rivers, for example, the middle barrier penetrated by the Swart River. These palaeochannels truncate the bedrock in Swartvlei and can be traced onto the adjacent continental shelf. Well-dated regional stratigraphy in this particular area (Bateman et al., 2004; Carr et al., 2010; Bateman et al., 2011) has allowed a thorough investigation of rivers numbered 11 - 16 (Table 5-2). The temporal control on the easternmost incision history provided a basis for fluvial correlation throughout this seismic record.

Table 5-2. South Coast fluvial systems and correlation to present rivers draining the area. The depth of incision is taken from below the WRS marking the base of the Holocene sediment wedge (seismic Unit N) to the base of the incised channel and includes adjacent flood plain deposits. The channel width measures the breadth of the thalweg. Both are presented in this table in metres (m).

River number (labelled from west to east)	Correlated fluvial system	Depth of incision (where intercepted on seismic profiles)	Channel width (where intercepted on seismic profiles)	Modern channel width (measured at the coastline)
R1	Goukou	6 m	1700 m	270 m
R2	Gouritz	Max. 11.5 m	18 000 m (separated by slight bathymetric highs and geological outcrop)	420 m
R3	Blinde	5 m	2000 m, 5000 m at the LGM	110 m
R4	Hartenbos	7 m	10 000 m at the LGM (combined with Klein Brak),	250 m
R5	Klein Brak	7.5 m	10 000 m at the LGM (combined with Hartenbos)	280 m
R6	Groot Brak	5.5 m	3500 m at the LGM, 1000 m in the bay	270 m
R7	Maalgate	10 m	750 m at the LGM	150 m
R8	Gwaing			190 m
R90	Skaapkop			80 m
R10	Kaaimans			190 m

R11	Touws	Max. 2.5 m	1350 m, 1000 m (divided by aeolianite)	280 m
R12	Touws (Tributary)	7 m	470 m	
R13	Hoekkraal	5 m	820 m	N/A (drains into Swartvlei)
R14	Swart	6 m	660 m	320 m
R15	Goukamma (west)	Max. 4.5 m	500 m, 100 m, 450 m, 150 m (divided by aeolianite)	350 m
R16	Goukamma (east)	3 m	1100 m	

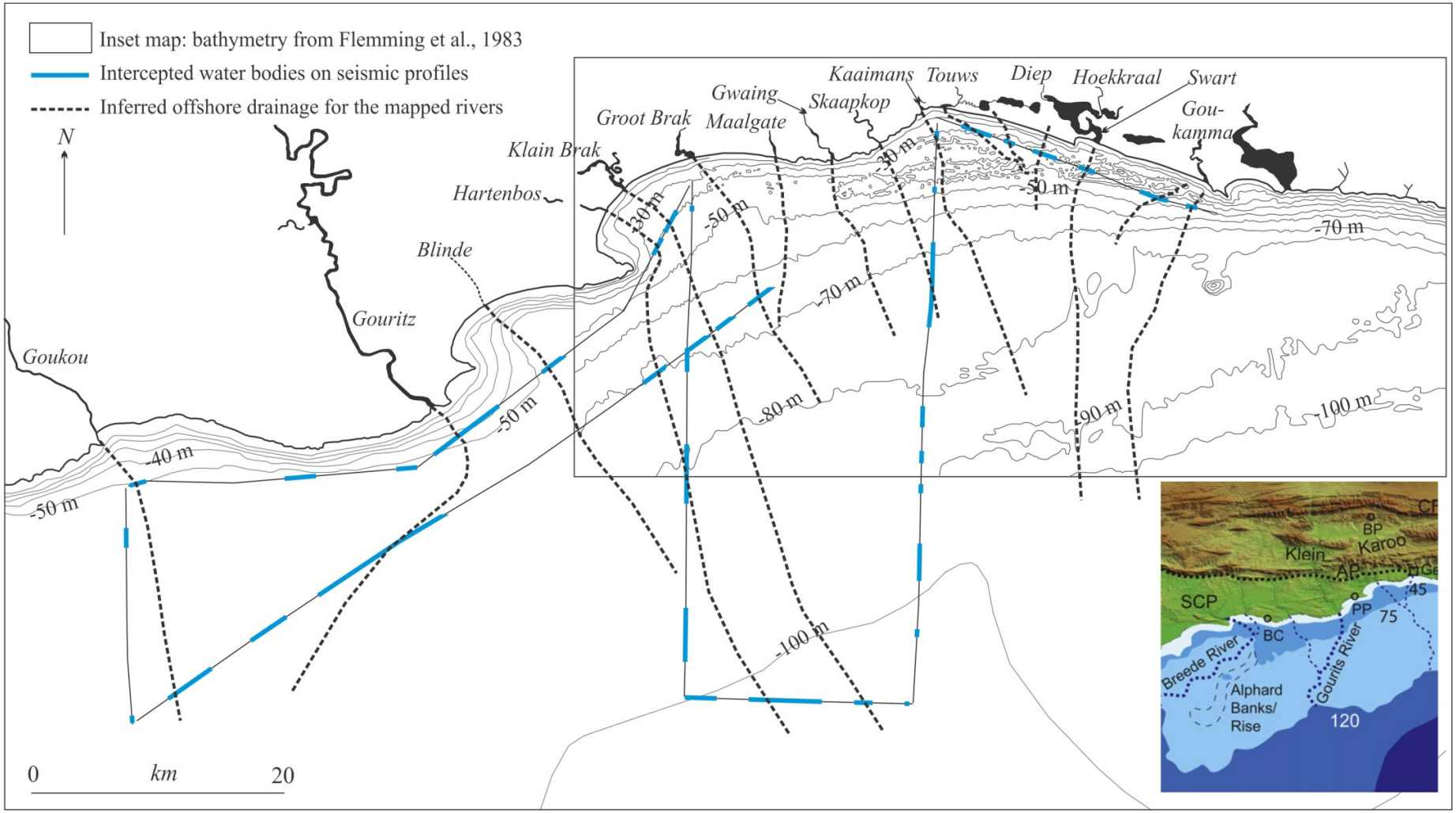

Figure 5-13. Palaeodrainage of the South Coast rivers in the study area, prior to infilling and subsequent burial of the channels to form the smooth surface of the continental shelf. Inset map shows inferred drainage on the shelf from Compton (2011). Unlike the Breede River to the west, which has a broadly defined valley, the valleys in this area are far less regionally defined and suggest that drainage was widely distributed over the surface. There is little to suggest they coalesce offshore to form a single, major drainage basin. The isobaths shown are derived from the GEBCO dataset.

5.5.2 Interpretation of the fluvial incision during sea-level lowstands

The adjacent floodplains on the shelf appear wider because the adjoining unconsolidated dune fields will also likely have been removed during the PMT. It is possible that river courses changed with each lowering and that the channels observed are the most recently formed with older ones all variably occurring laterally to them, accounting for the broad widths.

The South Coast rivers are currently associated with a relatively large bedload: the present Mean Annual Runoff of the Breede River on the South Coast is 1803 million m^3/a (DWAF, 2004a) and the Gouritz River 1680 million m^3/a (DWAF, 2004b). The sequence stratigraphic interpretations in this study showed, however, that sediment supply to this area was not consistent over time. In addition to the probability of a shallow braided stream network, the seismic architecture and antecedent geology of the shelf indicates that these channels were likely fixed, laterally stable incisions. The shallow, broad form may, however, facilitate the existence of extensive adjacent floodplain and wetland deposits during times of lowered sea-level. The distribution of channels on the shelf is closely associated with relative bathymetric lows observed on seismic profiles and when interpreted (Figure 5-4, Figure 5-8), these revealed infills of stratified sediments.

The associated sediment wedge of the Gouritz River is likely composed of silt, eroded off the Bokkeveld Group shale hinterland. Birch (1980) described a 35 m deep incised channel from a seismic profile acquired on the inner shelf, suggesting that the fluvial expression on the steeper gradient is more synonymous with the present-day situation. In all cases the incisions mapped in this study are broad and laterally extensive. The channel of the Blinde River can be traced towards the LGM shoreline (Figure 5-13). From Mossel Bay, extending eastward, the Mesozoic to Cenozoic Pletmos sub-basin deposits crop out on the Agulhas Bank on the inner shelf and are dominated by less competent strata consisting of siltstone, shale and limestone. With the prevalence of aeolianite on the shelf in this region, it is proposed that channel incision was closely related to dune depositional processes on a retreating shoreline.

In the Wilderness Embayment, deposition of the youngest seaward barrier (Bateman et al., 2011, Figure 5-13) would have been responsible for the most recent diversions. It seems that infilling of lowstand river channels by subsequent sedimentation made them less likely to be repeatedly incised and infilled as the river courses vary with contemporaneous sand dune development. Entry points to the embayment of rivers draining the wider hinterland, as at present were probably strongly controlled by the hard rock geology. Offshore, Birch et al. (1978) found no evidence for the extension of the Goukamma, Touws or Swart Rivers, although a potential palaeoestuary for the modern Touws and Swart Rivers was tentatively identified by Bateman et al. (2011). Birch et al. (1978) suggested that sediment entering the ocean could have been deposited into offshore interdune

depressions. Within the Wilderness Embayment, the oldest drainage system is interpreted to be the west-east oriented channel which lies seaward of the modern Swartvlei and adjacent to the landward barrier. This is represented on Figure 5-13 as River 12 (a tributary of the Touws River). Given that its incision is associated with the middle barrier, the channel associated with River 12 was likely incised between MIS 7 and MIS 5e, potentially during MIS 6 when lower eustatic sea levels would have increased the potential for fluvial incision. At this time the middle barrier sediments flanked this channel and it may have entered the sea at a palaeocoastline on the seaward edge of the middle barrier. Though definitive context is lacking, it is suggested that in the case of channel 11 that it links to the Touws River with the orientation of palaeoflow defined by the bedrock geology in the west. Channel 13 must post-date the middle barrier as it has incised the base of middle barrier in Swartvlei (Figure 5-13), which is known to have been deposited in MIS 7 (Bateman et al., 2011). It may also have flowed towards a shoreline that existed prior to the deposition of the seaward barrier. This Channel 13 event may have been fed by two rivers that flowed into the embayment and formed a confluence, which in the north re-used the existing depression from the very first/oldest landward channel. River 14 was either incised late or relatively dynamic stability enabled it to maintain flow during dune construction. Given intertidal beds within the Swartvlei Estuary that are known to date to MIS 5e (Carr et al., 2010) this channel probably existed at least pre MIS 5e. The channel may have cut through west of the present river mouth. Though only intercepted offshore, Rivers 15 and 16 may both be offshore extensions of the Goukamma and a palaeo-tributary that is now buried by the seaward barrier.

5.5.3 Sequence stratigraphy of incised channel infills

Buried incised channels/valleys are common features on continental shelves (Nordfjord et al., 2006). The accommodation provided by eroded topographic depressions offers space for deposition of early transgressive deposits (Vail, 1987) and, therefore, the opportunity to unravel the fluvial infill sequences deposited in these incised channels (Zaitlin et al., 1994; Foyle and Oertel, 1997; Nordfjord et al., 2006). On the South African shelf, recent attention has been paid to the seismic stratigraphy of incised valleys on the east coast (Green, 2009; Green and Garlick, 2011; Bosman, 2012). An idealised incised channel fill succession, deposited in response to a consistent sea-level rise and assuming steady sediment supply, includes basal fluvial deposits overlain by estuarine deposits and finally a zone of mixed-energy marine influence (Masselink and Hughes, 2003). These facies are bounded by bay flooding surfaces, tidal ravinement surfaces and wave ravinement surfaces, respectively (Allen, 1991; Zaitlin et al., 1994).

This study recognises four fill units within South Coast incised channels, based on seismic character of deposits, bounding horizons and observed geometries (Figure 5-14). The channel incision described above is associated with sequence boundaries of sub-aerial erosion. The four units, with varying degrees of preservation (Table 5-3),

can be traced across most of the sixteen incised channels of the South Coast shelf. The basal SFG i and stratigraphically higher SFK i (Table 5-1; Figure 5-14) are interpreted to represent the same facies, but are associated with different sequences. They are, therefore, temporally divided but reflect the same process of sedimentation. These facies are characterised by chaotic, variable-high amplitude reflectors and high acoustic impedance. They are typically laterally discontinuous and truncate against channel margins. Similarly, SFG ii and SFK ii are separated in time, but are remnant of a comparable sedimentary cycle across sequences. These facies consist of either semi-transparent deposits, or weakly layered successions characterised by parallel and sub-parallel clinoforms.

A prominent horizon, interpreted to be a maximum flooding surface (MFS), marks the boundary between SFG i and SFG ii (Figure 5-14). Most channel infill successions are capped by a WRS and overlying Seismic Unit O (the TST/PMT sediment wedge). In places, Unit O replaces SFK ii, but is differentiated by the presence of the distinctive basal WRS, associated with the base of Unit O. In some cases, few or no deposits of SFG i or SFK i may be preserved at the base of the infill package, although there may be evidence for their former existence. In this case, a marine TST rests directly on the incised channel.

This study proposes that SFG i and SFK i were deposited on FSST-LST systems tracts on the regressions from MIS 7 – 6 and MIS 5e – 2, respectively. SFG ii and SFK ii were deposited on TST and stillstand (LST/HST) systems tracts on the transgressions from MIS 6 – 5e and MIS 2 – 1, respectively. Although the incised channels may have been occupied prior to MIS 6, it seems most reasonable to interpret the preserved facies assemblages as post-dating this time, recording sedimentary events over the last and penultimate glacial – interglacial cycles (referred to in this study as Sequences 7 and 8). This work thus suggests that the incised channel deposits of the South Coast are the product of the last two sea-level cycles, incorporating FSST, LST and TST systems tracts deposits. The seismic architecture also suggests that the infill sequences can be interpreted to represent mixed fluvial and estuarine deposits, floodplain deposits and lastly, infilling by the most recent episode of marine sedimentation.

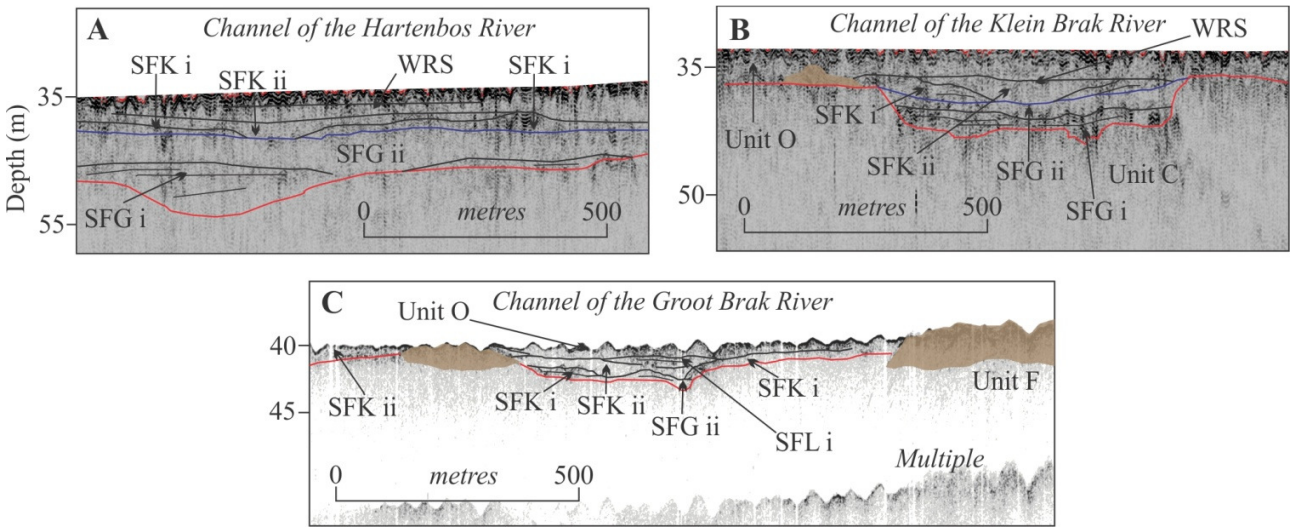

Figure 5-14. Incised channel fills, showing examples from A. the Hartenbos River (boomer seismic data), B. the Klein Brak River (boomer seismic data) and C. the Groot Brak River (pinger seismic data). For location please refer to the insets of Figure 5-6.

Table 5-3. Presence of seismic fill units and bounding horizons in the incised channels of palaeo river valleys mapped on the South Coast continental shelf. * indicates occurrence.

River number (labelled from west to east)	Correlated fluvial system (onshore rivers)	SFG i	MFS	SFG ii	SFK i	SFK ii	WRS	O
R1	Goukou				*	*		
R2	Gouritz			*	*	*	*	*
R3	Blinde			*				*
R4	Hartenbos	*		*	*	*	*	*
R5	Klein Brak	*	*	*	*	*	*	*
R6	Groot Brak			*	*	*	*	*
R7	Maalgate							
R8	Gwaing							
R9	Skaapkop							
R10	Kaaimans							
R11	Touws (west)				*	*	*	*
R12	Touws (east)				*	*	*	*
R13	Hoekkraal			*	*	*	*	*
R14	Swart				*	*	*	*
R15	Goukamma (west)				*	*	*	*
R16	Goukamma (east)					*	*	*

6 DEPOSITIONAL HISTORY OF THE MOSSEL BAY AREA

6.1 Introduction

This chapter combines all geophysical, geological and geochronological datasets to derive an interpreted depositional history of the study area. The preservation of geological deposits in this high-energy offshore environment is relatively limited (Gentle, 1987; this study) but interpretations based on seismic stratigraphy and surficial seafloor mapping provide a unique opportunity to piece together fragments of information within a framework of Quaternary palaeoenvironments. The implication is that in most cases, no exact modern analogues exist onland as direct frames of reference for what is preserved offshore, but *elements* of this submerged landscape can be recognised along the currently sub-aerially exposed Western- and Eastern Cape coasts. This stratigraphic model assumes a constant energy setting throughout the deposition of the sequences. Global studies of Holocene depositional systems, however, have indicated a complicated distribution of energy through sea-level cycles as a function of nearshore bathymetry, shelf width and tidal variation (Yoshida et al., 2007). Although it is acknowledged that this is also likely the case through the Quaternary record of Mossel Bay, the presence of rocky headlands and the overall nature of the strandline at different past sea levels allows proposed areas of focused and dispersed coastal wave energy to be determined.

6.2 Depositional age model (based on glacial-interglacial cycles, geochronology and seismic framework)

The South Coast geological deposits, seismic units, erosional structures and bounding horizons are discussed below in terms of the sequence stratigraphic model and nomenclature adopted in this study (Chapter 5). The seismic stratigraphy in particular has provided a platform from which to consider a process-driven explanation for the structures and deposits preserved in the study area. The contextualisation of this chronostratigraphic framework commences with the ~430 Ma Palaeozoic geological basement, and terminates with wave-induced ripples superimposed onto the Holocene sediment wedge by ocean swells generated by a frontal system two days prior to the acquisition of the geophysical dataset in April 2011. The time scales and cycles of deposits considered therefore bridge numerous orders of magnitude. The shelf depositional record is mostly absent by virtue of uplift and erosion, very little accommodation space and repeated sea-level fluctuations that have effectively eroded much of what was deposited. Yet sufficient evidence remains preserved to decipher a depositional history.

6.3 Palaeozoic deposits and structures: 'Acoustic basement'

Seismic Unit A is interpreted to represent the Silurian Skurweberg Formation of the Table Mountain Group, based on correlation to regional stratigraphy (Viljoen and Malan, 1993; Broad et al., 2006; Figure 5-11). This unit constitutes the sea cliffs between Dana Bay and Cape St. Blaize mapped in this study and extends offshore for a distance of 2 km eastward of the sub-aerially exposed limit of the coastal promontory (Chapter 4; section 4.1, 4.6.2). The Permo-Triassic Cape Orogeny which created the CFB is responsible for the anticlinal structure of bedding in the Mossel Bay sea cliffs (Viljoen and Malan, 1993). Bathymetric and seismic mapping in this study showed an abrupt termination of this unit to the south, with the near-vertical Skurweberg Formation cliffs being abutted by younger units directly offshore. This structure either attests to the nature of the steeply dipping folded strata, or suggests that this unit was subsequently down-faulted towards the south. Along the cliffs, mapped compressional structures associated with the Cape Orogeny (see Chapter 4, section 4.1) include tension fractures, foliation, fracture cleavage and reverse/low-angle thrust faults. Distribution of these Table Mountain Group sandstones relates to original fold structures, faults and to erosion with many of these erosional outliers of the CFB.

6.4 Mesozoic events and structures

The rift tectonic activity associated with the break-up of Gondwana is responsible for normal faulting (e.g. PP 1) and the creation of the offshore structural basins on the South Coast, including the Pletmos Basin. Extensional features documented along the Pinnacle Point coast in this study, including conjugate joints, offset veins and normal faults, were formed during this event. Down-faulting of seismic Unit A exposed the Pinnacle Point coastline during Gondwana rifting. Sedimentation patterns that developed during the accumulation of the Cretaceous and younger drift succession were controlled by the availability of seafloor accommodation space generated by tectonic subsidence on the continental margin (McMillan, 2003). The presence of significant unconformities through this stratigraphic succession attests to the tectonic instability at the time. Time-equivalent unconformities are recognised across the Southern African Mesozoic basins and are widely used in correlation of sequences and stratigraphic units (Broad et al., 2006). Tectonic uplift and associated with seafloor erosion results in non-deposition of sediment as it is bypassed into areas of positive accommodation space. Subsequent tectonic quiescence allowed the development of hardground crusts which preserved as the unconformity surfaces (McMillan, 2003).

6.5 Late Jurassic to early Cretaceous deposits and structures: Sequence 1

'Synrift' refers to the phase of sedimentation associated with active tectonics during the early stages of continental break-up (Broad et al., 2006). Seismic Unit B represents the Robberg Formation of the Uitenhage

Group and Unit C correlates to the Early Synrift sediments which are the onshore Enon and Kirkwood Formations. Sequence 1 deposits are capped by U/C 2 (this study) which correlates with unconformity 1At1 (regional stratigraphy of Broad et al., 2006), marking the onset of drift and transform movement along the AFFZ associated with Synrift II.

Early graben fill of Synrift I sediments in the Pletmos Basin date to the Kimmeridgian and consist of thick aggradational fluvial sediments in the north and marginal marine sediments in the south (Broad et al., 2006). A basal conglomerate has been correlated with the onshore Enon Formation (McMillan, 2003). The correlation of Seismic Unit C with the Mesozoic Enon and Kirkwood Formations of the Uitenhage Group is based on retrograding reflector geometry and spatial correlation to the onshore and deep offshore regional stratigraphy (Figure 5-11, Figure 6-1). These fining upward, dominantly fluvial and marine facies (Dingle et al., 1983; Viljoen and Malan, 1993) were deposited in response to a general rise in sea level. Younger Portlandian – Valanginian sediments are composed of fluvial, shallow marine and shelf deposits (Broad et al., 2006).

6.6 Early Cretaceous deposits and structures: Sequence 2

The HST deposits of Seismic Unit D are correlated with the offshore extent of the Buffelskloof and Hartenbos Formations of the Uitenhage Group (Viljoen and Malan, 1993), or the marine distal Agulhas Formation (Dingle et al., 1983). Unit D identified in this study is characterised by seaward-dipping aggradational to progradational parasequence sets and is separated from the underlying Unit C by an unconformity (U/C 1) which correlates with 1At1. The correlation with regional stratigraphy was based on the depositional environment of transitional marine deposits agreeing with the seismic architecture. The stratigraphy presented by Broad et al. (2006) displays these Early Cretaceous units being bounded by unconformities 1At1 at the base and 13At1 at the top of the succession. Late Cretaceous deposits were not identified in the study but crop out on the distal Agulhas Bank and on the edge of the continental margin (Dingle and Siesser, 1975). The basal Valanginian - Hauterivian graben infill successions in the Pletmos Basin generally suggest early phases of abrupt uplift and erosion followed by considerable subsidence (McMillan, 2003; Tinker et al., 2008b). The Pletmos Basin was subjected to uplift, followed by considerable subsidence during the Late Valangininan (1At1 times), resulting in the deposition of the upper graben infill consisting of deep water claystone and sandstone through the Late Valanginian into the Hauterivian (bounded by 1At1 and 6At1). The entire graben fill succession was planed off at the Hauterivian-Barremian boundary (6At1) prior the deposition of the drift sediments. Reflection 6At1 represents the final rift-drift boundary (Broad et al., 2006) and lies within the stratigraphy represented by Sequence 2 in this study (Figure 6-1).

The 6At1 – 12At1 Early Barremian deposits are only developed north of the Superior Fault and the Pletmos Basin was a significant depocentre for sandstones until mid-Aptian times (at 13At1). Seismic Unit D is interpreted to consist of sediments of Synrift II and early drift, terminating with unconformity 13At1. These sediments are characterised by aggradational deep-marine claystones and turbidites with organic-rich shales. Subsequent drift sedimentation is preserved as thin bands in the Pletmos Basin and consists dominantly of claystones (McMillan, 2003). Therefore, the Cretaceous exposed on the shelf in this study area is most likely a claystone.

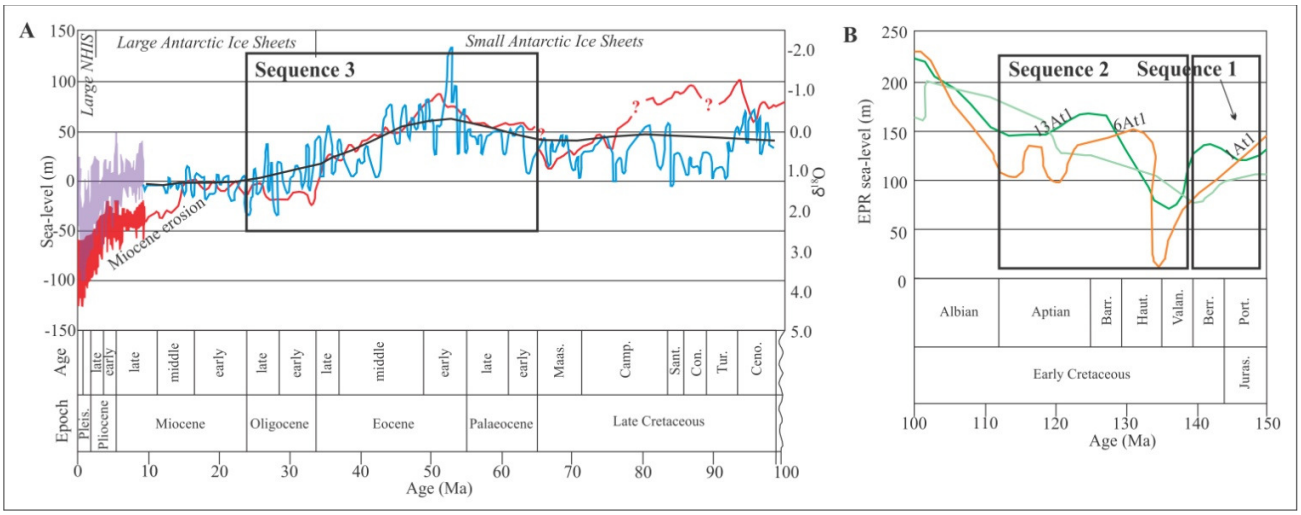

Figure 6-1. A. Mesozoic and early Cenozoic sea-levels and associated seismic sequences mapped in this study, after Miller et al. (2005b). A. Late Cretaceous – Pleistocene: global sea-level curve (blue) for the interval 7 to 100 Ma derived by backstripping data (van Sickel et al., 2004). Global sea-level (purple) for the interval 0 to 7 Ma derived from $\delta^{18}O$. Benthic foraminiferal $\delta^{18}O$ synthesis from 0 to 100 Ma shown in red. The portion of the $\delta^{18}O$ curve from 0 to 65 Ma from Miller et al. (1987). The $\delta^{18}O$ curve from 65 to 100 Ma is based on the data compiled by Miller et al. (2005a). The black line is the long-term fit to a backstripped curve. B. The Jurassic – Early Cretaceous shows Exxon Production Research data of Vail et al. (1977; light green), Haq et al. (1987; dark green), Haq and Al-Qahtani (2005; orange).

6.7 Cenozoic events and structures: Palaeogene deposits and structures: Sequence 3

Seismic Unit E (Sequence 3: Figure 6-1) is interpreted to represent drift deposits, now exposed by extensive planation since the Neogene and forming the Agulhas Bank. Unit E has been correlated with the Palaeogene Cape St. Blaize Group of Dingle et al. (1983). Although extensively planed off on the outer shelf and only intercepted offshore of Wilderness, the Cape St. Blaize Group outcrops in this region as upward fining cycles of coarse sandstone grading into calcareous clays like those described by Dingle et al. (1983). This corresponds well to the seismic expression of this TST deposit. Sediment starvation near the mid-Aptian (13At1) lower

boundary resulted in the deposition of organic-rich shales in the southern part of the Pletmos Basin. Late Cretaceous, Palaeogene and Neogene deposits of shelf origin consist of interbedded calcareous sandstones and limestones (Dingle et al., 1983). Unconformably overlying the Cretaceous strata across the South Coast shelf, is a 500 – 700 m thick succession of Palaeocene, Early to Late Eocene, Early Oligocene and Early Miocene aged units comprising deposits of interbedded glauconitic sandstone, claystone and carbonate (McMillan, 2003).

6.7.1 Continental shelf morphology and the resultant distribution of deposits

In this study, the seismic surface interpreted to have been planed extensively since the middle Miocene (Sequence Boundary 1) dips consistently with its onland profile and character in other South African offshore basins (Figure 6-2). This study, therefore, also supports the landscape evolution model for slow and uniform erosion of Bierman and Caffee (2001), Luft et al. (2005), Tinker et al. (2008a, b) and Kounov et al. (2007). For more detail, refer to Chapter 2. Lower Miocene carbonate-rich sediments cover a large portion of the shelf and upper slope of western and Southern Africa, forming a seaward-thickening wedge and tending to be flat-lying or dipping shallowly seaward (Dingle et al., 1983). The outer-shelf unconsolidated Miocene sediments are commonly capped by a <50 cm thick carbonate-cemented hardground (Birch, 1990), where extensive erosion during the late Miocene and the Pleistocene has planed off the upper surface of the lower Miocene unit (McMillan, 1989). The extensive occurrence of authigenic mineralisation on the continental shelf and widespread phosphatisation of calcareous sediments and limestones exposed at the seafloor has been linked to upwelling and the production of organic muds (Pether, 1994) since the late Oligocene.

The bimodality observed in the topographic and bathymetric elevations of Mossel Bay (steep coastal cliffs and an adjacent subdued coastal plain and continental shelf, Figure 6-2) is considered here to be predominantly controlled by lithology and preferential erosion of less competent geological units. The present coastline of the South Coast is characterised by a series of log-spiral bays. The regional distribution of lithologies is controlled by CFB structure, as modified by subsequent extensional deformation associated with Gondwana break-up (Hälbich, 1983; Toerien, 1979; Viljoen and Malan, 1993; Watkeys, 2006) and the formation of several half-grabens (e.g. Mossel Bay, Algoa Bay). The bedrock lithology of pre-Cenozoic strata along the South Coast is highly variable, creating variation in geomorphic expression. Resistant lithologies bounding the South Coast log-spiral embayments, such as Cape St. Blaize, tend to form rocky headlands of steep sea cliffs.

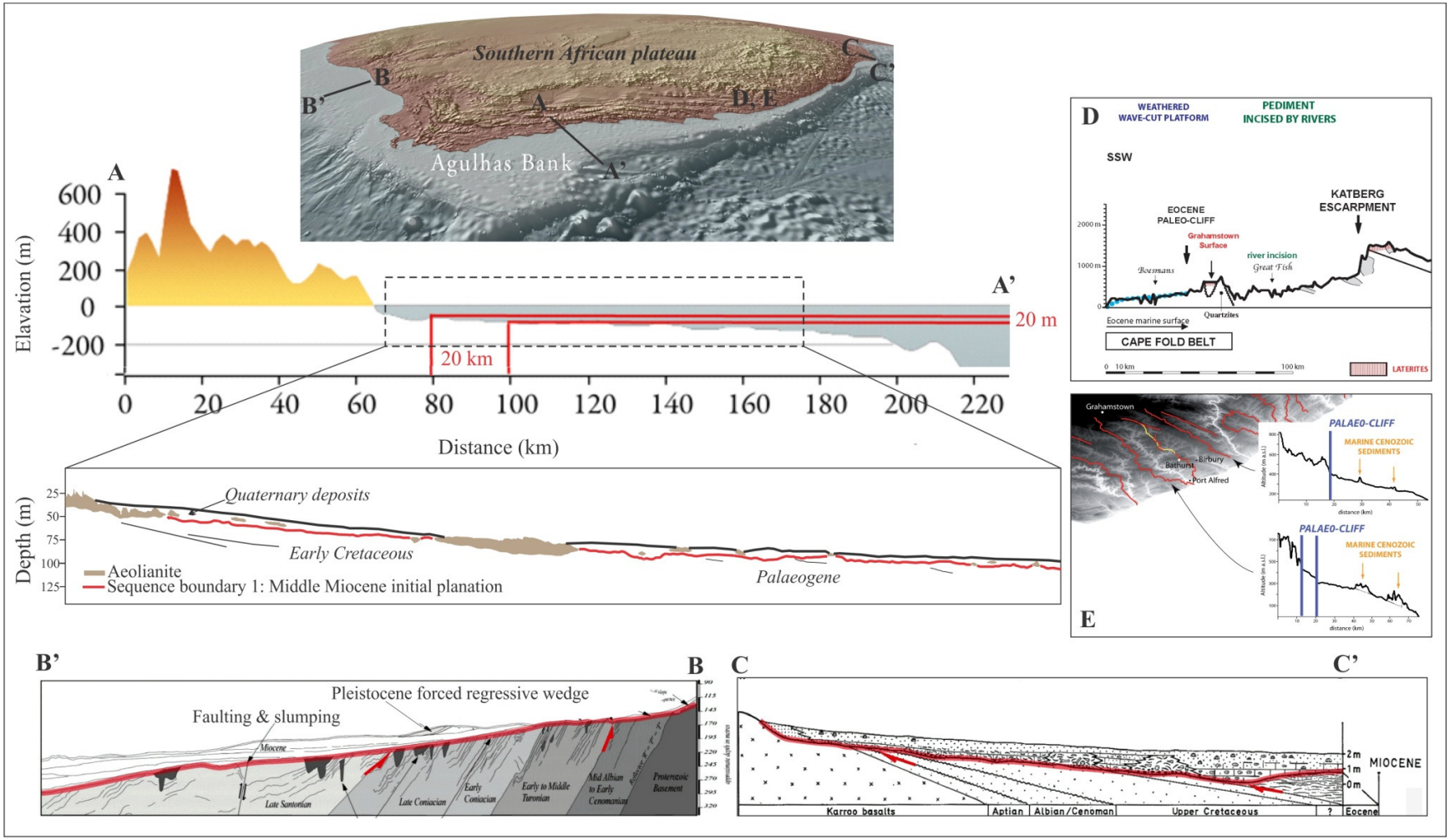

Figure 6-2. The shelf profile derived from this study in context compared to select existing Miocene erosional planation surfaces studied in Southern Africa. A. South Coast topographic/bathymetric profile (from Fisher et al., 2010). Inset: seismic profile offshore Mossel Bay (this study; Chapter 5). B. West coast profile showing the Miocene deposits and planation in red (from Stevenson and McMillan, 2004 in Guillocheau et al., 2013). C. Zululand Basin profile showing the red Miocene surface (from Förster, 1975 in Guillocheau et al., 2013). D and E. Eastern Cape topographic profiles showing scarps and wave-cut planation surfaces respectively (from Guillocheau et al., 2013).

Focusing in on the Mossel Bay area, which was mapped in the highest resolution, 7 submerged and significant geomorphic features were described in Chapter 4 that show a currently submerged terrestrial environment. Similar onshore structures were mapped by van Zyl (1997), but the geomorphic expression differs between the sub-aerial and sub-marine environments, likely as a function of accommodation space on a low-gradient expansive shelf. The planed-off nature of the Agulhas Bank and the variation in gradient on the shelf from the inner- to mid-zones are, therefore, attributed chiefly to its erodible lithologies. Antecedent resistant substrate led to the preservation of Quaternary strata in the Mossel Bay embayment, as lateral protection by the rocky headlands which bound the structural embayments sheltered these Cenozoic deposits from erosion by the prevailing southwesterly swell and storm surges in Mossel Bay. The unprotected outer shelf is an open, vast expanse of eroded underlying strata and generally lacks preserved Quaternary deposits when compared to its shallower counterpart. The closest possible analogue along the South Coast may be the region near Cape Agulhas and a further afield comparable region is thought to be the Maputaland Coastal Plain.

Near the present Mossel Bay shoreline, coastal and nearshore deposits have a tendency to stack vertically where there is limited highstand accommodation space (after the onshore models of Illenberger and Burkinshaw, 2008; Bateman et al., 2011), and further out on the continental shelf the submerged deposits accrete laterally (more akin to the dune plume model of Roberts et al., 2009 for the West Coast). It is proposed here that the difference in the character of this environment is related to the response of the low-gradient shelf to sea-level fluctuations and a distinct slope change from the onshore, to the inner shelf, to the mid- and outer parts of the shelf. This change in slope is expressed geomorphologically by the dominance of deposits at and near the shoreline and a relative absence of features on the low-relief, current-swept, deeper shelf environment.

A model of non-deposition rather than erosion is proposed to explain the relative lack of features offshore Vlees Bay compared to Mossel Bay as no significant rivers drain into Vlees Bay and both bays open at the same angle to the Indian Ocean. This hypothesis also accounts for the obvious lack of preserved deposits anywhere in the area other than within the Mossel Bay embayment, in close proximity to the three closely positioned river systems (the Hartenbos, Klein Brak and Groot Brak Rivers).

The dominantly regressive sea-level movement from the Neogene into the Pleistocene (Figure 5-12; Miller et al., 2005a) accounts for the non-deposition on the continental shelf which likely served as a zone of sediment by-pass and generated the hiatus that is expressed as SB 1. The initial planation of SB 1 is interpreted to have commenced during the middle Miocene. SB 1 is a prominent horizon capping Seismic Units A to E and marking the deposition of Sequence 7. The planed nature of SB 1 and correlation with existing sea-level models (Figure 5-12) and geological data of Dingle et al. (1983) suggest that this surface has been reworked since the middle Miocene through the Pleistocene, with the most recent reactivation during the regression from MIS 7 – 6. It was

not possible to differentiate individual erosional surfaces. As such, SB 1 is thought to be indicative of repeated erosional truncation and sediment by-pass associated with multiple forced regressive cycles. Since MIS 7, the younger strata deposited onto SB 1 have not yet been reworked by the last glacial cycle.

6.7.2 Shaping of the -45 m terrace (2.7 - 0.9 Ma)

The sea-level record derived from marine $\delta^{18}O$ record of benthic foraminifera since 3 Ma (Bintanja et al., 2005; Bintanja and van de Wal, 2008) indicates that sea level remained relatively high between 2.7 Ma and 2 Ma (Figure 6-3). More frequent regressions of sea level between 45 and 75 m BMSL occurred between 2 and 1.2 Ma. From 2.7 to 0.9 Ma the amplitude of sea-level fluctuations increased, and long-term oscillation near the -45 m isobath, led Compton (2011) to propose that this constrains the timing of the erosion of this prominent marine terrace on the South Coast. From MIS 21 –15, the earlier phase of the familiar sea-level cycle (Figure 6-3), deposits are rarely preserved but erosional structures can be linked to the oscillation of sea level. Incision of the offshore Cape St. Blaize caves likely occurred on these relatively lower sea levels (10 – 20 m BMSL) associated with the 40 kyr glacial-interglacial cycles between 2.7 and 0.9 Ma.

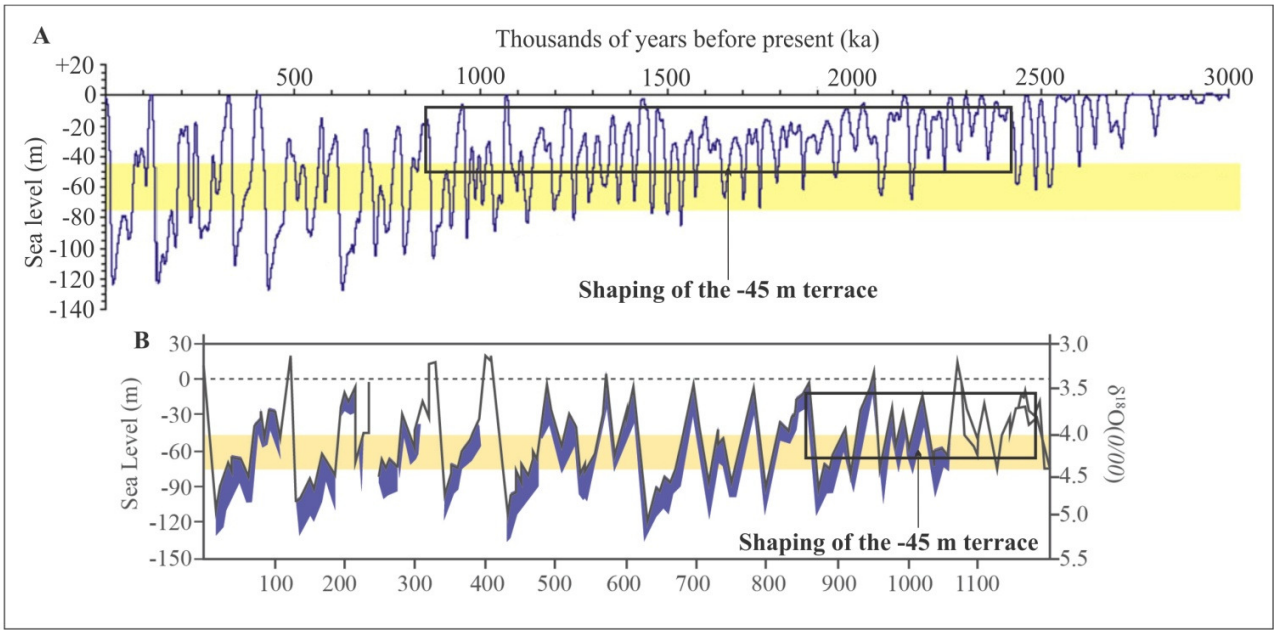

Figure 6-3. Early Quaternary sea levels and derived range in sea level since A. 3 Ma (Lisiecki and Raymo, 2005), and B. Since 1.2 Ma (Bintanja et al., 2005).

6.8 Middle Pleistocene deposits and structures: Sequence 4 (MIS 15; 621 – 563 ka)

The oldest Quaternary deposits mapped in this study, of MIS 15 age, lie adjacent to the mouth of the Klein Brak River and were only mapped geologically where they crop out along the present shoreline at ~1 m AMSL. A basal unit interpreted to represent deposition on the foreshore is overlain by aeolianite which was dated to 582 ka. These units could not be correlated seismically with features preserved in the offshore record. During deposition of this shoreline sequence, sea-level was situated relatively close to the present elevation, but possibly up to 10 m lower according to the glacio-eustatic sea-level record of Bintanja et al. (2005), which introduces doubt that at this time glacio-eustatic sea-level curves can be confidently applied in a South African context. These curves, however, have error envelopes that are likely to encompass such a discrepancy. According to the foreshore and regressive dune classification, these deposits are compositely interpreted to reflect progradational facies associated with normal regression along the palaeo-coastal zone. The palaeoshoreline at this time could not be delineated, owing to a general lack of preservation. Dune ridge stabilisation here is considered to be a function of sediment supply in relation to relative sea-level. The development of a stillstand from a purely sedimentological perspective has been documented only in close proximity to river mouths (Swift, 1976). Although conditions most favourable to dune construction occur during times of stillstand, and these geological units lie adjacent to the mouth of the Klein Brak River, it cannot be confidently confirmed that this deposit is in fact associated with a stillstand event, nor that the mouth of the Klein Brak River was situated in the same position during MIS 15. This interpretation of sedimentation in Mossel Bay during MIS 15 is, thus, speculative, owing to the scarcity of geological data. Carbonate diagenesis of MIS 15 deposits showed very little evidence for contemporaneous precipitation, and extensive alteration at grain boundaries to authigenic smectite, likely indicative of a long exposure.

6.9 Sequence 4 – Sequence 5 hiatus (MIS 15 – 11; 563 – 424 ka)

The retreat of sea level from the peak of the MIS 15 interglacial towards the MIS 14 glacial, the subsequent rise to the MIS 13 interglacial and the fall to the low base-level of MIS 12 is not convincingly represented geologically in the study area. Given the magnitude and sense of sea-level fluctuations over this time, (Figure 6-4), it is suggested that remnant deposits on the shelf were eroded. The sea-level curve of Bintanja et al. (2005), however, showed that the MIS 13 interglacial was not as high as either MIS 15 or MIS 11. Reactivation along the SB 1 surface likely continued the planation to contribute to the flat nature of the outer shelf, as sea-level regressions shifted palaeoshorelines in a basinward direction. Between 580 ka and 550 ka, sea level oscillated within the zone between 90 and 30 m BMSL and is interpreted to have planed the shelf above and below the pre-existing -45 m terrace during this time. In addition, the substantial sea-level stillstand at ~500 ka, at an elevation of ~30 m BMSL, may be responsible for the penultimate episode of incision along the submerged portion of the

Cape St. Blaize promontory, contributing to the creation of the now submerged coastal caves described in Chapter 4, section 4.6.2).

6.10 Sequence 5 (MIS 11; 424 – 374 ka)

Raised MIS 11 deposits mapped and dated in the vicinity of Mossel Bay (Jacobs et al., 2011; Roberts et al., 2012) represent a wave-energy, progradational shoreline succession that is presented as a transgressive – regressive sequence. Extrapolated seaward from up the Klein Brak River to the shoreline, the shoreline units identified in this study can be tied into a correlative chronostratigraphic context, considering the model of Roberts et al. (2012). Shoreline Unit Pm 3 was deposited in the upper shoreface environment as coastal retreat shifted seaward. Unit Pm 3 is closely associated with Unit Pm 4 (deposits of *in situ*, subtidal, *Ostrea atherstonei*), Unit Pm 5 (storm deposits), Unit Pm 6 (cobble conglomerate) and Unit Pm 7 (aeolianite), which provides evidence for the regression of sea level from the peak of the MIS 11 interglacial. Storm deposits suggest a high-energy, wave-dominated hydrodynamic environment at the time. At Pinnacle Point, this 13 m AMSL MIS 11 highstand washed out many of the existing cave deposits and incised others (Jacobs et al. 2011; Roberts et al. 2012). The MIS 15 beach and dune deposits (Pm 1, 2), as well as MIS 11 beach deposits (Pm 3, 4, 5, 6) contain isopachous microcrystalline rims at grain boundaries, interpreted to have precipitated during the MIS 11 interglacial, contemporaneous with the deposition of the littoral zone units. In addition, the aeolianites of MIS 11 (Pm 7) displayed the presence of microcrystalline rims; a diagenetic phase considered in this work to be an early feature of vadose zone diagenesis near the MIS 11 shoreline.

6.11 Sequence 5 – Sequence 6 hiatus (MIS 11 – 7; 374 – 243 ka)

No depositional evidence was identified in the study area to constrain conditions subsequent to the MIS 11 interglacial, for example during the MIS 11 – 10 retreat of sea-level (Figure 6-4). During this time climate, carbonate and resultant cementation by diagenetic processes are postulated to have been similar to conditions that prevail in the current interglacial, but owing to the extensive erosion since this time at elevations commonly revisited by sea-level, little evidence were retained in this lowstand environment. Deposits associated with MIS 10, 9 and 8 were not documented whatsoever and compelling evidence for these events was not observed in the seismic record. The lack of MIS 9 deposits is somewhat surprising, as this interglacial, according to the projections of Bintanja et al. (2005) reached a higher elevation than MIS 7 (Figure 6-4).

6.12 Sequence 6 (MIS 7; 243 – 191 ka)

MIS 7 palaeodunes have been dated in the area but were not mapped along the shoreline between the Hartenbos and Groot Brak Rivers but have been dated in the vicinity of Pinnacle Point. The position of Unit Pm 8 (Table 4-8) was fixed in the stratigraphic record according to its extent in the regional stratigraphy.

Dune deposition during MIS 7 is generally well documented by aeolianite preserved along the entire South African coastline (Illenberger, 1996; Roberts and Berger, 1997; Ramsay and Cooper, 2002; Bateman et al., 2004; Porat and Botha, 2008) as well as in the offshore Quaternary record of the East Coast (Cawthra et al., 2012a). The closest occurrence of significant MIS 7 deposits to the study area is the middle cordon of the Wilderness Embayment (Bateman et al., 2004), which indicated the propensity to accrete vertically in response to a lack of accommodation space.

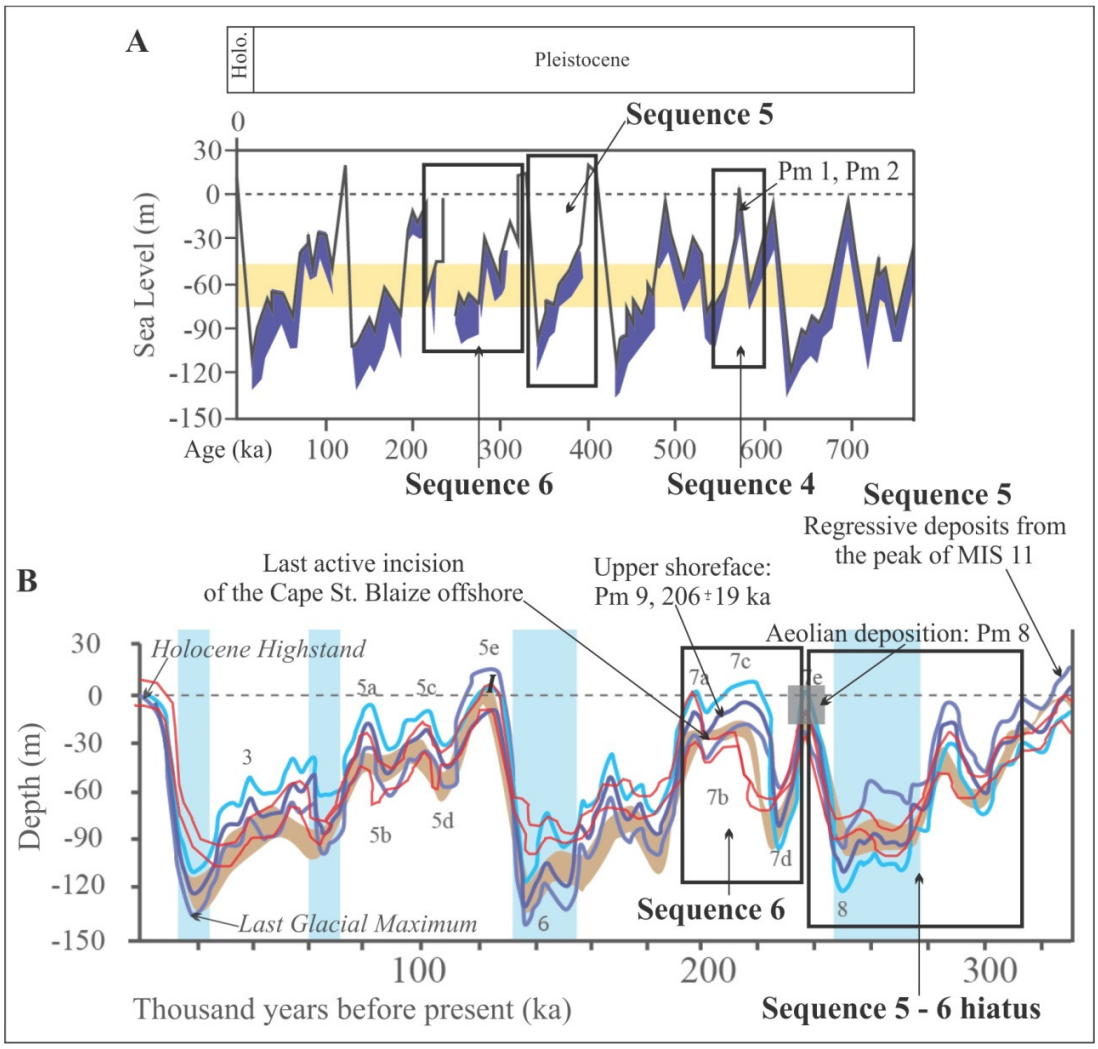

Figure 6-4. Sequences 4 5 and 6, plotted against A. Glacial to interglacial cycles from the record of Lisiecki and Raymo, 2005) and derived range in sea level since 1.2 Ma (Bintanja et al., 2005). B. Glacio-eustatic sea-level curves of Waelbroeck et al. (2002) in blue, Bintanja et al. (2005) in brown, Rohling et al. (2009) in red. Sea-level curves modified from Compton (2011).

6.13 Middle to Late Pleistocene deposits and structures: Sequence 7

6.13.1 MIS 7 - 6 transition

Deposition of the transgressive upper shoreface Unit Pm 9 (dated to 206 ± 19 ka; Appendix II) occurred during MIS 7c (Figure 6-5). A marine diagenetic cement, characterised by isopachous micrite at grain boundaries, is considered to be associated with this palaeoshoreline. A second phase of diagenesis also influenced the pre-existing strata of MIS 15 and MIS 11, with the second evidently cementation event forming isopachous marine phreatic rims in available pore spaces. This is specifically observed in Units Pm 2, 3, 5 and 7. The suggested

reason for this preservation is thought to be related to a time of high carbonate productivity during the transgression of a shoreline from MIS 7b to 7a. Biological productivity associated with the current interglacial at Mossel Bay is extremely high (Branch and Branch, 1992) and comparable conditions are thought to be traceable across past interglacials.

This period marks the last active reactivation interpreted along the SB 1 surface (Figure 6-5), as subsequent deposits are preserved on the erosional surface and remain volumetrically dominant on the continental shelf. By this time, the seafloor had been planed off to the familiar, flat surface of the Agulhas Bank. Unconformities can become compounded on palaeoshelfs (McMillan, 2003) and this, as suggested in the Miocene discussion (section 6.7.1), is what has occurred along the surface referred to as SB 1. The sea-level lowering at ~200 ka, from a depth of ~30 m BMSL, is interpreted to be responsible for the most recent episode of *significant* incision along the submerged portion of the Cape St. Blaize promontory. The later Holocene Transgression was rising rapidly when it exceeded this depth, associated with MWP 1B at 11 ka.

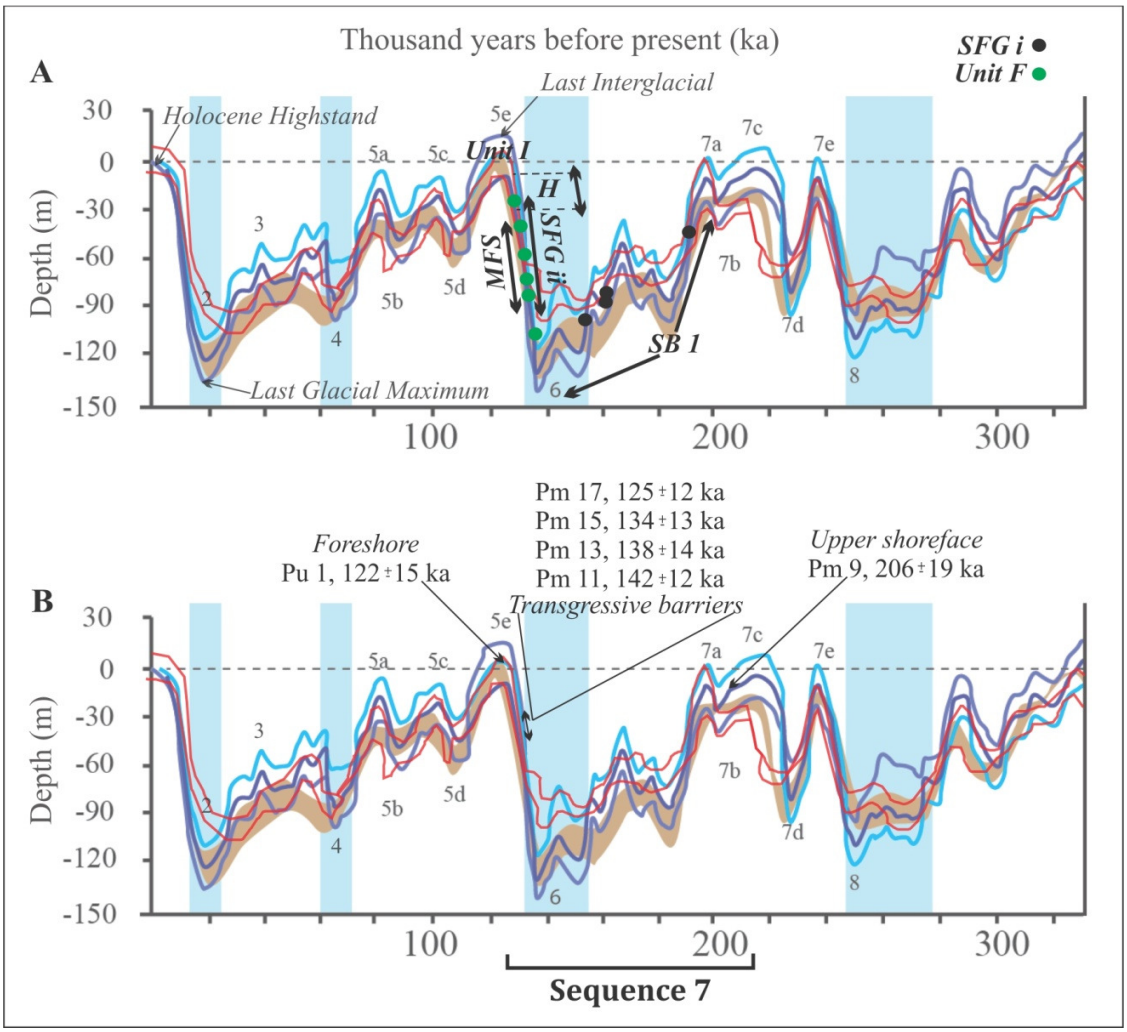

Figure 6-5. Deposits and features of Sequence 7 plotted on sea-level curves. Deposits and structures associated with Sequence 7 (A. seismic, B geological) superimposed onto the RSL data of Clark et al. (2009) Waelbroeck et al. (2002) in blue, Bintanja et al. (2005) in brown, Rohling et al. (2009) in red. Sea-level curves modified from Compton (2011).

Active incision of rivers, forming the incised channels on the shelf, is represented as bathymetric lows carved into strata where SB 1 dips and forms depressions. The character of the incision tends toward shallow, broad, relatively flat fluvial systems. By this time, with the shelf having been planed down to a very flat surface governed by SB 1, the fluvial systems incised accordingly, accounting for the geomorphic expression. Scattered deposits are preserved in the base of channels and these are expressed as SFG i. The depths of occurrence across the area suggest that these fluvial fills are associated with the regression of sea-level from MIS 7a (~195 ka) and towards the MIS 6 glacial (~160 ka). This work correlates the basal SFG i facies as fluvial lag deposits and compositely groups the fluvial, estuarine and tidal environments within this classification. Without cores or control on the sedimentary record, discernable features were not possible to interpret in the seismic data. The

chaotic reflectors directly overlying the incised surface imply deposition under relatively high-energy conditions. A dynamic set of facies is expected during deposition under energetic wave and current conditions (after Masselink and Hughes 2003). These deposits are patchy, likely due to subsequent erosion and back-filling by overlying transgressive deposit, and were only mapped in the palaeochannels of the Klein Brak- and Hartenbos Rivers of Mossel Bay and offshore of Still Bay within the Goukou River palaeochannel.

In addition to a variation in character across the mapped South Coast rivers from west to east, the down-dip profiles of the channels vary significantly from the current coastal plain to the (now submerged) continental shelf environment. This strong contrast of onshore channel widths with those in the offshore is clear as compared and documented in Table 5-3. This is partly the effect of planation by sea-level transgression(s) and subsequent infilling with marine sediments. Less incision took place and more lateral channel migration was possible. In the palaeo-coastal zones where a large graded fluvial system entered the ocean at the coastline and the littoral zone had been transgressing slowly for a long time, the graded slope of the shelf was less than the gradient of the lower course of the fluvial system being progressively transgressed. Because the exposed shelf had a gentler slope than the lower course of the fluvial system, rivers crossing the exposed shelf must have slowed down, and hence laterally deposited some of their load (e.g. Figure 6-6). Nummedal et al. (1993) presented numerical models which suggested that during deltaic progradation the longitudinal profile of a river will shift upward as the river mouth moves seaward creating accommodation space. Therefore, the trajectory of the river mouth has only an indirect relationship to the continental shelf. Despite the gradient of the shelf, a sea-level fall thus forces the river mouth to drop – so the gradient of the shelf is relevant to questions of accommodation space and lateral outbuilding of sediment as noted on the South Coast.

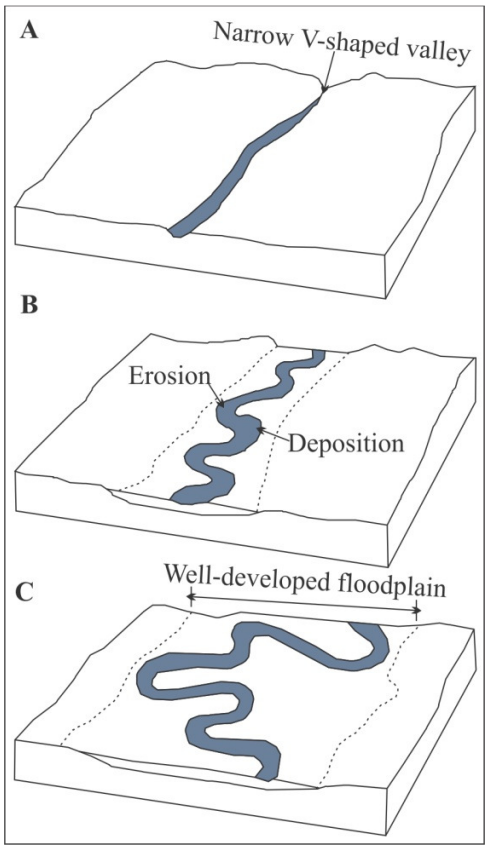

Figure 6-6. Schematic image showing typical stages of river development. A. Initial narrow valley. B. Reaching a more mature stage, meanders develop. C. Wide floodplain, oxbow lakes may develop.

The retreat of the shoreline from MIS 7a – 6 is likely responsible for the presence of calcite spar infilling available voids of deposits preserved on the depositional profile. The cement is composed of 'clean' carbonate, with no evidence for excessive mixing by organic or palaeosol material, lending to an inferred interpretation of a largely unvegetated dune field migrating rapidly seaward at this time. It may have been unvegetated due to strong prevailing winds that did not allow a plant community to take hold.

6.13.2 MIS 6 (183 - 134 ka)

Full exposure of the SB 1 surface occurred during the glacial of MIS 6 as sea-level reached a maximum regressive depth of ~130 m BMSL (Figure 6-5). At this time, very little of the remaining Pleistocene stratigraphy of the shelf had been deposited and the broad, but shallowly incised, rivers were well developed. In the vicinity of Vlees Bay, Table Mountain Group sandstones outcropped on the land surface as flat exposures. The MIS 6 glacial was a long lowstand and presumably would have developed well incised river channels, especially if the SCP was wetter during glacial periods as suggested by Bar-Matthews et al. (2010).

Mapped and dated deposits exposed surficially on the Mossel Bay shelf offshore of the Groot Brak River (Figure 4-22), appropriately illustrate excellent preservation of a transgressive barrier system migrating over a low-gradient palaeo-coastal zone. Geological Unit Pm 11 (a remnant, linear barrier dune) is closely associated with a beach deposit (Pm 12). Pm 11 was dated to 142 ± 12 ka (Figure 6-5). Directly inshore, the laterally stacked adjacent Pm 13 (dated aeolianite: 138 ± 14 ka) and associated beach (Pm 14) occurs directly landward of these deposits, Pm 15 (134 ± 13 ka aeolianite) and the Pm 16 beach complete the sequence (Figure 6-5, Figure 6-7). The depth range occupied by these deposits is 30 – 36 m BMSL and they flank the western palaeochannel bank of the Groot Brak River. Prograded barriers consist of parallel beach and commonly vegetated foredune ridges (Hesp, 1984), and reflect an environment with winds sufficiently strong to transport beach sand and a climate suitable to support the growth of the sediment-binding vegetation (Roy et al., 1994). Prograded barriers are closely associated with river mouths on wave-dominated coasts, although the sediment source is provided chiefly from the adjacent seafloor (Thom, 1984). Significant sediment supply is thus interpreted from MIS 6 – 5e to preserve transgressive barriers. The carbonate cementation showed that the aeolianite units in this transgressive package were dominated by dogtooth calcite spar as the first phase of diagenesis and the adjoining beaches, by micrite rims. The rapid translation of the barrier system was accompanied by rapid carbonate diagenesis, which kept pace with the rate of transgression out of the MIS 6 glacial. The coastline model of Fisher et al. (2010) based on GIS modelling and $^{87}Sr/^{86}Sr$ isotopes from speleothem at Pinnacle Point, showed that a maximum transgression with a velocity of 40 km per millennia was likely reached between 135 and 136 ka. These data correspond well to the geological evidence on the shelf for a rapidly transgressing shoreline.

When sea level rose rapidly, coastal barriers on the Mossel Bay shelf are interpreted to have overstepped during translation (Figure 6-7). In this model, a critical point is reached at the landward migration of a dune ridge where the barrier no longer maintains pace with the transgression, causing overstepping and landward remobilisation of the barrier structure. The sudden landward shift leaves a stranded barrier core in the shoreface, as documented in Nova Scotia (Penland et al., 1985), the US New Jersey coast (Stubblefield et al., 1984) and the South African East Coast (Green et al., 2012). On the South African East Coast the Aliwal Shoal (Bosman, 2012) was primarily deposited between 134 and 127 ka, on the same transgressive event. Near the commencement of the Last Interglacial cycle of warming and high sea level, the response to the termination is interpreted here to be associated with an influx of sediment and a propensity to prograde. The seismic data collected for this study showed that the remnant dune deposits on the South Coast shelf range from being low-relief and laterally extensive, to high-relief and occupying a narrow lateral basal band. This is suggested to be a consequence of cementation prior to the inundation of the encroaching sea level. The rapidly cemented units remain relatively intact, whereas the more unconsolidated dunes are thought to become flattened by the high wave energy associated with the transgressive shoreline.

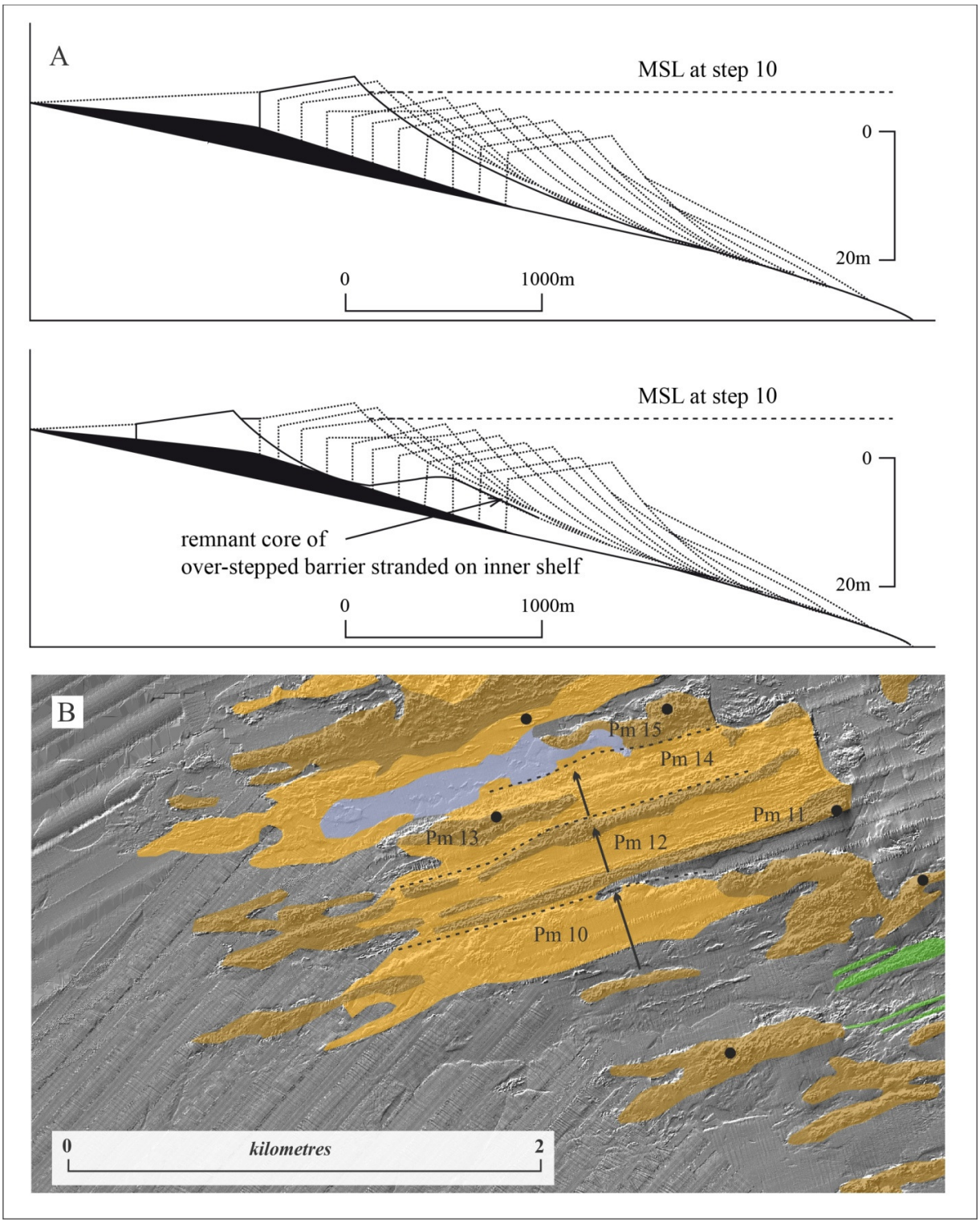

Figure 6-7. Barrier translation in response to sea-level transgression. A. Model modified from Cowell and Thom (1994). B. The MIS 6 transgressive barrier system mapped offshore of Mossel Bay. The black dots indicate sample locations and the stippled lines group composite units.

6.13.3 MIS 6 - 5 transition (134 – 131 ka)

Glacio-eustatic sea-level models suggest that the coast moved inland at speeds averaging 20 km/100 yr and the coastline model of Fisher et al. (2010) showed that at 137 ka ~73,000 km^2 of currently submerged bank was exposed. A maximum velocity of transgression (40 km/100 yr) was likely reached between 135 and 136 ka and by the time sea-level reached the shoreline of MIS 5e (Figure 6-5), an additional 400 km^2 of currently exposed land was submerged because of the 13 m AMSL maximum highstand.

Palaeosols that are interpreted to have deposited on the regression towards the MIS 6 glacial, associated with sub-aerial exposure of SB 2, were rapidly buried or destroyed by high-energy waves as sea-level transgressed landward. The actively incising rivers delivered unconsolidated sediment to the shelf during the sea-level lowstand of MIS 6 which was reworked into a TST wedge upon the MIS 6 – 5e transgression, preferentially infilling topographic depressions and notably river channels on the shelf as the shoreline shifted in a landward direction. Seismic facies SFG ii, is interpreted as TST channel infill deposits, linked to this event. The acoustically transparent and weakly layered deposits suggest homogeneity within facies SFG ii and likely represent transgressive sand sheets of an encroaching shoreline. SFG ii was mapped at depths ranging from 38 – 96 m BMSL across the study area, and is associated with the palaeochannels of most of the mapped rivers. Plotted against sea-level curves (Figure 6-5), these depths indicate deposition between ~140 and 135 ka as sea-level rapidly rose toward MIS 5e. Between depths of 93 and 52 m BMSL a prominent reflector interpreted to represent a maximum flooding surface separates the underlying SFG i from SFG ii and was identified within the channel infill succession of the Klein Brak River.

The infilling of depressions on the shelf during transgression can be considered in terms of self-organisation on sea-level stillstands, where broad low-energy sinks become channelised by marine sediments associated with encroaching sea-level. The basin fills until sediment bypassing is established, which represents steady-state conditions. Associated river mouths along the palaeoshorelines of the South Coast shelf may have become choked with sediment, promoting extensive tidal flats on a low gradient shelf. A possible analogue for the South Coast lowstand fluvial systems' river mouths is thought to likely be the Berg River on the South African West Coast whose tidal wedge extends 60 km inland due to the low coastal plain gradient.

6.13.4 The response of unconsolidated MIS 6 sediment to the MIS 5e transgression

On a rapid transgression, low gradient coasts are exposed to wave action and the associated transgressive sedimentary barriers which remain in vague equilibrium with rising sea level by the landward transfer of sediment from the shoreface to the back-barrier environment (described by Swift, 1976) (Figure 6-8). As sea level rises rapidly, low foredunes develop on the barrier surface, which is frequently punctuated by storm surge.

Associated washover horizons were mapped seismically in Mossel Bay comparable to the model provided in Figure 6-8. As the rate of sea-level rise slowed, more substantial dunes were developed and the frequency of washover was reduced, hindering barrier translation. This was also the case in the sub-aerially exposed Wilderness Embayment considered in this study. Barrier translation is considered to have been relatively continuous during rapid sea-level rise and intermittent with a reduced rate in rise. Assuming consistent sedimentation in the littoral zone, shoreface translation was predominantly governed by the gradient of the substrate. An erosional wave ravinement surface later developed on the shelf once the transgressive barrier passed, but low-energy sediments were preserved in topographic depressions on the shelf below the ravinement surface related to incisions in the antecedent substrate. The slope of the substrate is considered the most important factor in the preservation of deposits on the South Coast during rapid sea-level rise.

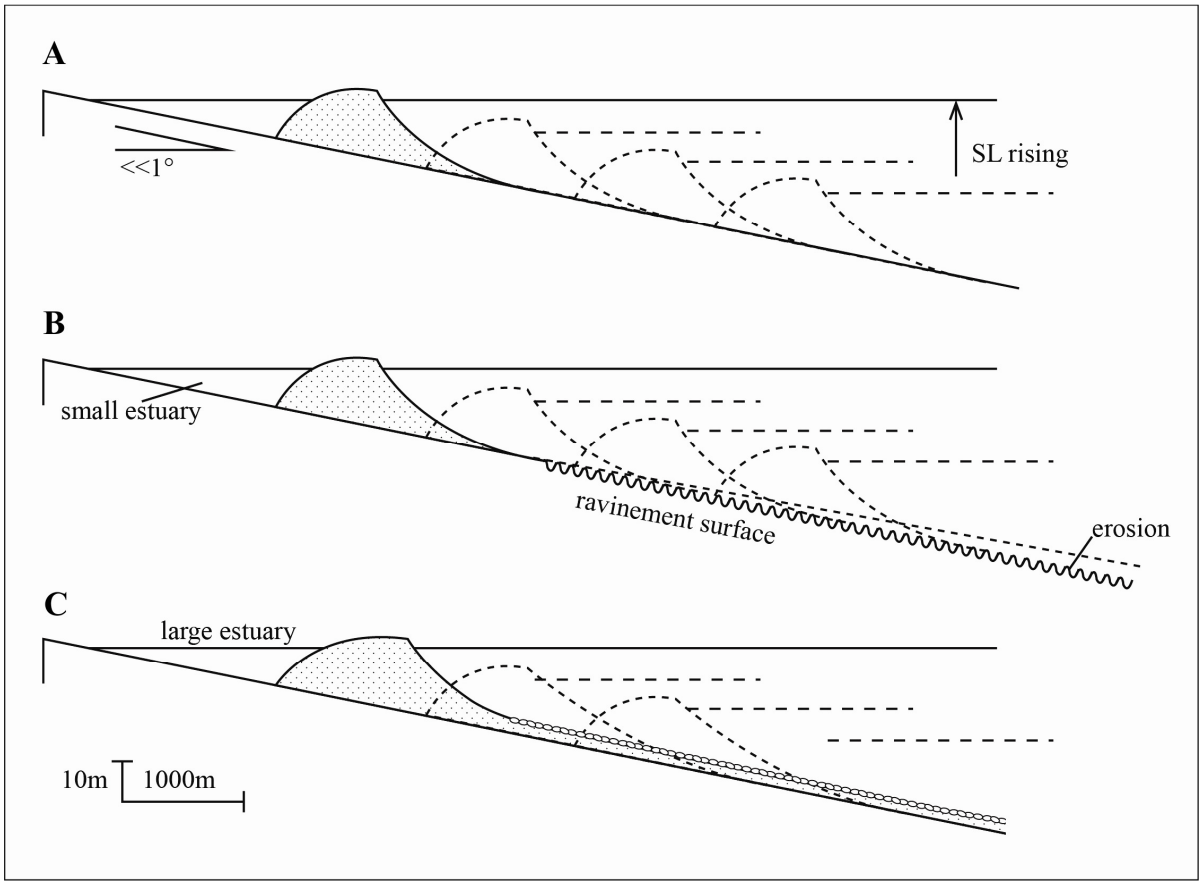

Figure 6-8. The variations in marine sediment budget will likely cause a transgressive barrier to erode the seafloor with a net loss of sediment (B) and result in the deposition of a trailing-edge sand sheet (C) if there is a net accumulation of sediment on the transgressive cycle. Modified from Cowell and Thom (1994).

In addition to the migration of the TST sediment wedge in a landward direction, the acoustically transparent Seismic Unit H (interpreted to be coastal wetland deposits indicative of maximum flooding) is preserved

offshore of Vlees Bay and is interpreted to be remnant of the MIS 6 – 5e transgression (Figure 6-5A, Figure 6-9B). Although these deposits would generally be subjected to immediate erosion (Carter, 2002), with an increase in the rate of sea-level rise or high sediment supply associated with the migrating TST, rapid burial and preservation has occurred. Unit H lies at a depth of 40 – 10 m BMSL and is underlain by SB 1. At this time the rate of sea-level rise was more rapid than the average calculated rate for this transgressive cycle (after the model presented in Figure 6-9A), which supports this hypothesis for preservation of Unit H, as mapped in the seismic record as a feature of maximum flooding.

Unit H has not been traced along strike in other sections of the mapped area, and it is proposed that the deposition and preservation of this unit is closely associated with the palaeodrainage of a river unable to incise the underlying bedrock substrate, thus promoting lateral deposition of sediment. Considering the relatively small Blinde River in Dana Bay and the basement outcrops at or near the seafloor in this region (the 'Infanta Arch'), this is considered plausible. Upon rapid transgression Seismic Unit H was perched directly on the geological substrate and subjected to rapid burial. Surficial sediment samples surrounding the locality of Unit H exhibit a low carbonate content (Figure 4-10). Assuming Unit H to represent a reworked wetland deposit, this hypothesis can be supported.

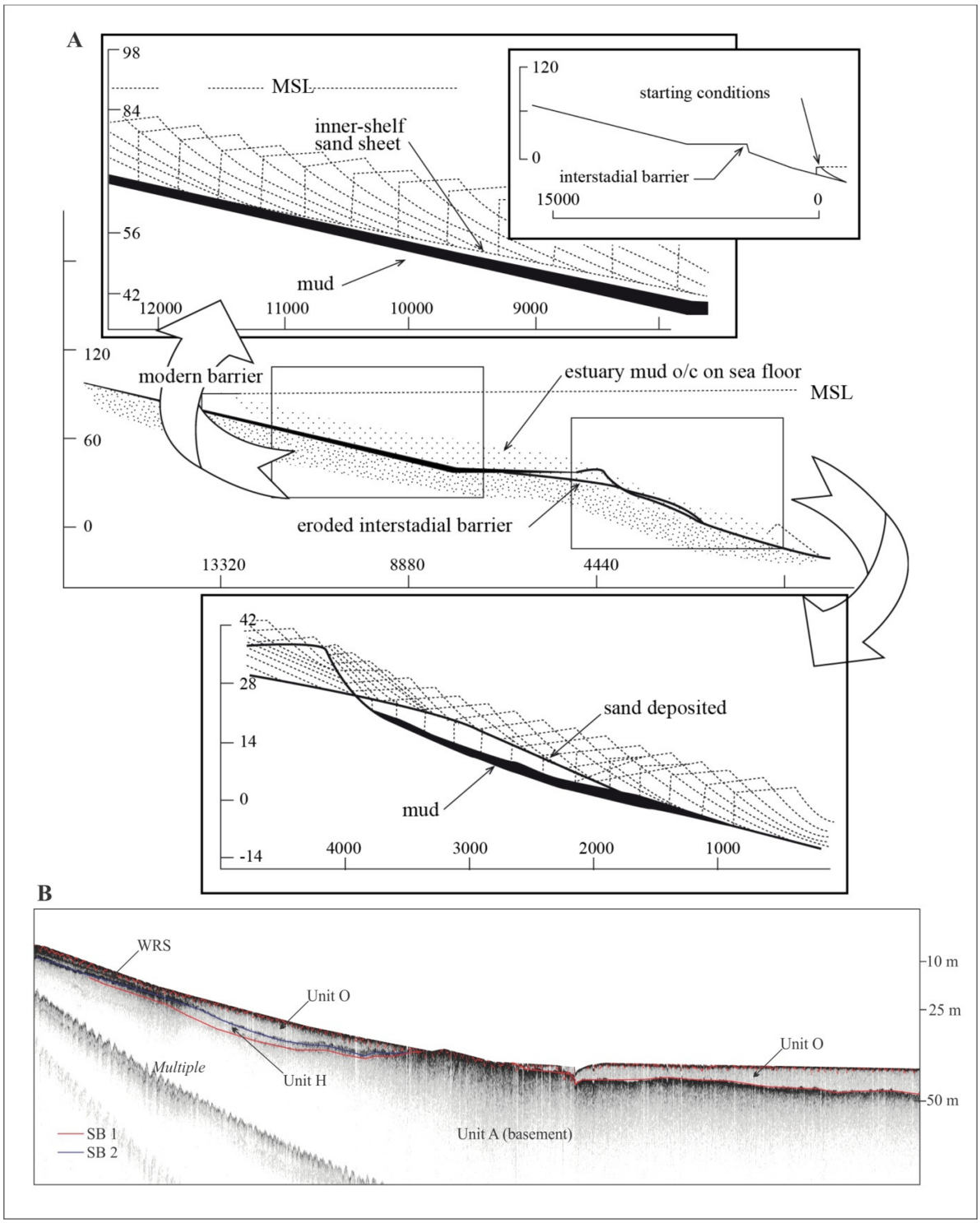

Figure 6-9. A. The modelled result of a marine transgression over a hard rock substrate from Cowell et al. (1992), applied to the preservation of Unit H. B. Seismic profile from Vlees Bay, showing transgressive deposits overlying a sequence boundary and shallow basement.

6.13.5 MIS 5e (131 - 113 ka)

The MIS 5e sea-level highstand is well represented on the South African coastline. Last Interglacial aeolianites and associated beach deposits along the South African coast have been constrained within a chronostratigraphic framework on the South Coast by Malan (1990), Carr et al., (2010) and Jacobs and Roberts (2009) where they crop out semi-continuously between Still Bay and Wilderness; up the west coast by Roberts and Berger (1997) and Compton and Franceschini (2005) and the east coast by Cooper and Flores (1991), Ramsay and Cooper (2002) and Porat and Botha (2008).

The beachrock facies identified in this study (Pm 18, Figure 6-5) on the shoreline is stratigraphically correlated to a transgressive facies deposited on the sea-level rise towards the peak of MIS 5e. This beachrock overlies older MIS 15 and MIS 11 aeolianite and the sedimentological characteristics and carbonate cements indicate deposition on an active intertidal zone. Cementation was likely rapid, as Pm 18 matches the beachrock sedimentology of accretion and rapid cementation in an intertidal zone.

The foreshore facies of MIS 5e has an OSL age of 122 ± 15 ka. This age range extends from 137 ka to 107 ka within the error, so technically could be MIS5e or 5d (Figure 6-5). Based on the age model, the sedimentological facies of an intertidal environment of deposition, correlation to sea-level curves, and field evidence, supported the interpretation to assign an age of MIS 5e. (Table 4-8, Appendix II). Geological Unit Pm 18 (transgressive beachrock) and Pu 1 (foreshore deposits) are both diagenetically characterised by fibrous micrite rims, indicative of precipitation in the marine mixing zone. Later dogtooth calcite spar borders grain boundaries and are likely associated with the regression from the peak of MIS 5e.

The presence of cusps on beaches (Pu 1 cobble conglomerate facies) reflects self-organisation of the system, driven by negative feedback between sedimentary environments on littoral zones (Werner and Fink, 1993). Cusps result from the morphodynamic interaction between swash, sediment transport and topographic variation on the foreshore and Pu 1 is interpreted to represent a cusp, deposited along the associated foreshore.

Aeolianite outcropping along the shoreline, and submerged aeolianites of Seismic Unit I mapped in Swartvlei are interpreted from field evidence to have been deposited on the MIS 5e HST. This unit, where sub-aerially exposed, has been dated in the Wilderness Embayment to the Last Interglacial (Bateman et al., 2004; Carr et al., 2010). Aeolianites of MIS 5e exposed sub-aerially along the Mossel Bay embayment coastline represent prograded barriers on a shoreline subsequent to the peak of the Last Interglacial termination, comparable to the active dunes deposited during the present interglacial since the peak of the Holocene Transgression. MIS 5e dunes (Seismic Unit I in Swartvlei, geological Unit Pu 2 in Mossel bay) were deposited on prograding shorelines subsequent to the peak of interglacial terminations. Dune build up in places is complex during MIS 5 and some

do span the entire range of 130 to 80 ka, which likely reflects the fact that sea level was fluctuating but not too far at times from near present day positions such that dunes could form by a complex amalgamation during MIS 5e, 5c and 5a.

Significant erosion of the sea cliffs at Pinnacle Point is associated with the MIS 5e highstand at 5 – 6 m AMSL (Hearty et al. 2007) which washed out unconsolidated archaeological deposits of lower-level caves (Fisher et al., 2010).

6.14 Late Pleistocene deposits: Sequence 8

6.14.1 The general MIS 5e – 2 transition

The period from the termination of the Last Interglacial to the early part of the Holocene Transgression was characterised by multiple oscillations of sea-level within a depth range of 70 – 20 m BMSL, which are superimposed on an overall regression towards the LGM (Lambeck and Chappell, 2001; Yokoyama et al., 2001) (Figure 6-10).

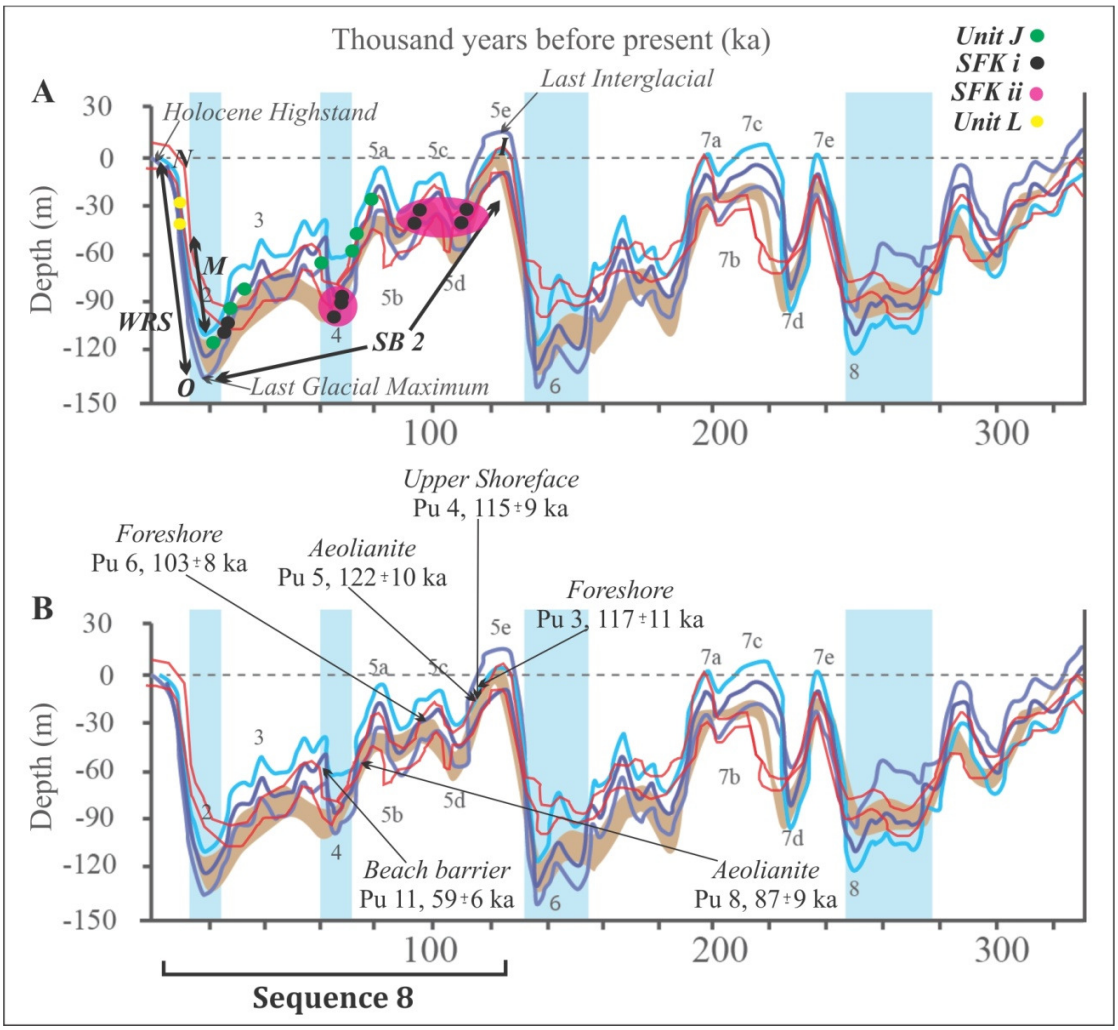

Figure 6-10. Deposits and structures associated with Sequence 8 (A. seismic, B geological) superimposed onto the RSL data of Clark et al. (2009) Waelbroeck et al. (2002) in blue, Bintanja et al. (2005) in brown, Rohling et al. (2009) in red. Sea-level curves modified from Compton (2011).

SB 2 (Figure 6-10A) represents erosional truncation of the underlying surface associated with this general sea-level regression and the commencement of deposition within Sequence 8. The basal truncated seismic units are Units F to I (Table 5-1) and the interpreted time scale for the creation of this surface extends from MIS 5e – 2. Despite the numerous interruptions of the general trend by stadial and interstadial events during MIS 5, SB 2 is particularly well preserved across the Wilderness Embayment and in Vlees Bay. Sub-aerial exposure of SB 2 during shoreline retreat in Vlees Bay is strongly suggested, as this surface can be traced onland to correlate with a distinct seaward-dipping palaeosol west of Dana Bay, adjacent to the Blinde River. The preservation of the potential palaeosol below more recently deposited shelf sediments is considered fortuitous, as these significant hiatuses are generally extensively eroded by ensuing transgressive cycles, if not subjected to rapid burial. The

form of the Vlees Bay embayment seems conducive to preservation of relatively low-energy and potentially erodible deposits, as was also the case with Unit H of Sequence 7.

The 52, 71 and 91 ka clusters of dunes are associated with normal regression at stillstands (LST) but occur on the overall forced regressive sea-level cycle of Sequence 8 (Figure 6-10B). In the case of these deposits, with the contemporary coast being far from these dunefields at the time of deposition, it is proposed that this environment may have been comparable to the Duynefontein dune plume (described by Roberts et al., 2009) or the Alexandria dunefield in the Eastern Cape. On the low-gradient coastal plain mobile dunes with a propensity to migrate landward are interpreted to have covered much of what is now the shelf. Transgressive dune fields are for the most part unvegetated (after Hesp, 1988), and remain relatively mobile. This mobility accounts for the lack of preservation on the open landscape, with remnant dunes from this time occurring in localised, protected, embayments along the Pinnacle Point coastline and within sheltered caves. Seismic Unit J aeolianites lie unconformably on SB 2 and are interpreted to have been deposited during the forced regression from MIS 5e – 2 (Figure 6-10A). The forced regression of Sequence 8, with its seaward migrating barrier systems, appeared to be associated with a higher sediment supply than the previous sea-level cycle. This is, however, argued to reflect a mass-balance of sediment in the system, which is reworked on each complete glacial-interglacial cycle. Although the rivers currently draining the South Coast deliver terrigenous sediment to the beaches and littoral zone, constant removal and redistribution by ocean current circulation on the shelf may account for relative stability in the sediment budget.

The MIS 5e – 2 transition can be traced through the record of carbonate diagenesis, as it is proposed that the dominant authigenic smectite infill was associated with this regressive cycle. This infilling phase contains trace elements suggesting the likely presence of overlying palaeosols. It is interesting to note, however, that authigenic smectite infill was not present in the Pm 8 aeolianite (~87 ka), which was deposited on this regressive cycle. The concept of an extensive dunefield as well as associated palaeosols is therefore plausible. Mobile dune cordons on the South Coast are generally less well developed than on the West Coast (Roberts et al., 2009) from the difference in total and, in particular, seasonal rainfall. If rainfall was less or more seasonal from MIS 5 to MIS 2, then the dunes may have remained unvegetated and mobile enough to move inland, but if palaeoclimate indicators suggest a wetter SCP during MIS 4 than today (e.g. Bar-Matthews et al., 2010), this would suggest that mobile dunes were restricted to near the coast as in present day.

6.14.2 MIS 5e – 4 (113 – 70 ka)

The retreat of sea-level from the peak of the Last Interglacial follows a complex path from MIS 5e – 5a (Figure 6-10). The highest resolution available record for this sea-level cycle is expressed by Last Interglacial corals

from the Huon Peninsula, Papua New Guinea, and Barbados were dated by Cutler et al. (2003) using ^{230}Th and ^{231}Pb techniques. MIS 5e ended prior to 113.1 ± 0.7 ka when sea-level was -19 m relative to the present elevation. The MIS 5c sea-level arguably reached a similar elevation to MIS 5e (Cutler et al., 2003). In Mossel Bay, luminescence dates and sedimentological analyses show the deposition of -26 m (present depth) foreshore deposits of Unit Pu 3 at 117 ± 11 ka on the regression from MIS 5e. In some respects the OSL date narrows the possibilities which the sea level curve can then further refine and despite the error range, correlations to the existing glacio-eutatic sea-level information is used to constrain the deposition of this unit. Sea-level may have experienced a brief transgressive phase, or alternatively high sediment supply facilitated significant progradation as upper shoreface deposits of 115 ± 9 ka crop out at a depth of 17 m BMSL (Unit Pu 4). Sedimentary deposits represent this regression well in Mossel Bay. Foreshore facies now lying at a water depth of 25 m BMSL were deposited at 103 ± 8 ka. During MIS 5b sea-level fell to -57 m by 92.6 ± 0.5 ka, having regressed ~40 m during the MIS 5c - MIS 5b transition (Figure 6-10). During the MIS 5c – MIS 5b fall in sea-level, regressive aeolianite is preserved at a water depth of 38 m BMSL and was dated to 87 ± 9 ka Sea-level then rose in excess of 40 m over 10 kyr from MIS 5b- 5a. MIS 5a lasted until approximately 76.2±0.4 ka at a level of -24 m. MIS 4 is interpreted to be associated with a -81 m sea-level at 70.8 ka, with sea-level falling almost 60 m in less than 6 kyr during the MIS 5a - 4 transition (Cutler et al., 2003). The MIS 4 glacial period extended from 75.1 (77 - 72) to 60.6 (63.5 - 56.4) ka.

The multibeam bathymetric dataset (Chapter 3, Chapter 4) showed that the palaeochannel of the Groot Brak River is exposed on the seafloor (Figure 4-9), and has incised the pre-existing Quaternary units lying adjacent to its channel margins. The implication is that this incision likely took place during the fall in sea-level from MIS 5e – 5d, as the depth of the channel extends to the seaward edge of the mapped area at 45 m BMSL. This additionally provides a minimum age for these cemented, subsequently incised, deposits which predate MIS 5e.

Unit K, and more specifically, facies SFK I (Figure 6-10A), is characterised by laterally discontinuous incised channel fill and onlapping clinoforms. This package displays relative acoustic impedance and is inferred to represent fluvial or estuarine facies deposited from MIS 5e – 4. This work correlates the basal SFK i facies as fluvial lag deposits and compositely groups the fluvial, estuarine and tidal environments within this classification. Unit K deposits have infilled depressions incised by the FSST of Sequence 8, initially exploited as sinks for Unit G sediments. Unit K therefore, represents a second phase of fluvial incision and deposition. SFK i is separated into three distinct clusters defined by the depth of occurrence at ~30 – 40 m, ~85 – 100 m, and 110 m BMSL. The shallowest (30 – 40 m package) is interpreted to reflect sea-level regressions within the MIS 5 sea-level fluctuations and because these are thought to be dominantly regressive deposits from the seismic architecture, they are assigned to MIS 5d or MIS 5b. The semi-transparent deposits adjacent to SFK i offshore of Mossel Bay are interpreted to represent lowstand floodplain sediments (SFK ii). The lateral accretion of

floodplain facies adjacent to a palaeochannel is in agreement with a model proposed by Wing (1984), which suggested two facies assemblages for floodplains: (1) tabular units interpreted to be deposits of gradually aggrading swamps; and (2) lenticular bodies that represent the fill of abandoned channels. This study proposes the former as a suitable explanation of the submerged LST. The LST deposits of SFK i lying at a depth of ~100 m BMSL are associated with a LST near the MIS 4 glacial (Figure 6-10). Progradation on this palaeoshoreline allowed the deposition of dominantly fluvial deposits into the pre-existing channels of most rivers draining the study area. In mature stages of sedimentary infilling fluvial deposits eventually prograded more seaward over the tidal delta. The transparent and weakly layered deposits suggest homogeneity within facies SFK ii. Where deposited adjacent to the relatively shallowly incised Groot Brak channel, it is proposed that antecedent fluvial topography on the shallowly dipping continental shelf created increased accommodation, which likely allowed the deposition of these lateral floodplain deposits. Over short periods of time high sediment supply distributary channels may tend to avulse and produce flooding surfaces (Catuneanu et al., 2009).

The two successive transgressive back-barrier units exposed surficially offshore of the Groot Brak River, preserved at depths of 29 and 35 m BMSL, are associated with TST cycles (seismic Unit L, Geological Units Pu 11, Pu 12, Figure 6-10). The 35 m BMSL deposit is ~59 ka in age. Further out to sea, a back-barrier environment lies in a water depth of ~50 m BMSL and display sediments deposited on a LST. These likely represent wave-dominated barrier environments with supratidal coastal barriers intersected by narrow entrance channels connecting the low energy back-barrier lagoons to the open coast. Seismic Unit L is broadly interpreted as a back-barrier sequence with SFL i at the base indicative of lagoonal, channel fill and floodplain facies, overlain by acoustically semi-transparent basin infill sediments. These facies are separated by Reflector *l*, thought to reflect washover into the system from intermittent action associated with the adjacent high-energy shoreline. It is proposed that during the regressive phase within this parasequence, the unconformity presented as reflector *l* formed during a temporary decrease in the rate of relative sea-level rise (stillstand) when the HST was deposited, and that an increasing rate of sea-level rise allowed the overlying LST to be deposited. These reflectors are, therefore, preserved where the facies reach their most proximal positions, determined in this study by the laterally bounding ridges. Unit L was only mapped in the east near Mossel Bay and Wilderness and is bounded at its landward and seaward margins by shore-parallel trending aeolianite and beach deposits. Wave-dominated barrier systems consist of estuarine lakes bounded by coastal barriers, have filled the mouths of lowstand incised valleys. The back-barrier environments of Mossel Bay are characterised by flat-bottomed basins and relatively shallow infills (up to 7 m as determined from seismic data).

The carbonate cements include an initial marine cement on the grain boundaries, followed by a second generation of carbonate-organic infill (associated with the back-barrier occurrence) and this is overprinted by a third event of marine rim cement. The development of these systems can be likened to three areas along the Cape

coast: the Wilderness Embayment, Still Bay back-barrier deposits and the Langebaan Lagoon. The evolution of a barrier during transgression will either continue to roll over (Leatherman, 1983) as sea level continues to rise, or will become overstepped. Overstepping occurs if the rate of rise is rapid, or if the substrate is steep. The beaches have shifted up the depositional profile at ~85 ka.

6.14.3 MIS 3 (57 – 29 ka)

Continuing the geological succession towards MIS 2 three sea-levels associated with interstadials occurred during MIS 3, with sea-level reaching elevations of between 85 and 74 m BMSL (60.6 ± 0.3 ka, 50.8 ± 0.3 ka and 36.8 ± 2 ka; Cutler et al., 2003) (Figure 6-10). The period between 60 ka and 12 ka (MIS 3-2) is a time of climate variation at long and short scales characterised by Heinrich and Dansgaard–Oeschger events (see Chapter 2), which had severe impacts on terrestrial Northern Hemisphere environments, but as yet the impact on the south is unclear although they are argued to be associated with sea-level fluctuations (Voelker, 2002). MIS 3 generally marks a warming in conditions relative to MIS 4 and sea level was highest from 60 - 50 ka then it dropped to around 38 ka before starting its final descent into MIS 2. Conditions became strongly glacial at ~30 ka, eventually reaching the LGM in MIS 2.

6.14.4 Response of coastal and barrier systems to forced regression

In the case of SFKii deposits lying at depths of 80 and 105 m BMSL, relative sea-level rapidly retreated on the shallow gradient outer shelf environment, and the highstand barrier prograded toward the shoreface with additional sediment derived from further offshore by erosion on the lower shoreface. The associated regressive barrier was constructed seaward into the eroded region where the substrate gradient of the palaeo-coastal zone was near horizontal and lateral outbuilding occurred. Lagoons situated behind prograding barriers become isolated from the ocean on embayed coasts, while those lying on linear clastic shorelines extend in the direction of longshore drift and ultimately close or become captured by adjacent water bodies (e.g. Cooper, 1994). Lagoons, estuaries and low-energy coastal environments are restricted spatially during a regression. Features cemented by meteoric water, were likely modified or destroyed with the following transgression.

According to Roy et al. (1994), regressive barrier and floodplain deposits are generally considered to be features of low-gradient, sediment rich shelves that have not been eroded during subsequent transgressions (Figure 6-11). Forced regressive barriers on the southeast Australian shelf are as wide as, or wider than, their stillstand equivalents, retaining approximately the same volume of sediment as the present onshore barriers. The reason for this is extensive sediment recycling and addition to the downdrift sediment budget. In this regard, and based on stratigraphic correlation across the South Coast, southeast Australia provides a suitable analogue to this study.

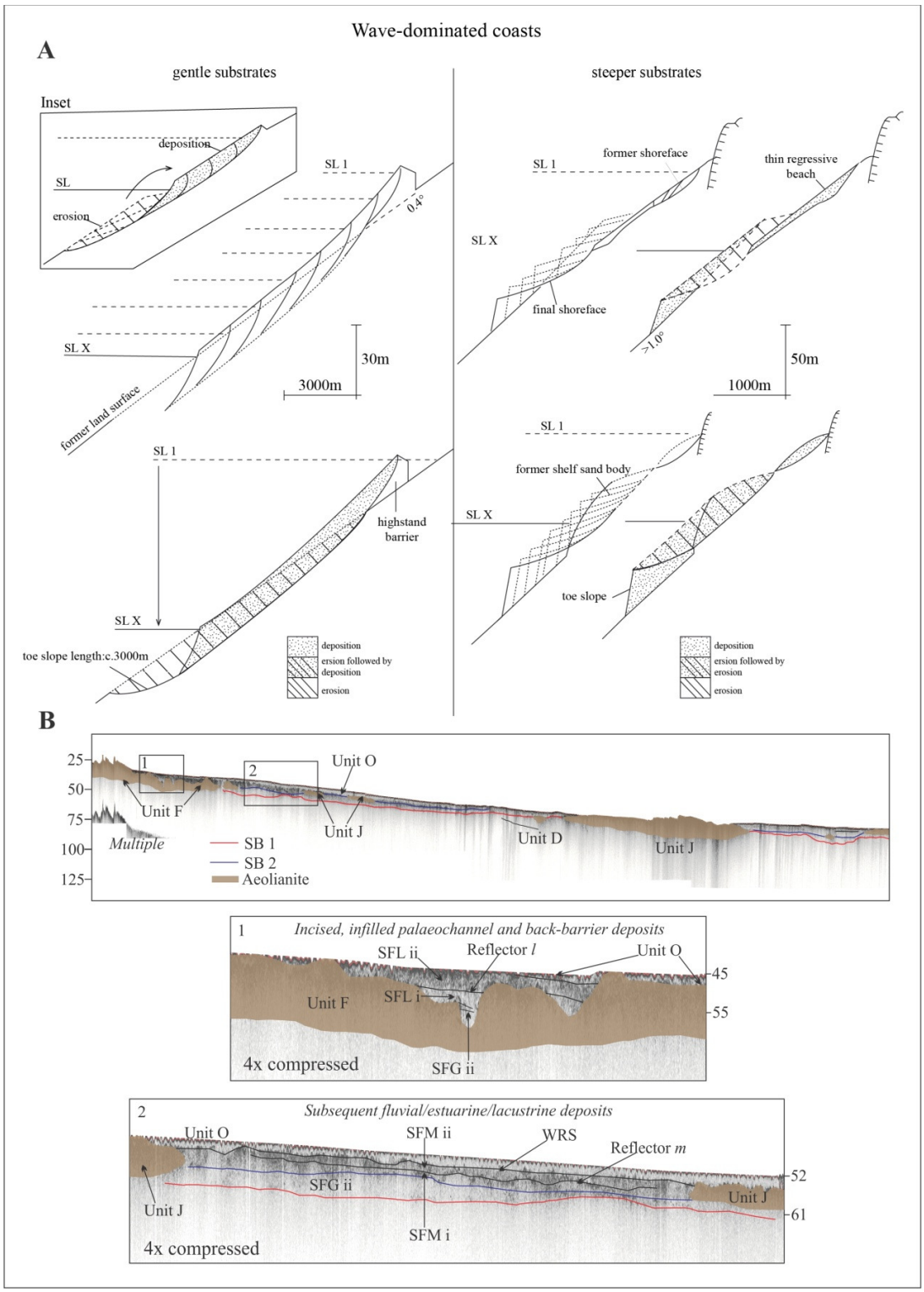

Figure 6-11. A. Regressive barrier development (modified from Cowell and Thom, 1994). B. Illustrated in the seismic record of Mossel Bay with respect to the down-profile migration of Seismic Unit J. Location of the enlarged areas represented by 1 and 2 is shown on the regional profile.

The continuum of shoreline retreat is also recorded in the shelf stratigraphy by the offshore/seismic record. Seismic Unit J (Figure 6-11B) lies conformably on the prominent SB 2 surface and these down-stepping palaeo-coastlines are preserved as dominantly aeolianite on the seafloor which track falling sea level. The deposition of these coastlines distal from the last HST shoreline traces the progressive down stepping as relative sea-level retreated towards the glacial lowstand of MIS 4. These deposits can therefore be further classified into "detached FSST" deposits (after Coe and Church, 2003). Though these units were deposited on the FSST they are interpreted here to be more closely associated with stillstands or pulses of sediment supply that periodically prevailed during FSST conditions, with a relative decrease in rate of base level fall on the FSST allowing significant dune accretion and deposition.

6.14.5 MIS 2 – 1 transition (36.5 – 7 ka)

This section describes the record of the post-glacial marine transgression (PMT) during which sea-level rose from the LGM -130 m 18 ka to 0 to +3 m MSL by ~7 ka (Figure 6-10). Preceding the PMT, sea level regressed to 107 m BMSL: at 23.7 ± 0.1 ka early in MIS 2, before reaching the LGM shoreline (121 m BMSL) at 26.5 ka (Cutler et al., 2003; Clark et al., 2009). The LGM ended at 18 ka (Clark et al., 2009. The glacial termination is marked by the moderate rise in sea level, before a rapid rise associated with MWP 1A at 14 ka. The melting of Northern Hemisphere ice sheets resulted in a ~25 m rise in sea-level until 14 ka (Clark et al., 2009).

The fall in sea-level towards the LGM coincides with the final incision and infilling of fluvial facies of SFK i within Unit K, which continued periodically from MIS 5 towards the outer shelf. The overlying transgressive deposits lying at a depth of ~110 m BMSL were deposited within incised river valleys and date to approximately 18 ka according to correlations to sea-level curves (Figure 6-10).

The PMT, which commenced during MIS 2 after the time of the LGM and the termination of this glacial cycle, left a prominent sediment wedge on the shelf (Seismic Unit O), which extends from the outer shelf to above present sea level where Holocene highstand sedimentation of the subsequent HST marks the end of the TST. Sedimentation within Unit O near the LGM shoreline (Figure 5-7; MIS 2) is interpreted to reflect LST deposition. Although intercepted along strike along the coast-parallel oriented deep seismic profile (110 m BMSL) between Mossel Bay and Wilderness, the sediment wedge of Seismic Unit O is relatively thick compared to units occurring higher up in the depositional profile. It is proposed that progradation of facies associated with a relatively high sediment supply over a sustained period of shoreline construction initially facilitated the development of Unit O. The sediment wedge is either underlain by a ravinement surface (WRS) which, where preserved, marks the regional flooding event, or by reflector *o* near the LGM shoreline (a surface of maximum regression). If neither element was present, Unit O would directly overlie elements of previously

deposited sequences that were outcropped on the seafloor. Although ravinement surfaces can also be dominated by tidal encroachment, the governing scouring mechanism of a WRS in this area is interpreted to be wave action in the shoreface (after Swift, 1975), assuming that the present high energy coasts prevailed throughout the late Pleistocene and Holocene. The mapped regional WRS erosionally truncates basal seismic units, for example Unit L, and it extends from MIS 2 – MIS 1 (the late Pleistocene into the late Holocene) (Figure 6-10). The more inshore sediment wedge of Unit O, lying on the transgressive WRS, likely formed initially in the shoreface and was later modified by current reworking on the mid- to outer-shelf. The thickness of the TST is dependent on the balance between sediment supply with much of the sediment supplied by reworking of older abandoned deposits of previous highstands and the rate of generation of accommodation space. With a rapid rise in base level, thin TST deposits (except where they intersect old dune systems) are preserved, hence these deposits are thinnest during the early rapid transgression. The depths of occurrence are also less likely to contain highstand sediment to rework.

The Holocene sediment wedge is the name traditionally given to this deposit across other parts of the South African continental shelf where it has been previously described (e.g. Martin and Flemming, 1986; Green, 2009; Cawthra et al., 2012b; Bosman, 2012 on the South- and East Coasts), but the author prefers to refer to the transgressive sedimentary deposits within a nomenclature describing the PMT because the late Pleistocene and Holocene are temporally inclusive in the depositional context of Unit O. The rise in sea level of the PMT was so rapid, most of the middle to outer shelf deposits of the world are relict sediment only reworked during the PMT (e.g. Sommerfield and Lee, 2004). Deposition of any significance did not occur until the Holocene highstand, such as the Holocene mudbelt on the West Coast. The mudbelt sits above the reworked deposits but in most places outside of the mudbelt this Holocene sediment exists as only a thin veneer (e.g. Wigley and Compton, 2006). The Seismic Unit O sediment wedge is distinct from later Holocene drape deposits, such as the South Coast mudbelt, which is best developed to the west of this study area. The 45 m BMSL nick point, which provides an inflection in the shelf dividing zones of different gradient, provides accommodation space for the inshore sediment wedge to be preserved and the slope is a likely area of accretion for mudbelt deposits, protected from open ocean swells compared to the flat Agulhas Bank. Low energy deposits are thought to accumulate in the lee of this terrace.

In this study, Seismic Unit O is acoustically transparent and contains low-amplitude, divergent clinoforms. Where this deposit is well developed, generally on the inner shelf, internal bounding surfaces truncating clinoforms can be observed. These, as per the previous discussion of associated surfaces of stillstands, either likely represent minor sea-level fluctuations on the overall transgression, or storm lag deposits. The divergent clinoforms are interpreted to represent variation in sea level as well as changes in sediment supply. Unit O generally thickens towards the east and is poorly developed in the vicinity of Still Bay.

Overstepping associated with the MWPs has recently been investigated up the East Coast by Green et al. (2014) for a case where sea level rose 20 m in 500 years. Unit M contains two distinct seismic facies separated by reflector *m*. Although facies SFM i is interpreted to consist of lagoonal deposits deposited on a stillstand, it is proposed that the preservation of these facies was promoted by subsequent maximum flooding of SFM ii. Carter (1988) suggested that reasons for overstepping include an increase in the rate of sea-level rise, high sediment influx, interplay of landward and seaward sediment transport processes, stranding on a topographic high and an interplay between different wave orientations. Cooper (1991) suggested, in addition, the contribution of early diagenesis (i.e. cementation) of bounding barrier sediments, making them less susceptible to reworking.

In terms of the carbonate diagenetic model, the transgression of sea level from MIS 2 – 1 is characterised by calcite spar infill, alteration of existing cements to microspar mosaics and, significantly, the presence of an organic-carbonate mixed cement. The presence of organic matter in the calcite cement suggests that the waters from which the calcite cement precipitated had abundant dissolved and particulate organic matter, typical of soils and tannin rich waters seen today in the low-lying coastal vleis. This attests to the presence of water-saturated sedimentary stratigraphy and can perhaps be extended to consider the presence of wetlands associated with floodplain sediments as described from the seismic record.

H 1 aeolianite, associated with the back-barrier Unit H 2 adjacent to the Klein Brak River in Mossel Bay, only showed the presence of dogtooth calcite spar at grain boundaries and contains unfilled voids. No authigenic smectite infilled pores, allowing for the previous interpretation for this diagenetic phase to be associated with a prior sea-level regression.

6.15 The Holocene evolution of the Wilderness Embayment: Sequence 9

The youngest sequence boundary, SB 3, is only observed in the Wilderness Embayment (Swartvlei) where the young sediments of Sequence 9 are preserved (Figure 6-12). SB 3 separates the underlying Unit O from the overlying Unit P. SB 3 therefore represents the most recent surface of sub-aerial erosion in the study area and is interpreted to have commenced with the termination of the 3 m AMSL Holocene highstand at ~4.5 ka (Compton, 2001; 2006).

The youngest sediments of Sequence 8 represent HST deposits and are represented by SFO iii in Swartvlei where they are interpreted to form the back edge margin and the basin infill associated with a stillstand on this systems tract. This occurred during the mid to Late Holocene, in response to the rising sea level reaching its maximum elevation. Within Swartvlei the FSST deposits (Seismic Unit P; MIS 1) present as progradational sedimentary facies now forming sandbanks along the lake margins. This is the youngest FSST deposit in the

study area as it is associated with a forced regression and its commencement is interpreted to date to the peak of the Holocene highstand circa 7 ka. The progradational parasequence represents basin infilling. Seismic Unit Q, the youngest deposit mapped in this study, represents modern back-barrier basin infill in Swartvlei. The active barrier sedimentation at Wilderness may be regarded as an intermediary feature between an eroded and prograded coast, associated with limited sediment for dune building and enclosure of water bodies (e.g. Roy and Thom, 1981). Dune construction in this case is asymmetrical alongshore with the largest dunes occurring at the downdrift embayment margin where there is the greatest exposure to onshore winds. The Holocene highstand likely allowed shoreward progradation of sediment to stabilise within the mouths of incised valleys, creating the back-barrier estuarine lakes.

The closest South African analogy to the Wilderness Embayment is the west coast Langebaan Lagoon, described by Flemming (1981), Roberts and Berger (1997), Compton (2001) and Compton and Franceschini (2005). This tidal current-dominated back-barrier system is bounded by Pleistocene aeolianites and Holocene barrier dunes. The West Coast embayment evolved on a broad coastal plain, which was planed off by sea-level oscillations eroding antecedent pre-Mesozoic strata (Roberts et al., 2006). The southeast Australian margin, which bares similarity to the South African context, showed that sedimentary infilling of incised valleys is closely related to Holocene sea-level fluctuations.

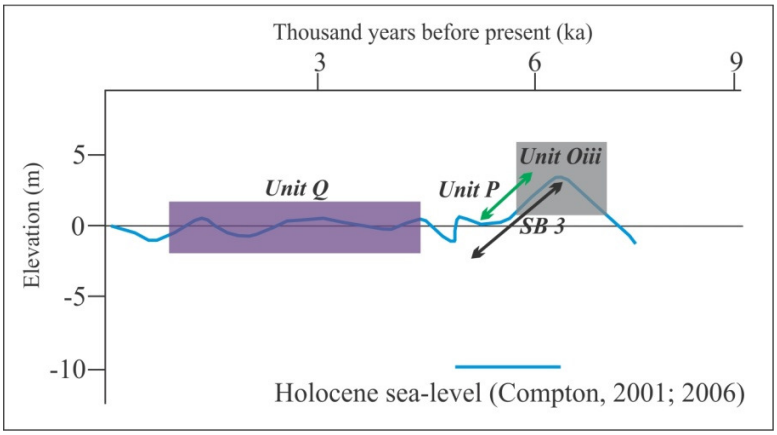

Figure 6-12. Deposits of Sequence 9, superimposed onto the local Holocene sea-level of Compton (2001, 2006) for the last 9 kyr.

6.16 The modern environment

The PMT sediment wedge on the inner shelf and a less well defined sand sheet on the low gradient mid- to outer shelf constitute the offshore active marine sedimentation in the study area. This unit rests on a discontinuous WRS. Bedforms, in the form of megaripples and sand ribbons, are observed in Mossel Bay associated with the

sediment wedge (Chapter 4), with the troughs exposing either antecedent deposits or the WRS. The widespread occurrence and the form of the transgressive sediment sheet reflect the autochthonous, sediment starved nature of the outer shelf of the South African South Coast. The 'modern' sedimentary deposits are likely to be relict and only more recently reworked sediment.

6.16.1 Inner shelf sediment deposits

On this generally sediment-starved shelf, aggradation of facies near terrestrially supplied sediment sources has occurred most significantly in the east and the shelf sediment wedge tends to thin toward the west. The Gouritz River, therefore, likely governs the main sediment distribution on this part of the South Coast shelf before it is transported eastward with longshore drift and bottom currents below wave base. An isopach map was constructed from digitising the base of the unconsolidated sediment wedge from seismic profiles within Mossel Bay (Figure 6-13). The shelf sediments are seen to be thickest in the lee of the offshore extension of the Cape St. Blaize promontory and in Vlees Bay, and thin towards the east where the prominent seafloor outcrops are exposed offshore of the Groot Brak River. The termination against the Groot Brak offshore outcrops suggests that these consolidated ridges are a major factor in reducing the littoral sediment transport in this region.

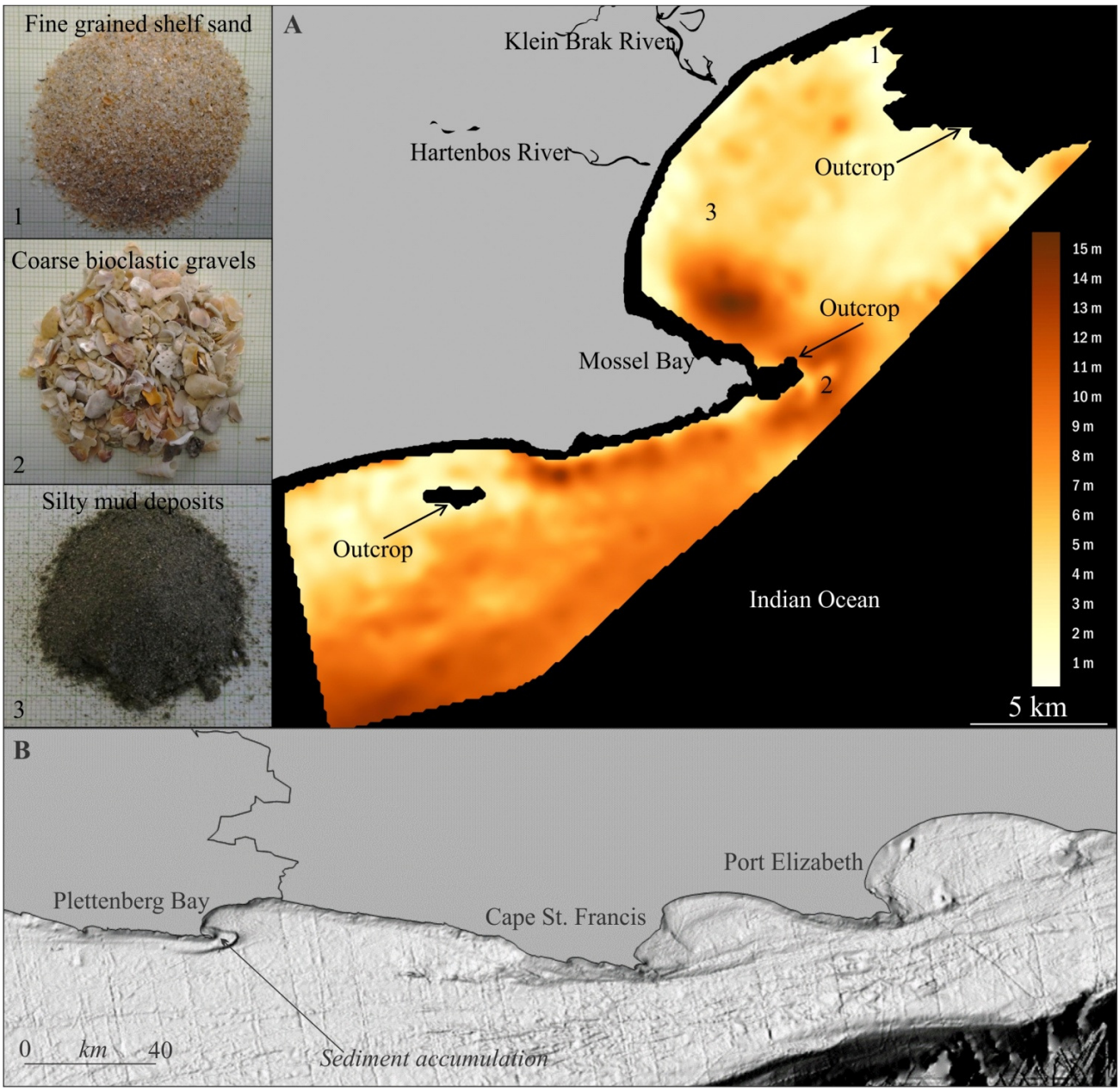

Figure 6-13. (Left) Three dominant unconsolidated sediment facies (shelf sand, bioclastic graves and silty mud). A. Isopach plot for the Mossel Bay study area, showing the form of the seafloor sediment wedge. B. Headland attached sand bodies in Mossel Bay and along the South Coast (from de Wet, 2013).

This shelf wedge was described as a geomorphic feature of the seafloor in Chapter 4. Approximately 43% of all bedload sediment on the South Coast is located between Cape St. Blaize and Plettenberg Bay, an area receiving only 3% of the total fluvial supply (Birch, 1980). This is interpreted to be dominantly associated with eastward transport of bedload sediment by the Breede and Gouritz Rivers. Sediment transported by these rivers is transported east by longshore drift and has ended up trapped in the Wilderness Embayment and off eastward-

facing headlands where there is accommodation space and protection from the further longshore transport. Between Cape St. Blaize and Knysna, the volume of Quaternary sediment mantling the shelf was determined to be 22 239 x 10^6 m^3 (Birch, 1980) or a total for the South Coast of 64 083 x 10^6 m^3. The sediment off the Gouritz River reaches 20 m in thickness. The region surrounding Mossel Bay is considered to be relatively sediment-starved and a swathe of sediment (>10 m thick) extends eastward from Cape St. Blaize across Mossel Bay. This wedge thickens towards Wilderness, reaching a maximum thickness of 25 m. The headland attached sand body has accreted adjacent to the offshore extension of Cape St. Blaize, which is interpreted to have accreted in response to dominant littoral drift from west to east. Linear, shore-parallel oriented similar features occur along the South Coast against almost every prominent headland (Figure 6-13).

The thickest sediment in Mossel Bay and Vlees Bay occurs within the embayments, where a well-developed inner shelf wedge is a prominent seafloor feature of the area. Birch (1980) argued that the relative lack of sediment surrounding the Breede River to the southwest is attributed to the sediment being contained within the substantial incised channel and wind removing sediment adjacent to the river mouth. In contrast, the sediment wedge associated with the Gouritz River, which is thickest west of the river mouth, was likely deposited in response to the south-facing headland, implying that the sediment is discharged further into the influence of deeper, westward-flowing currents (Rogers, 1971). The Gouritz River, in addition, drains argillaceous material from the Bokkeveld Group and has a maximum discharge in summer compared to the winter-dominated discharge of the Breede River (Tripp, 1967; Harris, 1978). The dominant westerly-flowing summer currents likely transport the fine-grained material in this direction. The Cape St. Blaize to Cape Seal area of the South Coast receives a low fluvial supply (0.1 x 10^6 tons bedload per year; Midgley and Pitman, 1969) yet is associated with the largest deposit of marine sediment (60 000 x 10^6 tons; Birch, 1980). This is likely a response of the trend of the coastline. The now filled Wilderness Embayment would have been a re-entrant on a smooth coastline upon lowered sea-level. The location of this embayment suggests that the lowstand shorelines between Cape St. Baize and Knysna would have been comparatively linear and may have served as a sediment trap for eastward-flowing longshore drift.

Sand delivered by rivers is transported east by longshore drift, while suspended mud is likely distributed further offshore and transported west by bottom currents to form the South Coast mudbelt to the west of this study area. This shelf sedimentary depositional model is analogous to the Orange River Holocene mudbelt on the West Coast (Meadows et al., 2002; Herbert and Compton, 2007).

7 EVIDENCE FOR FORMER LAND SURFACES ON THE EMERGENT SHELF OFF MOSSEL BAY

Submerged landscapes are areas of land that were once sub-aerially exposed but have been subsequently inundated by rising sea levels (Bailey and Flemming, 2008; Westley et al., 2011). Studies from neocoastal caves and other coastal archaeological deposits suggest that these currently submerged terrestrial ecosystems may have played a significant role in human evolution in South Africa during the Pleistocene, offering terrestrial as well as coastal and marine resources (Marean et al., 2007) and periodically served as a geographically isolated region for evolutionary divergence of groups living there (Compton, 2011). Although preservation of archaeological sites is unlikely after the repeated migration of a high-energy coast, constraining the now-submerged terrestrial landscape is strongly dependent on the geological features preserved.

7.1 Elements of submerged former land surfaces near Mossel Bay

7.1.1 Wetlands and water resources

Despite the presence of numerous rivers draining the study area (Chapter 5, Figure 5-13), no definitive evidence was found in this study for palaeodelta deposits, though these may have been reworked into the sediment wedge. With the slowly eroding hinterland (Tinker et al., 2008a; Scharf et al., 2013), it is unlikely that the fluvial systems delivered sediment to the coast more rapidly than marine processes could rework it, but sediment transport in general would have likely been low during glacials considering the low gradient beyond 45 m BMSL with much of the sediment trapped in lakes and floodplains.

On the broad Agulhas Bank with its Cretaceous organic-rich dominantly claystone sedimentary substrate on the inner shelf, palaeodrainage networks were shallowly incised and laterally extensive and are interpreted to facilitate a wetland environment and the probability of adjacent vast alluvial plains when the shelf is exposed. In the low-gradient offshore areas, rivers were free to meander. With the fluvial channels in the offshore environment exhibiting a tendency toward lateral accretion, it is likely that the steep onshore topography of the CFB served as a conduit of fine grained sediment to reach the shelf before being deposited into the extensive floodplains mapped and described in this study.

The character of fluvial incision, differing from the west to the east in this study area, is interpreted to be a function of geological substrate which governs shelf gradient. On the Infanta Arch (Still Bay and Vlees Bay)

where quartzite bedrock/basement is close to, or cropping out at, the surface, the river flow was controlled by the antecedent substrate.

The seismic data revealed the presence of bathymetric depressions containing low-reflectance sediments at dominant depths of 30 – 40 m, 50 – 60 m, 75 – 80 m and ~105 m BMSL across the entirety of the South Coast shelf between Still Bay and Wilderness. These, based on samples obtained from the inshore deposits, are interpreted to represent both interdune deposits and back-barrier sediments. They occur in close association with fluvial systems (e.g. off the Groot Brak River; Figure 7-1) and were likely also linked to estuaries in the palaeo record. A comparable analogue exposed along the modern coastline is the Wilderness Embayment, investigated in this study. In the embayment of Vlees Bay, SB 2 is overlain by Seismic Unit H, interpreted to represent a potential wetland deposit adjacent to the palaeoflow of the Blinde River. This, in close association with the palaeosol expected to reflect the SB 2 surface, provides a unique coastal setting compared to the currently exposed environment in close proximity (<10 km) to the Pinnacle Point archaeological site.

In addition to the presence of wetlands, the quartzite formations within the CFB are dissected by faults formed during orogeny that produced the Cape Fold Mountains and the later fragmentation of Gondwana (Hälbich, 1983). The CFB therefore contains large fractured aquifers (currently yielding ~2 litres per second; Roberts et al., 2008b) and freshwater springs rejuvenated by rainwater. Faure et al. (2002) propose that freshwater springs, associated with steepening of the coastal water table gradient and an increased hydrostatic head, appeared on emergent continental shelves during glacials. At the contact between the Table Mountain Group sandstone rocks and the Mesozoic to Cenozoic sediments of the Outeniqua Basin on the South Coast, in conjunction with mixing of salt water seepage from the Indian Ocean, the presence of wetlands and springs is thus expected to be supported in this region during cycles of sea-level regression. Groundwater presently obtained from Table Mountain Group sandstone aquifers is generally of excellent quality (DWAF, 2004b). Karstic springs may occur on the shelf where limestone is exposed at the surface, where overlain by Holocene sediments.

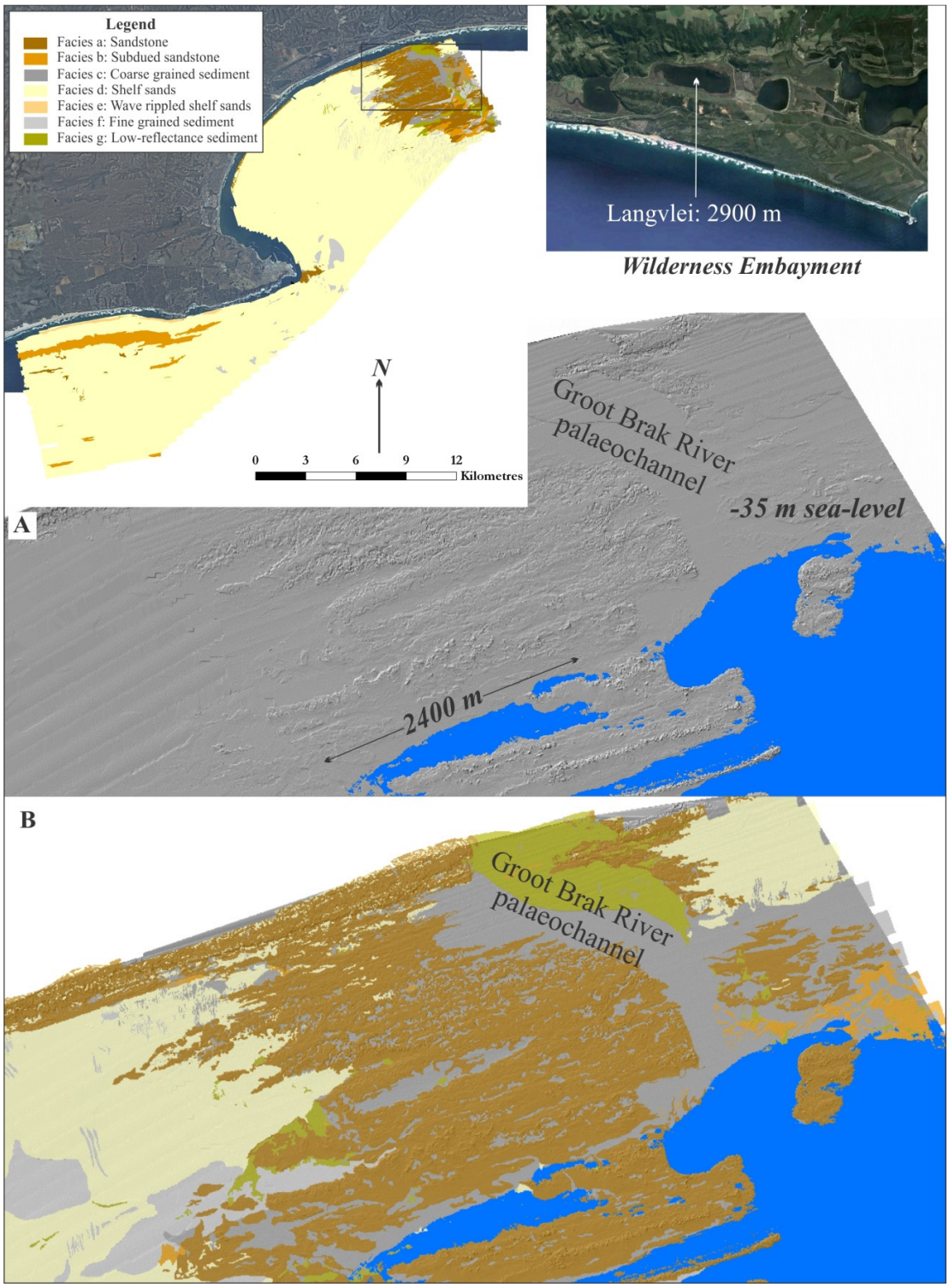

Figure 7-1. Back-barrier sediments associated with the Groot Brak palaeochannel, compared to the dimensions of Langvlei in the Wilderness Embayment. A. Multibeam bathymetric data with superimposed 35 m BMSL sea level, which inundated the back-barrier system. B. The same area, with interpreted acoustic facies draped over the multibeam bathymetric dataset.

This shelf environment is suggested to have been a locally water-saturated environment, confirmed by the carbonate cements analysed in this study and the seismic stratigraphy of fluvial systems. The presence of the reducing, organic-dominated matrix, black litho-clasts and authigenic smectite seen in thin section, as well as the nature of channel fills and lateral deposits seen on seismic profiles, attest to this. Organic matter noted in thin sections suggests well-watered, highly productive ecosystems important to humans who relied on wetland resources in addition to marine resources. Although the topography of the Agulhas Bank is relatively flat, the presence of Quaternary barrier systems likely promoted a landscape rich in wetlands and characterised by water bodies focussed locally in back barrier settings such as modern day Wilderness and along meandering river courses. Due to the high density of rivers along the South Coast (Table 5-2; Figure 5-13), fresh water resources were relatively evenly distributed across the emergent shelf and in close proximity to beaches on palaeoshorelines through the lowstand record of sea level.

7.2 Vegetation and soils

The modern day vegetation is determined largely by geological substrate, therefore it was probably the case when the sea level was lower. Given the high species diversity of the Cape Floral Region, and the broad landscape that would emerge upon lowered sea-level, geologically defined areas were considered in isolation when vegetating this submerged landscape. Vegetation types have been inferred and are presented in Figure 7-2 for the LGM and PMT. These can be broadly divided into dune environments, wetlands, floodplains, coastal lagoons and open grassland as defined by the underlying geology and described in the geomorphic features of Chapter 4. Compton (2011) created a vegetation map of the offshore environment from existing geological data (Figure 7-2A) and this has been built upon in the shallow nearshore where the shelf was mapped in high resolution for this study (Figure 7-2B). Vegetation on the Agulhas Bank and exposed shelf coast shelf has been postulated by Compton (2011) to be dominated by limestone Fynbos, grassland mosaics and shale Renosterveld, as determined by the underlying lithological substrate (Figure 7-2). Based on the results interpreted in this study, however, it is proposed that there was possibly a dominance of Uitenhage Group claystone sediments and outer shelf limestones at the surface, with floodplain and wetland sediments surficially outcropping adjacent to the fluvial incisions. Based on the seismic evidence resented here, these lithologies are anticipated to have locally outcropped at the surface when SB 1 and SB 2 were sub-aerially exposed during the retreat of sea level from MIS 7 – 6, and 5e – 2, respectively. At these times, scattered development of Strandveld Fynbos and a riparian system associated with wetlands (likely Cape Lowland Freshwater Wetlands) is envisaged to have formed mosaics in an area dominated by Renosterveld on the inner shelf, and limestone Fynbos on the outer shelf. The map presented in Figure 7-2B was inferred for the LGM and subsequent transgression. The projections are based primarily on geological substrate.

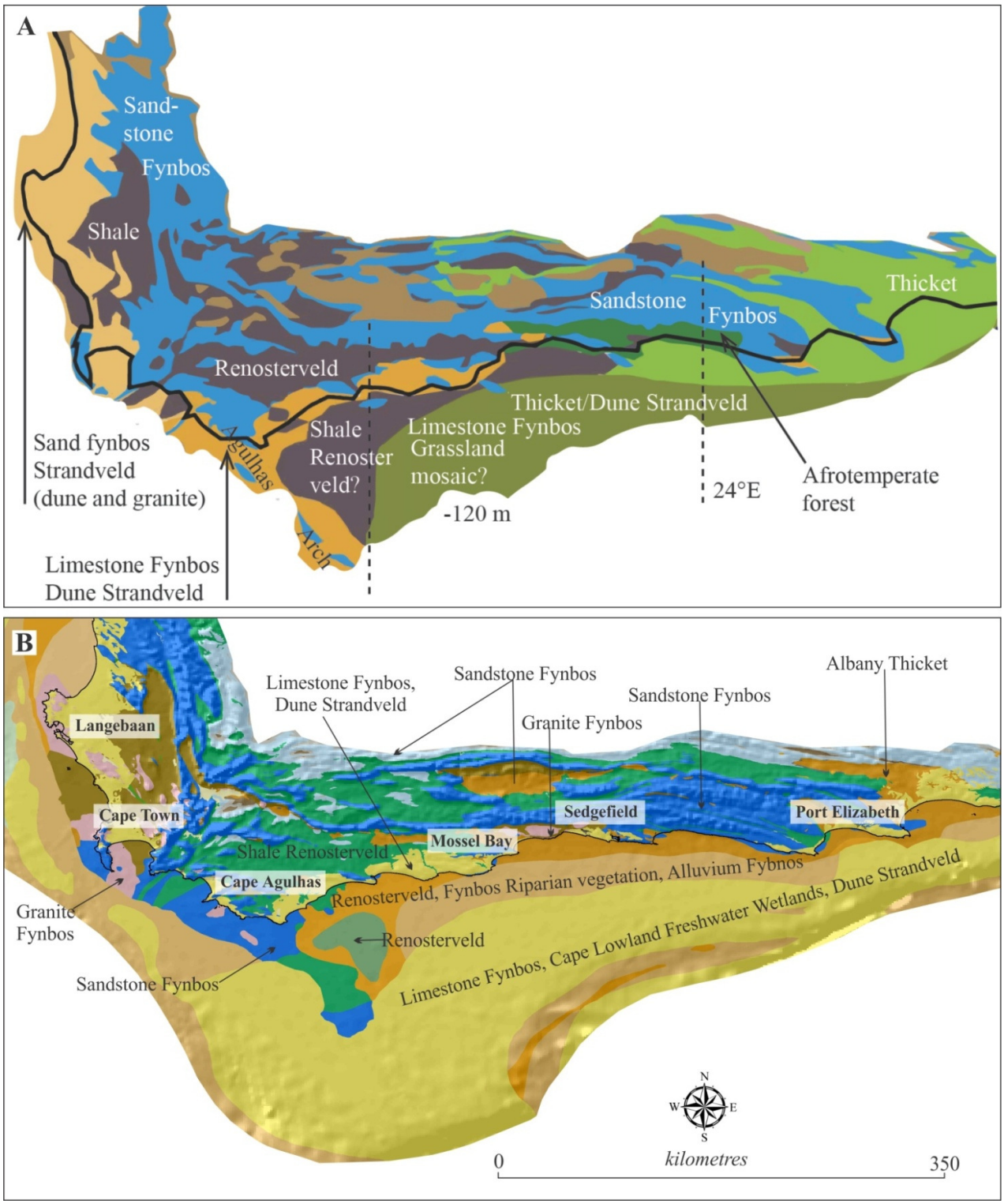

Figure 7-2. A. Vegetation model for the South Coast during lowered the lowered sea level of the LGM (modified from Compton, 2011). B. Proposed regional vegetation distribution from the work presented in this study, based on the geological substrate and a comparison to modern vegetation biomes and correlated to the onshore geological dataset compiled for Chapter 2 and vegetation biomes of Mucina and Rutherford (2006).

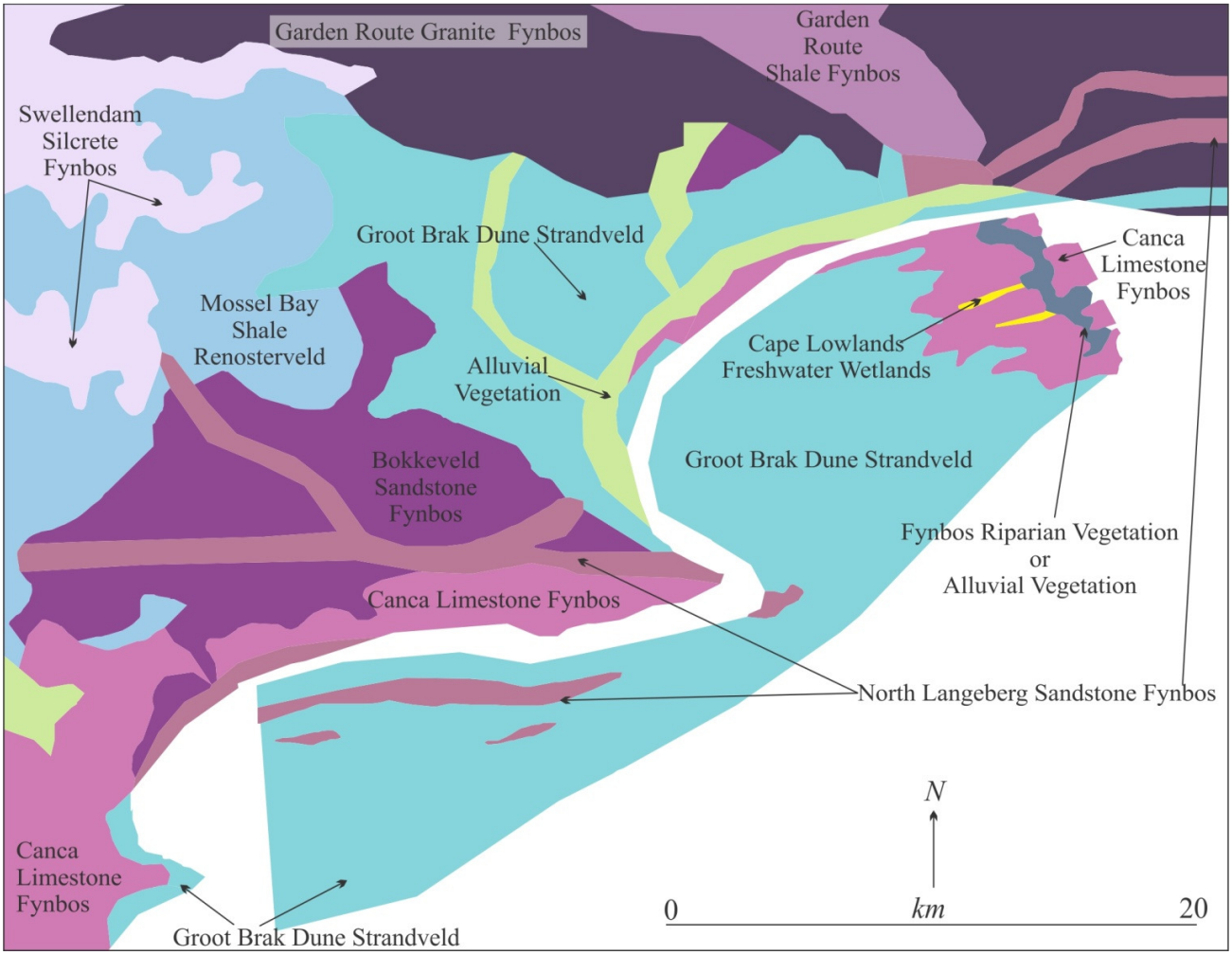

Figure 7-3. Vegetation reconstruction proposed for the high resolution study area of Mossel Bay, correlated to the onshore data of Mucina and Rutherford (2006).

The geographic area between Gans Bay and Mossel Bay, notably on the low-relief region near Bredasdorp and Arniston, comprises a complex array of soils and wetlands and has been suggested by Cowling (1990) to represent a likely analogue for the vegetation expression expected during glacials when the shelf is exposed. Most of the plant species present are associated with alkaline environments (Cowling and Holmes 1992) that would have been widespread on the now submerged shelf (Compton, 2011; Figure 7-2). This absorption of energy, for example by coastal Strandveld plants growing on dunes, may have offered protection to dunes from wind erosion in the palaeo record and promoted vertical accumulation of the dune systems. Fire destabilises Fynbos dune vegetation (Cowling, 1992) but the South Coast was probably less prone to fire, having had year round rainfall.

The South Coast was characterised by a more dominant summer rain-C4 signal during glacials (Bar-Matthews et al., 2010). Remains of large bodied open-habitat grazing ungulates are abundant at Klasies River (~180 km east of Mossel Bay) in archaeological layers from MIS 4 – MIS 3, and also at Boomplaas Cave (90 km north and inland). This open habitat grazing trend is further amplified in the LGM fauna at Nelson Bay Cave (~120 km east) and Boomplaas (Klein, 1972, 1976, 1983). This would suggest that the MIS 4 – MIS 3 trend at Pinnacle Point of greater summer rain, C4 grass and cool climate (Bar-Matthews et al., 2010) should accommodate substantial open habitats to support grazing herd species. The expansion of the SCP during glacial periods implied that animals were able to move easily from the interior to the coastal plain (Compton, 2011). The SCP can likely be considered as a glacial period refuge open to migratory herds from the north as climate conditions become more arid (Dupont et al., 2000), particularly if the SCP was unique in receiving year round rainfall (Bar-Matthews et al., 2010).

Extensive offshore deposits of phosphates and glauconite are known to occur on the South Africa continental shelf (Coles et al., 2002). Birch (1979b, 1990) (Figure 7-4) and Dingle et al. (1983) describe diagenetic phosphorites on the southern African continental shelf as being present as a near-continuous pavement, or capping veneers over extensive areas of the middle to outer shelf from Lüderitz to Port Elizabeth (Figure 7-4). The water depths vary from ~100 - 200 m BMSL along the South Coast, near the LGM shoreline. Partially and unphosphatised limestone hardgrounds have occasionally been dredged from these outer shelf areas. The Agulhas Bank phosphorite pavement covers an estimated 13 570 x 10^6 m^2 and has a projected 5500 x 10^6 metric tons of P_2O_5 (Birch, 1976). The high phosphorite content is proposed here to be one of the factors that make the South Coast shelf environment intrinsically unique. Given sufficient rainfall as projected by palaeoclimate models, the extensive wetlands and floodplains (Unit H, Unit K) as is evident from the seismic stratigraphy and the presence of phosphate, the now submerged platform is interpreted to have been a fertile coastal plain. Although it is not clear how easily this phosphate is mobilised in these soils once they are exposed, the combination with high rainfall and the substrate of Cretaceous Uitenhage Group deposits likely promoted the development of relatively high-nutrient soils capable of growing vegetation to support animals living on the glacial coastal plain.

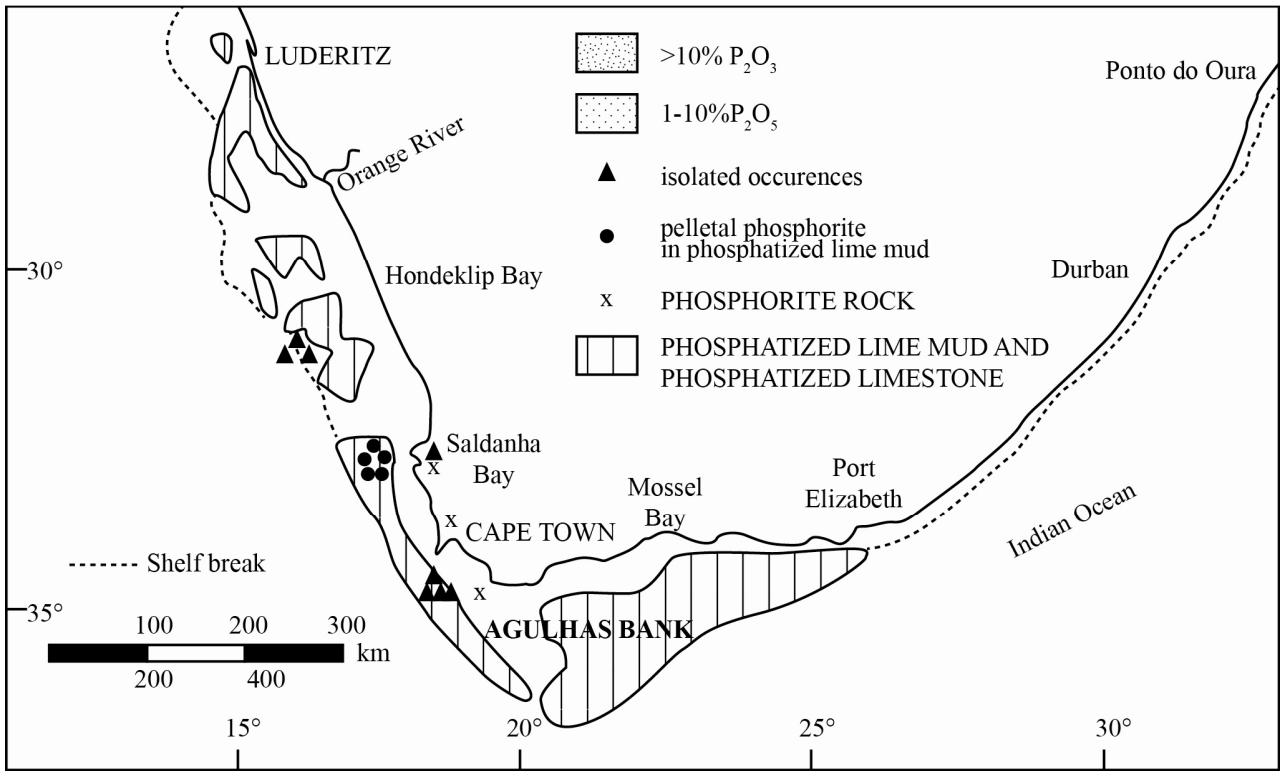

Figure 7-4. Pelletal and rock phosphorites on the continental margin of South Africa (modified from Birch, 1979b).

7.3 Beach environments and the shifting shoreline

The low angle gradient of the South Coast mid- to outer shelf results in a significant lateral migration of the shoreline with a relatively minor vertical oscillation in elevation. The palaeoscape model of Fisher et al. (2010) generated estimates of the distance and placement of the coastline at 1.5 ka increments through the last 440 kyr. This model showed that the shoreline was at times as far away as 100 km during glacial maxima and people likely moved with the shoreline in pursuit of a rich source of nutrients.

What is significant to note, based on this offshore geological investigation, is that a subtle vertical difference in topography associated with low-relief palaeodune deposits, may have a significant influence on the positions of the shorelines through time. The palaeo-coastal zones on the submerged shelf (Chapter 4; Figure 4-28) reach a maximum width of 1.5 km. In addition to the gradient of the shelf, periods associated with high sediment supply as defined by the seismic record (MIS 6, MIS 5, MIS 4, MIS 2), likely experienced significant progradation on HST and LST sea-level cycles, affecting the position and nature of the contemporary shorelines. Palaeoshorelines in Mossel Bay become linear on the outer shelf, beyond the extent of the present-day log-spiral embayment (Figure 7-5). For most of the Quaternary, coastal settings on the South Coast during all sea-level states of movement (regression, transgression, stillstand) have likely been low-gradient with linear barrier

shorelines (see Chapter 6). Linear beaches, accompanied by high sediment supply, will promote the formation of widespread sandy beaches through the palaeo-record and this is evident in the seismic data, as aeolianites crop out near the LGM shoreline. Changes in beach state may vary between dominantly rocky and dominantly sandy extremes (Figure 7-5) or an intermediate combination of both in association with embayed or linear planforms. Reflective beaches in this study area may have been associated with mixed rocky/sandy shorelines, and dissipative systems, with sandy beaches. Based on an inherited framework and assuming tectonic stability, the Mossel Bay palaeoshorelines can be classed into three dominant types of depositional morphologies: (1) Unbounded coastal plain coasts, which consist of linear barriers and shelf ridges with associated back-barrier deposits; (2) Bounded/embayed coasts where the protected sections of the log-spiral bays are characterised by the presence of inner shelf sand sheets; and (3) Protruding or cliffed coasts. In this case, headland-attached shelf sediment bodies exist. Figure 7-5 presents the planforms of coastlines at selected sea level depths (-18 m, -30 m, -40 m and -46 m) as examples. The selected depths displayed indicate changes in gradient on the shelf.

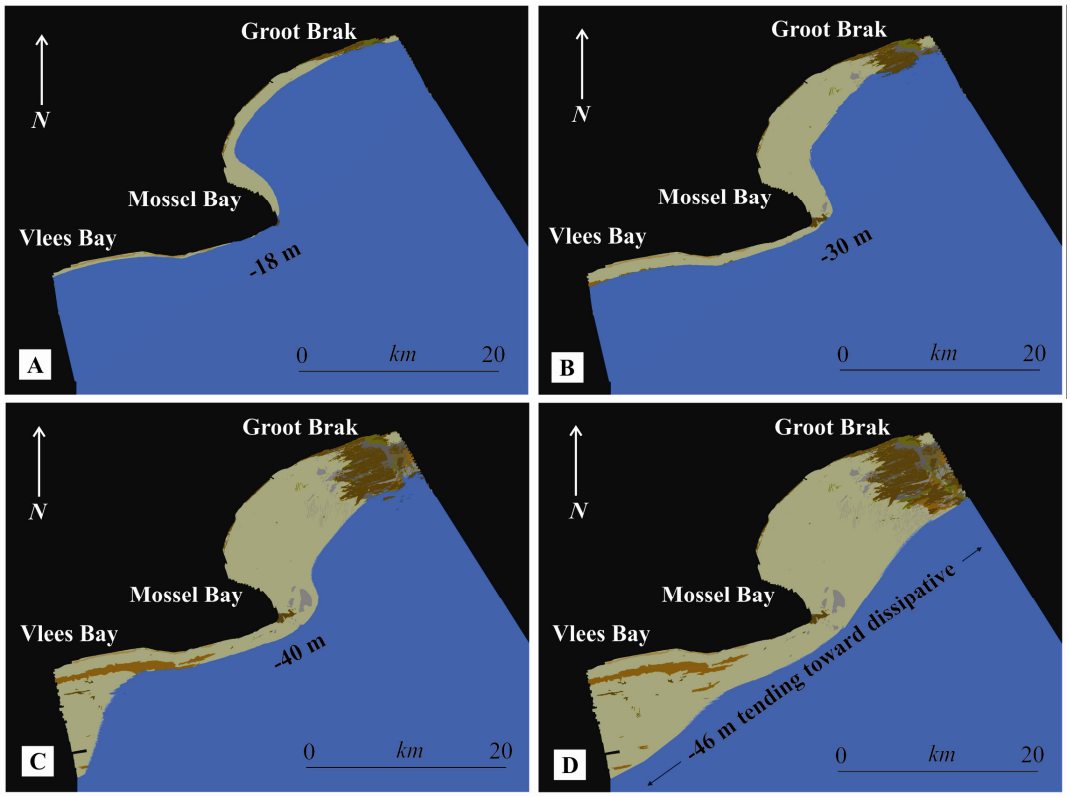

Figure 7-5. Beach morphology associated with a retreat of sea-level in Mossel Bay. The tendency to form log-spiral embayments, typical of the sub-aerially exposed South Coast, becomes more linear below a depth of 40 m BMSL. These depths were selected to link to the coastline model of Fisher et al. (2010).

The extent of cemented beachrock is less clear in the palaeo record and this would be an important variable in terms of rocky intertidal resources such as mussels and limpets. Although people could still harvest *Donax serra*

from sandy beaches, rocky intertidal beaches tend to have a richer assortment of marine foods. Ideally people would have benefitted most from a mixed sandy and rocky shore which is thought to have usually been the case except perhaps during glacial maxima when the coast may have been largely sandy coasts.

During the most recent PMT, the rapid transgression of sea-level was likely associated with a relatively shallow nearshore profile. With the stabilisation of the Holocene highstand, the inner shelf sediment profile is interpreted to have steepened in accordance with the dominant wave regime, resulting in the present environment. In terms of considerations of people on this landscape, the rapid shoreline shift through the PMT may have been noticeable during a lifetime. As conditions stabilised and progradation occurred, the establishment of the sandy beaches of Vlees Bay and Mossel Bay likely occurred.

Recent sedimentological studies along the South Coast suggest that the dunes dominantly formed during transgressive events (Bateman et al., 2004; Roberts, Carr et al., 2010). A large number of luminescence ages from Pinnacle Point shows pulses of dune formation near the MIS 6 – 5 boundary (144 ka, 126 ka; Bar-Matthews et al., 2010), as well as within MIS 5 at about 90 ka (Jacobs, 2010). These dune systems were likely associated with the presence of sandy beaches. The data presented in this study confirm dominant phases of dune deposition to include MIS 15, MIS 11, MIS 7, MIS 6, MIS 5, MIS 4 and MIS 1.

Table 7-1presents geological information, in conjunction with the coastline model of Fisher et al. (2010) and the distribution of shellfish from the PP 13B record (of Jerardino and Marean, 2010) to demonstrate the significance of geological substrate on these palaeoenvironmental constraints. The geological interpretations are extrapolated across the shelf from the seismic stratigraphic architecture, for example, the tendency of aeolianite (dunes) and wetlands or back barrier sediments to preferentially occur at specific depths across the South Coast study area. Aeolianite on the outer shelf (Seismic Unit J) crops out at specific depth bands between 40 and 110 m BMSL. Sediments interpreted to represent back-barrier, coastal lake or wetland environments (Seismic Units L and M) are concentrated between depths of 29 and 110 m BMSL.

Table 7-1. Combined coastline model of Fisher et al. (2010) and the geological information from this study at key time slices.

Time (ka)	**Coastline distance from Pinnacle Point (km)**	**Depth below current MSL**	**PP 13 B stratigraphy and shellfish species present (where applicable)**	**Expected geological substrate**	**Type of beach**	**Interpreted vegetation**
290 ka	38 km	27 m	N/A	Cretaceous claystone, aeolianite	Sandy beach/rocky shore	Dune Strandveld, Renosterveld
272 – 245 ka	65 km	100 – 80 m	N/A	Cretaceous claystone on the inshore,	Sandy beach/rocky	Dune Strandveld,

				Neogene and Palaeogene limestone beyond ~50 km, aeolianite	shore	Renosterveld, Limestone Fynbos
174–153 ka	Brief transgression at 167 ka to 10 km	70 – 40 m	LC-MSA Lower: *Perna perna*	Table Mountain Group sandstone, aeolianite and beach deposits	Rocky shore	Dune Strandveld, Sandstone Fynbos
150.5 ka	>100 km	120 m	N/A	Palaeogene limestone, calcrete	Mixed rocky and sandy	Limestone Fynbos
133–115 ka	1 km	60 - +5 m	LC-MSA Upper and LC-MSA Middle: *Perna perna*	Table Mountain Group sandstone, aeolianite and beach deposits	Rocky shore and sandy beaches	Dune Strandveld, Sandstone Fynbos
~91 ka	~3 km	42 m	West Upper Sands: dominant *Perna perna*	Table Mountain Group sandstone, aeolianite and beach deposits	Rocky shore	Dune Strandveld, Sandstone Fynbos
98–91 ka	<4 km	40 – 20 m	Upper Roof Spall/Shelly Brown Sand: *Donax Serra* (dominant), *Perna perna*, Limpet, Turbo sarmaticus (minor)	Table Mountain Group sandstone, aeolianite and beach deposits	Sandy beach/rocky shore	Dune Strandveld, Sandstone Fynbos
80 ka	1 km	25 m	N/A	Cretaceous claystone, aeolianite	Sandy beaches, dunes, coastal lakes and wetlands	Dune Strandveld and Renosterveld and riparian wetlands at the coast
70 ka	15 km	72 m	N/A	Aeolianite, back-barrier sediments	Sandy beaches, dunes, coastal lakes and wetlands	Dune Strandveld and riparian wetlands at the coast
62 ka	7 km	54 m	N/A	Aeolianite, back-barrier sediments	Sandy beaches, dunes, coastal lakes and wetlands	Dune Strandveld and riparian wetlands at the coast
33 ka	25 km	70 m	N/A	Aeolianite, back-barrier sediments	Sandy beaches, dunes, coastal lakes and wetlands	Dune Strandveld and riparian wetlands at the coast
31 ka	28 km	80 m	N/A	Aeolianite, back-barrier sediments	Sandy beaches, dunes, coastal lakes and wetlands	Dune Strandveld and riparian wetlands at the coast
30 ka	28 km	81 m	N/A	Aeolianite, beach deposits	Dominantly sandy beaches	Dune strandveld
29 ka	37 km	88 m	N/A	Aeolianite, beach deposits	Dominantly sandy beaches	Dune strandveld
29 – 28	37 – 55 km	95 – 100	N/A	Palaeogene	Mixed rocky	Limestone

ka		m		limestone, calcrete	and sandy	Fynbos
28 ka	55 km	100 – 105 m	N/A	Aeolianite, beach deposits, back-barrier sediments	Dominantly sandy beaches, coastal lakes and wetlands	Dune Strandveld, Riparian wetland
27 ka	55 km	110 m	N/A	Aeolianite, beach deposits	Dominantly sandy beaches	Dune strandveld

7.3.1 Distribution of shellfish in the archaeological record

The South Coast contains a diverse and dense shellfish population on the rocky intertidal zones of the quartz arenite substrate of the Table Mountain Group, coastal beach rocks, aeolianites and sandy beaches (Table 7-1). Rocky shore exploitation is signalled by the presence of mussel, limpet and *Turbo* shells. *Perna perna* (brown mussel), limpets (*Patella* sp.) and *Turbo sarmaticus* are some examples of rocky intertidal species common along the South Coast (Branch and Branch, 1992) that reach a size worth eating. The sandy beach is characterised by high frequencies of the sand (or white) mussel *Donax serra* (Kilburn and Rippey, 1982). No sites show an exclusive use of sandy beaches, (Jerardino and Marean, 2010; Table 7-1). Only *Perna perna* was found in oldest deposits (164 ka) but later, people started to exploit *Donax serra.* By the middle of MIS 5 (~90 ka), there is undisputed evidence for true coastal adaptations in the Pinnacle Point record (Marean et al., 2007; Marean, 2011). These are expressed in the form of expansion of the use of the intertidal zone, true shell middens, and the use of symbolic indicators obtained from the marine environment (Marean et al., 2007). In select cases, such as at PP 13B (Jerardino and Marean 2010) and Klasies River (Thackeray 1988) there is evidence for concentrated middens dominated by sand mussel (*Donax serra)*, showing that people travelled to dissipative beaches inhabited by this mollusc. Typical hunter-gatherers utilise a daily foraging radius of 8 – 12 km (Binford, 1980; 1982) and this study considers only the South Coast site of Pinnacle Point in the interpretations. Living near the coast would effectively halve a group's foraging range, so they required the coastal resources to make up for this loss.

Although during most of MIS 6 the coast was far from Pinnacle Point and the sea level record over this interval remains argued, the palaeoscape model of Fisher et al. (2010) does record a brief transgression starting at 171.5 ka and reaching a maximum sea level at 167 ka, which is concordant with the LC-MSA Lower stratigraphy at PP 13B: Table 7-1; Figure 7-7). The predicted rapid sea-level regression during MIS 5c – 5d likely promoted the formation of dunes and exposed sandy beaches. The presence of sandy beaches is confirmed by the presence of *Donax serra* in the fossil record at this time. Jerardino and Marean (2010) concluded that sandy beaches were likely well developed during MIS 5d and MIS 5c as a result of regression of sea level. The relatively intense collection of *Donax serra*, as reflected in the stratigraphy of PP 13B was possible probably because of rapid lowering of sea levels initiated at ~110 ka that resulted in the formation of long and exposed sandy beaches. As the coastline retreated onto a gradually sloping landscape without major cliff faces, it was postulated by

Jerardino and Marean (2010) that beachrock may have been present on these exposed surfaces explaining the rocky intertidal contexts. This study shows, however, that rocky intertidal zones dominated by calcarenite deposits of palaeobeaches and dunes lie outside the 12 km foraging radius and the rocky substrate responsible for the presence of *Perna perna* in the fossil record is rather Table Mountain Group sandstones (Figure 7-7, Figure 7-6) which crop out within 5 km of Pinnacle Point. These rocky substrates have more recently been buried by sand of the Holocene sediment wedge.

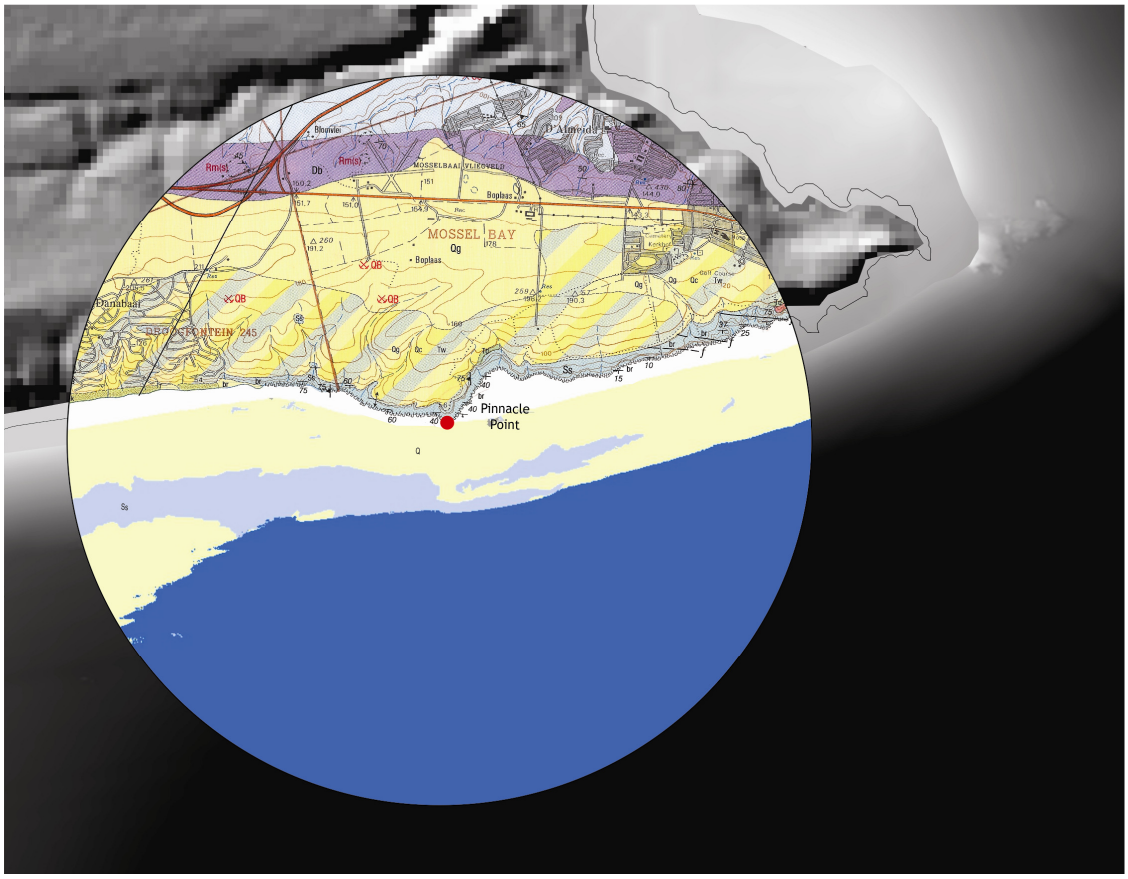

Figure 7-6. A 5 km radius extending outward from Pinnacle Point, showing the interception of both rocky and sandy substrates on the shelf, allowing foragers to harvest different species of shellfish in close proximity. The 5 km radius is presented, rather than a 12 km radius, based on the sea level at the time of the mixed rocky-sandy shorelines being located close to the Pinnacle Point cave complex.

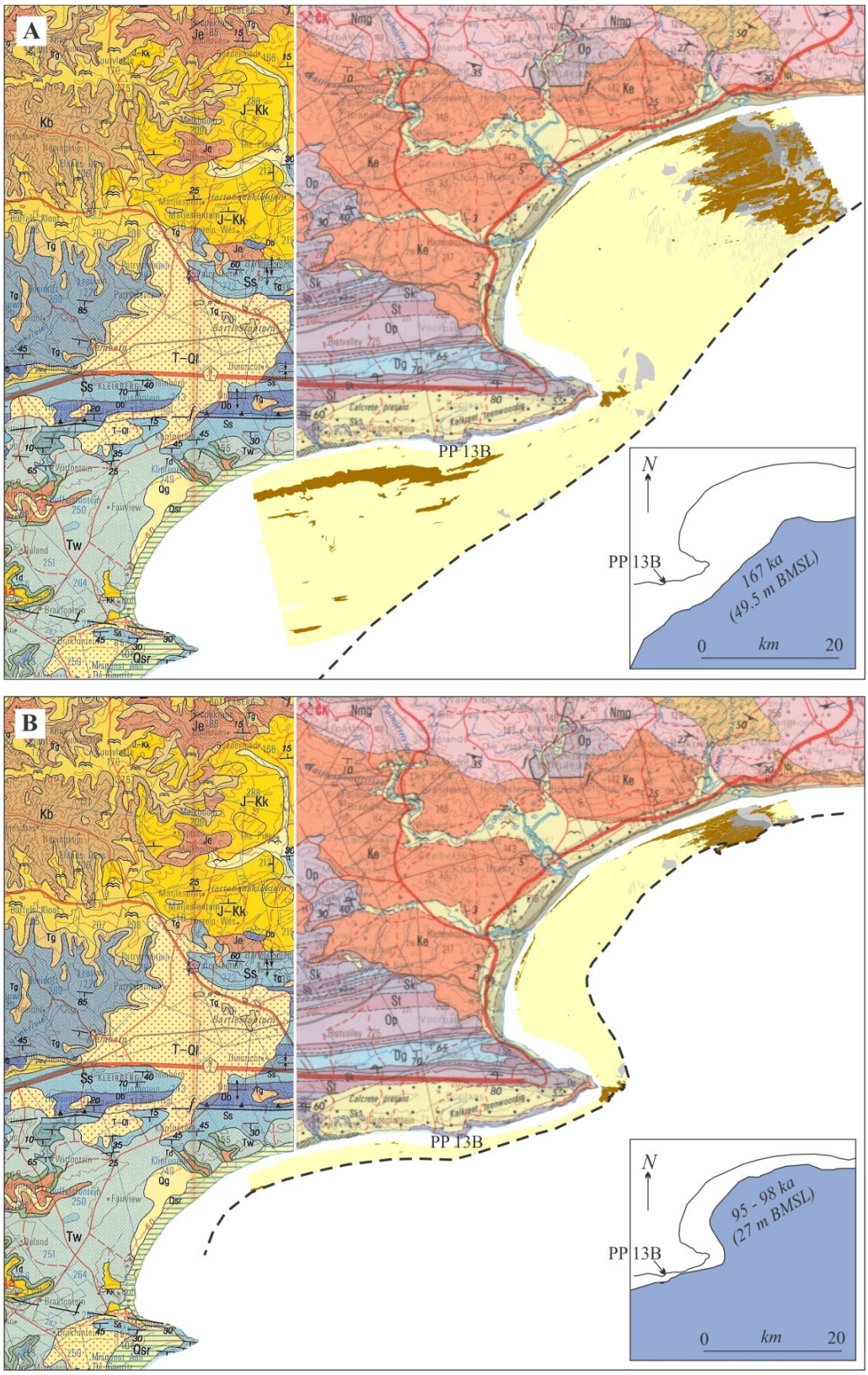

Figure 7-7. A. The -49.5 m coastline, with geological deposits expected to outcrop along the shoreline. Inset: Jerardino and Marean, 2010. B. The -27 m coastline, with geological deposits expected to outcrop along the

shoreline. Inset: Jerardino and Marean, 2010. The geological maps are the CGS 1:250 000 Riversdale and Oudtshoorn sheets. The nomenclature of significant geological units is as follows: Nmg: Goerge Granite Suite, Op, Ss, St: Table Mountain Group, Dg: Bokkeveld Group, Jr, J-Kk, Ke, Kb: Uitenhage Group, Tw, T-Qr, Qg: Bredasdorp Group.

7.4 Raw materials from the submerged environment

Given appropriate climatic conditions and sufficient exposure of the land surface, silcrete horizons are expected to be closely associated with rivers during periods of lowstand. Considering, as above, the likelihood to preserve unconformities represented as palaeosols, silcrete horizons may be intercepted in the seismic record, represented by unconformities. The dune environments also likely provide a substrate on which thicket can grow, yielding hard wood for the heat treatment of stone tools according to the methodology described by Brown et al. (2009). Limestone and phosphorite hardgrounds would form during submergence and later exposed as terrestrial surfaces.

In the vicinity of Pinnacle Point and offshore of Vlees Bay, surficially exposed and shallowly buried outcrops of Table Mountain Group sandstones occur as pebble and boulder beaches (Figure 7-8). These basal lag deposits unconformably overlying geological basement consist of well-rounded, tightly packed, unconsolidated clasts dominated by quartz arenite and are exposed when high energy conditions prevail in the shallow nearshore, removing beach sediments (Figure 7-8). Cobble beaches are, therefore, expected to be present on the shelf and near the present coastline in the shallow nearshore environment during phases of sediment starvation.

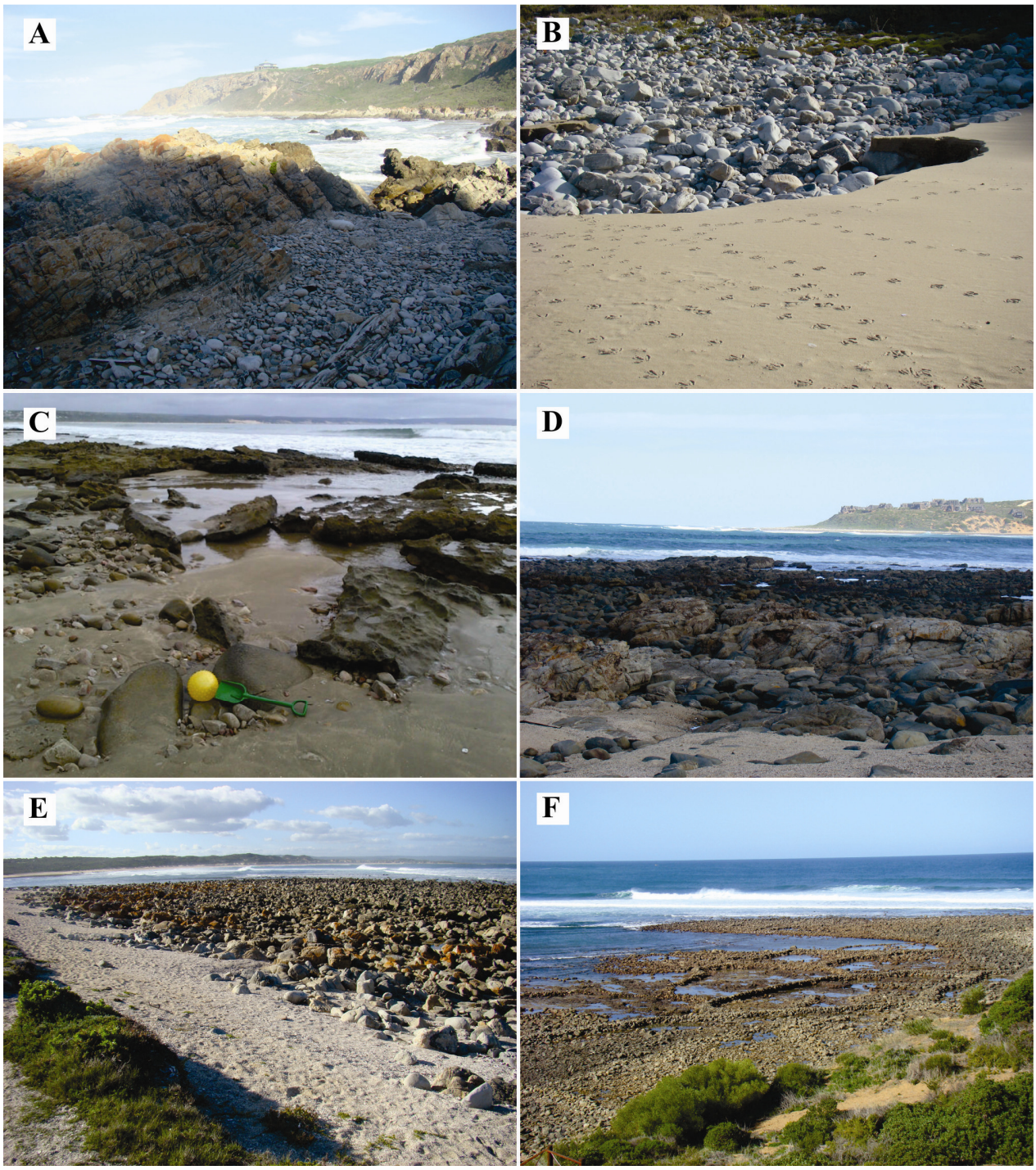

Figure 7-8. Boulder beaches along the modern South Coast shoreline exposed during storms or high swell events where Table Mountain Group sandstones crop out at or near the surface. A, B. North Beach, Pinnacle Point. C. Vlees Bay, photograph courtesy of Mrs Joan van Zyl. D, E, F. Still Bay. Image F also shows Holocene fish traps.

7.5 Geological interpretations for the last and penultimate glaciations

1. MIS 6 (183 – 134 ka)

Sea level reached a maximum depth of 130 m BMSL during MIS 6 and the seismic and geological record presented in this study attest to a vastly different environment. Wetlands and floodplains were present and broad, shallowly incised rivers carved what would have been a broad, flat, coastal plain. As sea level rapidly transgressed towards the Last Interglacial, coastal barrier systems shifted in a landward direction and were rapidly cemented by a relative abundance of carbonate in the system. MIS 6 is important to human evolution (Marean et al., 2007) because during the interglacial from 230 – 195 ka Africa was warm and wet, followed by the climate becoming cool and dry (Dupont et al., 2000). The warm, wet phase likely accounts for the available carbonate on the shelf and the environment on this shelf during the MIS 6 glacial may have provided a refuge for people at this time.

2. MIS 4/2 (71 – 57 ka/29 – 14 ka)

Instead of *Homo sapiens* populations contracting during MIS 4 as was the case in MIS 6 (Marean et al., 2007), archaeological sites remain abundant into this glacial. There was a marked shift in technology as new raw materials with different flaking properties rose in abundance and a change in the technologies to manufacture tools from silcrete (Brown et al., 2009). At Pinnacle Point, where heat treatment was first recognised in 164 ka deposits, silcrete microliths, blades and flakes were produced in deposits that date to ~71 - 60 ka at PP 5/6. The geological record of shelf evolution suggests that laterally extensive floodplains were infilled, and overspilled, with sediment into the channels carved during MIS 6. Extensive dunefields, extending up to 10 km inland from their associated palaeoshorelines, covered much of the emergent shelf (Figure 4-28). The closeness to water and dunes likely provided an attractive habitat to humans. This is shown during the Last Interglacial such as is the case at the Duynefontein archaeological site on the West Coast (Cruz-Uribe et al., 2003) where comparable palaeosols contain archaeological deposits. The environment offshore of Vlees Bay is envisaged to have been similar during MIS 4. The seismic stratigraphic record, as well as the diagenetic features, attest to a water table close to the surface. Dune ribbons across the shelf likely hindered river drainage during the retreat of sea level from MIS 5e. At this time, extensive dunefields, wetlands and rivers with sizeable floodplains are suggested to have existed. The sedimentary bedforms may have obstructed or slowed drainage as suggested by leached palaeosols and carbonate mixing observed in thin sections (see Chapter 4). Fertile grasslands are interpreted to be associated with glacials, as phosphate in the sediments likely represented a ‘natural fertiliser’. This, in conjunction with the abundant water present, attests to a landscape with abundant plant resources.

7.6 Extrapolation to the wider South Coast shelf

The detailed mapping in the vicinity of Mossel Bay was considered in high resolution, but to the west the Breede River region is significantly different. The bathymetric and fluvial expressions are considered here to be predominantly controlled by the nature of the geological substrate. The regional differences across the SCP (Dingle and Rogers, 1972; van Andel, 1989), therefore, most likely relate to basement geology. Prevalent zones of aeolianite mapped on the shelf near Mossel Bay (Table 7-1) are thought to extend approximately across the South Coast shelf. This suggests a propensity to find the development of dune and back-barrier sedimentary environments outcropping across the shelf, toward the LGM shoreline. The relative lack of shelf sediments below the 45 m BMSL nick point is thought to result in Mesozoic and lower Cenozoic strata at or near the surface.

The lowstand expression of the South Coast is envisaged to bare similarity to the currently exposed Maputaland Coastal Plain on the northeast coast of South Africa (Figure 7-9). The Maputaland Coastal Plain is underlain by Mesozoic to Pleistocene rocks which were deposited during drift (Broad et al., 2006). The coastal plain is bounded to the west by the Lebombo Mountain chain and the present shoreline is defined by a series of log-spiral embayments (Porat and Botha, 2008; Green, 2009). The landward bounding mountain chain, substrate of relatively erodible Cretaceous strata overlain by Cenozoic deposits and the recently developed coastal lakes and wetlands can be considered comparable to the environment on the South Coast shelf when it is exposed during times of low sea level. Much of the undulating Maputaland Coastal Plain is characterised by stabilised, vegetated dunes of whaleback-, parabolic- and linear forms (Porat and Botha, 2008). Additionally, widespread ephemeral interdune wetlands and grasslands sweep the landscape (Figure 7-9).

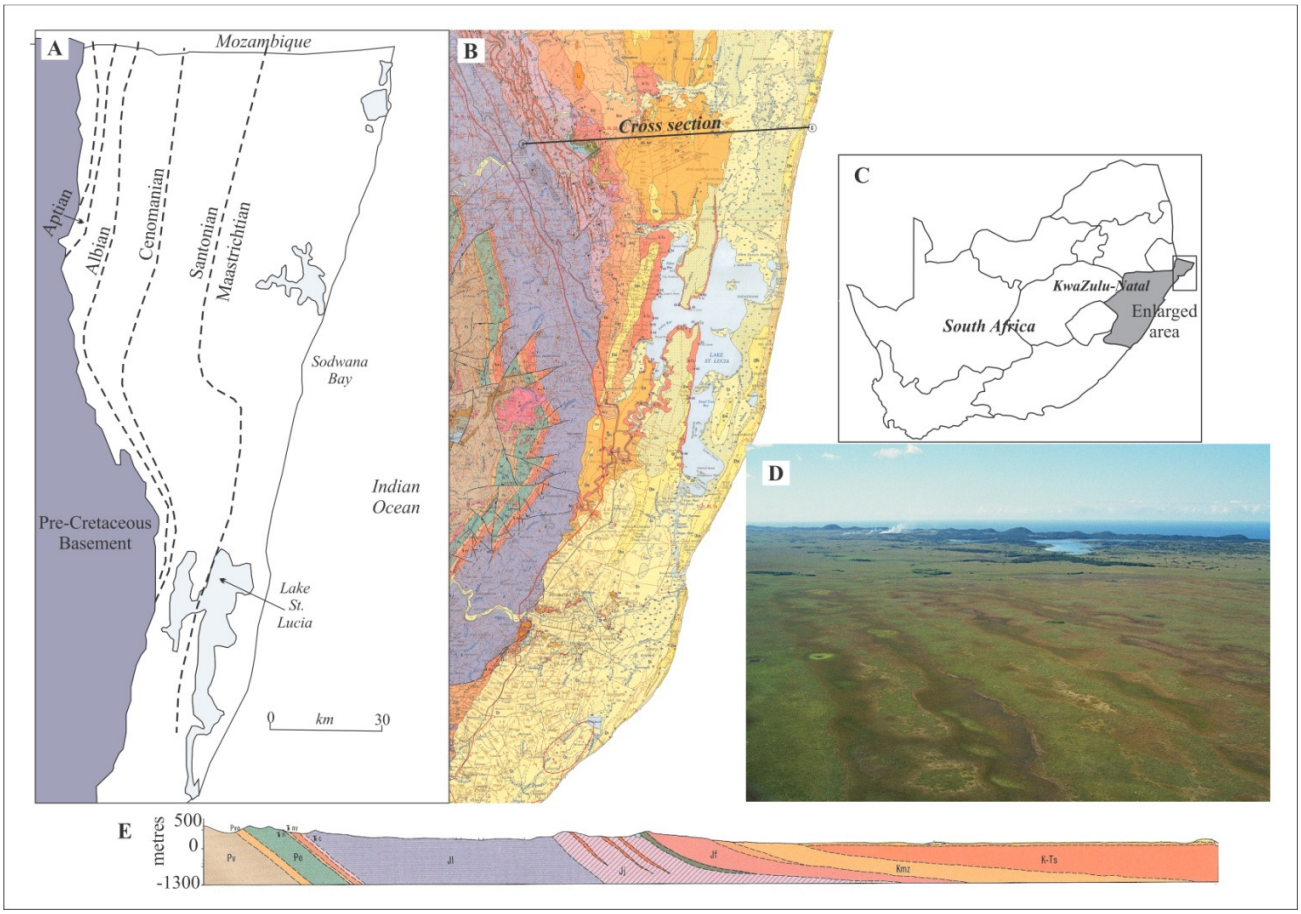

Figure 7-9. Geology and morphology of the Maputaland Coastal Plain, serving as a lowstand analogue for the environment on the South Coast shelf. From Wolmarans and du Preez (1985). B. From Viljoen and Malan (2008). C. Location. D. Photograph from Porat and Botha (2008).

7.7 Potential target locations for identifying archaeological sites on the emergent shelf

The scope of work in this study did not include the search for archaeological deposits on the seafloor, but this section describes potentially promising areas to explore on the shelf based on the geological investigations. Assigning priority and potential to areas attractive to early humans (see Westley et al, 2011), the following types of environment on the lowstand shelf are anticipated as significant to a *Homo sapiens* population and may be targeted for exploration of submerged archaeological sites: (1) Low-relief coastal dunes, with thicket vegetation growing on dune ridges. These low-relief ridges likely punctuated a dominantly low-relief, fertile plain and people would have exploited these shorelines. Additionally, thicket associated with dunes may have provided a source of fire wood. (2) Coastal middens may be preserved in the lee of dune ridges, protected from the westerly winds that prevailed through this late Quaternary record. Coastal middens, or disposal sites near the coast, would have likely been widespread through the palaeo record considering the documented coastal adaptation of Marean et al. (2007). (3) Wetlands and floodplains likely provided resources in the way of aquatic foods and plants.

Extensive wetlands are also desirable to animals. (4) Dune blow-outs associated with dunefields likely exposed deflation surfaces and palaeosols where stone tool artefacts may be preserved. Palaeosol surfaces are commonly associated with deflation surfaces (e.g. Fisher et al., 2013) of coarse gravel and pebble lags. At Pinnacle Point, Acheulean stone tools collected during trenching for road construction showed that here, as well as along much of the South Coast, archaeological material commonly occurs in concentrated layers associated with calcretes or palaeosols (Thompson, 2009). The offshore record has shown that this region, given the gradient of the shelf and the nature of the lithological substrate, has the propensity to generate palaeosols. As sea-level falls toward glacial maxima the exposed surfaces are subjected to widespread erosion and likely also compaction as is evident in the Quaternary seismic record in this study and notably at Sequence Boundaries 1 and 2. (5) Submerged caves extend seaward of Cape St. Blaize were likely occupied by populations of early modern humans. Although these were explored on scuba diving surveys and no evidence for archaeological sites was found, this environment was probably used by people when these caves were exposed along a shoreline when sea level was 30 – 13 m lower than present. It is assumed that the cave sediments were removed by the rapidly ensuing Holocene Transgression.

7.8 Summary

The geological deposits on the emergent shelf indicate a more extensive coastal plain, wetter from a combination of rain during glacials and low-gradient meandering rivers and more wetland lakes and vleis and may have been able to support more lush vegetation. Although not vastly different to the currently sub-aerially exposed Agulhas Plain, this is suggested to have been a good habitat for animals and people alike. Humans need water and wetlands and coastal lakes are considered here to be an important feature of the landscape on the emergent shelf during glacials. This study has showed what the river systems looked like and how they were likely to respond to lowstand conditions. Numerous relatively small rivers would have been flowing given the rainfall predicted by Bar-Matthews et al. (2010) and the multiple channels were not heavily incised, were characterised by high sinuosity, and were likely all flowing during glacials as was shown through the seismic record. The coastal exploitation described at Pinnacle Point (Marean et al., 2007; Jerardino and Marean, 2010) can be supplemented with proof for water resources at the coast for most of the lowstand record. This addresses an additional attraction of the SCP and contributes to the confluence of factors that make this environment unique.

8 CONCLUSIONS

8.1 Overview

The methods and approach in interpreting submerged deposits presented here, in conjunction with detailed coastal zone studies, provide new insights in our understanding of the complex land-ocean interface. When considered seamlessly, global coastal plain and continental shelf environments preserving Quaternary deposits comparable to those studied from the South Coast can be successfully placed into a holistic depositional model with the application of suitable geochronological and geophysical techniques. Offshore, three separate marine geophysical surveys were undertaken for this project applying the most appropriate techniques to address the objectives of this study, i.e. to examine evidence of past sea-level fluctuations and interpret geological deposits on the seafloor. Onshore, structural geological features and detailed lithology of the bedrock substrate of the basement rocks on the Pinnacle Point coastline were documented, and the distribution of sedimentological facies within Quaternary calcarenite deposits along the rocky shoreline of Mossel Bay was recorded at high resolution. The shoreline and offshore deposits are treated as one in this thesis, with the exception of the gap between the shoreline and inner continental shelf that make up the surf zone. Beach and dune deposits span from Marine Isotope Stage 15 (MIS 15) (582 ka) to Recent based on an age model that integrates OSL ages and the established eustatic sea-level record. This study presents new data from mapping carried out between Still Bay and Wilderness, and documents the presence of 9 discrete stratigraphic sequences spanning the last 600 kyr.

The Mossel Bay continental shelf and coastal plain have been shaped over a lengthy geological history. The hard bedrock promontory of Cape St. Blaize formed during orogenesis of the Cape Fold Belt. Subsequent rifting and extensional tectonics of Gondwana breakup allowed for the creation of accommodation space which was infilled by predominantly terrigenous sediments during two major pulses of deposition during the opening of the Atlantic and Indian Ocean basins. Repeated exposure of the shelf to sub-aerial conditions through the Cenozoic resulted in extensive erosion, as it served as a zone of sediment bypass to the adjacent margin, and the erodible lithologies were planed to the familiar elevation of the relatively featureless Agulhas Bank on the outermost portions of the broad South Coast shelf. With the onset of major Quaternary glacial-interglacial cycles at approximately 0.9 Ma, continental shelf deposits were preserved by processes of shallow burial and carbonate diagenesis in the littoral zone. Sedimentary response to shifting shorelines, defined by glacial and interglacial cycles, worked and reworked the sediment which currently occurs as deposits formed during the marine transgression of the last glacial termination.

8.2 Seismic stratigraphy

A total of 9 discrete seismic sequences are interpreted for the area from Still Bay in the west to Buffels Bay in the east and to a maximum water depth of 110 m. Seismic stratigraphic revealed 17 seismic units in the region (A – Q), some of which are further sub-divided into constituent seismic facies (SFi – iii). The 17 discrete seismic units are bounded by 2 unconformities (U/C 1 and 2), 3 regional sequence boundaries (SB 1, 2 and 3) and 1 wave ravinement surface (WRS). Unit A represents bedrock and is dominated in this region by the Silurian Table Mountain Group Skurweberg Formation arenaceous sandstones. Units B, C and D are associated with the Pletmos Basin stratigraphy, expressed onshore as the Cretaceous Uitenhage Group. Sequences 1 and 2 represent Synrift successions I and II, respectively. Unit E (Sequence 3) is interpreted as drift deposits, now exposed by extensive planation since the Neogene and forming the Agulhas Bank. A relative lowering of sea level since the Neogene accounts for non-deposition on the continental shelf that likely served as a zone of sediment by-pass and generated the hiatus that is expressed as SB 1. SB 1 is interpreted to have been formed as a planation surface extensively eroded since the middle Miocene. With the onset of major mid Pleistocene glacial – interglacials (e.g. Liesicki and Raymo, 2005), reactivation of existing surfaces formed deposits visible in the seismic record. Shelf sedimentation since at least MIS 7 and evolution of shifting shorelines dominate the offshore and littoral zone record of the South Coast and stratigraphically form part of the Bredasdorp Group sedimentary record. Sequence 7, commencing with SB 1, preserves systems tracts providing insight into the depositional and erosional processes from MIS 7 to the Last Interglacial (MIS 5e). Sequence 8, the most complete sequence documented in this study, commenced with the retreat of sea-level from MIS 5e and extends to the Holocene highstand (MIS 1). Within Sequence 8, the response of sedimentation to MIS 5 stages 5e-a, MIS 4, MIS 3 and MIS 2 is documented. Sequence 9 commences with the fall of sea level since the Holocene highstand and represents the ongoing evolution of the present shoreline within the Wilderness Embayment.

Active incision of rivers, forming channels on the shelf, is represented as bathymetric lows carved into strata where SB 1 dips and forms depressions. The incision shows shallow, broad, relatively flat fluvial systems. A total of 16 incised channels of varying scales were identified on the South Coast shelf within the study area. In the westernmost section of the study area (Still Bay to Vlees Bay) the channels are extremely broad and shallowly incised in comparison with the eastern areas where the channels are steeper but still considerably broader and shallower than their onshore equivalents. The adjacent floodplains on the shelf appear wider because the adjoining unconsolidated dune fields will also likely have been removed during the Post-glacial Marine Transgression (PMT). It is possible that river courses changed with each lowering and that the channels observed are the most recently formed with older ones all variably occurring laterally to them, accounting for the broad widths. This study recognised four fill units within South Coast incised channels, based on seismic character of deposits, bounding horizons and observed geometries. The seismic architecture suggested that the infill sequences can be interpreted to represent mixed fluvial and estuarine deposits, floodplain deposits and lastly,

infilling by the most recent episode of marine sedimentation. This study proposed that SFG i and SFK i were deposited on FSST-LST systems tracts on the regressions from MIS 7 – 6 and MIS 5e – 2, respectively. SFG ii and SFK ii were deposited on TST and stillstand (LST/HST) systems tracts on the transgressions from MIS 6 – 5e and MIS 2 – 1, respectively. Although the incised channels may have been occupied prior to MIS 6, it seems most reasonable to interpret the preserved facies assemblages as post-dating this time, recording sedimentary events over the last and penultimate glacial – interglacial cycles (Sequences 7 and 8).

Subtle shelf depressions expressed as bathymetric lows, mapped at depths between 30 and 110 m BMSL, are filled with fine grained silty material interpreted to represent back-barrier and interdune sediment (Seismic Units L and M, differentiated according to depth and therefore sea-level association). These likely represent wave-dominated barrier environments with dunes intersected by narrow entrance channels connecting the low energy back-barrier lagoons to the open coast. An OSL date of ~59 ka on one of these deposits near the Groot Brak River palaeochannel confirmed that they are transgressive barrier systems. These are interpreted here to be preserved as a result of over-stepping by a rapidly migrating shoreline associated with the Meltwater Pulses 1A and 1B. Evidence for the adjacent rapidly migrating shoreline is further present in the form of a PMT WRS consisting of unconsolidated cobbles. Though this surface was only mapped geologically on the inner shelf, it can be traced semi-continuously across the entirety of the shelf in the seismic record.

The SFKii regressive deposits lying at depths of 80 and 105 m BMSL formed when relative sea level rapidly retreated on the shallow gradient outer shelf environment. The highstand barrier prograded toward the shoreface with additional sediment derived from further offshore by erosion on the lower shoreface. The associated regressive barrier was constructed seaward into the eroded region where the substrate gradient of the palaeo-coastal zone was near horizontal and lateral outbuilding occurred. Lagoons situated behind prograding barriers become isolated from the ocean on embayed coasts, while those lying on linear clastic shorelines extend in the direction of longshore drift and ultimately close or become captured by adjacent water bodies.

8.3 Seafloor bathymetry

The bimodal topography and bathymetry of the Mossel Bay area characterized by steep coastal cliffs and an adjacent subdued coastal plain and continental shelf is predominantly controlled by lithology and preferential erosion of less competent geological units. Complex inner shelf geomorphology is defined by seafloor outcrops separated by troughs and fluvially incised valleys, in an area generally dominated by shelf sands. Features of a terrestrial landscape on the seafloor include sea cliffs, and submerged dune and beach deposits (compositely referred to as palaeo-coastal zones).The bathymetry in the mapped ranges from a minimum of 5 m BMSL to a maximum depth of 55 m BMSL. The morphology is relatively flat and smooth in the two embayments of Vlees

Bay in the west and Mossel Bay in the east, punctuated by features of noteworthy relief, but the inner shelf narrows significantly in the region adjacent to the Pinnacle Point coastline. A prominent nick-point at 45 m BMSL divides the inner- from the mid-shelf. Oscillation in sea level between ~2.7 and 0.7 Ma likely resulted in the formation of this erosional terrace.

The surficial geophysical datasets alluded to the presence of linear submerged palaeocoastlines offshore of the Groot Brak River. These, in terms of a morphodynamic model of beach evolution, indicate that below a water depth of ~40 m there is no tendency to create log-spiral embayments. This is interpreted to be directly related to the form of antecedent geological substrate. It is proposed here that there are several reasons why Mossel Bay contains preserved deposits of the lower- to mid-Pleistocene compared to a general scarcity of comparable stratigraphic units in other areas of South Africa. These include: the geomorphic form of the present-day embayment, the supply of sediment at glacial-interglacial terminations with a tendency to prograde as the rate of sea level rise slows, variations in the supply of sediment from the Gouritz and other river systems, a low gradient coastal plain and adjacent continental shelf, and lastly a significant source of existing sediment provided by the Devonian, Cretaceous, Palaeogene and Neogene antecedent deposits. This was confirmed by the prevalence of relatively young Quaternary deposits preserved seaward of the modern shoreline. The lack of a headland buffer, protruding into the bay during times of lowstand, is thought to be the reason for the scarcity of older deposits on the seafloor.

8.4 Quaternary deposits

Surficial texture of seafloor units was classified by the analysis of side-scan sonar data. Seven discrete acoustic facies were identified and sampled to classify shelf geology and sedimentary compartments. These included: silicified sandstone and calcarenite (Acoustic Facies a), subdued or eroded outcrops of Acoustic Facies a (Acoustic Facies b), coarse grained bioclastic sediment (Acoustic Facies c), shelf sands (Acoustic Facies d), wave rippled shelf sands (Acoustic Facies e), fine-grained sediment comprising silty mud (Acoustic Facies f), and low-reflectance, fine-grained sediment comprising mud (Acoustic Facies g).

8.4.1 Consolidated rocks

Five elements were considered in the analysis of Quaternary deposits and included: sedimentary facies, defined according to diagnostic sedimentological characteristics; the carbonate cements that are responsible for the consolidation of the deposits; geological units, consisting of cemented sedimentary facies contextualised in space and in time; palaeoshorelines, expressed as one-dimensional, linear features; and palaeo-coastal zones, constituting the area of active sedimentation associated with a palaeoshoreline and extending landward of that shoreline along a band of unchanged gradient. A total of 33 Pleistocene and Holocene geological units (Pm 1 –

18; Pu 1 – 13; H 1 - 2) were identified across the area. The dynamic shoreline environment showed a complex history of sedimentation and cementation and facies are preserved from the dune, foreshore, upper shoreface and intertidal environments, corresponding to highstands during MIS 15, 11, 7, 5 and 1. The lowstand sea-level record expressed in this area is dominated by the last- and penultimate glacial periods MIS 4 and 2 (termed Sequences 7 and 8 in the seismic stratigraphic model). The consolidated, cemented, sedimentary deposits on the shoreline and adjacent shelf preserve regressive coastal barrier systems, transgressive coastal barrier systems and coastal lagoons. Currently submerged aeolianites range in age from ~142 – 87 ka. The most prominent deposits date from the MIS 6 glacial to MIS 5 interglacial periods and include regressive aeolianites that extended at least 10 km inland from their associated palaeoshorelines. The transgressive deposits associated with the MIS 6 termination and early MIS 5 sea level rise (~140 – 130 ka) show that a critical point was reached at the landward migration of a dune ridge where the barrier no longer maintained pace with the transgression, causing overstepping and landward remobilisation of the entire coastal barrier structure.

The relative abundance of sediment since MIS 7 is likely responsible for the presence of dissipative (sandy) beaches on this emergent shelf, as confirmed with the presence of *Donax serra* in the archaeological record at Pinnacle Point. The retreat of sea level from the peak of the Last Interglacial follows a complex path from MIS 5e – 5a and this is reflected in the offshore stratigraphy of Mossel Bay. The MIS 5 deposits include transgressive beachrock, an extensive foreshore unit which prograded on the MIS 5e highstand, and regressive beach and dune deposits on the shelf associated with the MIS 5d fall in sea level. The excellent preservation, high-resolution accompanying seismic record and well-constrained luminescence dates demonstrate the fall in sea-level from the peak of MIS 5e towards the MIS 4 glacial. Seismic Unit J (aeolianite) lies conformably on the prominent SB 2 surface and these preserved down-stepping palaeo-coastlines track falling sea level. These deposits were classified into “detached FSST” deposits. MIS 4 lowstand incised river channels were infilled with sediment truncated during rapid landward shoreface migration at the MIS 4 termination. Low-energy, back-barrier MIS 4/3 sediments described above in the overview of the seismic stratigraphic model are preserved as a result of overstepping associated with meltwater pulses of the MIS 2 termination.

8.4.2 Carbonate diagenesis

Petrographic analysis of 120 thin of calcarenite, using transmitted light microscopy and SEM-EDS, revealed that the cements in the study area are freshwater LMC and marine phreatic micrite and aragonite altered to LMC by diagenesis upon exposure. It is proposed that marine phreatic diagenesis was initially associated with HMC but that this phase is poorly represented as a result of most of it being recrystallized as LMC over time. The LMC cements occur in six main morphologies, namely: cryptocrystalline coatings, isopachous prismatic rims, dogtooth spar, microspar mosaics, pseudo-pelloidal aggregates and radial aggregates. Other cements include

authigenic clays, occurring in two forms, and a mixed carbonate-organic matrix. The diagenetic cements occur as envelopes surrounding grain boundaries in the form of microcrystalline crystals forming meniscus layers as well as cements consisting of crystals growing from a substrate into a pore space (e.g. fibrous, dogtooth forms; or pore filling cements characterised by crystals increasing in size toward the centre of the void (e.g. blocky calcite spar). The alteration of select grain boundaries into authigenic clay minerals was the first diagenetic event. This suggests significant exposure of the deposits prior to the onset of diagenesis and cementation. If present, cryptocrystalline coatings at grain boundaries were the second diagenetic event to occur in the general sequence. The general diagenetic sequence of foreshore, intertidal and nearshore deposits commenced with an initial isopachous or fibrous micrite rim cement with later void infilling characterised by the presence of authigenic smectite, blocky calcite spar and microspar mosaics. In the case of aeolianites, the diagenetic sequence commenced with the formation of dog-tooth calcite, followed by calcite infill. Late-stage dissolution of the existing pore-infilling cements resulted in the occurrence of microspar mosaics. The red colouration in the fine grained matrix of the authigenic smectite diagenetic phase is interpreted to be caused by small percentages of iron oxide.

The MIS 15 beach and dune deposits, as well as MIS 11 beach deposits contain isopachous microcrystalline rims at grain boundaries, interpreted to have precipitated during the MIS 11 interglacial, contemporaneous with the deposition of the littoral zone units. The aeolianites of MIS 11 display the presence of microcrystalline rims; a diagenetic phase considered in this work to be an early feature of vadose zone diagenesis near the MIS 11 shoreline. The retreat of the shoreline from MIS 7a – 6 is likely responsible for the presence of calcite spar infilling available voids of deposits preserved on the depositional profile. The cement is composed of 'clean' carbonate, with no evidence for excessive mixing by organic or palaeosol material, suggesting they grew in a largely unvegetated dune field. A dominance of late-stage authigenic smectite is interpreted to be associated with leaching from overlying palaeosols in a dune environment. The smectite was likely formed in situ from chemical weathering of feldspar grains. The prevalence of authigenic smectite in deposits dated to post-MIS 5e suggests that these palaeosols were most abundant between MIS 5e and MIS 4 as sea level regressed towards the penultimate glacial maximum. The transgression of sea level from MIS 2 – 1 is characterised by calcite spar infill, alteration of existing cements to microspar mosaics and the presence of carbonate cement having organic matter inclusions. The presence of organic matter in the calcite cement suggests that the waters from which the calcite cement precipitated had abundant dissolved and particulate organic matter, typical of soils and tannin rich waters seen today in the low-lying coastal vleis.

8.4.3 Dunes and palaeowind distribution

The deposition of aeolianites is associated with sea-level still-stands which periodically prevailed, allowing the available sediment of the coastal zone to mobilise into dunes on the palaeocoastlines. Although now only relatively small cores remain, these may reflect the relics of extensive dune systems on a now partially submerged coastal plain: the inner continental shelf. Sedimentological analyses suggest that the palaeo-beach environment at the time of deposition of beach deposits was comparable to the beach morphology seen today and consisted of a relatively gently sloping beach on a wave-dominated coastline.

Wind distribution through the Quaternary record was determined from orientation of aeolian foresets measured in the field in the case of shoreline units, and from the trend of dune systems in the case of submerged aeolianites. The seismic data collected for this study showed that the remnant dune deposits on the South Coast shelf range from being low-relief and laterally extensive, to high-relief and occupying a narrow lateral basal band. Although during MIS 15 distribution of dominant winds differed slightly to the modern situation, through most of the palaeo-record since MIS 11, westerly winds have prevailed in Mossel Bay. On the more distal East Coast (Cawthra, 2010; Bosman, 2012) evidence was provided for significant shifts in wind direction from the glacials to the interglacials and on the West Coast a similar finding was documented by Roberts et al. (2013). The South Coast, however, appears to remain comparatively central to subtleties expressed in climate change further afield.

8.4.4 Surficial sediments

The PMT, which commenced during MIS 2 after the time of the LGM and the termination of this glacial cycle, left a prominent sediment wedge on the shelf which extends from the outer shelf to above present sea level where Holocene highstand sedimentation of the subsequent HST marks the end of the TST. The PMT sediment wedge on the inner shelf and a less well defined sand sheet on the low gradient mid- to outer shelf constitute the offshore active marine sedimentation in the study area. The PMT sediment wedge rests on a discontinuous WRS. The combination of multibeam bathymetric and side-scan sonar datasets allowed the outer shelf to be classified for the most part as sediment starved. The thickest sediment in Mossel Bay and Vlees Bay occurs within the embayments, where a well-developed inner shelf wedge is prominent on the seafloor. Sand delivered by rivers is transported east by longshore drift, while suspended mud is likely distributed further offshore and transported west by bottom currents to form the South Coast mudbelt to the west of this study area. This shelf sedimentary depositional model is considered analogous to the Orange River Holocene mudbelt on the West Coast (Meadows et al., 2002; Herbert and Compton, 2007). The 45 m BMSL nick point provides accommodation space for the inshore sediment wedge to be preserved and gentle slope of the mid shelf is a likely area of accretion for mudbelt deposits, protected from open ocean swells compared to the flat Agulhas Bank. Low energy deposits are thought

to accumulate in the lee of the 45 m BMSL terrace. The youngest sediments in the study area represent HST deposits and are represented in Swartvlei where they are interpreted to form the back edge margin and the basin infill associated with a stillstand on this systems tract. The brief Holocene highstand allowed final sedimentation in the structural embayment at Wilderness, and the resetting of base-level to the present elevation continues to prograde the existing shoreline.

8.5 Coastal cave formation

The Pinnacle Point cave complex holds 29 mapped and sequentially numbered separate cave/overhangs within a ~2 km stretch of coast. Structural features associated with compression (thrusts, reverse faults, tension/a-c fractures, shortening, foliation, fracture cleavage) and with an extensional regime (normal faults, joints, conjugate joints, offset veins) were documented in the vicinity of Pinnacle Point to investigate the susceptibility of the strata to cave formation. Four criteria were identified to explain the incision of coastal caves by high sea levels according to geological structure and therefore, zones of weakness. The features interpreted to be important for cave formation, in decreasing order, are lithology, faults, degree of silicification and joints. The Pinnacle Point promontory composed of Skurweberg Formation quartz arenites on the southern limb of an anticline lies close to the overlying Baviaanskloof Formation contact. These deposits contain a higher percentage of siltstone than the arenaceous Skurweberg Formation and are interpreted to have been more susceptible to erosion. Coastal caves near Pinnacle Point are dominantly incised into silt-rich layers in the stratigraphy, planes of thrust and normal faults, and to a lesser extent, the cave complexes are associated with conjugate joint sets and areas which were not highly silicified. When past high sea levels transgressed this coastal promontory, the zones of relative structural weakness were preferentially incised compared to unfaulted, massive, beds of quartz arenite.

8.6 Evidence for former land surfaces on the emergent shelf

The South Coast currently experiences year round rainfall. The palaeoclimate model of Bar-Matthews et al. (2010) proposed increased summer rainfall during glacial periods to make the exposed shelf area probably substantially wetter than the coastal plain is today. The geological deposits on the emergent shelf indicate a more extensive coastal plain, characterised by low-gradient meandering rivers and wetland lakes. The CFB served as a conduit of fine grained sediment to reach the shelf before being deposited into the extensive floodplains mapped in this study.

The geological substrate crops out near the surface on this current-swept shelf as a result of the poorly developed outer shelf sediment wedge and soils derived from weathered limestone, siltstone and shale bedrock likely formed during sea-level lowstands. The presence of phosphorite on the Agulhas Bank (described by Birch, 1976)

may have enhanced soil fertility in this emergent environment. Faunal assemblages in archaeological sites along the South Coast do suggest the presence of grazing taxa during glacials (e.g. Klein, 1983) and the soil formed from shale bedrock, as well as the presence of phosphate, is considered here to be capable of sustaining a productive ecosystem. A dominance of Uitenhage Group claystone on the inshore and outer shelf limestones which crop out on the seafloor is anticipated, with floodplain and wetland sediments outcropping adjacent to the fluvial incisions. Based on the seismic evidence presented here, these lithologies are anticipated to have locally outcropped at the surface when SB 1 and SB 2 were sub-aerially exposed during the retreat of sea level from MIS 7 – 6, and 5e – 2, respectively. At these times, scattered development of Strandveld Fynbos is envisaged to have formed mosaics in an area dominated by Renosterveld on the inner shelf and Limestone Fynbos on the outer shelf. Although relatively flat, topography on the Agulhas Bank induced by the presence of Quaternary palaeo-coastal zones likely promoted a landscape rich in wetlands and characterised by water bodies focussed locally in back barrier settings such as modern day Wilderness and along meandering river courses. Relict dune systems, extending up to 10 km inland from their associated palaeoshorelines, and in the vicinity of Vlees Bay, Table Mountain Group sandstones outcropped on the land surface as flat exposures. Palaeosols that are interpreted to have deposited on the regression towards the MIS 6 glacial and associated with sub-aerial exposure of SB 2, were rapidly buried or destroyed by high-energy waves as sea level transgressed landward. The geological lowstand expression of the South Coast during MIS 4 and 2 is envisaged to be similar to the currently exposed Agulhas Plain and the Maputaland Coastal Plain on the northeast coast of South Africa. These areas share in common a Cretaceous substrate variably drape by Quaternary sediment. The vegetation was, however, likely different to that of the Maputaland Coastal Plain.

8.7 Significance of shelf geology to the archaeological record

People rely strongly on water resourcs. The geological and geophysical record allowed submerged river systems to be mapped in close proximity to Pinnacle Point. A wetland or substantial water body closely associated with the palaeoflow of the Blinde River (Dana Bay) existed at a depth of 40 – 10 m BMSL in close proximity (<10 km) to Pinnacle Point until it was rapidly buried, preserved, and subsequently submerged by the ensuing Holocene Transgression. In Vlees Bay, eroded Table Mountain Group sandstones crop out close to the seafloor, suggesting the presence of mixed sand-cobble beaches when the shelf was exposed. The cobble layers are most likely exposed during high-energy wave or storm events and may have provided a source for raw materials used in stone tool manufacture.

In addition to water resources various factors are considered significant in the attraction to, and survival of, our early ancestors in this environment by Marean et al. (2007). These dominantly incorporate a rich biodiversity along shorelines and a coastal adaptation, in conjunction with geophyte resources from the Fynbos vegetation.

This work adds numerous unique features to the list as revealed by the geological record on the shelf. These include an abundance of drinking water, the presence of floodplains and wetlands, and the aquatic ecosystem associated with wetlands. The wet environment as suggested from the seismic and geological record is supported by high rainfall proposed by Bar-Matthews et al. (2010) during glacials. Aeolianite and broad coastal dune systems likely allowed thicket vegetation to grow in aggregations, providing wood to fuel fire. The marine diet described by Marean et al. (2007) and Jerardino and Marean (2010), linked to the coastline model of Fisher et al. (2010), can be further explained by the geological substrate. Broad palaeo-coastal zones were dominated by sandy beaches and mixed rocky-sandy beaches when sea level fell below 40 m BMSL. The shorelines in close proximity to Pinnacle Point on the inner shelf were likely dominated by outcrops of Table Mountain Group sandstone which supported the growth of *Perna perna* when the coast was relatively close.

Although not vastly different to the currently sub-aerially exposed Agulhas Plain, this is suggested to have been a suitable habitat for animals and people during glacial periods. The South Coast, currently lying at the junction of the warm Agulhas Current and cold Benguela Upwelling System, bridges the winter versus summer rainfall domains and experiences the mildest climate in southern Africa, may well have been characterised by comparable environmental stability through time as far back as MIS 11. Perhaps this predictability, in part, buffered our ancestors from the extremes of global Pleistocene climatic instability and allowed the survival of reduced populations through periods of climactic instability and provided a refuge during harsh climatic periods.

8.8 Key findings

1) This work demonstrates that within sea-level cycles, accommodation space for coastal deposits is controlled by antecedent drainage pathways and gradient of the adjacent inner continental shelf.
2) Through offshore and lakefloor seismic profiling, this work has linked the well-documented sub-aerially exposed stratigraphy to the currently submerged geological and sedimentological record on the South Coast.
3) The resistant geological substrate in Mossel Bay led to the preservation of Quaternary strata in the embayment, as lateral protection by the rocky headland of Cape St. Blaize sheltered submerged Cenozoic deposits from erosion by the prevailing southwesterly swell and storm surges. The unprotected outer shelf is an open, vast expanse of eroded underlying strata and generally lacks preserved Quaternary deposits when compared to its shallower counterpart. The closest possible analogue along the South Coast may be the region near Cape Agulhas and a further afield comparable region is thought to be the Maputaland Coastal Plain.
4) Bathymetric mapping of the shelf in this study has shown a distinct bimodality in onshore-offshore elevation, resulting in the presence of a now submerged area with no exact sub-aerially exposed

analogue. Upon this notably flat shelf a small fall in sea level beyond 45 BMSL results in the development of extensive coastal plains. These coastal plains include rivers and floodplains close to the present coast.

5) The palaeoshoreline was defined here as a linear definition of past sea level, whereas the palaeo-coastal zone represents deposition along an active coastal environment, which encompasses the entire area extending from the shallow nearshore to the coastal dunes.
6) Aeolianite, beachrock, foreshore deposits and cemented upper shoreface sediments have been dated and placed within a sequence stratigraphic framework. The deposits are associated with a combination of forced regressive, normal regressive, still-stand and landward transgressive events.
7) It is proposed that there is no strict pattern for preferential dune and beach deposition related to sea level as previously suggested in South African continental shelf studies (Ramsay, 1996; Cawthra et al., 2012a; Bosman, 2012). Dune deposition is not limited to sea-level regressions and beach deposits are not exclusively deposited on transgressive cycles as argued in these East Coast investigations. This study has shown that suitable gradient, promoting the development of broad palaeo-coastal zones is of more importance in terms of depositional preservation than the direction of sea-level movement. The presence of aeolian deposits near the present shoreline during glacials (i.e. when the strandline was situated far offshore), in conjunction with a unique carbonate diagenetic history, supports the hypothesis that dune cordons extended far inland.
8) The South Coast may well have been characterised by comparable environmental and climatic stability through time as far back as MIS 11. The mild climate is suggested to have created a suitable habitat for animals and people during glacial periods.

8.9 Recommendations for follow-up studies

1) Cores have recently been obtained from parts of the shelf. These will be analysed during 2014 by the author.
2) Mathematical modelling of energy along past shorelines to refine the character of palaeo-coastal zones using the data from this project would contribute significantly to the way Quaternary lowstand deposits and environments in South Africa are understood.
3) Revisit existing geophysical datasets from other areas on the South African continental shelf for palaeoenvironmental reconstructions.

9 REFERENCES

Abe-Ouchi, A., Saito, F., Kawamura, K., Raymo, M., Okuno, J., Takahashi, K., Blatter, H., 2013. Insolation-driven 100,000-year glacial cycles and hysteresis of ice-sheet volume. Nature 500, 190-194.

Ager, D., 1993. The new catastrophism: the importance of the rare events in geological history. Cambridge University Press, Cambridge, 231 pp.

Aitken, M. J., 1985. Thermoluminescence dating. Academic press.

Alexandersson, T., 1972. Intergranular growth of marine aragonite and Mg-calcite: Evidence of precipitation from supersaturated seawater. Journal of Sedimentary Petrology 42(2), 441-460.

Allen, G.P., 1991. Sedimentary processes and facies in the Gironde estuary: a recent model for macrotidal estuarine systems. In: Smith, D.G., Reinson, G.E., Zaitlin, B.A. & Rahmani, R.A. (Eds): Clastic Tidal Sedimentology: Canadian Society of Petroleum Geologists Memoir 16, 29-40.

Ashley, G.M., 1990. Classification of large-scale subaqueous bedforms: A new look at an old problem. Journal of Sedimentary Petrology 60, 160-172.

Bailey, G.N., Flemming, N.C., 2008. Archaeology of the continental shelf: marine resources, submerged landscapes and underwater archaeology. Quaternary Science Reviews 27, 2153–2165.

Bar-Matthews, M., Marean, C.W., Jacobs, Z., Karkanas, P., Fisher, E.C., Herries, A.I.R., Brown, K., Williams, H.M., Bernatchez, J., Ayalon, A., Nilssen, P.J. 2010., A high resolution and continuous isotopic speleothem record of paleoclimate and paleoenvironment from 90 to 53 ka from Pinnacle Point on the south coast of South Africa. Quaternary Science Reviews 29, 2131-2145.

Bard, E., Hamelin, B., Fairbanks, R. G., 1990. U-Th ages obtained by mass spectrometry in corals from Barbados: sea level during the past 130, 000 years. Nature 346(6283), 456-458.

Bard, E., Hamelin, B., Delanghe-Sabatier, D., 2010. Deglacial Meltwater Pulse 1B and Younger Dryas Sea Levels Revisited with Boreholes at Tahiti. Science 327, 1325-1327.

Bateman, M.D., Holmes, P.J., Carr, A.S., Horton, B.P., Jaiswal, M.K., 2004. Aeolianite and barrier dune construction spanning the last two glacial-interglacial cycles from the Southern Cape coast, South Africa. Quaternary Science Reviews 23, 1681-1698.

Bateman, M.D., Carr, A.S., Murray-Wallace, C.V., Roberts, D.L., Holmes, P.J., 2008. A dating intercomparison study on Late Stone Age coastal midden deposits, South Africa. Geoarchaeology 23, 715-741.

Bateman, M.D., Carr, A.S., Dunajko, A.C., Holmes, P.J., Roberts, D.L., McLaren, S.J., Bryant, R.G., Marker, M.E., Murray-Wallace, C.V., 2011. The evolution of coastal barrier systems: a case study of the Middle-Late Pleistocene Wilderness barriers, South Africa. Quaternary Science Reviews 30, 63-81.

Beach, D.K., Ginsburg, R.N., 1980. Facies succession of Pliocene-Pleistocene carbonates, northwestern Great Bahama Bank. AAPG Bulletin 64(10), 1634-1642.

Behar, D.M., Villems, R., Soodyall, H., Blue-Smith, J., Pereira, L., Metspalu, E., Scozzari, R., Makkan, H., Tzur, S., Comas, D., Bertranpetit, J., Quintana-Murci, L., Tyler-Smith, C., Wells, R.S., Rosset, S., The Geongraphic Consortium, 2008. The dawn of human matrilineal diversity. American Journal of Human Genetics 82, 1130-1140.

Bell, W.T., Zimmerman, D.W., 1978. The effect of HF acid etching on the morphology of quartz inclusions for thermoluminescence dating. Archaeometry 20(1), 63-65.

Bell, W. T., 1979. Thermoluminescence dating: radiation dose-rate data. Archaeometry 21(2), 243-245.

Berner, R.A., Westrich, R.G., Smith, J., Martens, C., 1978. Inhibition of aragonite precipitation from supersaturated seawater; a laboratory and field study. American Journal of Science 278, 816–837.

Bierman, P.R., Caffee, M.W., 2001. Slow rates of rock surface erosion and sediment production across the Namib Desert and escarpment, Southern Africa: American Journal of Science 301(4-5), 326-358.

Bintanja, R., van de Wal, R.S.W., 2008. North American ice-sheet dynamics and the onset of 100,000-year glacial cycles. Nature 454, 869-872.

Bintanja, R., van de Wal, R.S.W., Oerlemans, J., 2005. Modelled atmospheric temperatures and global sea levels over the past million years. Nature 437, 125-128.

Binford, L.R., 1980. Willow smoke and dogs tails: hunter-gatherer settlement systems and archaeological site formation. American Antiquity 45, 4–20.

Binford, L.R., 1982. The archaeology of place. Journal of Anthropological Archaeology 1, 5–31.

Birch, G.F., 1976. A short report on the glauconite and phosphate reserves on the margin of South Africa. Report 1946-0011 of the Joint Geological Survey/University of Cape Town Marine Geology Program.

Birch, G.F., De Plessis, A., Willis, J.P., 1978. Off shore and on land geological and geophysical investigations in the Wilderness Lakes region. Transactions of the Geological Society of South Africa 81, 339-352.

Birch, G.F., 1979a. The Karbonat-Bombe: a precise, rapid and cheap instrument for determining calcium carbonate in sediment rocks. Technical report, Joint Geological Survey – University of Cape Town Marine Geoscience Unit 11, 122-126.

Birch, G.F., 1979b. Phosphorite pellets and rock from the western continental margin and adjacent coastal terrace of South Africa. Marine Geology 33 (1-2), 91-116.

Birch, G.F., 1980. Nearshore Quaternary sedimentation off the south coast of SA (CT to PE). Geological Survey Bulletin 67, 20pp.

Birch, G.F., 1981. The bathymetry and geomorphology of the continental shelf and upper slope between Durban and Port St. Johns. Annuals of the Geological Survey of South Africa 15(1), 55-62.

Birch, G. F., 1990. Phosphorite deposits on the South African continental margin and coastal terrace. In: Burnett, W. C. and Riggs, S. R., (eds)., Phosphate deposits of the world: Volume 3, Genesis of Neogene to recent phosphorites: Cambridge, Cambridge University Press, 153-166 .

Bond, G., Broecker, W.S., Johnsen, S., McManus, J., Labeyrie, L., Jouzel, J., Bonani, G., 1993. Correlations between climate records from North Atlantic sediments and Greenland ice. Nature 365, 143-147.

Bonfil, R., Meyer, M., Scholl, M.C., Johnson, R., O'Brien, S., Oosthuizen, H., Swanson, S., Kotze, D., Paterson, M., 2005. Transoceanic migration, spatial dynamics, and population linkages of white sharks. Science 310, 100 – 103.

Bosman, C., Uken, R., Smith, A. M., 2005. The bathymetry of the Aliwal Shoal, Scottburgh, South Africa. South African Journal of Science 101(5/6), 255.

Bosman, C., 2012. The marine geology of the Aliwal Shoal, Scottburgh, South Africa. Ph.D. Thesis, University of KwaZulu-Natal, South Africa.

Bradley, R. S., 1999. Palaeoclimatology: reconstructing climates of the Quaternary (2nd Ed.) Academic Press San Diego, 613pp.

Branch, G.M., Branch, M., 1992. The Living Shores of Southern Africa. Struik Publishers, Cape Town.

Branch, G.M., Menge, B.A., 2001. Rocky intertidal communities. In: Bertness, M.D., Gaines, S.D., Hay, M.E. (Eds.), Marine Community Ecology. Sinauer Associates, Inc., Sunderland, pp. 221-251.

Broad, D. S., Jungslager, E. H. A., McLachlan, I. R., Roux, J., 2006. Offshore Mesozoic Basins. In: Johnson, M. R., Annhauser, C. R. and Thomas, R. J. (Eds.), The Geology of South Africa. Geological Society of South Africa, Johannesburg/Council for Geoscience, Pretoria, 553-571.

Broad, D. S., Jungslager, E. H. A., McLachlan, I. R., Roux, J., van der Spuy, D., 2012. South Africa's offshore Mesozoic Basins. Phanerozoic Passive Margins, Cratonic Basins and Global Tectonic Maps, pp. 535-560.

Brown, K.S., Marean, C.W., Herries, A.I.R., Jacobs, Z., Tribolo, C., Braun, D., Roberts, D. L., Meyer, M.C., Bernatchez, J., 2009. Fire as an engineering tool of early modern humans. Science 325, 859-862.

Brown, K.S., Marean, C.W., Jacobs, Z., Schoville, B.J., Oestmo, S., Fisher, E.C., Bernatchez, J., Karkanas, P., Matthews, T., 2012. An early and enduring advanced technology originating 71,000 years ago in South Africa. Nature 491(7425) 590-593.

Brown Jr., L.F., Benson, J.M., Brink, G.J., Doherty, S., Jollands, A., Jungslager, E.H.A., Keenan, J.H.G., Muntingh, A., van Wyk, N.J.S., 1995. Sequence stratigraphy in offshore South African divergent basins: an atlas on exploration for cretaceous lowstand traps by Soekor (Pty) Ltd. AAPG Studies in Geology 41.

Brown, R.W., Summerfield, M.A., Gleadow, A.J.W., 2002, Denudational history along a transect across the Drakensberg Escarpment of southern Africa derived from apatite fission track thermo-chronology: Journal of Geophysical Research 107, 1-17.

Burke, K., 1996. The African Plate. South African Journal of Geology 99, 341–409.

Burton, E.A., Walter, L.M., 1991. The effects of PCO2 and temperature on magnesium incorporation in calcite in seawater and MgCl2– CaCl2 solutions. Geochimica et Cosmochimica Acta 55, 777–785.

Carr, A.S., Bateman, M.D., Holmes, P.J., 2007. Developing a 150 ka luminescence chronology for the barrier dunes of the Western Cape, South Africa. Quaternary Geochronology 2, 110–116.

Carr, A.S., Bateman, M.D., Roberts, D.L., Murray-Wallace, C.V., Jacobs, Z., Holmes, P.J., 2010. The last interglacial sea-level high stand on the southern Cape coastline of South Africa. Quaternary Research 73, 351–363.

Carr, A.S., Botha, G.A., 2012. Coastal geomorphology. In: Holmes, P., Meadows, M. (Eds.), Southern African geomorphology: Recent trends and new directions. SUN Press Bloemfontein, 267-305.

Carter, R.W.G., 1988. Coastal environments: an introduction to the physical, ecological and cultural systems of coastlines. Academic Press.

Carter, R.W.G., Woodroffe, C.D., 1994. Coastal evolution: an introduction. In: Carter, R.W.G., Woodroffe, C.D. (Eds.), Coastal Evolution: late Quaternary shoreline morphodynamics. Cambridge University Press, 1-31.

Carter, R.W.G., 2002. Coastal environments: An introduction to the physical, ecological and cultural systems of coastlines. Elsevier, London. 634 pp.

Catuneanu, O., 2006. Principles of sequence stratigraphy. Elsevier.

Catuneanu, O., Abreu, V., Bhattacharya, J.P., Blum, M.D., Dalrymple, R.W., Eriksson, P.G., Fielding, C.R., Fisher, W.L., Galloway, W.E., Gibling, M.R., Giles, K.A., Holbrook, J.M., Jordan, R., Kendall, C. G.St.C., Macurda, B., Martinsen, O.J., Miall, A.D., Neal, J.E., Nummedal, D., Pomar, L., Posamentier, H.W., Pratt, B.R., Sarg, J.F., Shanley, K.W., Steel, R.J., Strasser, A., Tucker, M.E., Winker, C., 2009. Towards the standardization of sequence stratigraphy. Earth Science Reviews 92, 1-33.

Cawthra, H.C., 2010. The Cretaceous to Cenozoic evolution of the Durban Bluff and adjacent continental shelf. Unpublished M.Sc. Thesis, University of KwaZulu-Natal, South Africa.

Cawthra, H.C., 2011a. A guideline to the interpretation and classification of marine geophysical data (bathymetry, side-scan sonar and sub-bottom profiling). 2011-0102, Marine Geoscience Unit, Council for Geoscience, Cape Town, South Africa, 12 pp.

Cawthra, H.C., 2011b. Cruise report for the Mossel Bay seismic survey, southern Cape, South Africa. Phase 2: Boomer and pinger sub-bottom profiling. 2011-0134, Marine Geoscience Unit, Council for Geoscience, Cape Town, South Africa, 33 pp.

Cawthra, H.C., Uken, R., Oveckhina, M., 2012a. New insights into the geological evolution of the Bluff Ridge and adjacent Blood Reef, Durban, South Africa. South African Journal of Geology 115(3), 291-308.

Cawthra, H.C., Neumann, F.H., Uken, R., Smith, A.M., Guastella, L., Yates, A.M., 2012b. Sedimentation on the narrow (8 km wide), oceanic current-influenced continental shelf off Durban, KwaZulu-Natal, South Africa. Marine Geology 323-325, 107-122.

Cawthra, H. C., Uken, R., 2012. Modern beachrock formation in Durban, KwaZulu-Natal. South African Journal of Science 108 (7/8), 84-88.

Chase, B.M., Meadows, M.E., 2007. Late Quaternary dynamics of southern Africa's winter rainfall zone. Earth Science Reviews 84, 103-138.

Clark, P. U., Pollard, D., 1998. Origin of the middle Pleistocene Transition by ice sheet erosion of regolith. Paleoceanography 13, 1-9.

Clark, P. U., Mc Cabe, A. M., Mix, A. C., Weaver, A. J., 2004. Rapid rise of sea level 19,000 years ago and its global implications. Science 304(5674), 1141-1144.

Clark, P. U., Archer, D., Pollard, D., Blum, J. D., Rial, J. A., Brovkin, V., Roy, M., 2006. The middle Pleistocene transition: characteristics, mechanisms, and implications for long-term changes in atmospheric pCO_2. Quaternary Science Reviews 25(23), 3150-3184.

Clark, P.U., Dyke, A.S., Shakun, J.D., Carlson, A.E., Clark, J., Wohlfarth, B., Mitrovica, J.X., Hostetler, S.W., McCabe, A.M., 2009. The Last Glacial Maximum. Science 325, 710-714.

Cockcroft, M.J., Wilkinson, M.J., Tyson, P.D., 1987. The application of a present-day climatic model to the Late Quaternary in southern Africa. Climatic Change 10, 161-181.

Coe, A.L., Church, K.D., 2003. Sea-level change. In: Coe, A.L. (Ed.), The sedimentary record of sea-level change. Cambridge University Press, pp. 34-56.

Cohen, A.L., Tyson, P.D., 1995. Sea surface temperature fluctuations during the Holocene off the south coast of Africa: implications for terrestrial climate and rainfall. Holocene 5, 304–312.

Coles, S.K.P., Wright, C.I., Sinclair, D.A., Van den Bossche, P., 2002. The Potential for Environmentally Sound Development of Marine Deposits of Potassic and Phosphatic minerals offshore, Southern Africa. Marine georesources and Geotechnology (20), 87-110.

Compton, J.S., 2001. Holocene sea-level fluctuations inferred from the evolution of depositional environments of the southern Langebaan Lagoon salt marsh, South Africa. The Holocene 11(4), 395-405.

Compton, J.S., Franceschini, G., 2005. Holocene geoarchaeology of the sixteen mile beach barrier dunes in the Western Cape, South Africa. Quaternary Research 63(1), 99-107.

Compton, J.S., 2006. The mid-Holocene sea-level highstand at Bogenfels Pan on the southwest coast of Namibia. Quaternary Research 66(2), 303-310.

Compton, J.S., Wiltshire, J.G., 2009. Terrigenous sediment export from the western margin of South Africa on glacial/interglacial cycles. Marine Geology 266, 212-222.

Compton, J. S., 2011. Pleistocene sea level fluctuations and human evolution on the southern coastal plain of South Africa. Quaternary Science Reviews 30 (5-6), 506-527.

Cooper, J.A.G., 1991. Shoreline changes on the Natal coast: Mkomazi River mouth to Tugela River mouth. Natal Town and Regional Planning Commission Report 77, Pietermaritzburg, South Africa, 57 pp.

Cooper, J.A.G., Flores, R.M., 1991. Shoreline deposits and diagenesis resulting from two Late Pleistocene highstands near +5 and +6 metres, Durban, South Africa. Marine Geology 97, 325–343.

Cooper, J.A.G., 1994. Shoreline changes on the Natal coast: Mtamvuma River mouth to Mkomazi River mouth. Natal Town and Regional Planning Commission Report 79, Pietermaritzburg, South Africa 53 pp.

Cooper, J.A.G., 2001. Geomorphological variability among microtidal estuaries from the wave-dominated South African coast. Geomorphology 40, 99-122.

Cooper, J.A.G., Flores, R.M., 1991. Shoreline deposits and diagenesis resulting from two Late Pleistocene highstands near +5 and +6 metres, Durban, South Africa. Marine Geology 97, 325–343.

Cowell, P.J., Roy, P.S., Jones, R.A., 1992. Shoreface translation model: computer simulation of coastal-sand-body response to sea level rise. Mathematics and Computers in Simulation 33, 603-608.

Cowell, P.J., Thom, B.G., 1994. Morphodynamics of coastal evolution. In: Carter, R.W.G., Woodroffe, C.D. (Eds.), Coastal Evolution, Late Quaternary Shoreline Morphodynamics. Cambridge University Press, pp. 33-86.

Cowling, R.M., 1990. Diversity Components in a Species-Rich Area of the Cape Floristic Region. Journal of Vegetation Science 1(5) 699-710.

Cowling, R.M., 1992. The ecology of fynbos: nutrients, fire and diversity. Oxford University Press Southern Africa.

Cowling, R.M., Holmes, P.M., 1992. Endemism and speciation in a lowland flora from the Cape Floristic Region. Biological Journal of the Linnean Society 47, 367-383.

Cronin, T.M., 1999. Principles of Climatology. Columbia University Press. New York 204 pp.

Cruz-Uribe, K., Klein, R. G., Avery, G., Avery, M., Halkett, D., Hart, T., Milo, R. G., Sampson, C.G., Volman, T, P., 2003. Excavation of buried Late Acheulean (Mid-Quaternary) land surfaces at Duinefontein 2, Western Cape Province, South Africa. Journal of Archaeological Science 30(5), 559-575.

Cutler, K.B., Edwards, R.L., Taylor, F.W., Cheng, H., Adkins, J., Gallup, C.D., Cutler, P.M., Burr, G.S., Bloom, A.L., 2003. Rapid sea-level fall and deep-ocean temperature change since the Last interglacial period. Earth and Planetary Science Letters 206, 253-271.

Dansgaard, W., Johnsen, S.J., Clausen, H.B., Dahl-Jensen, D., Gundestrup, N.S., Hammer, C.U., Hvidberg, C.S., Steffensen, J.P., Sveinbjornsdottir, A.E., Jouzel, J., Bond, G., 1993. Evidence for general instability of past climate from a 250-kyr ice-core record. Nature 364(6434), 218–220.

Davies, J.L., 1980. Geographical variation in coastal development. Longman, New York, 212 pages.

Day, R.W., 1986. Magnetometric mapping of the False Bay dolerites. Joint Geological Survey/University of Cape Town Marine Geoscience Unit Technical Report 16, 217-227.

Department of Water Affairs and Forestry, South Africa (DWAF), 2004a. Breede Water Management Area: Internal Strategic Perspective. Prepared by Ninham Shand (Pty) Ltd in association with Jakoet & Associates, Umvoto Africa and Tlou and Matji, on behalf of the Directorate: National Water Resource Planning. DWAF Report No P WMA18/000/00/0304.

Department of Water Affairs and Forestry, South Africa (DWAF), 2004b. Gouritz Water Management Area: Internal Strategic Perspective. Prepared by Ninham Shand (Pty) Ltd in association with Jakoet &

Associates and Umvoto Africa, on behalf of the Directorate: National Water Resource Planning. DWAF Report No P WMA16/000/00/0304.

De Decker, R.H., 1983. The Sediments of Plettenberg Bay and the Submerged Robberg Spit. Joint Geological Survey/ University of Cape Town Technical Report 14, 255 - 265.

De Decker, R.H., 1987. The geological setting of diamondiferous deposits on the inner shelf between the Orange River and Wreck Point, Namaqualand. Bulletin of the Geological Survey of South Africa 86, 99 pp.

De Swardt, A. M. J., McLachlan, I. R., 1982. Petroleum exploration in the South African offshore: the geological framework and ydrocarbon potential. In: Glen, H. W. (Ed.) Proceedings of the 12th CMMI Congress, Johannesburg, South African Institute of Mining and Metallurgy, 147-166.

de Wet, W., 2013. Bathymetry of the South African continental shelf. Unpublished MSc thesis, University of Cape Town.

de Wit, M.J., Ransome, I.G.D., 1992. Regional inversion tectonics along the southern margin of Gondwana. In: de Wit, M.J., Ransome, I.G.D. (Eds.), Inversion Tectonics of the Cape Fold Belt, Karoo and Cretaceous Basins of Southern Africa. A.A. Balkema, Rotterdam, pp. 15–21.

de Wit, M.J., 2007. The Kalahari Epeiorogeny and climate change: differentiating cause and effect from core to space. Inkaba yeAfrica special volume. South African Journal of Geology 110, 367–392.

Dingle, R.V., Rogers, J., 1972. Pleistocene palaeogeography of the Agulhas Bank. Transactions of the Royal Society of South Africa 40, 155-465.

Dingle, R. V. and Siesser, 1975. Geology of the continental margin between Walvis Bay and Ponta do Ouro. Government Printer, 1pp.

Dingle, R.V., Siesser, W.G., Newton, A.R., 1983. Mesozoic and Neogene geology of southern Africa. Balkema, Rotterdam, 375pp.

Duncan, R.A., Hooper, P.R., Rehacek, J., Marsh, J.S., Duncan, A.R., 1997. The timing and duration of the Karoo igneous event, southern Gondwana. Journal of Geophysical Research 102, 18127–18138.

Dupont, L.M., Jahns, S., Marret, F., Ning, S. 2000. Vegetation change in equatorial West Africa: time-slices for the last 150 ka. Palaeogeography, Palaeoclimatology, Palaeoecology, 155 (1-2) 95-122.

Doucoure, C.M., de Wit, M.J., 2003. Old inherited origin for the present near-bimodal topography of Africa. J. Afric. Earth Sci. 36 (4), 31–388.

Du Toit, A., 1937. Our Wandering Continents. Oliver and Boyd, U.K., 366pp.

Du Toit, A., 1954. The Geology of South Africa, 3rd ed. Oliver and Boyd, U.K., 611pp.

Du Toit. S.R., 1976. Mesozoic geology of the Agulhas Bank, South Africa. Ph.D. Thesis, Faculty of Science, University of Cape Town, South Africa.

Eagles, G., 2007. New angles on South Atlantic opening. Geophysical Journal International 166, 353–361.

Edwards, R.L., Beck, J.W., Burr, G.S., Donahue, D.J., Chappell, J.M.A., Bloom, A.L., Druffel, E.R.M., Taylor, F.W., 1993. A large drop in atmospheric 14C/12C and reduced melting in the Younger Dryas, documented with 230Th ages of coral. Science 260(5110), 962–968.

Elderfield, H., Ferretti, P., Greaves, M., Crowhurst, S., McCave, I.N., Hodell, D., Piotrowski, A.M., 2012. Evolution of ocean temperature and ice volume through the Mid-Pleistocene climate transition. Science 337(6095), 704-709.

Elliott, T., 1986. Siliciclastic shorelines. In: Reading, H.G. (Ed.), Sedimentary Environments and Facies. Blackwell, Oxford, 155–188.

EPICA Community Members, 2004. Eight glacial cycles from an Antarctic ice core. Nature 429, 623-628.

EPICA Community Members, 2006. One-to-one coupling of glacial climate variability in Greenland and Antarctica. Nature 444, 195-198.

Erlanger, E.D., Granger, D.E., Gibbon, R.J., 2012. Rock uplift rates in South Africa from isochron burial dating of fluvial and marine terraces. Geology 40(11), 1019-1022.

Fagundes, N.J.R., Ray, N., Beaumont, M., Neuenschwander, S., Salzano, F.M., Bonatto, S.L., Excoffier, L., 2007. Statistical evaluation of alternative models of human evolution. Proceedings of the National Academy of Sciences 104, 17614–17619.

Faure, H., Walter, R. C., Grant, D. C., 2002. The coastal oasis: ice age springs on emerged continental shelves. Global and Planetary Change 33, 47-56.

Fenna, D., 2006. Cartographic science: a compendium of map projections, with derivations. CRC Press.

Fisher, E.C., Bar-Matthews, M., Jerardino, A., Marean, C.W., 2010. Middle and Late Pleistocene Paleoscape Modeling along the Southern Coast of South Africa. Quaternary Science Reviews 29, 1382-1398.

Fisher, E.C., Albert, R-M., Botha, G.A., Cawthra, H.C., Esteban, I., Harris, J., Jacobs, Z., Jerardino, A., Marean, C.W., Neumann, F.H., Pargeter, J., Poupart, M., Venter, J., 2013. Archaeological Reconnaissance for Middle Stone Age Sites along the Pondoland Coast, South Africa. Palaeoanthropology. 104-137.

Fleming, K., Johnston, P., Zwartz, D., Yokoyama, Y., Lambeck, K., Chappell, J., 1998. Refining the eustatic sea-level curve since the Last Glacial Maximum using far-and intermediate-field sites. Earth and Planetary Science Letters 163(1), 327-342.

Fleming, A., Summerfield, M.A., Stone, J.O.H., Fifield, L.K., Cresswell, R.G., 1999. Denudation rates for the southern Drakensberg escarpment, SE Africa, derived from in-situ-produced cosmogenic 36Cl: initial results. Journal of Geological Society (London) 156, 209–212.

Flemming, B. W., 1978. Underwater sand dunes along the southeast African continental margin—observations and implications. Marine Geology 26(3), 177-198.

Flemming, B. W., 1981. Factors controlling shelf sediment dispersal along the southeast African continental margin. Marine Geology 42, 259–277.

Flemming, B.W., Eagle, G.A., Fricke, A.H., Hunter, I.T., Martin, A.K., Schumann, E.H., Swart, V.P., Zoutendyk, P., 1983. Agulhas Bank Studies Report 11, Stellenbosch National Research Institute for Oceanology Memo 8319, 78 pp.

Flügel, E., 2004 Microfacies of Carbonate Rocks: Analysis, Interpretation and Applcation. Springer-Verlag, Berlin, Heidelberg, New York, 976pp.

Folk, R.L., 1959. Practical petrographic classification of limestones: American Association of Petroleum Geologists Bulletin 43, 1-38.

Folk, R. L., 1974: Petrology of sedimentary rocks. Hemphill Pub. Co, Austin, Texas, 182 pp.

Foyle, A.M., Oertel, G.F., 1997. Transgressive systems tract development and incised-valley fills within a Quaternary estuary-shelf system: Virginia inner shelf, USA. Marine Geology 137, 227-249.

Förster, R., 1975. The geological history of the sedimentary basin of southern Mozambique, and some aspects of the origin of the Mozambique Channel. Palaeogeography, Palaeoclimatology, Palaeoecology 17(4), 267-287.

Frimmel, H.E., Fölling, P.G., Diamond, R., 2001. Metamorphism of the Permo-Triassic Cape Fold Belt and its basement, South Africa. Mineralogy and Petrology 73 (4), 325–346.

Gentle, R. I., 1987. The geology of the inner continental shelf and Agulhas Arch: CT to PE . Geological Survey Bulletin 20, 129pp.

Gilchrist, A. R., Summerfield, M. A., 1991. Denudation, isostasy and landscape evolution. Earth Surface Processes and Landforms 16(6), 555-562.

Ginsburg, R.N., 1953. Beachrock in south Florida. Journal of Sedimentary Petrology 23(2), 85-92.

Gonder, M.K., Mortensen, H.M., Reed, F.A., de Sousa, A., Tishkoff, S.A., 2007. WholemtDNA genome sequence analysis of ancient African lineages. Molecular Biology and Evolution 24, 757–768.

Grabau, A.W., 1904. On the classification of sedimentary rocks. American Geologist 33, 228-247.

Green, A.N., 2009. Palaeo-drainage, incised valley fills and transgressive systems tract sedimentation of the northern KwaZulu-Natal continental shelf, South Africa, SW Indian Ocean. Marine Geology 263: 46-53.

Green, A., Luke Garlick, G., 2011. A sequence stratigraphic framework for a narrow, current-swept continental shelf: The Durban Bight, central KwaZulu-Natal, South Africa. Journal of African Earth Sciences 60(5), 303-314.

Green, A., Leuci, R., Thackeray, Z., Vella, G., 2012. Number One Reef: An overstepped segmented lagoon complex on the KwaZulu-Natal continental shelf. South African Journal of Science 108, pages.

Green, A.N., Cooper, J.A.G., Salzmann, L., 2014. Geomorphic and stratigraphic signs of postglacial meltwater pulses on continental shelves. Geology 42, 151-154.

Gresse, P. G., von Veh, M. V., Frimmel, H. E., 2006. Namibian (Neoproterozoic) to Early Cambrian successions. In: Johnson, M. R., Annhauser, C. R. and Thomas, R. J. (Eds.), The Geology of South Africa. Geological Society of South Africa, Johannesburg/Council for Geoscience, Pretoria, 395-421.

Griggs, G. B., Trenhaile, A. S., 1994. Coastal cliffs and platforms. In: Carter, R.W.G., C.D. Woodroffe (Eds.), Coastal Evolution: late Quaternary shoreline morphodynamics. Cambridge University Press Cambridge University Press, 425-450.

Guérin, G., Mercier, N., Adamiec, G., 2011. Dose rate conversion factors: update. Ancient TL 29, 5–8.

Guillocheau, F., Dauteil, O., de Wit, M., Hassen, S., Linol, B., 2013. Evolution of the South African Plateau: uplift and relief growth. TopoAFRICA Conference field excursion guidebook 21 – 25 January, 64 pp.

Gunatilaka, H.A., Till, R., 1971. A precise and accurate method for the quantitative determination of carbonate minerals by X-ray diffraction using a spiking technique. Mineralogical Magazine 38, 481-487.

Hälbich, I.W., 1983. A geodynamic model for the Cape Fold Belt. In Söhnge, A. P. G and Hälbich, I. W. (Eds.) Geodynamics of the Cape fold Belt Special Publication of the Geological Society of South Africa 12, 177-184.

Haq, B.U., Hardenbol, J., Vail, P.R., 1987. Chronology of fluctuating seal levels since the Triassic. Science 1, 1156–1167.

Haq, B. U., Al-Qahtani, A. M., 2005. Phanerozoic cycles of sea-level change on the Arabian Platform. GeoArabia 10(2), 127-160.

Haq, B.U., 2007. The geological time table: Sixth revised enlarged and updated version. Elsevier. 1pp.

Harris, T.F.W., 1978. Review of coastal currents in Southern African waters. South African national scientific programme report 10, 103 pp.

Hays, J. D., Imbrie, J., Shackleton, N. J., 1976. Variation in the Earth's orbit: Pacemaker of the ice ages. Science 194, 1121-1132.

Heap, A. D., Harris, P. T., 2008. Geomorphology of the Australian margin and adjacent seafloor. Australian Journal of Earth Sciences 55(4), 555-585.

Hearty, P.J., Hollin, J.T., Neumann, A.C., O'Leary, M.J., McCulloch, M., 2007. Global sea-level fluctuations during the Last Interglaciation (MIS 5e). Quaternary Science Reviews 26(17), 2090-2112.

Heine, K., 1982. The main stages of the late Quaternary evolution of the Kalahari region, southern Africa. Palaeoecology of Africa 15, 53-76.

Helland-Hansen, W., 2009. Towards the standardization of sequence stratigraphy. Earth-Science Reviews 94(1), 95-97.

Hendey, Q.B., 1983. Cenozoic geology and palaeogeography of the Fynbos region. In: Deacon, H.J., Hendey, Q.B., Lambrechts, J.J.N. (Eds.), Fynbos palaeoecology: A preliminary synthesis, South African National Scientific Programmes 75, 35-61.

Henshilwood, C.S., D'Errico, F., Yates, R., Jacobs, Z., Tribolo, C., Duller, G.A.T., Mercier, N., Sealy, J.C., Valladas, H., Watts, I., Wintle, A.G., 2002. Emergence of modern human behavior: Middle Stone Age engravings from South Africa. Science 295, 1278-1280.

Henshilwood, C., d'Errico, F., Vanhaeren, M., van Niekerk, K., Jacobs, Z., 2004. Middle Stone Age shell beads from South Africa. Science 304, 404.

Henshilwood, C.S., d'Errico, F., van Niekerk, K.L., Coquinot, Y., Jacobs, Z., Lauritzen, S.E., Menu, M., García-Moreno, R., 2011. A 100,000-Year-Old Ochre-Processing Workshop at Blombos Cave, South Africa. Science 334(6053), 219-222.

Herbert, C., Compton, J.S., 2007. Geochronology of Holocene sediments on the western margin of South Africa. South African Journal of Geology 110, 327–338.

Hesp, P.A., 1984. The formation of sand 'beach ridges' and foredunes. Search 15, 289-291.

Hesp, P.A., 1988. Surfzone, beach, and foredune interactions on the Australian south east coast. Journal of Coastal Research 3, 15-25.

Heydorn, A.E.F., Tinley, K.L., 1980. Estuaries of the Cape part 1: Synopsis of the Cape coast, natural features, dynamics and utilisation. CSIR Research Report 380.

Holmes, P.J., Bateman, M.D., Carr, A.S., Marker, M.E., 2007. The place of aeolian coversands in the geomorphic evolution of the southern Cape coast, South Africa. South African Journal of Geology 110, 127-138.

Hunt, D., Tucker, M. E., 1992. Stranded parasequences and the forced regressive wedge systems tract: deposition during base-level fall. Sedimentary Geology 81(1), 1-9.

Huntley, D.J., Wintle, A.G., 1981. The use of alpha scintillation counting for measuring Th-230 and Pa-231 contents of ocean sediments. Canadian Journal of Earth Sciences 18(3), 419-432.

Huybers, P., 2007. Glacial variability over the last two million years: an extended depth-derived agemodel, continuous obliquity pacing, and the Pleistocene progression. Quaternary Science Reviews 26(1), 37-55.

Illenberger, W.K., 1996. The geomorphic evolution of the Wilderness dune cordons, South Africa. Quaternary International 33, 11-20.

Illenberger, W.K., Burkinshaw, J.R., 2008. Coastal dunes and dunefields. In: Lewis C.A. (ed.), Geomorphology of the Eastern Cape, NICS Grahamstown, 85-106.

Ingman, M., Kaessmann, H., Paabo, S., Gyllensten, U., 2000. Mitochondrial genome variation and the origin of modern humans. Nature 408, 708–713.

Jacobs, Z., 2004. Development of luminescence techniques for dating Middle Stone Age sites in South Africa. Unpublished Ph.D. Thesis, University of Wales, Aberystwyth.

Jacobs, Z., Roberts, D.L., 2009. Last Interglacial age for the Nahoon Fossil Human Footprints, Southeast Coast of South Africa. Geochronology 4, 160-169.

Jacobs, Z., 2010. An OSL chronology for the sedimentary deposits from Pinnacle Point Cave 13B - a punctuated presence. Journal of Human Evolution 59 (3-4), 289-305.

Jacobs, Z., Roberts, R.G., Lachlan, T.J., Karkanas, P., Marean, C.W., Roberts, D.L. 2011. Development of the SAR TT-OSL procedure for dating Middle Pleistocene dune and shallow marine deposits along the southern Cape coast of South Africa. Quaternary Geochronology 6, 491–513.

Jelsma, H.A., de Wit, M.J., Thiart, C., Dirks, P., Viola, G., Basson, I.J., Anckar, E., 2004. Preferential distribution along transcontinental corridors of kimberlites and related rocks of Southern Africa. South African Journal of Geology 107 (1/2), 301–324.

Jerardino, A, Marean, C.W., 2010. Shellfish gathering, marine paleoecology and modern human behavior: perspectives from cave PP13B, Pinnacle Point, South Africa . Journal of Human Evolution 59, 412-424.

Johnson, M.R., van Vuuren, C.J., Visser, J.N.J., Cole, D.I., Wickens, de V., Christie, A.D.M., Roberts, D.L., Brandl, G., 2006. Sedimentary rocks of the Karoo Supergroup. In: M.R. Johnson, C.R., Annhauser, R.J. Thomas (Eds.), The Geology of South Africa. Geological Society of South Africa/Council for Geoscience Pretoria, 461-501.

Johnson, R., Bester, M. N., Dudley, S. F. J., Oosthuizen, W. H., Meyer, M., Hancke, L., Gennari, E., 2009. Coastal swimming patterns of white sharks (Carcharodon carcharias) at Mossel Bay, South Africa. Environmental Biology of Fishes 85, 189-200.

Johnson, R., Kock, A., 2006. South Africa's White Shark cage-diving industry – is there cause for concern? In: Nel, D.C. & Peschak, T.P. (eds) Finding a balance: White shark conservation and recreational safety in the inshore waters of Cape Town, South Africa; proceedings of a specialist workshop. WWF South Africa Report Series – 2006/Marine/001.

Jones, E.J.W., 1999. Marine Geophysics. John Wiley &Sons Ltd. Chichester, 466pp.

Kilburn, R., Rippey, E., 1982. Sea Shells of Southern Africa. Macmillan, Johannesburg.

King, L.C., 1951. South African Scenery, 2nd edn. Oliver and Boyd, U.K. 379pp.

King, L.C., 1962. Morphology of the Earth: a study and synthesis of world scenery. Oliver and Boyd Ltd, Edinburgh, 726 p.

Kitano, Y., Hood, D.W., 1965. The influence of organic material on the polymorphic crystallization of calcium carbonate. Geochimica et Cosmochimica Acta 29, 29–41.

Klein, R.G., 1972. The late quaternary mammalian fauna of Nelson Bay Cave (Cape Province, South Africa): its implications for megafaunal extinctions and environmental and cultural change. Quaternary Research 2, 135-142.

Klein, R.G., 1976. The mammalian fauna of the Klasies River Mouth sites, southern Cape Province, South Africa. South African Archaeological Bulletin 31, 75-98.

Klein, R.G., 1983. Palaeoenvironmental implications of quaternary large mammals in the fynbos region. In: Deacon, H.J., Hendey, Q.B., Lambrechts, J.J.N. (Eds.), Fynbos Palaeoecology: a Preliminary Synthesis, pp. 116-138.

Kounov, A., Niedermann, S., de Wit, M.J., Viola, G., Andreoli, M., Erzinger, J., 2007. Present day denudation rates bearing on erosion processes along selected west- and south-facing sections of the South African Great Escarpment and its interior derived from in situ produced cosmogenic 3He and 21Ne. South African Journal of Geology 110, 235–248.

Krige, A.V., 1927. An examination of the Tertiary and Quaternary changes of sea-level in South Africa, with special stress on the evidence in favour of a recent world-wide sinking of ocean-level. Annuals of the University of Stellenbosch, 1-48.

Lambeck, K., Chappell, J., 2001. Sea level change through the last glacial cycle. Science 292(5517), 679-686 Lawrence, K.T., Zhonghui, L., Herbert, T.D., 2006. Evolution of the eastern tropical Pacific through Plio-Pleistocene glaciation. Science 312, 79-83.

Lear, C. H., Elderfield., H., Wilson, P. A., 2000. Cenozoic deep-sea temperatures and global ice volumes from Mg/Ca in benthic foraminiferal calcite. Science 287, 269-272.

Leatherman, S.P., 1983. Barrier dynamics and landward migration with Holocene sea-level rise. Nature 301, 415-418.

Leinfelder, ¸1987. Formation and significance of black pebbles from the Ota Limestone (Upper Jurassic, Portugal). Facies 17(1), 159-169

Lisiecki, L.E., Raymo, M.E., 2005. A Pliocene–Pleistocene stack of 57 globally distributed benthic δ18O records. Paleoceanography 20, 1003–1020.

Lisiecki, L. E., 2010. Links between eccentricity forcing and the100,000-year glacial cycle. Nature Geoscience 3, 349–352.

Luft, F.F., Luft, J.L., Jr., Chemale, F., Jr., Lelarge, M.L.M.V., Avila, J.N., 2005. Post-Gondwana break-up record constraints from apatite fission track thermochronology in NW Namibia, Radiation Measurements 39 (6), 675-679.

Lutjeharms, J.R.E., 1981. Features of the southern Agulhas Current circulation from satellite remote sensing. South African Journal of Science 77, 231–236.

Lutjeharms, J.R.E., 2006. The Agulhas Current. Springer-Verlag, Berlin, 329 pp.

MacHutchon, M.R., 2012. The geological evolution and sedimentary dynamics of Hout Bay, South Africa. Unpublished M.Sc. Thesis, University of Cape Town, South Africa.

Mackay, A., Welz, A., 2008. Engraved ochre from a Middle Stone Age context at Klein Kliphuis in the Western Cape of South Africa. Journal of Archaeological Science 35, 1521-1532.

Malan, J.A., 1990. The stratigraphy and sedimentology of the Bredasdorp Group, southern Cape Province. Unpublished M.Sc. Thesis, University of Cape Town, South Africa.

Malan, J. A., Viljoen, J. H. A., 2008. Southern Cape Geology: evolution of a rifted margin. AAPG International Conference and Exhibition field excursion FT07 guidebook 30 October – 3 November, 60 pp.

Marean, C.W., Assefa, Z., 2005. The Middle and Upper Pleistocene African record for the biological and behavioral origins of modern humans. In: Stahl, A.B. (Ed.), African Archaeology. Blackwell, New York, pp. 93-129.

Marean, C.W., Bar-Matthews, M., Bernatchez, J., Fisher, E., Goldberg, P., Herries, A.I.R., Jacobs, Z., Jerardino, A., Karkanas, P., Minichillo, T., Nilssen, P.J., Thompson, E., Watts, I., Williams, H., 2007. Early human use of marine resources and pigment in South Africa during the Middle Pleistocene. Nature 449, 905-908.

Marean, C.W., 2010. Pinnacle Point Cave 13B (Western Cape Province, South Africa) in context: The Cape Floral kingdom, shellfish, and modern human origins. Journal of Human Evolution 59, (3-4) 425-443.

Marean, C. W., 2011. Coastal South Africa and the co-evolution of the modern human lineage and coastal adaptations, In: Trekking the Shore: Changing Coastlines and the Antiquity of Coastal Settlement, N. Bicho, J. A. Haws, L. G. Davis, eds., New York: Springer, pp. 421-440.

Marker, M.E., 1987. A note on marine benches of the southern Cape. South African Journal of Geology 90, 120–123.

Marker, M.E., Miller, D.E., 1993. A mid-Holocene high stand of the sea at Knysna. South African Journal of Science 89, 100–102.

Marker, M.E., Holmes, P.J., 2005. Landscape evolution and landscape sensitivity: the case of the southern Cape. South African Journal of Science 101, 53-60.

Marker, M.E. Holmes, P.J., 2010. The geomorphology of the Coastal Platform in the southern Cape. South African Geographical Journal 92(2), 105-116.

Marshall, S.J., 2013. Solution proposed for ice-age mystery. Nature 500, 159-160.

Martin, A. K., 1985. The geology of the seafloor between the Mossel Bay/Stilbaai coast and the EM and FA drill sites, Marine Geoscience division National Institute for Oceanology Council for Scientific and Industrial Research report C/SEA, 8510.

Martin, A.K., Flemming, B.W., 1986. The Holocene shelf sediment wedge off the south and east coast of South Africa. In: Knight, R.J. & McLean, J.R. (eds) Shelf Sands and Sandstones. Canadian Society of Petroleum Geologists Memoir 2, 27–44.

Martin, A.K., Hartnady, C.J.H., 1986. Plate tectonic development of the southeast Indian Ocean: A revised reconstruction of East Antarctica and Africa. Journal of Geophyiscal Research 91, 4767-4786.

Martin, A.K., Flemming, B.W., 1987. Aeolianites of the South African coastal zone and continental shelf as sea-level indicators. South African Journal of Science 83, 507-508.

Martin, A.R.H., 1962. Evidence relating to the Quaternary history of the Wilderness lakes. Transactions of the Geological Society of South Africa 65, 19-45.

Maslin, M., Seidov, D., Lowe, J., 2001. Synthesis of the nature and causes of rapid climate transitions during the Quaternary. Geophysical Monograph 126, 9–52.

Masselink, G., Hughes, M., 2003. An Introduction to Coastal Processes and Geomorphology. Hodder Arnold, London.

Matthews, T., Rector, A., Jacobs, Z., Herries, A.I.R., Marean, C.W., 2011. Environmental implications of micromammals accumulated close to the MIS 6 to MIS 5 transition at Pinnacle Point Cave 9 (Mossel Bay, Western Cape Province, South Africa). Palaeogeography, Palaeoclimatology, Palaeoecology 302, 213-229.

Maud, R. R., Botha, G. A., 2000. Deposits of the south eastern and southern coasts. In: Partridge, T. C., Maud, R. R. (Eds.) The Cenozoic of southern Africa. Oxford University Press, 19-32.

Maud, R. R., 2012. Macroscale geomorphic evolution. In: Holmes, P., Meadows, M. (Eds.), Southern African geomorphology: Recent trends and new directions. SUN Press Bloemfontein, 5-23.

Mayer, L., Hughes-Clarke, J.E., 1995 STRATAFORM Cruise Report: R/V Pacific Hunter, Multibeam Survey, July 14 – 28, 1995.

McDougall, I., Brown, F.H., Fleagle, J.G., 2005. Stratigraphic placement and age of modern humans from Kibish, Ethiopia. Nature 433, 733–736.

MacGregor, D. 2013 - Manganese Deposits of the Cape Peninsula, South Africa. Unpublished M.Sc. Thesis, University of Cape Town, South Africa.

McMillan, I.K., 1989. Victoriella conoidea (Rutten, 1914): a guide to foraminifera for the later Aquitanian (Early Miocene) marine rocks of southern Africa. South African Journal of Geology 92 (2), 95–101.

McMillan I.K., 2003. Foraminiferally defined biostratigraphic episodes and sedimentation pattern of the Cretaceous drift succession (Early Barremian to Late Maastrichtian) in seven basins on the South African and southern Namibian continental margin. South African Journal of Science 99(11/12), 537-576.

Meadows, M.E., Rogers, J., Lee-Thorp, J.A., Bateman, M.D., Dingle, R.V., 2002. Holocene geochronology of a continental-shelf mudbelt off southwestern Africa. Holocene 12, 59–67.

Miall, A.D., 1997. The geology of stratigraphic sequences. Springer, 433pp.

Midgley, D.C., Pitman, W.V., 1969. Surface water resources of South Africa: Hydrological research unit report 2(69). University of the Witwatersrand, 128 pp.

Milani, E.J., de Wit, M.J., 2008. Correlations between classic Parana and Cape-Karoo basins of South America and southern Africa and their basin infills flanking the Gondwanides: Du Toit revisited. InWest Gondwana: Pre-Cenozoic Correlations Across the South Atlantic Region. In: Pankhurst, R.J., Trouw, R.A.J., de Brito Neves, B.B., de Wit, M.J (Eds.), Geological Society, London, Special Publication, 294, pp. 319–342.

Miller, K. G., Fairbanks, R. G., Mountain, G. S., 1987. Tertiary oxygen isotope synthesis, sea level history, and continental margin erosion. Paleoceanography 2(1), 1-19.

Miller, K. G., Kominz, M. A., Browning, J. V., Wright, J. D., Mountain, G. S., Katz, M. E., Sugarman, P.J., Cramer, B.S., Christie-Blick, N., Pekar, S. F., 2005a. The Phanerozoic record of global sea-level change. Science 310(5752), 1293-1298.

Miller, K. G., Wright, J. D., Browning, J. V., 2005b. Visions of ice sheets in a greenhouse world. Marine Geology 217(3), 215-231.

Mitchum, R.M. Jr., Vail, P.R., 1977. Seismic Stratigraphy and global changes in Sea-level, part 7, seismic stratigraphic interpretation procedure. In: Payton, C.E. (Ed.), Seismic Stratigraphy - Applications to Hydrocarbon exploration. Amreican Association of Petroleum Geology Memoir Memoir, 26 Boulder, Colorado, 135-143.

Montenat, C., 1981. Observations nouvelles sur les croûtes calcaires pleistocènes du Sud-Est de l'Espagne (Province d'Alicante et de Murcia). Géol. Mediterr. 8/3, 137–154.

Mucina, L., Rutherford, M.C., 2006. The Vegetation of South Africa, Lesotho, and Swaziland. South African National Biodiversity Institute, Pretoria.

Mucina, L., Rutherford, M.C., Powrie, L.W., 2006. Vegetation atlas of South Africa, Lesotho and Swaziland. In: Mucina, L., Rutherford, M.C. (Eds.), The Vegetation of South Africa, Lesotho, and Swaziland. South African National Biodiversity Institute, Pretoria, pp. 748-790.

Murray-Wallace, C.V., Brooke, B.P., Cann, J.H., Belperio, A.P., Bourman, R.P., 2001. Whole-rock aminostratigraphy of the Coorong Coastal Plain, South Australia: towards a 1 million year record of sea-level highstands. Journal of the Geological Society, London 158, 111-124.

Neumeier, U., 1999. Experimental modelling of beachrock cementation under microbial influence. Sedimentary Geology 126(1-4), 35-46.

Newton, A.R., Shone, R.W., Booth, P.W.K., 2006. The Cape Fold Belt. In: Johnson, M. R., Annhauser, C. R. and Thomas, R. J. (Eds.), The Geology of South Africa. Geological Society of South Africa, Johannesburg/Council for Geoscience Pretoria, 521-531.

Nichols, G., 2009. Sedimentology and Stratigraphy Second Edition. Wiley-Blackwell, 432 pp.

Nordfjord, S., Goff, J.A., Austin, J.A., Gulick, S.P.S., 2006. Seismic facies of incised valley fills, New Jersey continental shelf: implications for erosion and preservation processes acting during the latest Pleistocene-Holocene transgression. Journal of Sedimentary Research 76, 1284-1303.

Nordfjord, S., Goff, J. A., Austin, J. A. Jr., Duncan, L. S., 2009. Shallow stratigraphy and complex transgressive ravinement on the New Jersey middle and outer continental shelf. Marine Geology 266, 232-243.

North Greenland Ice Core Project Members, 2004. High-resolution record of Northern Hemisphere climate extending into the last interglacial period. Nature 431, 147-151.

Nummedal, D., Swift, D. J. P., 1987. Transgressive stratigraphy at sequence-bounding unconformities: some principles derived from Holocene and Cretaceous examples. In: Nummedal, D., Pilkey, O. H., Howard, J. D. (Eds.), Sea Level Fluctuation and Coastal Evolution. SEPM, Tulsa, 241-260.

Nummedal, D., Riley, G.W., Templet P.L., 1993. High-resolution sequence architecture; a chronostratigraphic model based on equilibrium profile studies. In: H.W. Posamentier, C.P. Summerhayes, B.U. Haq, G.P. Allen (Eds.), Sequence Stratigraphy and Facies Associations, Special Publication of the International Association of Sedimentologists, 55–68.

Nyblade, A.A., Sleep, N.H., 2003. Long lasting epeirogenic uplift from mantle plumes and the origin of the Southern African Plateau. Geochemistry, Geophysics, Geosystems 4(12).

Parker, R.J., 1975. The petrology and origin of some glauconitic and glauco-conglomeratic phosphorites from the South Africa continental margin. Journal of Sedimentary Petrology 45(1), 230-242.

Parker, R. J., Siesser, W. G. 1972. Petrology and origin of some phosphorites from the South African continental margin. Journal of Sedimentary Research 42(2), 434-440.

Parkinson, R., 2001. High-resolution site surveys. Taylor and Francis, London, 230pp.

Partridge, T.C., Maud, R.R., 1987. Geomorphic evolution of southern Africa since the Mesozoic. South African Journal of Geology 90, 179-208.

Partridge, T.C., Maud, R.R., 2000. Macro-scale geomorphic evolution of southern Africa. In: Partridge, T.C. and Maud, R.R. (Eds.), The Cenozoic of Southern Africa. Oxford Monographs on Geology and Geophysics 40, 3-18.

Paton, D.A., Macdonald, D.I.M., Underhill, J.R., 2006. Applicability of thin or thick skinned structural models in a region of multiple inversion episodes, southern. South African Journal of Structural Geology 28, 1933-1947.

Peltier, W.R., 1998. Postglacial variations in the level of the sea: Implications for climate dynamics and solid earth geophysics. Reviews of geophysics 36(4), 603-689.

Peltier, W. R., Fairbanks, R. G., 2006. Global glacial ice volume and Last Glacial Maximum duration from an extended Barbados sea level record. Quaternary Science Reviews 25(23), 3322-3337.

Penland, S., Suter, J.R., Boyd, R., 1985. Barrier island arcs along abandoned Mississippi River deltas. Marine Geology 63, 197-223.

Pether, J. 1994. Molluscan evidence for enhanced deglacial advection of Agulhas water in the Benguela Current, off southwestern Africa. Palaeogeography, Palaeoclimatology, Palaeoecology, 111, 99–117.

Pether, J., Roberts, D.L., Ward, J. 2000. Deposits of the West Coast. In: Partridge, T.C., Maud, R.R. (eds) The Cenozoic of Southern Africa. Oxford Monographs on Geology and Geophysics, 40, 33–54.

Petroleum Agency South Africa (PASA), 2012. Northern Pletmos Basin. Exploration opportunities offshore South Africa's south coast. Petroleum Agency South Africa information brochure, 4pp.

Pickering, R., Jacobs, Z., Herries, A.I., Karkanas, P., Bar-Matthews, M., Woodhead, J.D., Kappen, P., Fisher, E., Marean, C.W., 2013. Paleoanthropologically significant South African sea caves dated to 1.1-1.0 million years using a combination of U-Pb, TT-OSL and palaeomagnetism. Quaternary Science Reviews 65, 39-52.

Plint, A.G., 1988. Sharp-based shoreface sequences and offshore bars in the Cardium formation of Alberta; their relationship to relative changes in sea level. In: Wilgus, C.K., Hastings, B.S., Kendall, C.G.St.C., Posamentier, H.W., Ross, C.A., Van Wagoner, J.C. (Eds.), Sea Level Changes—An Integrated Approach, 42. SEPM Special Publication 42, 357–370.

Porat, N., Botha, G., 2008. The luminescence chronology of dune development on the Maputaland coastal plain, southeast Africa. Quaternary Science Reviews 27, 1024-1046.

Portenga, E.W., and Bierman, P.R., 2011, Understanding Earth's eroding surface with 10Be: GSA Today 21(8), 4–10.

Posamentier, H.W., Jervey, M.T, Vail, P.R., 1988. Eustatic controls on clastic deposition, part 1, conceptual framework. In: Wilgus, C.K., Hastings, B.S., Kendall, C. G. St. C., Posamentier, H.W., Ross, C.A. and Van Wagoner, J.C. (Eds.), Sea-level Changes and integrated approach. Society of Economic Palaeontologists and Mineralogists Special Publication 42, 109-124.

Posamentier, H.W., Vail, P.R., 1988. Eustatic controls on clastic deposition, part 2, sequence and systems tracts. In: Wilgus, C.K., Hastings, B.S., Kendall, C. G. St. C., Posamentier, H.W., Ross, C.A. and Van Wagoner, J.C. (Eds.), Sea-level Changes and integrated approach. Society of Economic Palaeontologists and Mineralogists Special Publication 42, 125-154.

Posamentier, H.W., Allen, G.P., 1999. Siliciclastic sequence stratigraphy: concepts and applications. Concepts in Sedimentology and Palaeontology. Society of Economic Palaeontologists and Mineralogists (SEPM) 7, 210pp.

Prescott, J.R., Hutton, J.T., 1994. Cosmic ray contributions to dose rates for luminescence and ESR dating: large depths and long-term time variations. Radiation Measurements 23, 497-500.

Pye, K., 1983. Coastal dunes. Progress in Physical Geography 7, 531-557.

Pysklwec, R.N., Mitrovica, J.X., 1999. The role of subduction induced subsidence in the evolution of the Karoo Basin. J. Geol. 107, 155–164.

Ramsay, P.J., 1995. 9000 Years of sea-level change along the Southern African coastline. Quaternary International 31, 71-75.

Ramsay, P.J. 1996. Quaternary marine geology of the Sodwana Bay continental shelf, northern KwaZulu-Natal. Council for Geoscience Bulletin, 117, 86 pp.

Ramsay, P.J., Cooper, J.A.G., 2002. Late Quaternary sea-level change in South Africa. Quaternary Research 57, 82-90.

Raymo, M. E., 1994. The initiation of Northern Hemisphere glaciation. Annual Review of Earth and Planetary Sciences 22, 353-384.

Reddering, J.S.V., 1988. Evidence for a middle Holocene transgression, Keurbooms estuary, South Africa. Palaeoecology of Africa 19, 79–86.

Rees-Jones, J., 1995. Optical dating of young sediments using fine-grain quartz. Ancient TL 13(2), 9-14.

Reinhold, C., 1999. Dog-tooth cements: indicators of different diagenetic environments. Zetralblatt für eologie und Paläontologie 1, 1221-1235.

Reinson, G.E., 1984. Barrier-island and associated strand-plain systems. In: Reading, H.G. (Ed.), Facies Models, Geoscience Canada Reprint Series, Geological Association of Canada, 119–140.

Richter, D.K., 1979. Die Stufen der meteorisch-vadosen Umwandlung von Mg-Kalzit in Kalzit in rezenten bis pliozänen Biogenen Griechenlands. Neues Jahrbuch für Geologie und Paläontologie 158, 277–333.

Rohling, E.J., Grant, K., Bolshaw, M., Roberts, A.P., Siddall, M., Hemleben, C., Kucera, M., 2009. Antarctic temperature and global sea level closely coupled over the past five glacial cycles. Nature Geoscience 2, 500-504.

Roberts, D.L., Berger, L., 1997. Last Interglacial (c. 117 kyr) human footprints, South Africa. South African Journal of Science 93, 349-350.

Roberts, D.L., Botha, G.A., Maud, R.R., Pether, J., 2006. Coastal Cenozoic deposits. In: M.R. Johnson, C.R., Annhauser and R.J. Thomas (Eds.), The Geology of South Africa. Geological Society of South Africa/Council for Geoscience Pretoria, 605-628.

Roberts, D.L., Bateman, M.D., Murray-Wallace, C.V., Carr, A.S., Holmes, P.J., 2008a. Fossil elephant trackways, sedimentation and diagenesis in OSL/AAR-dated Late Quaternary coastal aeolianites: Still Bay, South Africa. Palaeogeography, Palaeoclimatology, Palaeoecology 257, 261-279.

Roberts, D. L., Viljoen, J. H. A., Macey, P., Nhleko, L., Cole, D. I., Chevallier, L. P., Gibson, L., Stapelberg, F., 2008b. The geology of George and environs. Council for Geoscience map explanation: sheets 3322CD and 3422AB, 76 pp.

Roberts, D.L., Bateman, M.D., Murray-Wallace, C.V., Carr, A.S., Holmes, P.J., 2009. West coast dune plumes: climate driven contrasts in dunefield morphogenesis along the western and southern South African coasts. Palaeogeography, Palaeoclimatology, Palaeoecology 271, 24-38.

Roberts, D.L., Matthews, T., Herries, A.I.R., Boulter, C., Scott, L., Dondo, C., Mthembi, P., Browning, C., Smith, R. H., Haarhoff, P., Bateman, M.D., 2011. Regional and global context of the Late Cenozoic Langebaanweg (LBW) palaeontological site: West Coast of South Africa. Earth-Science Reviews 106(3-4), 191-214.

Roberts, D.L., Karkanas, P., Jacobs, Z., Marean, C.W., Roberts, R.G., 2012. Melting ice sheets 400,000 yr ago raised sea level by 13 m: Past analogue for future trends. Earth and Planetary Science Letters 357–358, 226–237.

Roberts, D.L., Cawthra, H.C., Musekiwa, C., 2013. Dynamics of late Cenozoic aeolian deposition along the South African coast: A record of evolving climate and ecosystems. In: Martini, I. P., Wanless, H. R. (Eds.), Sedimentary Coastal Zones from High to Low Latitudes: Similarities and Differences. Geological Society, London, Special Publications 388.

Rogers, J. 1971. Sedimentology of Quaternary deposits on the Agulhas Bank. Unpublished MSc Thesis, University of Cape Town.

Rohling, E.J., Grant, K., Bolshaw, M., Roberts, A.P., Siddall, M., Hemleben, Ch, Kucera, M., 2009. Antarctic temperature and global sea level closely coupled over the past five glacial cycles. Nature Geoscience 2, 500-504.

Roy, P.S., Thom, B.G., 1981. Latequaternary marine deposition in New South Wales and southern Queensland: an evolutionary model. Journal of Geology Society of Australia 28, 471-489.

Roy, P.S., 1984 New South Wales estuaries: their origin and evolution, In Thom, B.G. (Ed.), Coastal Geomorphology in Australia. Academic Press, Sydney. 99–121.

Rozendaal, A., Gresse, P.G., Scheepers, R., Le Roux, J.P., 1999. Neoproterozoic to Early Cambrian crustal evolution of the Pan-African Saldania Belt, South Africa. Precambrian Research 97 (3–4), 303–323.

Rust I.C., Theron, J.N., 1964. Some aspects of the Table Mountain Series near Vanrhynsdorp. Transactions of the Geological Society of South Africa 62, 131–136.

Ryklief, R., 2012. Population dynamics of the white shark, Carcharodon carcharias, at Mossel Bay, South Africa. Master of Science Thesis, Nelson Mandela Metropolitan University, 116 pp.

Scharf, T., Codilean, A.T., de Wit, M.J., Jansen, J.D., Kubik, P.W., 2013. Strong rocks sustain ancient postorogenic topography in southern Africa. Geology 41(3), 331-334.

Scheepers, R., Schoch, A. E., 2006. The Cape Granite Suite. In: Johnson, M. R., Annhauser, C. R. and Thomas, R. J. (Eds.), The Geology of South Africa. Geological Society of South Africa, Johannesburg/Council for Geoscience, Pretoria, 421-433.

Schink, J.C., Stockwell, J.H., Ellis, R. A., 1979. An improved device for gasometric determination of carbonate in sediment. Journal of Sedimentary Petrology 48, 651-653.

Schulz, M., 2002. On the 1470-year pacing of Dansgaard–Oeschger warm events. Paleoceanography 17, 41-49.

Schumm, S. A., 1985. Patterns of alluvial rivers. Annual Review of Earth and Planetary Sciences 13, 5.

Siesser, W.G., 1978. Leg 40 results in relation to continental shelf and onshore geology. Initial Reports of the Deep Sea Drilling Project 40, 965-979.

Smith, T.M., Tafforeau, P., Reid, D.J., Grün, R., Eggins, S., Boutakiout, M., Hublin, J.-J., 2007. Earliest evidence of modern human life history in North African early *Homo sapiens*. Proceedings of the National Academy of Science 104, 6128-6133.

Sommerfield, C.K., Lee, H.J., 2004. Across-shelf sediment transport since the Last Glacial Maximum, southern California margin. Geology 32, 345–348.

Stanford, J.D., Rohling, E.J., Hunter, S.E., Roberts, A.P., Rasmussen, S.O., Bard, E., McManus, J., Fairbanks, R.G., 2006. Timing of meltwater pulse 1a and climate responses to meltwater injections. Paleoceanography 21, 4103.

Stankiewicz, J., Ryberg, T., Schultze, A., Lindique, A., Weber, M.H., de Wit, M.J., 2007. Results from the wideangle seismic refraction lines in the southern Cape. Inkaba yeAfrica special volume. South African Journal of Geology 110, 407–418.

Steig, E. J., Brook, E. J., White, J. W. C., Sucher, C. M., Bender, M. L., Lehman, S. J., Clow, G. D., 1998. Synchronous climate changes in Antarctica and the North Atlantic. Science 282(5386), 92-95.

Stevenson, I. R., McMillan, I. K., 2004. Incised valley fill stratigraphy of the Upper Cretaceous succession, proximal Orange Basin, Atlantic margin of southern Africa. Journal of the Geological Society 161(2), 185-208.

Stocker, T.F., Johnsen, S.J., 2003. A minimum thermodynamic model for the bipolar seesaw. Paleoceanography 18(4), 1087.

Stubblefield, W.L., McGrail, D.W., Kersey, D.G., 1984. Recognition of transgressive and post-transgressive sand ridges on the New Jersey continental shelf. In: Tillman, R.W., siemers, C.T. (Eds.), Siliciclastic shelf sediments. Society of Econimic Palaeontologists and Mineralogists Special Publication 34, 1-23.

Swift, D.J.P., 1976. Coastal sedimentation. In: Stanley, D.J., Swift, D.J.P., (Eds.) Marine sediment and transport and environmental management. Wiley New York, 255-310.

Swift, D. J. P., Holliday, B., Avignone, N., Shideler, G., 1972. Anatomy of a shoreface ridge system, False Cape, Virginia. Marine Geology 12, 59-84.

Taljaard, J.J., 1996. Atmospheric circulation systems, synoptic climatology and weather phenomena of South Africa. Part 6, Rainfall in South Africa, 98 pp.

Tankard, A.J., Schweitzer, F.R., 1974. Geology of Die Kelders Cave and environs – palaeoenvironmental study. South African Journal of Science 70(12), 365-369.

Texier, P.J., Porraz, G., Parkington, J., Rigaud, J.P., Poggenpoel, C., Miller, C., Tribolo, C., Cartwright, C., Coudenneau, A., Klein, R., Steele, T., Verna, C., 2010. A Howiesons Poort tradition of engraving ostrich eggshell containers dated to 60,000 years ago at Diepkloof Rock Shelter, South Africa. Proceedings of the National Academy of Sciences 107, (14) 6180-6185.

Thackeray, F., 1988. Molluscan fauna from Klasies River, South Africa. South African Archaeological Bulletin 43, 27-32.

Thamm, A.G., Johnson, M.R., 2006. The Cape Supergroup. In: Johnson, M. R., Annhauser, C. R. and Thomas, R. J. (Eds.), The Geology of South Africa. Geological Society of South Africa, Johannesburg/Council for Geoscience Pretoria, 443-461.

Thompson, E., 2009. Acheulean Artifact Accumulation and Early Hominin Land Use, Garden Route Casino Road, Pinnacle Point, South Africa. Geoarchaeology 24(4), 402–428.

Tinker, J.H., de Wit, M.J., Brown, R., 2008a.Mesozoic exhumation of the southern Cape, South Africa, quantified using apatite fission track thermochronology. Tectonophysics, 455, 77–93.

Tinker, J.H., de Wit, M.J., Brown, R.W., 2008b. Linking source and sink: evaluating the balance between onshore erosion and offshore sediment accumulation since Gondwana break-up, South Africa. Tectonophysics 455, 94–103.

Tinley, K.L., 1985. Coastal Dunes of South Africa. South African National Scientific Programmes Report No. 109. Foundation for Research Development Council for Scientific and Industrial Research, Pretoria, 300 pp.

Tishkoff, S.A., Gonder, M.K., Henn, B.M., Mortensen, H., Knight, A., Gignoux, C., Fernandopulle, N., Lema, G., Nyambo, T.B., Ramakrishnan, U., Reed, F.A., Mountain, J.L., 2007. History of Click-Speaking Populations of Africa Inferred from mtDNA and Y Chromosome Genetic Variation. Molecular Biology and Evolution 24, (10) 2180-2195.

Toerien, D.K., 1979. Die geologie van die gebied Oudtshoorn. Toeligting van blad 3322, Skaal 1: 250 000. Department van Mynwese, Geologiese Opname van Suid-Afrika, 34 pp.

Trenhaile, A.S., 1987. The geomorphology of rock coasts. Clarendon Press, Oxford. 384 pp.

Tripp, R.T., 1967. An atlas of coastal drifts, Cape Town to Durban. University of Cape Town Department of Oceanography, 10 pp.

Trumbull, R.B., Reid, D.L., de Beer, C., van Acken, D., Romer, R.L., 2007. Magmatism and continental breakup at the West Margin of Southern Africa: a geochemical comparison of dolerite dikes from NW Namibia and the Western Cape. South African Journal of Geology 110, 477–502.

Tucker, M.E., Wright, V.P., 1990. Carbonate sedimentology. Blackwell Scientific Press, Oxford. 482 pp.

Tyson, P.D., 1999. Late-Quaternary and Holocene palaeoclimates of southern Africa: a synthesis. South African Journal of Geology 102, 335–349.

Uenzelmann-Neben, G., Sclutter, P., Weigelt, E., 2007. Cenozoic ocean circulation within the South African gateway: indications from seismic stratigraphy. South African Journal of Geology 110, 275–294.

Uenzelmann-Neben, G., Huhn, K., 2009. Sedimentary deposits on the southern South African continental margin: Slumping versus non-deposition or erosion by oceanic currents? Marine Geology 266(1), 65-79.

Vail, P. R., Mitchum Jr., R. M., Todd, R. G., Widmier, J. M., S. Thompson III, J.B. Sangree, J. B., Bubb, J. N., Hatlelid, W. G., 1977. Seismic stratigraphy and global changes of sea level. In Payton, C.E. (Ed.), Seismic stratigraphy -Applications to hydrocarbon exploration. American Association Petroleum Geologists Memoir 26, 49-212.

Vail, P.R., 1987. Seismic stratigraphy interpretation using sequence stratigraphy. Part 1: seismic stratigraphy interpretation procedure. In A.W. Bally, (Ed.), Atlas of Seismic Stratigraphy Volume 1: AAPG Studies in Geology 27, 1–10.

Van Andel, T.H., 1989. Late Pleistocene sea levels and human exploitation of the shore and shelf of southern South Africa. Journal of Field Archaeology 16, 133-155.

Van Der Beek, P.A., Summerfield, M.A., Braun, J., Brown, R.W., Fleming, A., 2002. Modeling postbreakup landscape development and denudational history across the Southeast African (Drakensberg Escarpment) margin. J. Geophys. Res. 107, 2351.

Van Sickel, W. A., Kominz, M. A., Miller, K. G., Browning, J. V., 2004. Late Cretaceous and Cenozoic sea-level estimates: backstripping analysis of borehole data, onshore New Jersey. Basin Research 16(4), 451-465.

Van Zinderen Bakker, E.M., 1976. The evolution of late-Quaternary palaeoclimates of southern Africa. Palaeoecology of Africa 9, 160-202.

Van Zyl, M., 1997. Landscape evolution of the Garden Route between the Bloukrans River and Mossel Bay. Master of Science thesis, University of Port Elizabeth. 133 pp.

Vieira, M.M., De Ros, L.F., 2006. Cementation patterns and genetic implications of Holocene beachrocks from northeastern Brazil. Sedimentary Geology 192, 207-230.

Viljoen, J.H.A., Malan, J.A., 1993. Die geologie van die gebeide 3421BB Mosselbaai en 3422AA Herbertsdale. Toeligting tot blaaie 3421BB en 3422AA, Skaal 1: 50 000. Geologise Opname van Suid-Afrika, 79pp.

Visser, D.J.L. 1998. The geotectonic evolution of South Africa and offshore areas. Council for Geoscience, Pretoria, 319pp.

Voelker, A.H.L., 2002. Global distribution of centennial-scale records for Marine Isotope Stage (MIS) 3: a database. Quaternary Science Reviews 21, 1185–1212.

Waelbroeck, C., Labeyrie, L., Michela, E., Duplessy, J.C., McManus, J.F., Lambeck, K., Balbon, E., Labracherie, M., 2002. Sea-level and deep water temperature changes derived from benthic foraminifera isotopic records. Quaternary Science Reviews 21, 295-305.

Walker, N.D., 1990. Links between South African summer rainfall and temperature variability in the Agulhas and Benguela Current systems. Journal of Geophysical Research 95, 3297–3319.

Walker, R.G., 1992. Facies, facies models and modern stratigraphic concepts. In Walker, R.G., James, N.P. (Eds.), Facies Models: Response to Sea Level Changes, Geological Association of Canada, 1–14.

Watkeys, M.K., 2006. Gondwana break-up: A South African perspective. In: Johnson, M. R., Annhauser, C. R. and Thomas, R. J. (Eds.), The Geology of South Africa. Geological Society of South Africa, Johannesburg/Council for Geoscience Pretoria, 531-539.

Weaver, A. J., Saenko, O. A., Clark, P. U., Mitrovica, J. X., 2003. Meltwater pulse 1A from Antarctica as a trigger of the Bølling-Allerød warm interval. Science 299(5613), 1709-1713.

Werner, B.T., Fink, T.M., 1993. Beach cusps as self-organized patterns. Science 260(5110), 968-971.

Westley, K., Quinn, R., Forsythe, R., Plets, R., Bell, T., Benetti. S., McGrath, F., Robinson, R., 2011. Mapping Submerged Landscapes Using Multibeam Bathymetric Data: a case study from the north coast of Ireland. The International Journal of Nautical Archaeology 40(1), 99-112.

White, T.D., Asfaw, B., De Gusta, D., Gilbert, H., Richards, G.D., Suwa, G., Clark Howell, F., 2003. Pleistocene *Homo sapiens* from Middle Awash, Ethiopia. Nature 423(6941) 742-747.

Whitfield, A.K., 1983. Effect of prolonged aquatic macrophyte senescence on the biology of the dominant fish species at Swartvlei. South African Journal of Science 79, 153-157.

Wigley, R.A., 2004. Sedimentary facies from the Head of the Cape Canyon: Insights into the Cenozoic evolution of the western margin of South Africa. Unpubl PhD Thesis, University of Cape Town, South Africa.

Wigley, R.A., Compton, J.S., 2006. Late Cenozoic evolution of the outer continental shelf at the Head of the Cape Canyon, South Africa. Marine Geology 226, 1–23.

Wing, S.L., 1984. Relation of paleovegetation to geometry and cyclicity of some fluvial carbonaceous deposits. Journal of Sedimentary Research 54(1).

Wolmarans, L.G., du Preez, J. W., 1985. The geology of the St. Lucia area. Geological Survey map explanation: sheet 2732, 42 pp.

Woodborne, M.W., 1991. The geology of the diamondiferous inner shelf off Namaqualand between Stompneus Bay and White Point, just north of the Buffels River. Bulletin of the Geological Survey of South Africa 99, 68 pp.

Woodroffe, S. A., Horton, B. P., 2005. Holocene sea-level changes in the Indo-Pacific. Journal of Asian Earth Sciences 25(1), 29-43.

Yokoyama, Y., Esat, T.M., Lambeck, K., 2001. Coupled climate and sea-level changes deduced from Huon Peninsula coral terraces of the last ice age. Earth Planetary Science Letters 193, 579-587.

Yoshida, S., Steel, R.J., Dalrymple, R.W., 2007. Changes in depositional processes—an ingredient in a new generation of sequence-stratigraphic models. Journal of Sedimentary Research 77(6), 447-460.

Zaitlin, B.A., Dalrymple, R.W., Boyd, R., 1994. The stratigraphic organisation of incised valley systems associated with relative sea-level change. In: Dalrymple, R.W., Boyd, R.J., Zaitlin, B.A., (Eds.), Incised valley systems: Origin and sedimentary Sequences. SEPM Special Publication 51, 45-60.

Zecchin, M., 2010. Towards the standardization of sequence stratigraphy: Is the parasequence concept to be redefined or abandoned? Earth-Science Reviews 102(1), 117-119.

Zhong, S., Mucci, A., 1989. Calcite and aragonite precipitation from seawater solutions of various salinities: precipitation rates and overgrowth compositions. Chemical Geology 78, 283–299.

APPENDIX I

Rock sample numbers, locations and classifications. Prefix O denotes offshore rock samples, all other letters are shoreline samples (A-V, excluding O).

Sample No.	Easting	Northing	Rock type	Thin sections	Sample No.	Easting	Northing	Rock type	Thin sections
A1	600534	6214412	Calcarenite	1	O11	613501	6228615	Calcarenite	1
A2	600534	6214412	Calcarenite	1	O22	613018	6229302	Calcarenite	1
B1	592696	6214061	Calcrete	1	O23	612554	6228579	Calcarenite	1
C1	608022	6216619	Quartz arenite	1	O24	615613	6225541	Calcarenite	1
C2	608270	6216887	Quartz arenite	1	O26	614071	6227063	Calcarenite	1
C3	607630	6216371	Quartz arenite	1	O27	613061	6227076	Calcarenite	1
D1	603360	6224107	Calcarenite	1	O28	616126	6226504	Calcarenite	1
D2	603360	6224107	Cemented back-barrier	1	O29	616795	6227038	Calcarenite	1
E1	6085300	6228640	Calcarenite	1	O3	615796	6227038	Calcarenite	1
E6	6087970	6228760	Calcarenite	1	O30	616251	6227111	Calcarenite	1
E2	6085260	6228630	Calcarenite	1	O32	615402	6230000	Calcarenite	1
E3	6085260	6228570	Calcarenite	1	O33	615308	6227366	Calcarenite	1
E4	6085580	6228590	Calcarenite	1	O35	615157	6227757	Calcarenite	1
E5	6085170	6228610	Calcarenite	1	O36	615620	6228543	Calcarenite	1
E7	6085400	6228580	Calcarenite	1	O37	613841	6229915	Calcarenite	1
E8	6085120	6228620	Calcarenite	1	O38	615443	6228712	Calcarenite	1
E9	6087400	6228710	Calcarenite	1	O39	615101	6229193	Calcarenite	2
F1	6069300	6227880	Calcarenite	1	O4	615531	6227271	Calcarenite	1
F2	6070500	6227910	Calcarenite	1	O40	616195	6229492	Calcarenite	1
F3	6070400	6227920	Calcarenite	1	O41	614325	6229067	Calcarenite	2
F4	6070790	6227900	Calcarenite	1	O42	612521	6228855	Calcarenite	1
F5	6072050	6228020	Calcarenite	1	O43	613529	6228215	Calcarenite	1
F6	6072850	6228010	Calcarenite	1	O44	613540	6227771	Calcarenite	1
F7	6076250	6228240	Calcarenite	1	O45	616633	6228493	Calcarenite	2
F8	6076170	6228220	Calcarenite	1	O46	614656	6228345	Calcarenite	1
G1	6061050	6227035	Calcarenite	1	O6	614300	6227685	Calcarenite	1
G2	6060750	6226997	Calcarenite	1	O7	614388	6227609	Calcarenite	1
G3	6060600	6226994	Calcarenite	1	O9	618294	6227111	Calcarenite	1
H1	6094260	6229077	Calcarenite	1	P1	608696	6228719	Calcarenite	1
I1	6073990	6228103	Calcarenite	1	Q1	6108470	6229729	Calcarenite	1
I2	6075670	6228200	Calcarenite	1	R 1	6086430	6228703	Calcarenite	1
I3	6099970	6228417	Calcarenite	2	R 2	6088030	6228771	Calcarenite	1
I4	6079740	6228405	Calcarenite	2	R 3	609216	6228975	Calcarenite	1
I5	608350	6228575	Calcarenite	1	R 4	609216	6228975	Calcarenite	1
J1	6054110	6227152	Calcarenite	1	R 5	609216	6228975	Calcarenite	1
J2	6055950	6227005	Calcarenite	2	R 6	6094320	6229085	Calcarenite	1
J3	6058980	6226993	Calcarenite	1	R 7	6093920	6229060	Calcarenite	1
J4	6058890	6226991	Calcarenite	1	R 8	6095790	6229137	Calcarenite	1
J5	6058980	6226992	Calcarenite	1	R 9	6099120	6229295	Calcarenite	1
J6	6058790	6226952	Calcarenite	1	R 10	609912	6229295	Calcarenite	1
J7	6059370	6226869	Calcarenite	1	R 11	6099040	6229292	Calcarenite	1
J8	6058640	6226901	Calcarenite	1	R 12	6099040	6229292	Calcarenite	1
J9	6057800	6226764	Calcarenite	1	S1	6099810	6229337	Calcarenite	1
K1	6055860	6226484	Calcarenite	1	SH	608760	6228710	Calcarenite	1

K2	605510	6226460	Calcarenite	1	T1	610585	6229542	Calcarenite	1
K3	6054550	6226419	Calcarenite	1	T2	610951	6229743	Calcarenite	1
K4	6053690	6226295	Calcarenite	1	T3	610955	6229746	Calcarenite	1
L1	605281	6226262	Calcarenite	1	T4	621255	6229855	Calcarenite	1
L2	605290	6226262	Calcarenite	1	T5	621255	6229855	Calcarenite	1
L3	605125	6229560	Calcarenite	1	U1	611281	6229853	Calcarenite	1
M1	6048220	6225690	Calcarenite	1	V1	611540	6229951	Calcarenite	1
N1	6041640	6223031	Calcarenite	1	V2	611825	6230050	Calcarenite	1
N2	6041560	6225009	Calcarenite	1	V3	611983	6230109	Calcarenite	1

APPENDIX II

Geochronological data table showing dose rate data, D_e values and optical ages for twelve samples from the continental shelf offshore of Groot Brak (Mossel Bay). Analysis was conducted by Dr Zenobia Jacobs, University of Wollongong, Australia.

Sample code	Moisture content (%)	Radionuclide concentrations [a] U ($\mu g\ g^{-1}$)	Th ($\mu g\ g^{-1}$)	K (%)	Dose rates (Gy kyr^{-1}) Beta [b]	Gamma [c]	Cosmic [d]	Total dose rate [e, f] (Gy kyr^{-1})	D_e (Gy)	Number of grains [g]	σ_d [h] (%)	Optical age [i] (ka)
HC-SH	10 ± 3	0.71 ± 0.01	0.60 ± 0.13	0.21 ± 0.03	0.22 ± 0.02	0.21 ± 0.01	0.18	0.63 ± 0.04	76.1 ± 8.1	24	35 ± 5	122 ± 15
HC-37	13 ± 3	1.11 ± 0.05	1.99 ± 0.36	0.22 ± 0.03	0.29 ± 0.02	0.24 ± 0.02	0.10	0.66 ± 0.05	136.6 ± 6.6	22	21 ± 4	206 ± 19
HC-32	9 ± 2	1.22 ± 0.06	2.81 ± 0.46	0.79 ± 0.04	0.69 ± 0.04	0.43 ± 0.02	0.07	1.22 ± 0.07	139.7 ± 7.1	60	26 ± 5	115 ± 9
HC-39	11 ± 3	0.92 ± 0.03	1.64 ± 0.29	0.64 ± 0.04	0.53 ± 0.03	0.31 ± 0.02	0.05	0.91 ± 0.06	94.3 ± 4.6	24	23 ± 4	103 ± 8
HC-40	15 ± 4	1.60 ± 0.09	2.33 ± 0.44	0.31 ± 0.04	0.40 ± 0.03	0.32 ± 0.02	0.05	0.79 ± 0.06	92.9 ± 5.3	21	24 ± 4	117 ± 11
HC-35	17 ± 4	1.47 ± 0.09	2.81 ± 0.48	0.40 ± 0.04	0.44 ± 0.03	0.34 ± 0.02	0.04	0.85 ± 0.06	113.7 ± 6.7	24	28 ± 4	134 ± 13
HC-36	22 ± 6	1.04 ± 0.04	1.59 ± 0.30	0.34 ± 0.03	0.32 ± 0.02	0.23 ± 0.01	0.04	0.61 ± 0.05	77.0 ± 4.1	21	24 ± 4	125 ± 12
HC-6	17 ± 4	2.72 ± 0.25	3.88 ± 0.69	0.61 ± 0.07	0.71 ± 0.04	0.54 ± 0.04	0.04	1.32 ± 0.10	77.8 ± 5.6	20	29 ± 5	59 ± 6
HC-26	25 ± 5	2.20 ± 0.18	3.60 ± 0.66	0.48 ± 0.05	0.54 ± 0.03	0.43 ± 0.03	0.04	1.03 ± 0.08	142.6 ± 8.1	21	28 ± 5	138 ± 14
HC-30	12 ± 3	1.79 ± 0.10	1.58 ± 0.34	0.19 ± 0.04	0.35 ± 0.02	0.29 ± 0.02	0.03	0.70 ± 0.05	99.5 ± 4.4	21	19 ± 3	142 ± 12
HC-29	21 ± 5	1.43 ± 0.08	2.58 ± 0.45	0.37 ± 0.04	0.40 ± 0.02	0.31 ± 0.02	0.03	0.77 ± 0.06	94.0 ± 3.3	24	16 ± 3	122 ± 10
HC-24	17 ± 4	2.73 ± 0.22	1.92 ± 0.44	0.42 ± 0.05	0.57 ± 0.03	0.43 ± 0.03	0.03	1.05 ± 0.07	91.8 ± 6.9	24	35 ± 5	87 ± 9

Geochronological data table showing optical ages for 44 samples from Mossel Bay. Analysis was conducted by Dr Zenobia Jacobs, University of Wollongong, Australia.

Site Name	**Age Final (ka)**		**Site Name**	**Age Final (ka)**
Crevice Cave	88		PP13B	128
Crevice Cave	88		PP13C	116
Crevice Cave	89		PP29	123
Crevice Cave	91		PP5-6	64
Crevice Cave	94		PP5-6	70
Crevice Cave	124		PP5-6	71
Crevice Cave	124		PP5-6	74
Crevice Cave	126		PP5-6	69
Crevice Cave	127		PP5-6 embayment dune	71
Crevice Cave	127		PP5-6 embayment dune	125
Crevice Cave	130		PP5-6 embayment dune	67
Crevice Cave	144		PP7	124
Crevice Cave	145		PP9	128
Dana Bay	395		PP9B	88
Klein Brak	385		PP9B	89
Klein Brak	403		PP9B	91
PP13B	93		PP9B	129
PP13B	93		PP9C	75
PP13B	122		PP9C	130
PP13B	125		PP9C	72
PP13B	125		PP9C	91
PP13B	128		PP9C	255

APPENDIX III

Carbonate content values, for (1) unconsolidated marine sediments (prefix MB), (2) crushed rock samples (prefix denoted with a letter, O being offshore, all else is from the shoreline) and (3) modern reference samples (prefix REF).

Sample No.	Easting	Northing	Carbonate%	Sample No.	Easting	Northing	Carbonate%
MB-1	607980.18	6214907.46	26.56	MB-41	614889.47	6221973.72	26.51
MB-2	603411.41	6211643.61	12.9	MB-44	612402.46	6223798.44	23.45
MB-4	601768.19	6209636.26	10.47	MB-47	604573.53	6224251.8	27.81
MB-5	601006.44	6208761.73	10.99	MB-48	606232.56	6222882.72	18.31
MB-6	599915.58	6207510.28	12.55	MB-50	603594.82	6222007.47	43.2
MB-7	607253.48	6215386.41	23.6	MB-54	609812.07	6218267.59	33.33
MB-8	606512.3	6214470.29	18.76	MB-56	608024.21	6216938.08	24.51
MB-9	605857.82	6214967.37	19.17	MB-57	607520.28	6217741.09	22.6
MB-10	606514.89	6212771.44	14.93	MB-58	608416.63	6217910.67	30.79
MB-11	606338.06	6213164.04	18.71	MB-59	609411.59	6217104.02	21.68
MB-13	605762.74	6213697.09	8.45	MB-60	609243.39	6217187.18	28.05
MB-14	603650.85	6213062.85	18.71	MB-61	609738.48	6215911.64	28.15
MB-15	602606.39	6210890.03	12.36	MB-62	609456.61	6215723.82	27.93
MB-17	601793.74	6212116.12	13.63	MB-63	609174.35	6215794.77	60.96
MB-18	596624.99	6213710.35	16.3	MB-64	608247.44	6216173.17	58.95
MB-19	595611.74	6213814.27	16.43	MB-66	615844.3	6228584.29	33.89
MB-20	598491.12	6213793.68	16.07	MB-71	615994.82	6229979.45	23.96
MB-21	600322.12	6213701.56	14.31	MB-75	615862.35	6226126.59	25.31
MB-23	601476.29	6213006.45	22.87	MB-76	615797.1	6225917.28	23.77
MB-24	599642.32	6210471.61	12.18	MB-78	618842.62	6225934.86	19.24
MB-26	596947.59	6207541.82	8.62	MB-79	617925.61	6226466.07	52.9
MB-27	598610.46	6205907.24	9.91	MB-80	613859.63	6229454.07	53.26
MB-29	593122.26	6205913.6	8.23	MB-81	614158.59	6229707.64	38.59
MB-31	595925.8	6212797.12	23.34	MB-83	614684.62	6229736.59	28.95
MB-32	591382.72	6212401.48	18.17	MB-86	615766.76	6229423.97	35.18
MB-33	593983.05	6210036.21	15.78	MB-88	616954.04	6228488.27	56.52
MB-35	609555.94	6224102.16	26.87	MB-89	615612.7	6228386.96	46.01
MB-36	613858.67	6223383.37	26.09	MB-90	615499.34	6228228.52	20.99
MB-38	609024.82	6221844.68	25.51	MB-97	611450.53	6228804.35	26.12
MB-40	614993.48	6223463.48	19.87	MB-98	611095.3	6228275.08	21.25
MB-101	610674.56	6227361.61	29.15	MB-108	606197.21	6225618.57	23.36
MB-102	611424.39	6226164.77	30.29	MB-110	608786.18	6226409.06	24.11
MB-103	611579.78	6226526.09	16.53	MB-113	609833.75	6224989.78	21.57
MB-104	609982.45	6225791.4	22.35	MB-114	610427.82	6224983.32	20.6
MB-105	610778.46	6226790.23	25.03	MB-117	604483.63	6224518.69	27.79
MB-106	610338.9	6228648.85	28.86	MB-118	604464.39	6224685.22	29.64
MB-107	608909.64	6227654.28	30.86				

Sample No.	Carbonate%	Sample No.	Carbonate%	Sample No.	Carbonate%
03	69.38	045-B	54.66	F3	42.34
06	35.69	046	50.14	F4	41.95
07	38.36	A1	21.18	F5	41.31
09	27.38	A2	27.28	F6	27.16
011	59.83	B1	47.63	F7	33.91

022	38.68	C1	30.58	F8	32.33
023	30.57	C2	39.16	G1	55.4
024	31.91	C3	45.89	G2	47.74
026	56.45	D1	59.37	K2	30.3
027	49.59	D2	57.41	K3	37.3
028	40.43	E1	50.02	K4	46.55
029	37.84	E2	40.92	L1	53.15
030	39.23	E3	48.58	L2	26.88
032	48.11	E4	73.55	L3	50.19
033	48.34	E5	52.9	M1	22.47
034	41.81	E6	52.17	N1	33.7
035	39.18	E7	1.41	N2	31.8
036	52.12	E8	2.55	P1	49.91
037	29.93	E9	2.23	Q1	65.86
038	43.71	F1	16.42	R1	33.73
039-A	62.37	F2	24.59	R2	39.92
039-B	26.34	I3	48.32	R3	52.19
040	54.61	I4	41.59	R4	45.48
041-A	43.62	I5	46.23	R5	42.15
041-B	27.95	J1	43.55	R6	50.81
042	56.14	J2	61.71	T2	41.87
043	63.45	J3	78.92	T3	26.81
044	28.93	J4	50.28	T4	31.48
045-A	50.13	J6	43.86	T5	38.03
G3	64.14	J7	56.82	U1	60.88
H1	94.32	J8	37.89	V1	44.02
I1	35.29	J5	44.02	V2	29.74
I2	34.53	J9	59.81	V3	22.15
K1	31.5	R7	39.81	R8	36.15
R9	33.95				

Sample No.	**Easting**	**Northing**	**Carbonate%**	**Sample No.**	**Easting**	**Northing**	**Carbonate%**
REF-1	610842	6229743	21.64	REF-11	605815	6227224	26.03
REF-2	610847	6229729	22.43	REF-12	606127	6227134	40.48
REF-3	610848	6229723	33.25	REF-13 (Top)	606139	6227129	58.76
REF-4	610844	6229714	33.51	REF-13 (Bot)	606139	6227129	22.13
REF-5	610846	6229709	46.87	REF-14	609077	6228902	88.5
REF-6	610846	6229698	47.62	REF-15	609826	6229262	94.41
REF-7	610453	6229542	61.23	REF-16	606050	6227100	39.01
REF-8	608287	6228550	93.28	REF-17	606450	6226450	25.49
REF-9	608287	6228554	29.84	REF-18	610100	6229400	64.95
REF-10	608280	6228561	24.33	REF-19	609700	6229250	29.6

APPENDIX IV

SEM-EDS data for the 16 selected samples (for location and details, see Appendix II) analysed by this technique.

Sample: G2 Processing option : All elements analysed (Normalised)								
All results in weight%								
Spectrum	In stats.	C	O	Mg	Si	Ca	Fe	Total
Spectrum 1	Yes	18.79	52.67	0.47	0.28	27.78	0	100
Spectrum 2	Yes	18.93	49.08	0.42	0.64	30.94	0	100
Spectrum 3	Yes	15.72	46.13	0.55	0.41	36.39	0.8	100
Mean		17.81	49.29	0.48	0.44	31.71	0.27	100
Std. deviation		1.82	3.28	0.07	0.18	4.36	0.46	
Max.		18.93	52.67	0.55	0.64	36.39	0.8	
Min.		15.72	46.13	0.42	0.28	27.78	0	

Sample: D1 Processing option : All elements analysed (Normalised)									
All results in weight%									
Spectrum	In stats.	C	O	Mg	Al	Si	Ca	Fe	Total
Spectrum 1	Yes	16.91	53.02		1.03	1.92	24.76	2.36	100
Spectrum 2	Yes	17.34	54.44			0.67	27.55		100
Spectrum 3	Yes	17.12	51.3	0.66	0.78	1.54	26.75	1.84	100
Max.		17.34	54.44	0.66	1.03	1.92	27.55	2.36	
Min.		16.91	51.3	0.66	0.78	0.67	24.76	1.84	

Sample: O24 Processing option : All elements analysed (Normalised)									
All results in weight%									
Spectrum	In stats.	O	Mg	Al	Si	K	Ca	Fe	Total
Spectrum 1	Yes	55.96	0.82	1.21	10.92	0.44	29.21	1.43	100
Spectrum 2	Yes	57.3	1.92	4.09	18.3	1.08	12.7	4.62	100
Spectrum 3	Yes	55.9	0.83	2.39	13.7	1.17	22.55	3.45	100
Mean		56.39	1.19	2.56	14.31	0.9	21.49	3.17	100
Std. deviation		0.79	0.63	1.44	3.73	0.4	8.31	1.62	
Max.		57.3	1.92	4.09	18.3	1.17	29.21	4.62	
Min.		55.9	0.82	1.21	10.92	0.44	12.7	1.43	

Sample: J1 Processing option : All elements analysed (Normalised)							
All results in weight%							
Spectrum	In stats.	C	O	Al	Si	Ca	Total
Spectrum 1	Yes	52.52	30.03		13.49	3.97	100

Spectrum 2	Yes	20.15	52.49	0.81	2.04	24.5	100
Spectrum 3	Yes	23.47	49.11		3.52	23.9	100
Max.		52.52	52.49	0.81	13.49	24.5	
Min.		20.15	30.03	0.81	2.04	3.97	

Sample: O3 Processing option : All elements analysed (Normalised)										
All results in weight%										
Spectrum	In stats.	C	O	Al	Si	S	K	Ca	Fe	Total
Spectrum 1	Yes	59.17	28.6			1.11		11.12		100
Spectrum 2	Yes	65.31	19.14		15.55					100
Spectrum 3	Yes	49.43	30.95	2.1	13.55	1.13	0.48		2.36	100
Max.		65.31	30.95	2.1	15.55	1.13	0.48	11.12	2.36	
Min.		49.43	19.14	2.1	13.55	1.11	0.48	11.12	2.36	

Sample: L1 Processing option : All elements analysed (Normalised)										
All results in weight%										
Spectrum	In stats.	C	O	Mg	Al	Si	K	Ca	Fe	Total
Spectrum 1	Yes	11.52	55.72	1.38	3.52	11.91	1.07	13.54	1.33	100
Spectrum 2	Yes	13.83	47.69	2.15	2.99	8.18	1.02	21.97	2.17	100
Spectrum 3	Yes	15.14	55.43	1.33	3.53	12.55	0.76	9.89	1.37	100
Mean		13.5	52.95	1.62	3.35	10.88	0.95	15.13	1.62	100
Std. deviation		1.84	4.55	0.46	0.31	2.36	0.17	6.19	0.47	
Max.		15.14	55.72	2.15	3.53	12.55	1.07	21.97	2.17	
Min.		11.52	47.69	1.33	2.99	8.18	0.76	9.89	1.33	

Sample: D2 Processing option : All elements analysed (Normalised)							
All results in weight%							
Spectrum	In stats.	C	O	Mg	Si	Ca	Total
Spectrum 1	Yes	21.45	56.2	2.07	1.74	18.55	100
Spectrum 2	Yes	19.87	56.99	1.73	1.28	20.14	100
Spectrum 3	Yes	18.39	57.86	2.24	1.81	19.71	100
Mean		19.9	57.01	2.01	1.61	19.47	100
Std. deviation		1.53	0.83	0.26	0.29	0.82	
Max.		21.45	57.86	2.24	1.81	20.14	
Min.		18.39	56.2	1.73	1.28	18.55	

Sample: O32 Processing option : All elements analysed (Normalised)										
All results in weight%										
Spectrum	In stats.	C	O	Mg	Al	Si	K	Ca	Fe	Total
Spectrum 1	Yes	0	49.97	2.94	8.74	22.94	3.36		12.04	100
Spectrum 2	Yes	0	61.71		5.88	16.3	3	13.1		100
Spectrum 3	Yes	18.36	52.32		1.17	4.86		23.29		100

Max.		18.36	61.71	2.94	8.74	22.94	3.36	23.29	12.04	
Min.		0	49.97	2.94	1.17	4.86	3	13.1	12.04	

Sample: O6 Processing option : All elements analysed (Normalised)													
All results in weight%													
Spectrum	In stats.	O	Na	Mg	Al	Si	S	Cl	K	Ca	Ti	Fe	Total
Spectrum 1	Yes	55.65	0.9	0.99	2.93	17.68	2.12	1.32	1.39	9.65		7.36	100
Spectrum 2	Yes	52.27		1.52	5.2	11.39		1.11	2.76	14.15	1.66	9.95	100
Spectrum 3	Yes	62.37	1.12	1.08	2.27	6.01		0.73	0.86	20.7		4.87	100
Max.		62.37	1.12	1.52	5.2	17.68	2.12	1.32	2.76	20.7	1.66	9.95	
Min.		52.27	0.9	0.99	2.27	6.01	2.12	0.73	0.86	9.65	1.66	4.87	

Sample I5 Processing option : All elements analysed (Normalised)										
All results in weight%										
Spectrum	In stats.	C	O	Na	Al	Si	Cl	Ca	Fe	Total
Spectrum 1	Yes	13.57	39.22			0.91		46.3		100
Spectrum 2	Yes	21.19	44.44	1.37	0.63	26.38	1.55	2.3	2.13	100
Spectrum 3	Yes	22.01	42.12	1.19	0.42	7.91	1.73	23.33	1.29	100
Max.		22.01	44.44	1.37	0.63	26.38	1.73	46.3	2.13	
Min.		13.57	39.22	1.19	0.42	0.91	1.55	2.3	1.29	

Sample: SH Processing option : All elements analysed (Normalised)											
All results in weight%											
Spectrum	In stats.	C	O	Na	Mg	Al	Si	Cl	K	Ca	Total
Spectrum 1	Yes		50.05	4.58	0.76	6.35	9.68	5	1.91	21.67	100
Spectrum 2	Yes	10.14	41.83			0.63	3.12	0.71		43.58	100
Spectrum 3	Yes		59.5	1.29	0.81	2.59	4.76	1.86	0.88	28.32	100
Max.		10.14	59.5	4.58	0.81	6.35	9.68	5	1.91	43.58	
Min.		10.14	41.83	1.29	0.76	0.63	3.12	0.71	0.88	21.67	

Sample: O35 Processing option : All elements analysed (Normalised)								
All results in weight%								
Spectrum	In stats.	C	O	Mg	Si	Ca	Fe	Total
Spectrum 1	Yes	18.75	47.42	2.04	3.03	26.6	2.17	100
Spectrum 2	Yes	8.16	29.05			62.79		100
Spectrum 3	Yes	14.18	45.42	2.06	1.96	36.38		100
Max.		18.75	47.42	2.06	3.03	62.79	2.17	
Min.		8.16	29.05	2.04	1.96	26.6	2.17	

Sample: O39 Processing option : All elements analysed (Normalised)								
All results in weight%								
Spectrum	In stats.	C	O	Mg	Al	Si	Ca	Total

Spectrum 1	Yes	14.21	53.79	0.56			31.44	100
Spectrum 2	Yes	16.54	49.19	0.57		0.53	33.16	100
Spectrum 3	Yes	15.59	53.59	0.58	0.43	1.18	28.63	100
Max.		16.54	53.79	0.58	0.43	1.18	33.16	
Min.		14.21	49.19	0.56	0.43	0.53	28.63	

Sample: O29 Processing option : All elements analysed (Normalised)									
All results in weight%									
Spectrum	In stats.	C	O	Na	Mg	Al	Si	Ca	Total
Spectrum 1	Yes	14.88	60.02		1.3	1.23	5.39	17.18	100
Spectrum 2	Yes	16.05	55.38	3		2.54	16.63	6.39	100
Spectrum 3	Yes	17.53	56.23		1.58	1.57	7.09	15.99	100
Max.		17.53	60.02	3	1.58	2.54	16.63	17.18	
Min.		14.88	55.38	3	1.3	1.23	5.39	6.39	

Sample: O27 Processing option : All elements analysed (Normalised)											
All results in weight%											
Spectrum	In stats.	C	O	Na	Mg	Al	Si	K	Ca	Fe	Total
Spectrum 1	Yes	0	57.23		0.82	1.45	5.08	0.75	29.92	4.74	100
Spectrum 2	Yes	11.61	53.46	0.65	1.08	1.08	3.89	0.52	24.65	3.06	100
Spectrum 3	Yes		56.98		0.92	1.38	6.74	0.75	28.47	4.76	100
Max.		11.61	57.23	0.65	1.08	1.45	6.74	0.75	29.92	4.76	
Min.		0	53.46	0.65	0.82	1.08	3.89	0.52	24.65	3.06	

Sample: R1 Processing option : All elements analysed (Normalised)									
All results in weight%									
Spectrum	In stats.	C	O	Mg	Al	Si	Ca	Fe	Total
Spectrum 1	Yes	18.46	52.2	2.03	0.8	1.01	25.01	0.5	100
Spectrum 2	Yes	18.47	52.39	1.96	0.48	1.02	24.83	0.84	100
Spectrum 3	Yes	19.14	52.21	2.28		0.53	25.01	0.82	100
Max.		19.14	52.39	2.28	0.8	1.02	25.01	0.84	
Min.		18.46	52.2	1.96	0.48	0.53	24.83	0.5	

APPENDIX V

A3 fold-outs of the two detailed tables presented in Chapters 4 and 5, respectively (Table 4-8 and Table 5-1). These tables do not differ to the ones in the text and are provided only for convenience.